Appendix I

The Impact of IRIS on the Geosciences

THE IMPACT OF IRIS ON THE GEOSCIENCES

In 1984, the seismological community created a consortium of research institutions to build the necessary facilities to support seismological research. Today, IRIS has become the primary data source for one of our major scientific frontiers — understanding the Earth's interior. By most objective measures, IRIS has been a success; and that success continues as each year, more data are requested, more experiments are supported, and more scientists and students participate in IRIS programs.

What IRIS's founders did not anticipate, however, was the extent of the Consortium's impact on the culture of seismology. As described elsewhere in this proposal, seismology is no longer restricted to the few research institutions that can support large data management facilities and maintain instrumentation. Seismological data are now readily available to a broad range of researchers and educators. Consequently, many of the traditional barriers in Geoscience research and education are beginning to dissolve. Boundaries are routinely crossed in such areas as structural geology and crustal imaging, tomography and mineral physics, earthquakes and metamorphic processes, and inner-core structure and geomagnetism. In addition, IRIS contributions to education and outreach, the monitoring of the Comprehensive Nuclear Test-Ban Treaty, and earthquake hazard mitigation are helping to foster a new generation of "scientist-educator-citizens".

While all of IRIS contributions are important, the fundamental value of the facilities must be measured by the science that is produced. The purpose of Appendix I is to provide specific examples of both the scope and depth of IRIS's impact. The beginning of this section consists of one-page project descriptions, contributed by researchers, that illustrate the role of IRIS data in advancing our understanding of topics ranging from global tomography and continental structure to the mechanics of volcanic eruptions and the development of educational programs and products. Following this collection of one-pagers is a list of publications that specifically acknowledge IRIS data or instrumentation. This collection of projects and publications is by no means complete. It is meant simply to illustrate the breadth of scientific and educational endeavors to which IRIS resources contribute.

The one-pagers begin with some advances in global tomography. The examples demonstrate how we have been able to go beyond broad-scale mantle convection and begin detailed study of smaller-scale processes related to subducting slabs, oceanic ridges, the core-mantle boundary, mineralogical phase-transitions, and differential rotation of the inner core. Following the collection on global tomography are examples of seismological investigations of oceanic and continental structure that tie surface observations with processes within the lower-crust and mantle. The examples provide evidence that we now stand at a threshold of integrative breakthroughs in understanding local and regional scale processes such as subduction, continental rifting, ocean basin evolution, the uplift of mountains, the assemblage of continents, and earthquakes and volcanoes. Continued high-quality seismological observations will play a key role in addressing these inherently multi-disciplinary problems.

Also included are a series of one-page descriptions that demonstrate the role of IRIS data and instruments for understanding the earthquake process and for advancing the applications of seismology. In particular, we have included examples of IRIS's role in improving our assessments of seismic risk, predicting ground motion, and in enhancing our ability to monitor compliance with international treaties that prohibit the testing of nuclear weapons. IRIS data have now become fully integrated into both the research and the operational systems associated with the National Earthquake Information Center and the International Monitoring System for the Comprehensive Nuclear Test-Ban Treaty.

A final group of one-pagers constitutes examples of contributions to education. The availability of real-time global seismic data, the opportunity for students to participate in fieldwork, and the development of classroom seismic stations has stimulated interest in Geoscience at all levels. These educational and outreach projects serve not only to advance public knowledge of Geoscience, but also to create a new generation of students with an improved understanding of the scientific process and scientific data.

Following the one-pagers is a list of IRIS-related publications that appeared in 1999. The list is intended to complement the one-pagers by further demonstrating the extent of IRIS influence.

Together, the one-page descriptions and the sample reference list provide evidence not only for the impact of IRIS on seismology, but also for seismology's role as a cornerstone for Earth Science. One of the next major steps in understanding the Earth is to connect processes observed at the surface with the structure and dynamics of the Earth's interior that we infer through seismology. As evidenced by this Appendix, IRIS is contributing to these advances by providing the data necessary to make these

One-Page Project Descriptions

Data Resolution and Visualization

Y. J. Gu, A. M. Dziewonski, W.-J. Su, and G. Ekström, Harvard University

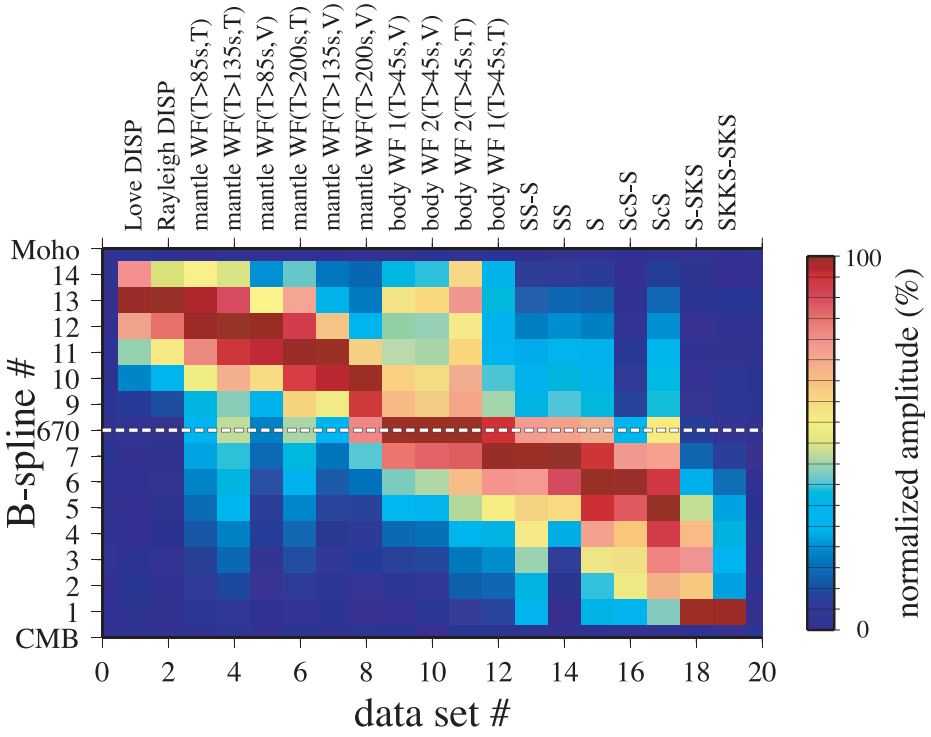

Sensitivity of individual data sets to the 14 radial B-spline functions used in a 3-D inversion of shear velocities in the mantle. B-spline functions are labeled in an increasing order from the CMB to the Earth surface. Normalized sensitivity of the data set in resolving the 14 B-spline functions are shown: large sensitivities are shown in intense red, and small, dark blue. It is evident that the surface wave dispersion measurements are highly sensitive to the near-surface splines. The mantle wave waveforms are sensitive to the upper mantle structure, while body wave waveform and travel time measurements have the largest contributions to depths below 500 km. WF 1 represents a waveform data set with recordings from 1977-1990; WF 2 represents a more recently compiled waveform data set.

To achieve good resolution in full range of depths it is often important to combine data sets such as body- and mantle-wave waveforms, travel times, surface waves phase velocities, etc., for the three-dimensional (3-D) inversion of shear velocities in the mantle. The diversity of data warrants a closer examination on the sensitivity of each data set to a given model parameter. We hereby describe a simple method to visualize the contribution of individual data sets to an inversion that is radially parameterized in 14 localized B-spline functions (Gu et al, 2000). Because the data sensitivity to the spline function centered at each radial knot is directly related to the corresponding diagonal elements of the A^TA matrix, we can define a simple normalized diagonal average for each data set: for the k-th data set and the i-th spline, a diagonal element of the averaged $(A^TA)^{(k)}$ matrix

$$(A^TA)^{(k)}_i = (1/N) \sum_{j=1}^{N} [\mathrm{diag}\,(A^TA)^{(k)}]_{i,j} \qquad 1 \le i \le M;$$

is w_k is the weight of the data set, N is the total number of horizontal splines (362 nodes) and M is the number of radial splines. By assuming unit weights, we compute the contributions of all data sets of this study to the individual spline functions (normalized to the peak amplitude within each data set) and a color-coded representation is shown. It clearly illustrates the varying contributions of different subsets of data to the maximum resolution at various depths. For example, the inclusion of surface wave dispersion measurements allows us to resolve the structure in the top 200 km; various sets of mantle-wave waveforms provide adequate sampling in the upper mantle and transition zone, and body wave waveforms, in mid-mantle depths. The absolute travel time measurements help to constrain structure immediately below the 670-km discontinuity to mid-mantle, whereas the differential travel times of S-SKS, ScS-S and SKKS-SKS are particularly sensitive to the structure in the lowermost mantle. All of these data sets have been obtained from analysis of digitally recorded seismograms from the GSN, retrieved from the DMC over the years.

For further reading:

Gu, Y.J., Dziewonski, A.M., Su, W-J, Ekstrom, G., Shear velocity model of the mantle and discontinuities in the pattern of lateral heterogeneities, submitted, 2000.

Global 3-D Models and Event Location

Michael Antolik, Göran Ekström, and Adam Dziewonski, Harvard University

Experiments performed using 3-D models of various resolution show that the event location with respect to the ground truth is not a simple function of the number of parameters in a model. To this effect we have compared the results obtained using a 'high-resolution' model described by 250,000 parameters, a 'medium-resolution' model described by 25,000 parameters, and a 'low-resolution' model described by 2,500 parameters. The result was that the corrections predicted by the 'low-resolution' model led to the most precise locations, while the 'high-resolution' model gave corrections that led to the best variance reduction.

Our previous experiments with the quality of the location used data from ISC Bulletins, which may not be representative of the IDC (International Data Centre, Vienna) data set. To investigate the effect of the smaller number of the reporting stations, we have artificially reduced the number of observations. The results reveal that 3-D corrections are even more important when the station coverage is sparser. The figure shows mislocation resulting from location trials using a group of 86 explosions and well-located earthquakes (Kennett and Engdahl, 1991) for four 3-D mantle models of increasing complexity from top to bottom, as well as the spherically symmetric model PREM (Dziewonski and Anderson, 1981). Models SP12 and MK12 (Su and Dziewonski, 1997) use spherical harmonic functions up to degree 12, model BDP98 (Boschi and Dziewonski, 1999) uses constant-velocity blocks of dimension 5° x 5° at the equator, and model VWE97 of van der Hilst et al. (1997) uses blocks with a dimension of 2°. We relocated each test event multiple times using different random selections of either 30 or 8 teleseismic P phases recorded by the GSN. As the figure shows, the more detailed 3-D models do not produce better results. The average mislocation resulting from the location trials is smallest for model SP12.

To accommodate future regional 3-D models, we have begun construction of a reference global model, using local function representation (3-D cubic splines) roughly equivalent to degree 18 in spherical harmonics. The model will be constructed using waveforms, surface wave dispersion measurements, and travel times in order to achieve better resolution in the upper mantle than contained in most existing block models. An arbitrary part of this model can be replaced by a regional model, and travel time corrections can be computed at regional distances using the regional model. At teleseismic distances, the corrections would be evaluated for a combination of regional and global structure.

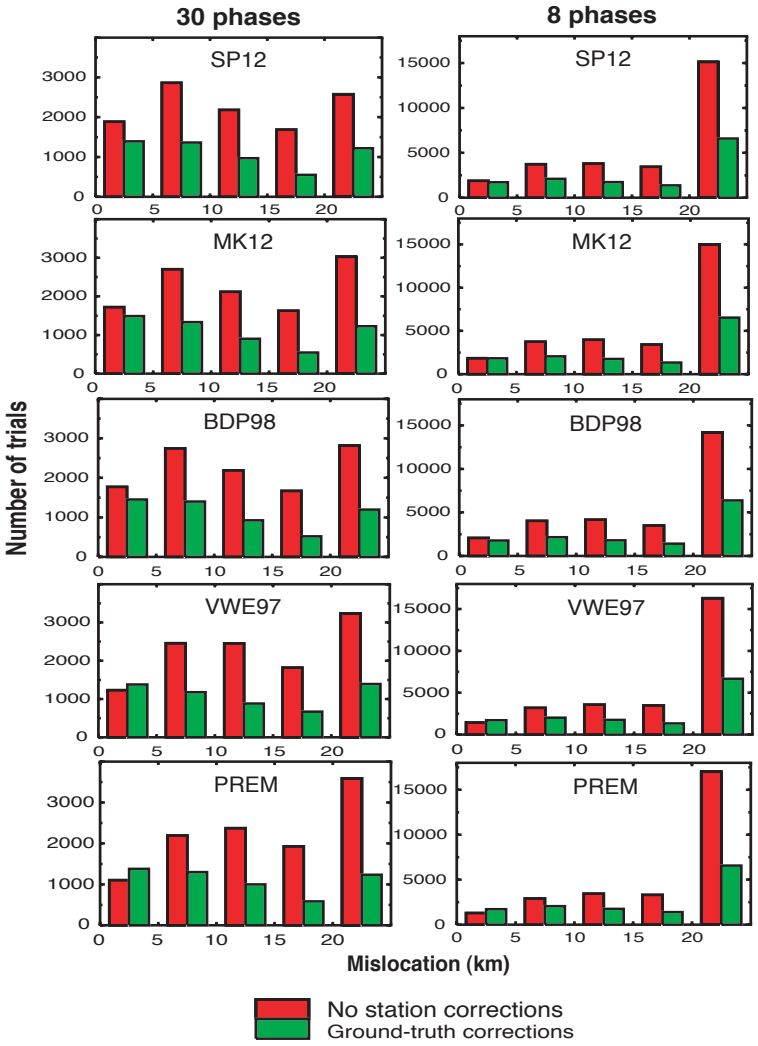

Histograms depicting the distribution of location errors for trials using 30 phases (left) and 8 phases (right) for four 3-D models and for PREM. The data set consisted of 86 explosions and earthquakes with well-constrained locations. The height of each bar represents the number of location trials resulting in a mislocation within a 5-km wide bin, except that the last bin contains all of the location trials with a mislocation larger than 20 km. Red bars show results for location trials using no empirical station corrections while the green bars are for trials using station corrections computed relative to ground-truth. The green bars do not include results for the reference events used to calculate the ground-truth corrections.

For further reading:

Boschi, L., and Dziewonski, A.M., High and low-resolution images of the Earth's mantle: Implications of different approaches to tomographic modeling, *J. Geophys. Res.*, **104**, 25,567-25,594, 1999.

Dziewonski, A. M., and Anderson, D.L., Preliminary reference earth model, *PEPI*, **25**, 297-356, 1981.

Kennett, B. L. N., and Engdahl, E.R., Travel times for global earthquake location and phase identification, *Geophys. J. Int.*, **105**, 429-465, 1991.

Su, W., and Dziewonski, A.M., Simultaneous inversion for 3D variations for shear and bulk sound velocity in the mantle, *PEPI*, **100**, 135-156, 1997.

van der Hilst, R. D., Widiyantoro, S., and Engdahl, E.R., Evidence for deep mantle circulation from global tomography, *Nature*, **386**, 578-584, 1997.

Global Mantle Tomography: The Resolving Power of Low-Degree Spherical Harmonic Parameterization

Lapo Boschi and Adam M. Dziewonski, Harvard University

One important application of the data collected by IRIS, in the GSN and PASSCAL programs, is the derivation of the three-dimensional structure of Earth's interior. In the last two decades, as the discipline of seismic tomography was developing, the reliability of different computational techniques has been debated. In fact, the determination of global 3-D velocity models, by a least-squares fit of seismic travel-time data, requires very intense computational procedures, both in terms of time and computer memory. In the early years of global tomography, it was therefore unavoidable to parameterize such seismic models of the Earth in terms of a limited number of basis functions; quite frequently, the lateral variations of P or S velocity within the Earth were described as a linear combination of spherical harmonic functions (up to a relatively low degree), multiplied by Chebyshev polynomials (which accounted for the radial dependence of the anomalies). More recently, it has been suggested (Pulliam and Stark, 1993; Megnin et al., 1997) that tomographic inversions based on low-degree parameterizations tend to generate artifacts and overestimate the spectral power at low degrees.

We believe that the validity of those early, long wavelength models, can be demonstrated by means of an *ad-hoc* synthetic test. We use the high-resolution model BDP98 (Boschi and Dziewonski, 1999) to compute theoretical delay times resulting from 3-D P-velocity anomalies. We then carry out a tomographic inversion of those "synthetic" data to determine a degree 12 spherical harmonics/degree 13 Chebyshev polynomials image of the Earth's mantle. The similarity of the "input" and "output" models is a measure of the resolving power of this low-degree parameterization.

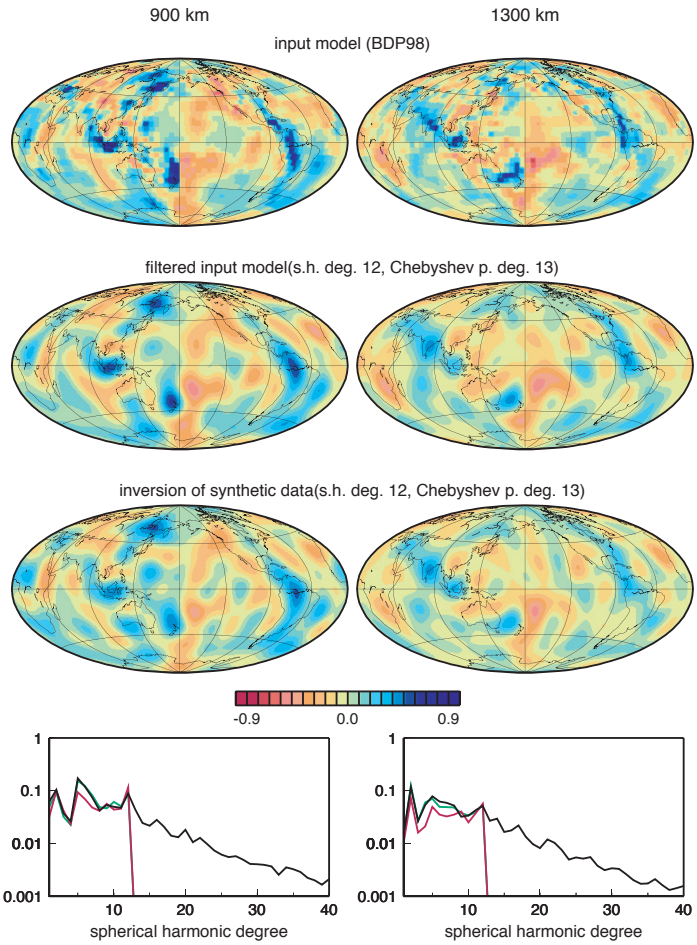

Degree 12 spherical harmonics/degree 13 Chebyshev polynomials synthetic inversion for 3-D mantle structure. We focus on the depths of (left) 900 km and (right) 1300 km in the mid mantle. (top) Input model BDP98. (top middle) A low-pass-filtered version of BDP98, obtained by finding the linear combination of degree 12 spherical harmonics/ degree 13 Chebyshev polynomials that best fits BDP98, sampled at the center of each block. (top bottom) The result of the actual synthetic inversion. (bottom) Spherical harmonic power spectra corresponding to each depth: the spectrum of the input model is in black, the spectrum associated with the synthetic experiment is in red, and the spectrum of the filtered version of BDP98 is in green.

For further reading:

Boschi, L., and Dziewonski, A.M., "High" and "low" resolution images of the Earth's mantle: Implications of different approaches to tomographic modeling, *J. Geophys. Res.*, **104**, 25,567-25,594, 1999.

Megnin, C., Bunge, H.-P., Romanowicz, B., and Richards, M.A., Imaging 3-D spherical convection models: What can seismic tomography tell us about mantle dynamics?, *Geophys. Res. Lett.*, **24**, 1299-1302, 1997.

Pulliam, R. J., and Stark, P.B., Bumps on the core-mantle boundary: Are they facts or artifacts?, *J. Geophys. Res.*, **98**, 1943-1955, 1993.

Global and Regional Tomographic Maps from Surface-Wave Phase Velocity Anomalies

Lapo Boschi, Göran Ekström, and Adam Dziewonski, Harvard University

In the last few years, a large number of Rayleigh and Love wave phase anomaly measurements, based on seismic records from the GSN, have been collected by the Harvard seismology group, making use of the technique described by Ekström, Tromp and Larson (1997). Through tomographic inversion, these data have provided new images of the lateral variations of phase velocity at different periods, as well as three-dimensional (3-D) models of the shear and compressional velocity structure of Earth's upper mantle, including significant anisotropic features (e.g., Ekström and Dziewonski, 1998; Ekström, 2000).

Recent developments in this research, made possible by the good quality of our measurements, include: (1) determination of 3-D images of the upper mantle based upon a 3-D starting model, accounting for the effect of the crust and the associated lateral variation in the sensitivity of our data to the underlying structure and (2) use of a locally varying parameterization, finer within a certain, well-sampled, region of interest.

For further reading:

Ekström, G., Tromp, J., and Larson, E.W.F., Measurements and global models of surface waves propagation, *J. Geophys. Res.*, **102**, 8137-8157, 1997.

Ekström, G., and Dziewonski, A.M., The unique anisotropy of the Pacific upper mantle, *Nature*, **394,** 168-172, 1998.

Ekström, G., Mapping the lithosphere and asthenosphere with surface waves: Lateral structure and anisotropy, in *The History and Dynamics of Global Plate Motions*, edited by M. Richards *et al.*, AGU monograph, in press, 2000.

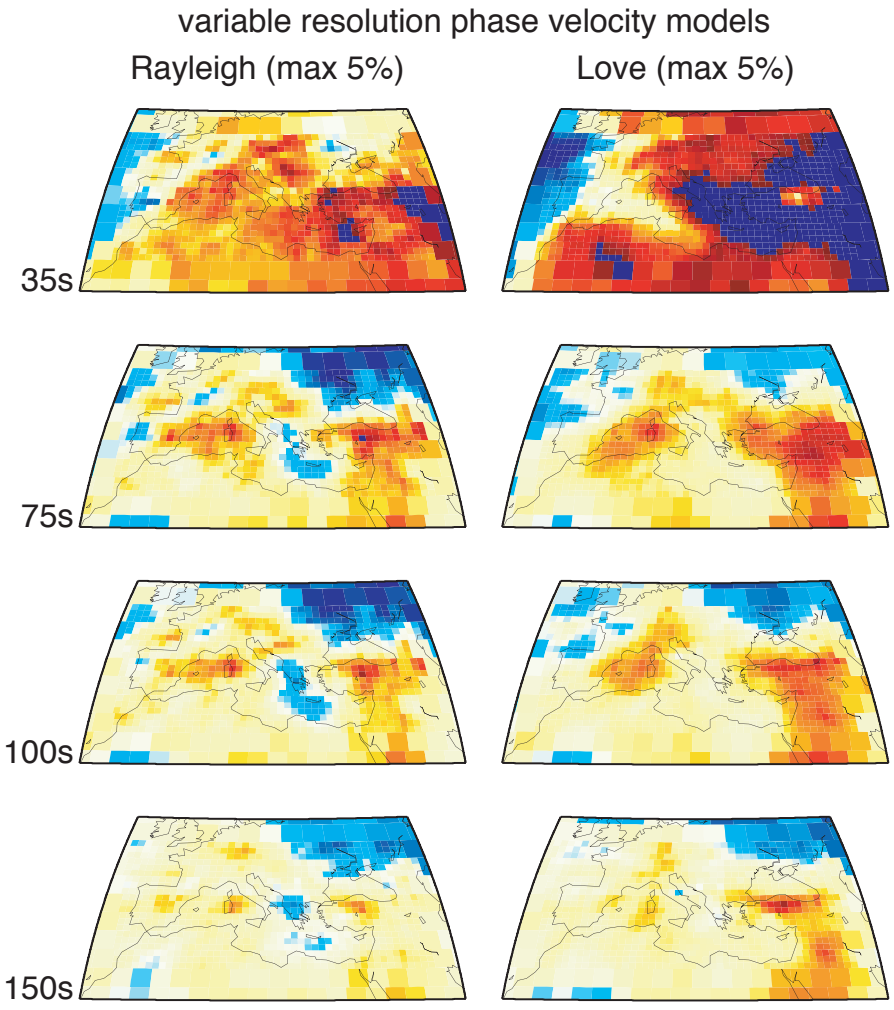

Eight 1-degree by 1-degree phase velocity maps of the Mediterranean region, corresponding, as indicated, to surface waves of different periods and types. Each of these images is part of a global model, parameterized everywhere outside the region of interest in terms of 3-degree by 3-degree blocks. This variable resolution approach has two important advantages. First, it allows us to refine our model exclusively in one region, without dealing with the inconveniences of an exceedingly large number of free parameters. Second, it accounts explicitly for the sensitivity of global data to lateral velocity variations outside the region of interest; global data can thus be used to map regional structure.

Seismic Travel Times at Finite Frequency: The Next Step in Seismic Tomography

Guust Nolet, Tony Dahlen and Shu-Huei Hung, Princeton University

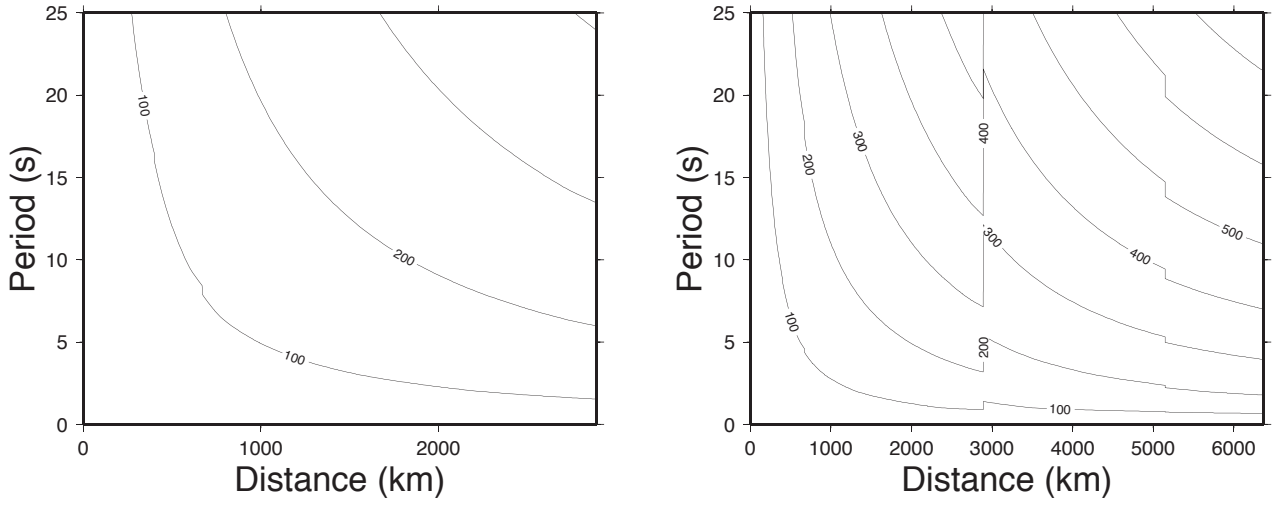

The resolvable width in km of a low-velocity body as a function of distance between the heterogeneity and the seismometer (or source) along the ray path. Left: S waves. Right: P waves. The wavelength of the P or S pulse is assumed to be that of a wave vertically propagating in PREM. Contours are labeled in km, and represent widths for which the fractional group delay has dimished by wavefront healing to 80% of its original value. After this, healing soon becomes catastrophic as the wave travels further, and the tomographic signal is lost. Kinks in the isolines are caused by velocity discontinuities in PREM.

Although it is well known that anomalies in wavefronts heal as the wave propagates, the effects of this are generally ignored in global tomography. As shown in Dahlen et al (2000) and Huang et al (2000), the complexities of the raypath in realistic Earth models create a complicated, often counter-intuitive, relationship between the travel time of a broadband P or S pulse and the velocity structure inside the Earth. As a consequence, modeling errors are likely to affect interpretation of all but the shortest period travel time anomalies. For larger velocity contrasts, nonlinear effects may appear that are even more baffling to a classical seismologist whose intuition is sharpened by ray theory, but not necessarily by the realities of wave propagation inside the Earth.

In a recent analytical study of the phenomena in Nolet and Dahlen (2000), we concluded that the effects of wavefront healing for surface waves traveling in 2D are less severe than those for body waves in 3D; that the healing of delays is likely to contribute significantly to the scatter of observed travel-time anomalies; that tomographic inversions of long-period body waves face perceptible limitations in theoretical resolving power; and that positive travel-time anomalies evolve differently from negative ones. The figure shows the theoretical limits of resolution inside the Earth (assuming otherwise perfect ray coverage). For heterogeneities smaller than the ones in this figure, finite frequency effects are serious. Many of the current global models are based on travel times, or differential travel times, measured from the GSN at periods of 20 seconds or more. Such data effects of wavefront healing must certainly be taken into account in the interpretation.

For further reading:

Dahlen, F.A., Hung S.-H., and Nolet, G., Frechet kernels for finite-frequency traveltimes — I. Theory, *Geophys. J. Int.*, **141**, 157-174, 2000.

Hung,S.-H., F.A. Dahlen and G. Nolet, Frechet kernels for finite-frequency traveltimes — II. Examples, *Geophys. J. Int.*, **141**, 175-203, 2000.

Nolet, G. and F.A. Dahlen, Wavefront healing and the evolution of seismic delay times, *J. Geophys. Res.*, in press, 2000.

Discontinuities in the Pattern of Lateral Heterogeneities

Y. J. Gu, A. M. Dziewonski, and G. Ekström, Harvard University

To obtain a reliable snapshot of shear velocities in the mantle, particularly near the transition zone, we use a diversified data set consisting of body- and mantle-wave waveforms, travel times and surface wave phase velocities. Nearly all of these data have been obtained using seismograms recorded by the GSN. We conduct inversions using a local B-spline support for the lateral and radial dimensions. By parameterizing the radial variations of velocity using one or more sets of B-splines, we allow the velocities to vary smoothly (former), or discontinuously (latter) across depths at which the mantle is split. Our experiments suggest a significant change in the long-wavelength anomalies of the transition zone from those below. The attached figure shows a best-fit model for the Earth with two imposed discontinuities (400 km and 670 km). They are well established as global discontinuities in seismic velocities. The amplitudes of the heterogeneities at both discontinuities are comparable. Our experiment is intended to explore how the pattern of lateral heterogeneity changes across these boundaries. Near 400 km, only minor changes in the large-scale features are observed (panels a and b). The power spectra (panel c) shows a moderate decrease in degree 1 and 5 in the transition zone, which implies a decrease of the continent-ocean signature that characterizes the lithosphere. The overall change at 400 km, however, is too gradual to signify a flow boundary. In contrast, the amplitudes of fast velocities related to subducted slabs in the western Pacific and South America decrease notably in the lower mantle (panels d and e). The Pacific mantle, which is dominated by large-scale slow velocities at 650 km, is overtaken by small-scale fast velocities at the 690-km depth. The degree-2 spherical harmonic (panel f), which is the most pronounced signal in the transition zone, is strongly attenuated at the top of the lower mantle. Resolution tests show that these results are robust which suggest a possible reorganization of the flow between the upper and lower mantle.

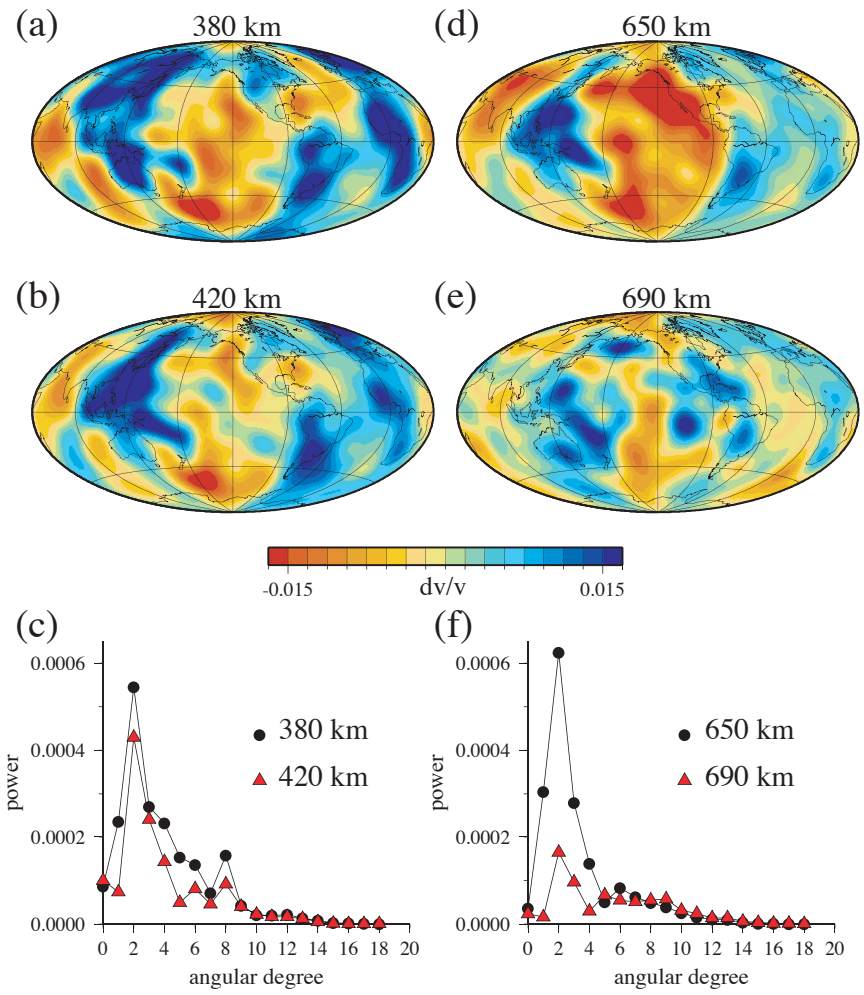

Constraining Three-Dimensional Mantle Structure Using Normal-Mode Splitting Data and the Earth's Gravity Field

Miaki Ishii and Jeroen Tromp, Harvard University

A normal mode, or free oscillation, of the Earth is a standing wave resulting from the constructive and destructive interference of traveling waves. The resonance peak of a normal mode is split as a result of rotation, hydrostatic ellipticity and lateral heterogeneity. The effects of Earth's rotation and hydrostatic ellipticity can be predicted, and the remaining splitting, represented as splitting function coefficients, can be used to constrain lateral variations in the mantle.

Recently, a large number of splitting function coefficients has become available through analysis of seismograms recorded after large earthquakes in 1994-1996. With the new data set, obtained using seismograms from world-wide stations including GSN, Geoscope and IDA, we have been able to invert not only for perturbations in shear velocity, but also for perturbations in compressional velocity and density. Inversion for density heterogeneity is a unique advantage gained by using long-period normal-mode data. Body-wave data, normally used in the construction of mantle models, are not sensitive to lateral variations in density.

An additional constraint on the density structure of the mantle is provided by the Earth's gravity anomaly. This signal depends on density variations within the mantle and topography on internal discontinuities and the surface. We include the gravity data in our inversion by taking advantage of models of boundary topography determined previously through seismic and geodynamic studies.

Shear and compressional velocity models obtained from normal-mode inversion are consistent with those obtained using travel-time or waveform data. Comparison of shear (β) and compressional (α) velocity models shows reasonable correlation throughout the mantle, consistent with a thermal origin of lateral variations. However, comparison of shear velocity and bulk sound velocity ($v_\phi = \sqrt{\alpha^2 - 4\beta^2/3} = \sqrt{\kappa/\rho}$, where κ denotes the isentropic incompressibility and ρ density) shows a decrease in correlation from the top to the bottom of the mantle. Near the core-mantle boundary, shear and bulk sound velocity are strongly anti-correlated (correlation coefficient of -0.63), which suggests the importance of variations from a non-thermal origin. This is further supported by the comparison of density and shear velocity models which shows regional anti-correlation near the core-mantle boundary.

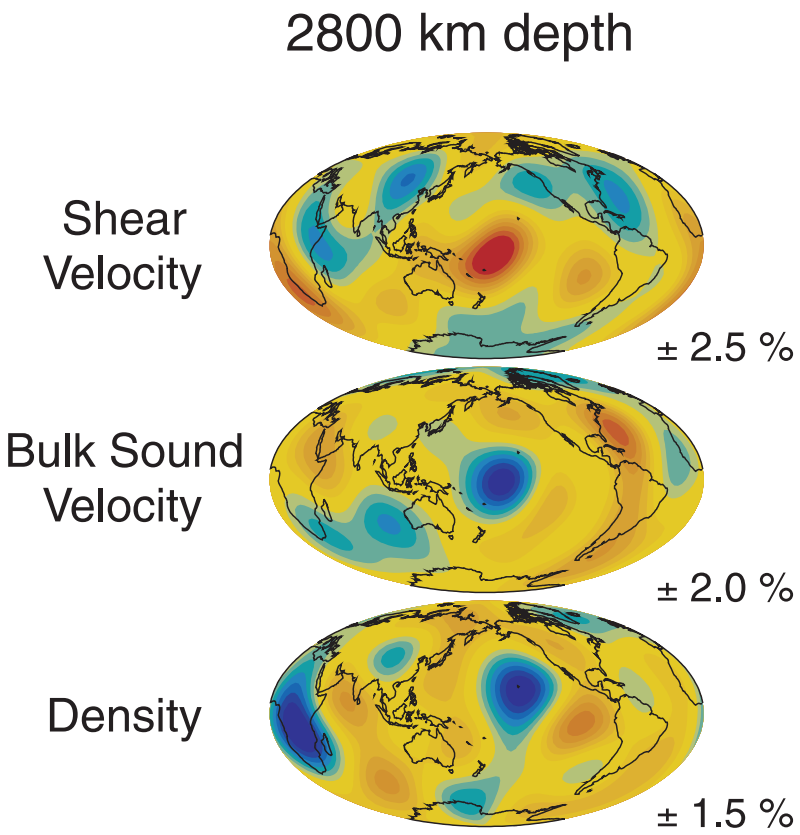

Shear velocity, bulk sound velocity and density models at 2800km depth. Map views of lateral variations in shear velocity, bulk sound velocity and density near the core-mantle boundary relative to PREM. Blue colors indicate regions of higher than average velocities or density and red colors indicate regions of slower than average velocities or lower than average density. For each depth, the saturation value is indicated beside each of the maps. Coast lines have been superimposed for reference. The maximum harmonic degree of these models is 6.

For further reading:

Degree 24 3D Shear Velocity Model of the Mantle Obtained Using NACT Waveform Inversion

Charles Megnin and Barbara Romanowicz, University of California, Berkeley

Most global tomographic models to date are derived using a combination of surface wave (or normal mode) data and body wave travel time data. The former provide resolution in the upper mantle, and the latter, in the lower mantle. However, the travel time approach restricts the number of phases available for inversion by requiring them to be isolated on the seismogram. This may ultimately result in limiting the resolution of 3-D structure, at least in some depth ranges in the mantle. In previous work, we successfully derived a degree 12 whole mantle SH velocity tomographic model (SAW12D; Li and Romanowicz, 1996), expanded laterally in spherical harmonics up to degree 12 and radially in Legendre polynomials, using exclusively waveform data. In this inversion, a normal mode formalism suitable for body waveforms, the nonlinear asymptotic coupling theory (NACT; Li and Romanowicz, 1995), was combined with a body-wave windowing scheme, which assigns individual weights to different body-wave energy packets, and thus can enhance lower energy signals such as that of S diffracted waves. This can be contrasted with a more standard technique in which a single time window is considered from the first body wave arrival to the fundamental mode surface waves. Under NACT, the broadband body wave kernels correctly reproduce the sensitivity to structure along and around the theoretical ray-path, in contrast to the standard "path-average" (PAVA) approximation, suitable for surface waves, in which the effect of 3-D structure is averaged horizontally between the source and the receiver. We have shown that the NACT approach is particularly important at mid-mantle depths (sampled by phases such as S and SS), whereas the windowing scheme improves resolution near-the core mantle boundary (Megnin and Romanowicz, 1999).

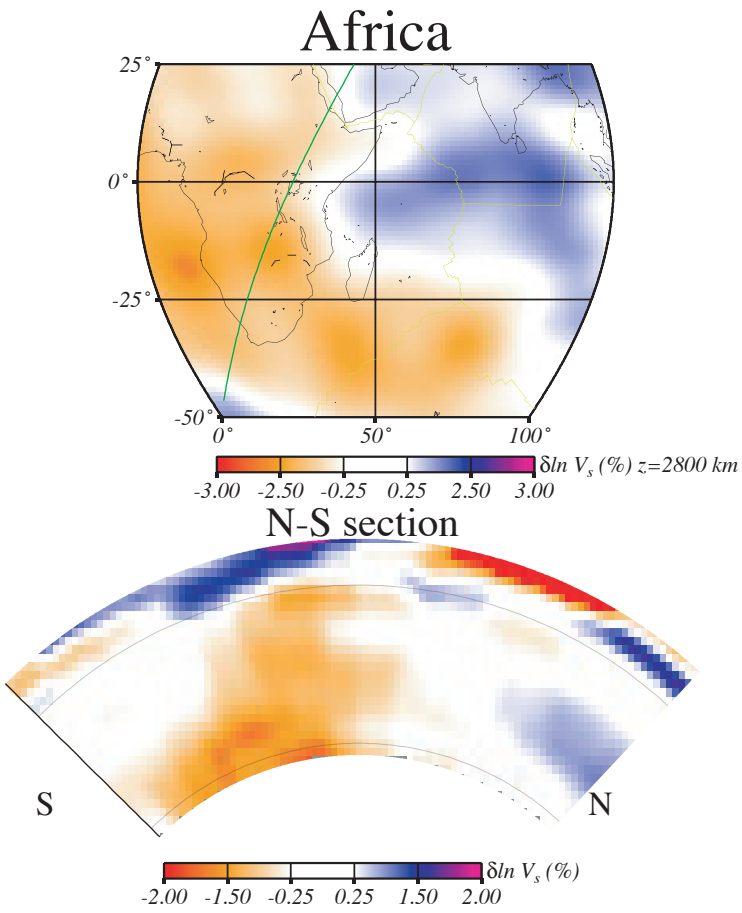

Top: horizontal cross-section of SH velocity model SAW24B16 at a depth of 2800 km beneath Africa. Bottom: vertical North-South cross-section along the green line shown in the top figure (from Megnin and Romanowicz, 2000)

We now have applied the NACT approach to a larger dataset of SH waveforms, and have derived a higher resolution model, SAW24B16 (Megnin and Romanowicz, 2000), expanded laterally up to degree 24 and radially in cubic b-splines. The adoption of local basis functions in the radial parametrization allows to accommodate the varying ray sampling of mantle structure with depth, which is precluded by the use of global basis functions. The present model was derived from the inversion of 31,000 body waves, 9300 fundamental and 1400 overtone surface waves. The data were extracted from the IRIS DMC and the Geoscope data center, and correspond to events of magnitude larger than 5.5 for the period 1977-1994. To illustrate our model, we give an example of vertical cross-section across the African "plume" (figure), distinctly showing a strong and wide low velocity anomaly at the base of the mantle, narrowing as it rises high into the lower mantle, and shifting to the northeast with increasing radius. This anomaly appears to continue into the upper mantle and is deflected horizontally as it encounters the cold African continental root.

For further reading:

Li, X.D. and Romanowicz, B., Comparison of global waveform inversions with and without considering cross-branch modal coupling, *Geophys. J. Int.*, **121**, 695-709, 1995.

Li, X.D. and Romanowicz, B., Global mantle shear-velocity model developed using nonlinear asymptotic coupling theory, *Geophys. J. R. Astr. Soc.*, **101**, 22,245-22,272, 1996.

Megnin, C. and Romanowicz, B., The effects of the theoretical formalism and data selection on mantle models derived from waveform tomography, *Geophys. J. Int.*, **138**, 366-380, 1999.

Megnin, C. and Romanowicz, B., The 3D velocity structure of the mantle from the inversion of body, surface, and higher mode waveforms, *Geophys. J. Int.*, in revision, 2000.

An Analysis of Large Scale Variations in Small-Scale Mantle Heterogeneity: Using IRIS GSN Recordings of Precursors to PKP

Michael A.H. Hedlin and Peter M. Shearer, University of California, San Diego

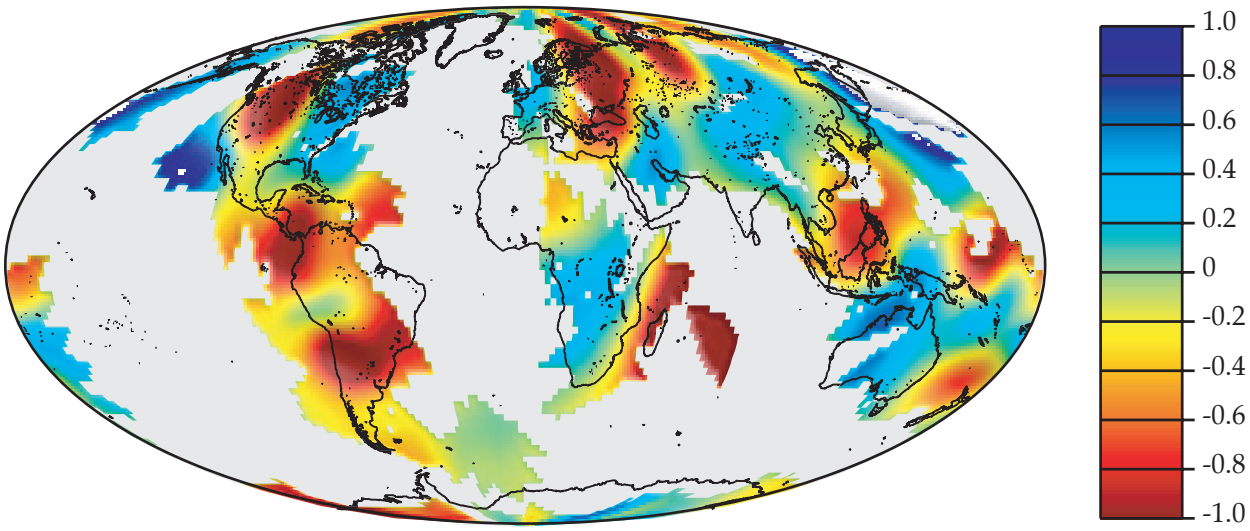

A conjugate gradient inversion of the GSN precursor dataset. The color scale shows the logarithm (base 10) of the rms amplitude of small-scale velocity heterogeneity in the model relative to the global average. Blue indicates stronger heterogeneity and scattering, red indicates weaker heterogeneity and scattering.

High-frequency precursors to the core phase PKP are caused by scattering off heterogeneities in the lowermost mantle and D" regions and provide a unique window into the small-scale structure of the deep Earth. We study lower mantle scattering by analyzing 412 high-quality PKP precursor records at ranges between 120° and 137.5° as obtained from the IRIS GSN during the last ten years. To examine regional variations in scattering strength, we compare individual records with the globally averaged PKP precursor stack of Hedlin et al. (1997). We identify strong differences in apparent scattering strength among specific source-receiver paths. Inversion of these data for scattering source regions is complicated by ambiguity between source- and receiver-side scattering and the sparse and uneven data coverage. Synthetic tests, however, suggest that inversions with applied smoothness constraints can resolve large-scale differences in scattering strength over significant parts of the lower mantle. We use a conjugate gradient method based on an approximation to Rayleigh- Born scattering theory to image differences in the average strength of scattering within the lowermost 1000 km of the mantle. Our results, shown in the figure above, indicate particularly strong scattering beneath central Africa, parts of North America, and just north of India, whereas weaker scattering in seen beneath South and Central America, eastern Europe and Indonesia. Some regions of strong scattering correlate roughly with large-scale anomalies revealed by seismic tomography including the African plume and the Tethys trench. These correlations are tentative rather than definitive because bootstrap resampling tests show that many details in our model are not reliably resolved and the network data alone do not permit complete resolution of the source-receiver ambiguity in all areas. Further progress in this area will require integration of available network recordings with data collected by regional networks and arrays, and consideration of the phase velocity of the precursors as well as their temporal variations.

For further reading:

Hedlin, M.A.H., Shearer, P.M., and Earle, P., Seismic Evidence for Small-Scale Heterogeneity Throughout the Earth's Mantle, *Nature*, **387**, 145-150, 1997.

A New S Velocity Model for the Western Pacific and Southeast Asia

Sergey Lebedev and Guust Nolet, Princeton University

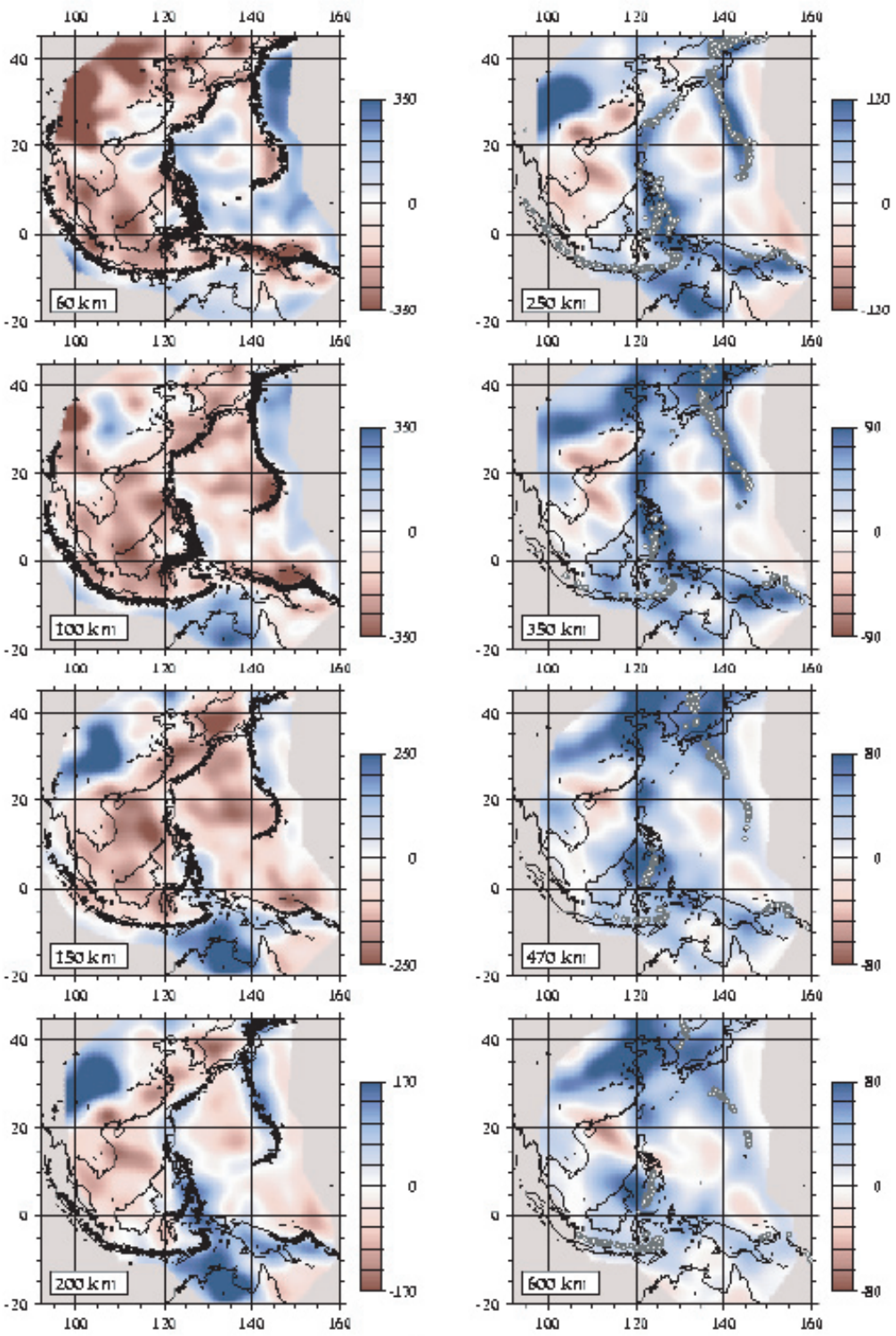

This figure shows the S velocity anomalies beneath the Western Pacific and South East Asia as derived from a waveform inversion of 4038 regional seismograms from the Global Seismographic Network. The high-velocity root beneath the western Yangtze Craton is the fastest anomaly in the whole region in the 120-300 km depth range. Sites of abundant Cenozoic intraplate volcanism are located in the northeastern corner of the East China Foldbelt, South China including the Hainan Island, and eastern Indochina. Prominent low-velocity anomalies underly these locations at 150 km and deeper. A significant slow anomaly is located beneaIth the Hainan Island region and seems to be continuous in the 100-660 km depth range. A major high-velocity anomaly occupies the transition zone beneath the eastern Sino-Korean Craton.

For further reading:

Lebedev, S., The Upper mantle beneath the Western Pacific and Southeast Asia, PhD thesis, Princeton University, 2000.

Seismic Structure of the Mantle Beneath the Western Pacific

Liangjun Chen, Li Zhao, and Thomas H. Jordan, Massachusetts Institute of Technology

To improve the tomographic resolution of upper-mantle structure beneath the western Pacific basin, we collected extensive sets of frequency-dependent travel times from circum-Pacific earthquakes recorded by broadband seismometers in this region. A variety of seismic phases were analyzed in the band 10-50 MHz, including direct and multiple S waves, Love and Rayleigh surface waves, and ScS reverberations. We primarily employed sources from the seismic zones from Tonga to Japan distributed at distances of 40-75 degrees around the Hawaiian Islands, and particular emphasis was placed on event sets spanning the full range of focal depths. In our initial experiments, we inverted the data from individual source arrays in the New Hebrides, Solomon, Mariana, Izu Bonin-Ryukyu, and Japan island arcs for two-dimensional vertical tomograms of mantle structure using the technique described by Katzman, Zhao, and Jordan (1998) in their initial study of the Tonga-Hawaii corridor. The 2-D tomograms for these corridors were generally consistent with previous tomographic results, although they show upper-mantle features that are smaller in scale and larger amplitude than published global models. Resolution tests confirmed the ability of the data sets to resolve upper-mantle shear-velocity structures along individual corridors with scale lengths less than 1000km horizontally and 200km vertically, although this resolving power diminishes rapidly below the 660 discontinuity. We then inverted the entire data set from all corridors for a 3-D model of the western-Pacific upper mantle. At low wavenumbers, this regional model is consistent with large-scale features found from global tomography. For example, the uppermost mantle (< 200 km depth) shows fast anomalies in the interior of the Pacific plate and slow anomalies in the marginal basins along the Pacific rim, while this pattern is reversed in the transition zone (400-700 km). However, our model displays greater lateral heterogeneity in both isotropic and anisotropic structure than the global models, especially in the 200-400 km depth range, which can be attributed to the better resolution of small-scale features by our data set. Fast and slow anomalies in isotropic shear speed, some extended subparallel to the Pacific plate motion, are observed in the upper mantle. In particular, the Hawaiian Swell is underlain by a fast anomaly in the uppermost mantle and a slow anomaly in the transition zone. Near Hawaii, the amount of radial anisotropy is smaller than its surrounding regions, which is inconsistent with a recent study of global anisotropy by Ekström and Dziewonski (1998). Our tomographic results for the southwestern Pacific indicate that the upper mantle in this region is chemically heterogeneous and dynamically active.

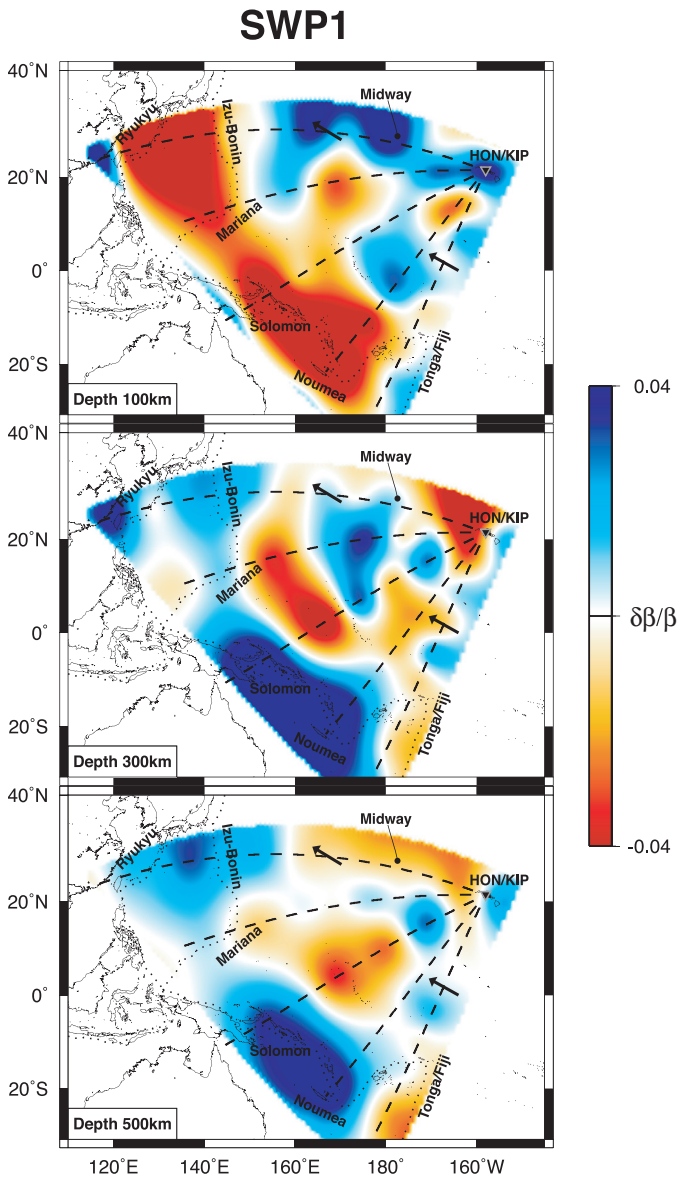

Horizontal sections through 3-D shear-speed model SWP1 displayed as velocity perturbations relative to the 1-D model PA5 for Pacific at 100km, 300km, and 500km depth.

For further reading:

Katzman, R., Zhao, L., and Jordan, T.H., High-resolution, 2D vertical tomography of the central Pacific mantle using ScS reverberations and frequency-dependent travel times, *J. Geophys. Res.*, **103**, 17,933-17,971, 1998.

Ekström, G. A., and Dziewonski, A.M., The unique anisotropy of the Pacific upper mantle, *Nature*, **394**, 168-172, 1998.

Survey of Precursors to P'P': Constraints on Mantle Discontinuities

Fei Xu, Paul S. Earle, and John Vidale, University of California, Los Angeles

Abrupt jumps in velocity and density near 410- and 660-km depths have been postulated to mark phase changes, however, because the reported details of these discontinuities vary in different studies, it has been difficult to say whether the phase-change explanation has difficulties.

We have systematically collected high-quality recordings of the seismic phase P'P' and its precursors. The phase P'P' reflects from the surface once 145° from the earthquake, then arrives at the station 290° away (70° the other way round). The data come from the GSN FARM database, regional networks in California and the LASA array in Montana.

First, we searched the FARM database for P'P' precursors. In order to collect precursors with the highest signal-to-noise ratio, we collected more than 1200 vertical-component, broadband records of events larger than Mw 6.3 recorded in the distance range 67° to 73°. The broadband traces were filtered to retain mainly 1-s-period motions and the records with low signal-to-noise ratios or protracted P'P' coda were discarded. This reduced the dataset to 91 seismograms.

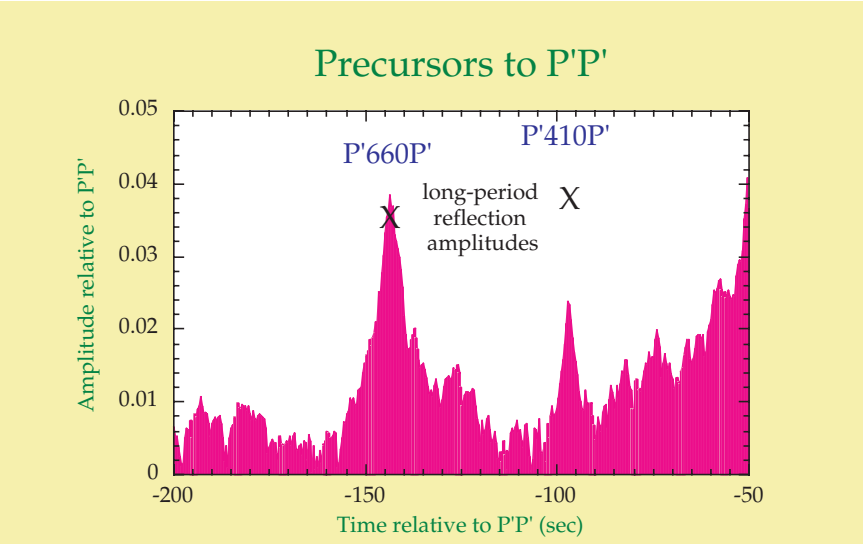

A stack of the envelopes of network recordings, corrected for noise and attenuation (Der et al., 1982). We selected the 20 events with the lowest noise before P'P' from our selection of LASA and the Northern and Southern California Seismic Network data. 15 are earthquakes, 5 are nuclear tests. We remove background noise with the assumption that it is 6% of the peak of P'P'. The noise is expected to contribute in an r.m.s. sense. The signal plotted is the square root of the difference of the squares of the total amplitude and noise. The expected times of P'660P' and P'410P' are shown. The crosses show the predicted reflection coefficients from the model of Shearer and Flanagan (1999).

An increase in the envelope is visible at the expected time for P'660P'. The amplitude of the P'660P' arrival, 4% of P'P' after correction for attenuation, matched that observed at long period. The distribution of bounce points for the 91 P'P' arrivals is mostly beneath the middle Americas and Asia, but spans several styles of surface tectonics. We expect this sampling of the upper mantle discontinuities to be relatively unbiased.

Next, we examine network data, which has greater sensitivity due to a larger numbers of stations. As we did with the GSN data, we filter, select good traces, and stack. P'P' has two more transits through the shallow mantle than its precursors, which will cause more attenuation than experienced by the precursors.

The stack of the network records is shown in the figure. It is clear that "660" is generally more reflective than the "410" for 1-s period P waves. Further, the amplitude of the precursors from the "660" are consistent with most of the velocity contrast occurring with just a few km, and the "410" being more diffuse.

These new data are consistent with the details predicted for the "410" by Stixrude (1997), rendering additional complications such as compositional variation, nonequilibrium transformation, or the influence of water unnecessary across the region that we sampled.

For further reading:

Der, Z.A., McElfresh, T.W., O'Donnell, A., An investigation of regional variations and frequency dependence of anelastic attenuation in the mantle under the United States in the 0.5-4 Hz band, *Geophys. J. Roy. astr. Soc.*, **69**, 67-99, 1982.

Shearer, P.M., and Flanagan, M.P., Seismic velocity and density jumps across the 410- and 660-km discontinuities in Earth's upper mantle, *Science*, **285**, 1545-1548, 1999.

Stixrude, L., Structure and sharpness of phase transitions and mantle discontinuities, *J. Geophys. Res.*, **102**, 14835-14852, 1997.

Topography on the 410-km Discontinuity Near Slabs

Megan P. Flanagan, Lawrence Livermore National Laboratory
Peter M. Shearer, University of California, San Diego

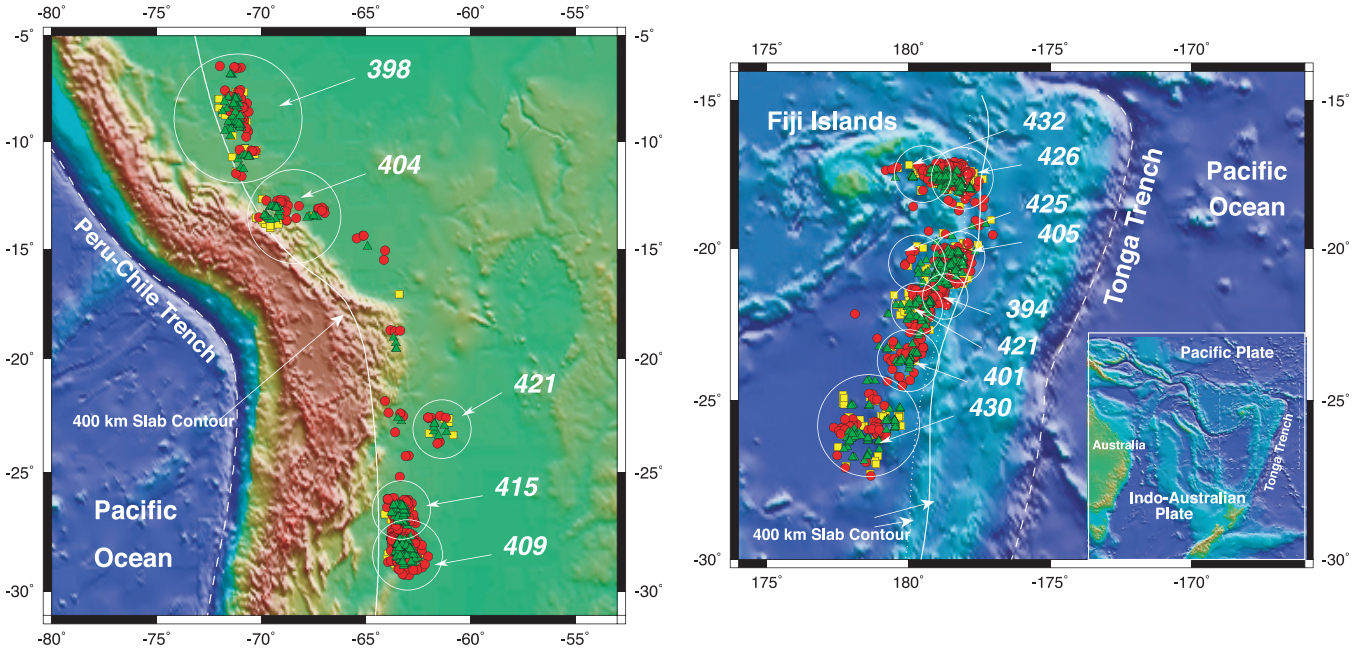

Mercator projection of the South America and Tonga subduction zones together with the bounce point locations of s410S (red circles), s410P (green triangles), and p410P (yellow squares) as they sample 400 km depth. Contours of the subducted lithosphere are shown at the surface trench (long-dashed line) and at 400 km depth (solid line) as taken from Gudmundsson and Sambridge (1998), and from an earlier study of Billington (1980) in Tonga (short-dashed line). Clusters of bounce points for which we obtain estimates of the 410 discontinuity are circled with labels corresponding to the 410 depths we measure from the waveform stacks. The circles show only the approximate locations of the different clusters; there is no sharing of data between subgroups in the actual data stacks.

Topography on the 410-km discontinuity in several subduction zones is measured from examining sS, sP, and pP precursors as observed from stacking long-period records from deep earthquakes. Rather than focusing on a single subduction zone or phase geometry, we adopt a comprehensive approach which incorporates all data currently available from the global digital archives maintained at the IRIS DMC in order to identify consistent features in the data and map lateral variations in the 410 wherever possible. We stack the teleseismic depth phases sS, sP, and pP produced by deep focus earthquakes to image precursory arrivals that result from near-source, underside reflections off the 410-km discontinuity and use differential time measurements between these phases and their precursors to compute discontinuity depths near seven subduction zones around the Pacific Ocean margin. We find approximately 30 km peak-to-peak topography on the 410 near some slabs which is consistent with the expected thermodynamic response of the olivine phase changes at 410-km depth to the colder temperatures of subducted lithosphere. Near most slabs the results indicate little change in the average depth to the 410-km discontinuity in the local areas sampled by the precursor bounce points compared to broad regional depths inferred from SS precursor results (Flanagan and Shearer, 1998). This implies that any large variations in depth to the 410-km discontinuity near subduction zones are limited to a narrow zone within the slab itself where they may be difficult to resolve with long-period data. Coverage for the Tonga and Peru-Chile subduction zones is sufficiently dense that we can observe lateral variations in 410 depths. The discontinuity depth appears to vary from the northern to the southern part of the slab beneath South America with the 410 being uplifted by about 10 to 18 km in the northern region. In Tonga the results suggest depth variations perpendicular to the slab of up to 33 km, after correcting for probable lateral heterogeneity in velocity above 400 km depth, and variations parallel to the slab orientation as large as 13 km. The cross-slab variation is consistent with the elevation of olivine phase transformations in cold regions; the variation along strike suggests a more complex thermal heterogeneity that may be related to the subduction history of the Tonga-Fiji region.

For further reading:

Flanagan, M. P. and Shearer, P.M., Topography on the 410-km seismic velocity discontinuity near subduction zones from stacking of sS, sP, and pP precursors, *J. Geophys. Res.*, **103**, 21,165-21,182, 1998.

Flanagan, M.P. and Shearer, P.M., Global mapping of topography on transition zone velocity discontinuities by stacking SS precursors, *J. Geophys. Res.*, **103**, 2673-2692, 1998.

Precise Transition Zone Constraints from Triplicated Multiple-S

Tim Melbourne, Central Washington University
Don Helmberger, California Institute of Technology

We analyze whole broadband seismograms containing triplicated S, SS, SSS and ScS which sample the sub-East Pacific Rise mantle to assess Transition Zone topography. We simultaneously model all body waves traversing depths from the lithosphere to the core-mantle boundary, thereby eliminating depth-velocity ambiguities. Data consist of western North American broadband recordings of EPR-affiliate transform events that form a continuous record section from 26° to 82° and sample nearly the entire East Pacific Rise. We find no discernible variation in apparent depths of the 405 and 660 Km discontinuities over ridge-orthogonal distances on the order of 1000 Km (or 20 MA crust). High frequency waveform comparisons indicate we can resolve discontinuity depths to 5 Km, providing an upper limit to Transition Zone topography. These depth estimates exclude the possibility of short-wavelength Transition Zone topography which could escape previous SS precursor analyses, and show that nowhere along the sub-EPR Transition Zone is markedly different from the global average. The striking homogeneity of the sub-EPR upper mantle requires that spreading ridge can not be actively supplied from the local lower mantle, and that tomographically imaged lateral variation beneath the ridge likely reflects lateral smearing of outlying velocity gradients. Dynamically, the Transition Zone therefore appears vertically decoupled from overlying East Pacific Rise.

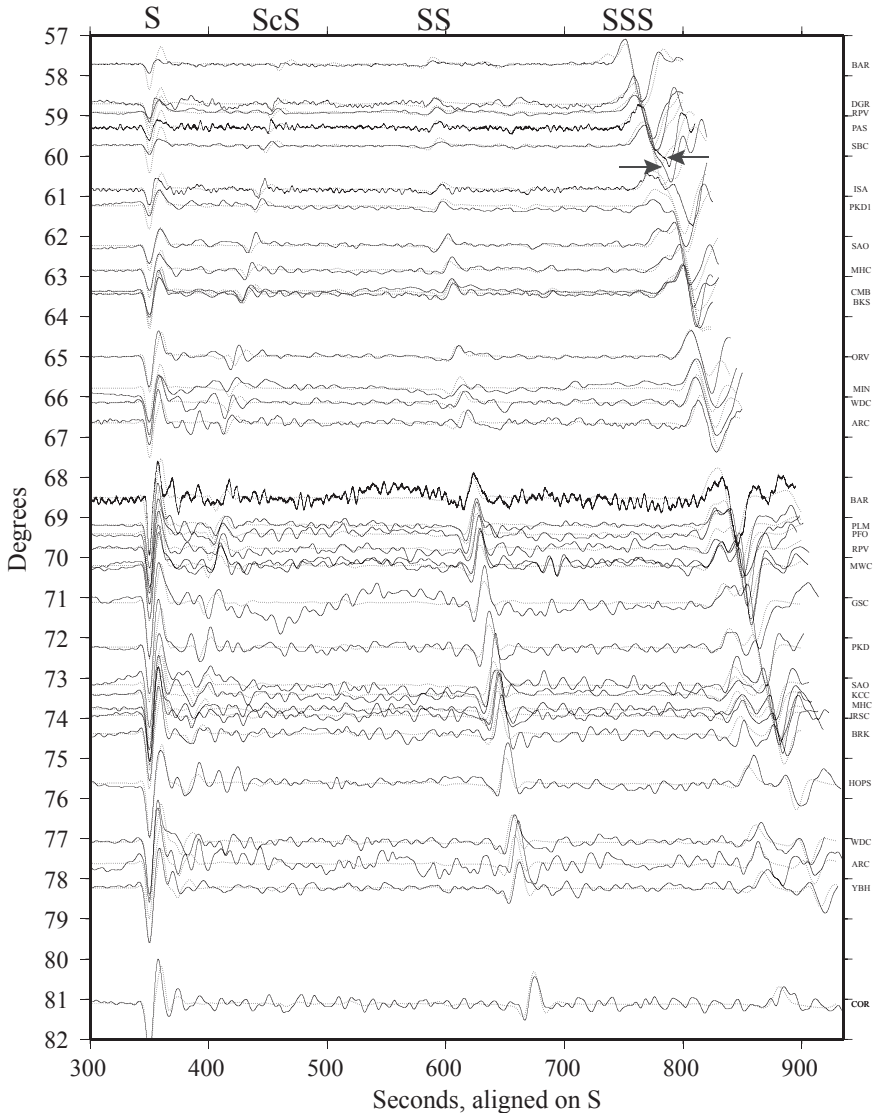

Modeled S, SS, SSS, and triplicated ScS. Regional Transition Zone thickness variation would be manifested as systematic misfit in sub-phases of the SSS triplication, which is not observed. These data are fit with three different lithospheric Lid thicknesses (V_s 4.55 Km/S). At 57° to 61° (sampling oceanic plate with age ~12 Ma), the synthetics are computed with a Lid of 73 Km, which grows to 76 Km for data between 62° and 66° (~13Ma). At ranges of 68° to 78°, the modeled Lid thickness is 58 Km thick, reflecting the first surface bounce near the East Pacific Rise ridge crest. The largest mis-fit in the record section is the ScS phase on stations ARC, WDC, MIN, and ORV, may reflect heterogeneity in D".

Imaging Upper Mantle Discontinuities Using GSN Data

Peter M. Shearer, University of California, San Diego
Megan P. Flanagan, Lawrence Livermore National Laboratory

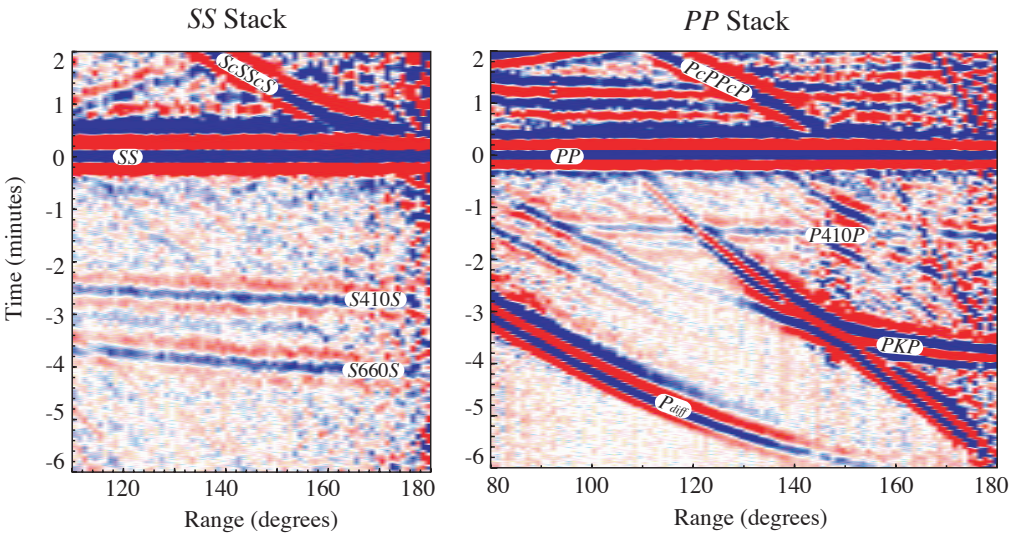

The upper mantle seismic discontinuities provide important constraints on models of mantle composition and dynamics. New observations of reflected and converted phases from the discontinuities have made possible more detailed measurements of discontinuity structure than are provided by traditional analyses of refracted waveforms. This figure shows stacks of long-period data from the global seismic networks obtained from the IRIS DMC, including over 13,000 transverse component and 25,000 vertical component records between 1976 and 1997. To enhance the visibility of the discontinuity reflections, we align the seismograms on the maximum amplitudes of SS and PP and stack the data in bins of constant source-receiver range. The underside discontinuity reflected phases S410S and S660S are visible in the transverse component stack, arriving 2 to 4 minutes before the direct SS phase, while the underside P reflection off the 410-km discontinuity, P410P, is seen in the vertical component stack. By analyzing the timing differences between these discontinuity reflections and the main phases, it is possible to map large-scale variations in discontinuity topography (e.g., Flanagan and Shearer, 1998, 1999). These maps indicate the following: (1) The amplitude of the large-scale 660 topography is significantly greater than the 410 topography, (2) The topographies of the 410 and 660 discontinuities are largely uncorrelated, (3) The power in the observed topography at long wavelengths is dominated by low spherical harmonic degree, and (4) Depressions in the 660 km discontinuity are correlated with subduction zones, consistent with the response of the 660 phase change to cooler temperatures. A depression in the 660-km discontinuity near the subduction zones in the northwest Pacific is particularly well-resolved due to the dense data coverage in this region.

The amplitudes of the 410 and 660 underside reflections are also examined to measure the velocity and density jumps across these discontinuities. This is done by modeling the observed range dependence of the S410S, S660S, P410P, and P660P phases. The PREM is within our computed 95% confidence ellipse for the 410-km discontinuity but well outside the allowed jumps across the 660-km discontinuity. Current pyrolite mantle models appear consistent with our constraints for the 410-km discontinuity but overpredict amplitudes for the 660-km reflections. The density jump across the 660-km discontinuity is between 4% and 6%, substantially below the PREM value of 9.3% commonly used in mantle convection calculations.

The potential of upper-mantle discontinuity phases to resolve mantle structure has only begun to be tapped. Migration methods (e.g., Shearer et al., 1999) can be used to improve the resolution of the images and reduce diffraction artifacts. The amplitudes of the discontinuity phases provide direct constraints on the velocity and density jumps across the interfaces. Because individual discontinuity phases are very weak, large numbers of seismograms must be analyzed to obtain reliable results. The IRIS program has been a key factor in the success of these efforts, facilitating ready access to high-quality global datasets.

For further reading:

Flanagan, M.P. and Shearer, P.M., Global mapping of topography on transition zone velocity discontinuities by stacking SS precursors, *J. Geophys. Res.*, **103**, 2673-2692, 1998.

Flanagan, M.P. and Shearer, P.M., A map of topography on the 410-km discontinuity from PP precursors, *Geophys. Res. Lett.*, **26**, 549-552, 1999.

Shearer, P.M., Flanagan M.P. and Hedlin, M.A.H., Experiments in migration processing of SS precursor data to image upper mantle discontinuity structure, *J. Geophys. Res.*, **104**, 7229-7242, 1999.

Shearer, P.M. and Flanagan, M.P., Seismic velocity and density jumps across the 410-and 660-kilometer discontinuities, *Science*, 1545-1548, 1999.

Looking at ULVZs With Data Available Through the IRIS DMC

John Castle, Massachusetts Institute of Technology

The details of the state of the bottom of Earth's mantle are difficult to characterize. However, these "details" may have large effects on Earth processes such as hotspot genesis, heat transport across the core-mantle boundary (CMB), and magnetic field reversals.

Excitingly, distorted waveforms suggest that 5-40 km thick zones of distinct material with ultra-low V_p wavespeeds (ULVZs) exist just above the CMB (e.g., Garnero, 2000). Evidence for these zones is found most frequently within broader slow regions at the base of the mantle but also found within some broad fast regions, such as at the base of the mantle beneath the Gulf of Alaska. Additionally, evidence for ULVZs has come from V_p observations but not V_s observations.

Because of the archive and data request facilities available at the IRIS DMC, I was able to investigate ULVZs beneath the Gulf of Alaska and Central America regions (Castle and van der Hilst, 2000). The datasets available from IRIS included seismic waveforms from high-density seismic networks. By comparing waveform shapes and amplitudes, these seismograms showed that the waveforms of phases reflected at the CMB (PcP, ScP) beneath Central America can be well-modeled using the PREM model. Similar waveforms from the Gulf of Alaska cannot be modeled by the PREM or AK135 model. Furthermore, including an ULVZ with a V_s decrease makes the waveform fit worse. The best way to model the waveforms in this region is with very low shear wave attenuation ($Q_s > 600$ @ 1Hz) and high, not low, V_s wavespeeds. Either this area is an ULVZ for V_p and a high-velocity zone for V_s or the previous observation of an ULVZ in this region is in error.

Should the latter be true, it would reinforce a one-to-one correlation between broad slow regions at the base of the mantle and the presence of ULVZs. If ULVZs are found only in slow regions, regions that are likely to be warmer than the surrounding ambient mantle, and not found in cold regions, it becomes more plausible that ULVZs are accomplices in plume genesis.

As further data from dense seismic networks become easily available, such as through the IRIS DMC, we will be able to better describe the base of the mantle and understand its many influences.

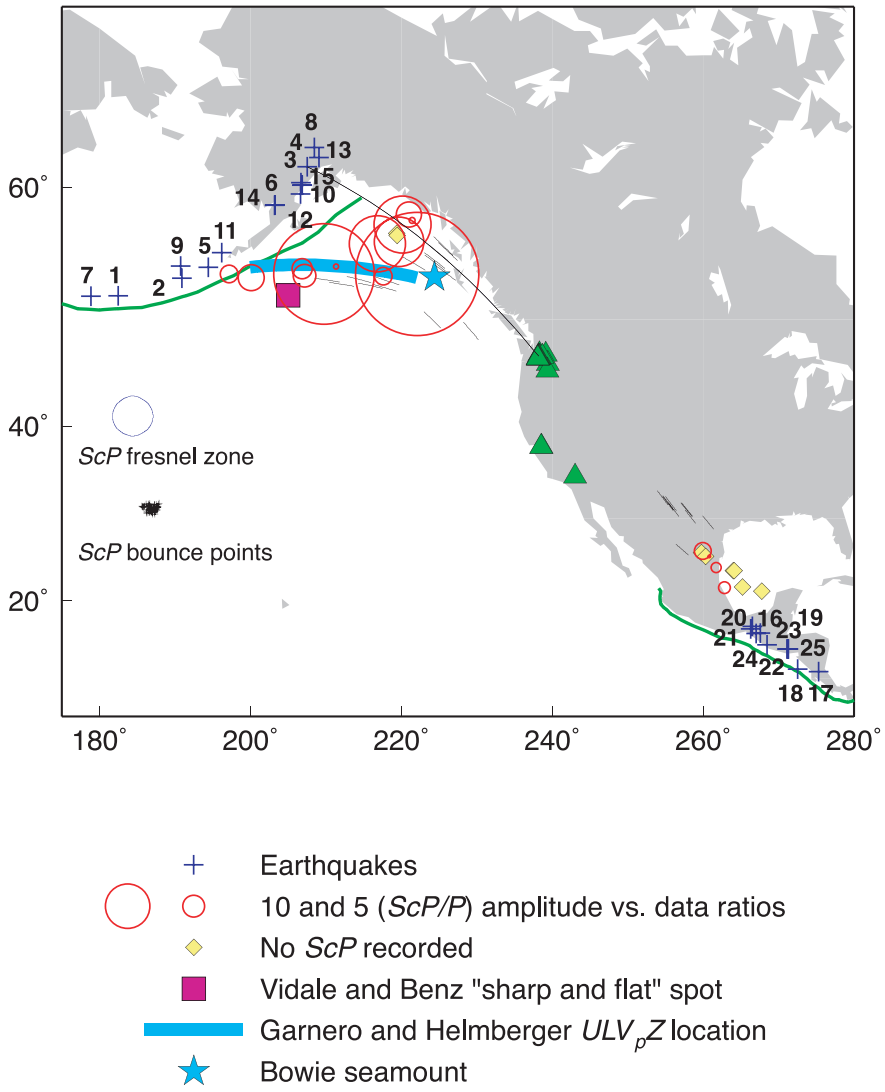

Map of earthquake locations (crosses), mean stations location (triangles), and ScP reflection points (yellow diamonds and red circles). Yellow diamonds indicate that the ScP time window was not saved while red circles show recorded ScP phases. Circle sizes are proportional to the observed ScP versus P amplitude ratio relative to the PREM synthetic ratio.

For further reading:

Garnero, E.J., Revenaugh, J., Williams, Q., Lay, T., and Kellogg, L.H., Ultralow velocity zone at the core-mantle boundary, in: The Core-Mantle Boundary Region Geodynam. Ser., **28**, AGU, 319-334, 1998.

Castle, J. and van der Hilst, R.D., The core-mantle boundary under the Gulf of Alaska: no ULVZ for shear waves, *Earth Planet. Sci. Lett.*, **176**, 311-321, 2000.

3-D Variations in Shear Wave Anisotropy Within the Lowermost Mantle Beneath the Pacific

Matthew J. Fouch, Carnegie Institution of Washington
Karen M. Fischer, Brown University
Michael E. Wysession, Washington University

In this study we investigated seismic structure near the core-mantle boundary (CMB) beneath two regions of the Pacific Ocean. In particular, we evaluated variations in the strength and orientation of anisotropy within D", the region just above the CMB. Data for this study came from several PASSCAL seismometer arrays, including MOMA, NOMAD, TWIST, and Abitibi, as well as a number of IRIS/GSN, CNSN, and USNSN permanent broadband seismometers.

To examine patterns of shear wave splitting in diffracted phases that traverse the CMB, we developed a new master station method that provides more precise estimates of splitting than previous studies. Using this method, we obtained nearly 250 new measurements of shear wave splitting which clearly indicate early arrivals of SH relative to SV in nearly all cases (denoted as positive splitting values). To estimate the magnitude of anisotropy, we assumed an appropriate regional velocity model for each area— SYLO for the northern Pacific (Young and Lay, 1990) and M1 for the central Pacific (Ritsema et al., 1997)— and that the anisotropy is uniformly distributed along the entire raypath that samples D". This analysis indicates that the strength of anisotropy is moderately weak (range of -0.25% to 0.90%; average value of 0.3%) for regions beneath the northern Pacific, but is stronger (range of 0.1% to 5.3%; average value of 1.3%) for regions beneath the central Pacific (Figure). Because ray coverage is dense, we divided the data into depth bins based on ray bottoming depth and applied a 5 degree Gaussian cap-average to each data bin. Using this approach, we detected areas of very strong anisotropy in the uppermost portion of D" (Figure, box A).

Our results, combined with the results of Wysession et al. (1999), place firm constraints on the geometry of anisotropy in both of these regions. Beneath the northern Pacific, anisotropy may be due to lateral flow along the CMB induced by spreading of downwelling paleoslab material. Beneath the central Pacific, anisotropy may represent CMB reaction products or lenses of partial melt, and their distribution may be related to inflow of mantle material to the Hawaiian plume source.

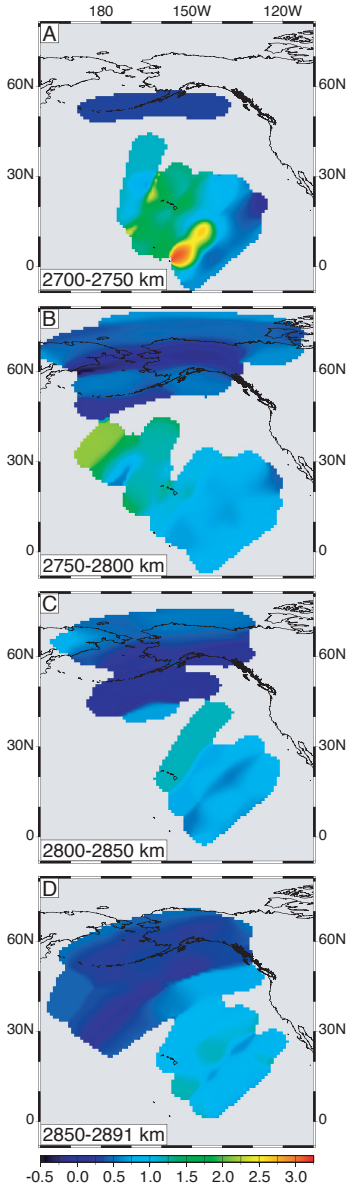

Cap-average values of lowermost mantle anisotropy for four depth slices beneath the Pacific Ocean. Colored zones correspond to regions sampled by source-receiver raypaths assuming both a local 1-D velocity model and that the observed splitting is evenly distributed along the portion of the raypath that traverses D". The northern Pacific region shows very small degrees of anisotropy at all depths. The largest anisotropy values are located in the uppermost portion of D" near the Hawaiian Island chain (A). A localized column of stronger anisotropy persists with depth to the CMB beneath Hawaii (B-D).

For further reading:

Ritsema, J., E. Garnero, and T. Lay, A strongly negative shear velocity gradient and lateral variability in the lowermost mantle beneath the Pacific, *J. Geophys. Res.*, **102**, 20,395-20,411, 1997.

Wysession, M. E., A. Langenhorst, M. J. Fouch, K. M. Fischer, G. I. Al-Eqabi, P. J. Shore, and T. J. Clarke, Mantle flow inferred from lateral variations in compressional/shear velocities at the base of the mantle, *Science*, **284**, 120-125, 1999.

Young, C.J., and T. Lay, Multiple phase analysis of the shear velocity structure in the D" region beneath Alaska, *J. Geophys. Res.*, **95**, 17, 385-17,402, 1990.

Using MOMA Broadband Array ScS-S Data to Image Smaller-Scale Structures at the Base of the Mantle

Michael E. Wysession, Ghassan I. Al-eqabi, and Patrick J. Shore, Washington University, St. Louis
Karen M. Fischer, Brown University

ScS-S travel time residuals obtained at stations of the PASSCAL Missouri-to-Massachusetts (MOMA) temporary broadband seismic array are used to delineate variations in seismic velocity structure above the core-mantle boundary (CMB) at scales smaller than observable with tomographic models. The best-covered region of our study is the junction of South America, Central America, and the Caribbean Sea, with 152 residuals from 10 earthquakes. The waves are travelling south-to-north to the MOMA array, which trends west-east. The cross-MOMA profiles are very coherent, both within a single profile and between adjacent profiles, suggesting that the signals are well above noise levels. The most obvious feature is a region of large positive residuals centered at (7N, 76W), suggestive of slow D'' shear velocities, surrounded by negative residuals. This is seen not only in the raw residuals , but also in the residuals that are path-corrected with tomographic models.

An interesting corroboration comes from the amplitude ratios of ScS and S. In the central part of our slow anomaly, the ScS wave amplitude actually exceeds that of S. This is partly due to a decrease in S amplitudes, but primarily due to an increase in ScS amplitudes. This is expected based on wave propagation behavior. The S wave is interacting with the fast anomaly of the mid-mantle subducting Farallon slab, so it is refracted away from the anomaly, and amplitudes decrease. The ScS wave is interacting with a slow anomaly at the base of the mantle, so waves are refracted toward the anomaly and amplitudes increase. The consistency of the amplitude anomalies for the profiles is striking.

This anomalously slow seismic features could have several possible interpretations. It is usually expected that a purely thermal origin of D'' heterogeneity would not give rise to small-scale variations, but if the subducted Farallon slab should drape itself across the core, then a small pocket of hot ambient lower mantle could become trapped beneath the falling cold slab rock. Alternatively, the anomaly could represent chemical heterogeneity, either through the presence of dense iron-rich mineral phases or of partial melt. The correlation between slow velocities and large ScS amplitudes favors a chemical origin, because a hot thermal anomaly would be isostatically compensated by an uplift of the CMB, and this doming would contribute to a decrease in ScS amplitudes. A seismically slow chemical anomaly would likely be iron-rich, which would depress the CMB, causing a focusing of ScS waves reflecting off of it, and the increase in amplitudes that are observed.

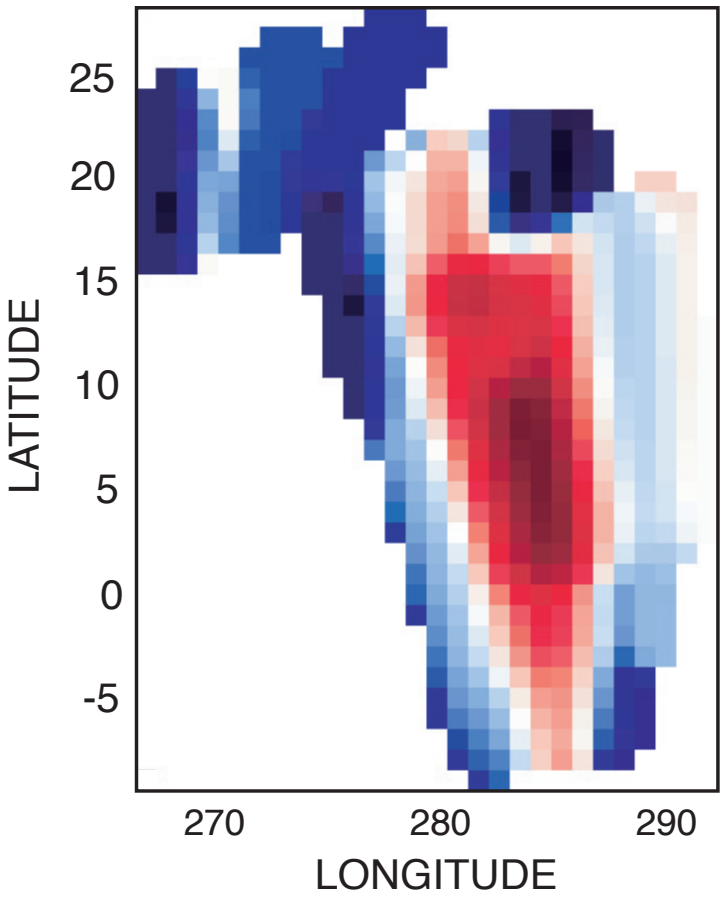

A slow velocity anomaly of at least -1.0% exists at (7N, 76W) in a region that was previously identified as having only anomalously fast velocities. The S and ScS times are mantle-path corrected using a recent tomographic model (S. Grand, personal communication). The ScS-S travel time residuals are then mapped onto their paths through D'', and these paths are then regionally smoothed to obtain the image. Though the slow anomaly appears 1000 km long (north-south), this is exaggerated by the south-north path smearing, and is therefore likely to be less. The east-west width of the D'' anomaly is 300 km, and while smearing is not a problem here, this value is at the same scale as the ScS Fresnel zone, so should be viewed as a maximum limit. Our cross-profile ScS-S residuals show steady variations of up to 4 s over distances of 550 km along the MOMA array (CMB distances of 150 km). The smoothed velocities show a variation of more than 3% (1.1% to -2.1%) over a distance of 440 km at the CMB, for a velocity gradient of 0.008 1/s. These are steep lateral gradients, and represent minimum values because of the smoothing technique and the fact that significant waveform annealing occurs in ScS waveforms after interaction with CMB anomalies.

For further reading:

Wysession, M. E., Fischer, K.M., Al-eqabi, G.I., Shore, P.J., Using MOMA Broadband Array ScS-S Data to Image Smaller-Scale Structures at the Base of the Mantle, *Geophys. Res. Lett.*, submitted, 1999.

Complex Structure at the Base of the Mantle as Revealed by S and SKS Waves

Ludovic Breger and Barbara Romanowicz, University of California, Berkeley

Comparison of trends of observed and predicted differential travel times of S-SKS phases as a function of epicentral distance along narrow azimuthal corridors under the Pacific Ocean indicates that existing global S velocity tomographic models are able to map the position and lateral extent of S velocity heterogeneity at the base of the mantle rather well, in regions where the sampling is adequate. However, these models underestimate the strength of the lateral variations significantly, in some locations by factors of at least 2 to 3 (Breger et al., 1998).

Starting with the global SH velocity model SAW12D (Li and Romanowicz,1996), we have performed forward modeling of differential S-SKS and Sdiff-SKS travel times on several narrow azimuthal profiles from sources in the Fiji Islands to stations in north America. The dataset consists of digital records accumulated by the GSN over the last few years. The forward modeling procedure uses standard ray theory and consists in adjusting the amplitude of the velocity anomalies to best fit the data, keeping the boundaries of the zones of high and low velocity practically fixed. A family of best fitting models indicates that the base of the large zone of low velocity in D" in the "Central Pacific Plume" reaches a strength of at least -4% with respect to the reference 1D model PREM, is broad at its base near the core-mantle boundary, and narrows as it rises at least 1000 km above the core-mantle boundary. On its eastern border, a rapid transition (over less than 500 km) separates it from a narrow zone of very high velocities (+5% with respect to PREM). The base of the Central Pacific Plume also seems to be bordered by a zone of strong S wave anisotropy, as revealed by analysis of SVdiff data (e.g., Vinnik, et al., 1998). The strong velocity contrasts observed cannot be explained by thermal affects alone, and one needs to invoke either partial melting in the low velocity "plume" region, and/or possibly chemical heterogeneity, which would account for the exceptionally high velocities observed on the eastern border of the plume.

A similar strong low velocity zone rising into the lower mantle has recently been documented under Africa by Ritsema et al. (1999) and ultra-low velocity zones have been documented in the vicinity of both regions (e.g., Garnero et al., 1998). The borders of these two major structures at the base of the mantle appear to be the loci of sharp structure and anisotropy gradients that are closely related to the dynamics of the upwellings. Such localized gradients will strongly affect differential travel times of core sensitive phases such as PKP(AB)-PKP(DF) for paths which interact with the plumes, yielding large anomalies when one of the branches falls outside the plume and the other inside. These effects need to be taken into account when making inferences on the structure of the core, and particularly inner core anisotropy (Breger et al., 1999).

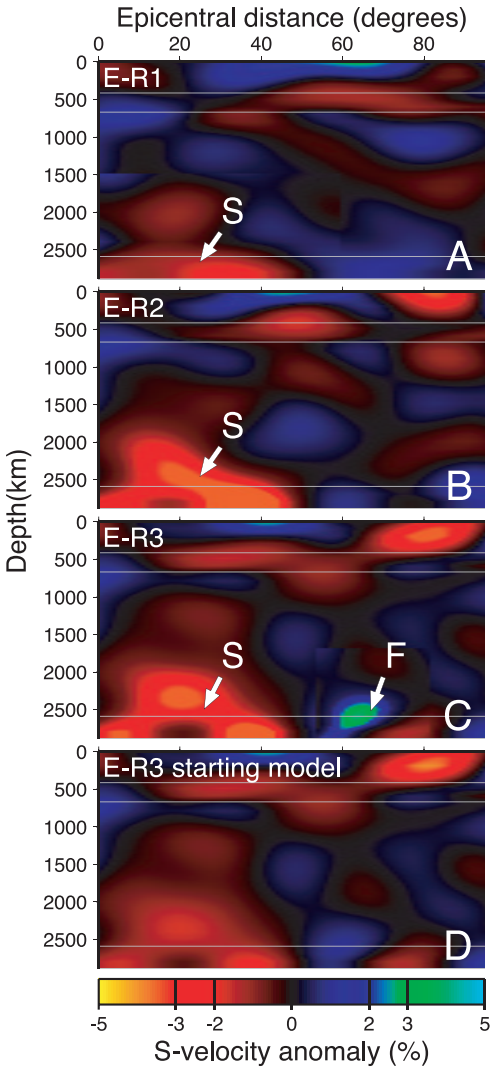

Examples of vertical cross-sections through the modified tomographic model of Breger and Romanowicz (1998). The cross-sections (A-C) show a velocity structure that depends strongly on the path chosen, which indicates a complex 3D structure. Note the presence of a large slow anomaly [S] where S-velocity are reduced by approximately 3.5 to 4%, and of a smaller region [F] where the heterogeneity reaches 4 to 5%. These two domains are required to fit the travel time residual data. The fast velocity region [F] does not need to extend much above D".

For further reading:

Breger, L. and Romanowicz, B., Thermal and chemical 3D heterogeneity in D", *Science*, **282**, 718-720, 1998.

Breger, L., Romanowicz, B. and Vinnik, L., Tests of tomographic models in D" using differential travel times, *Geophys. Res. Lett.*, **25**, 5-8, 1998.

Breger, L., Tkalcic, H., and Romanowicz, B., PKP travel times: Inner core anisotropy or complex structure in the deep mantle?, submitted to E.P.S.L., 1999.

Garnero, E.J., Revenaugh, J., Williams, Q., Lay, T., Kellogg, L.H., in: The Core-Mantle boundary, eds Gurnis, M., Buffett, B.A., Knittle, E. and M. E. Wysession, 319-334, American Geophysical Union, Washington, DC., 1998.

Ritsema, J., Ni, S., Helmberger, D.V., Crotwell, H.P., Evidence for strong shear velocity reductions and velocity gradients in the lower mantle beneath Africa, *Geophys. Res. Lett.*, **25**, 4245-4247, 1998.

Vinnik, L., Breger, L., and Romanowicz, R., Anisotropic structures at the base of the mantle, *Nature*, **393**, 564-567, 1998.

Modelling of D” Using High-Quality PKP(AB-DF) Datasets

Hrvoje Tkalcic, Barbara Romanowicz, and Ludovic Breger
University of California, Berkeley

The effects of complex structure in the deep mantle and D” on PKP differential travel times should be accurately estimated in order to reach reliable conclusions about the physical and chemical properties of Earth’s inner and outer core. In particular, it is important to assess how much of the data can be explained by mantle structure alone. To achieve a robust coverage of PKP paths in the lowermost mantle, we compiled several independent, hand-picked high quality PKP(AB)-PKP(DF) differential travel time datasets and inverted them, together with our own collection of measurements, to retrieve the P velocity anomalies in the lowermost part of the mantle. By using differential travel times, we assume that effects of near-source and receiver structure and source mislocation are minimized, and that the dataset is mostly sensitive to the D” and the core, where paths of the two phases differ the most.

The main strength of this study is in its usage of exclusively high-quality PKP(AB-DF) differential travel time data, obtained mostly via the IRIS DMC and measured by only several seismologists (Creager, 1999; McSweeney et al., 1997; Souriau, personal communication; Wysession, personal communication; Tkalcic et al., in prep.) through the cross-correlation from vertical components of broadband and short-period instruments worldwide. Our results demonstrate that, with only about 1500 PKP differential travel time data, we are able to retrieve a D” map of quality comparable to other maps derived using a much large number of ISC data. The influence of several P and S tomographic mantle models, stripped of D”, on PKP(AB-DF) residuals is tested in order to choose a model which achieves the best variance reduction in our dataset. This analysis shows that the mantle without the D” can account for about 10-15% in differential travel time PKP(AB-DF) data. An S velocity model (Megnin and Romanowicz, 2000), converted to P using a constant scaling factor, is our preferred model for correcting PKP(AB-DF) travel times due to significantly larger variance reduction in comparison with other models. The mantle corrections do not change significantly for slightly different scaling between S and P velocity perturbations. A constant scaling of 1.8 yields in a variance reduction of 13.2% and not much better results can be achieved for different combinations of scaling, even if we allow changes in the scaling with depth. Existing P velocity models derived from P travel time data give a significantly smaller variance reduction (about 3% and less). This is most likely due to the poorer global coverage achieved than for waveform derived S velocity models. P-wave velocity structure in the lowermost 300 km layer of the mantle is obtained by using two methods of parametrization: a regular equiangle block grid in which the size of blocks is set to 5 degrees, and a variable-size block grid which allows us to consider smaller-size of blocks in regions with good coverage, and at the same time increase the size of the blocks in poorly sampled regions. The “allowed” shapes are chosen in such a way that the final grid consists of shapes with a small aspect ratio. Our maps of P velocity anomalies in D” show prominent fast features in northeastern Asia, Arabian Sea, South Atlantic, Caribbean Sea and Alaska, as well as slow features in the southwest Pacific, North America and under southern Africa (Figure). We

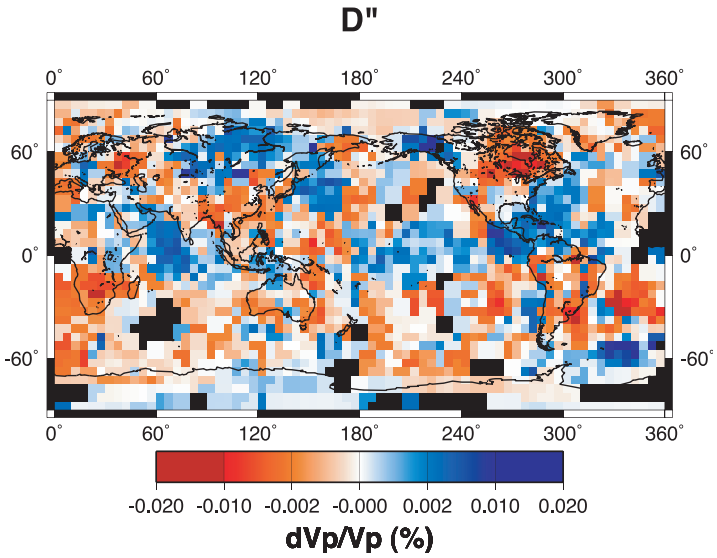

Map of P-wave velocity perturbations in the lowermost 300 km thick layer of the mantle, obtained from the PKP(AB-DF) dataset. The reference model is ak135 (Kennett et al., 1995). Unsampled regions are black.

compare models obtained with and without polar paths (paths with angles of less than 35 degrees with respect to Earth’s spin axis) and find that their inclusion or exclusion does not significantly affect the D” model. One way to increase the coverage (and improve the uncertainty imposed by coupling effects between source and receiver side of D” sampled by the same ray), is to consider phases like PcP (PcP-P differential times) which can also put a constrain on resolving small wavelength structure. Preliminary maps of PcP-P anomalies, plotted at the PcP bouncing points, correlate well with the PKP(AB-DF) maps of D” under Americas in places where coverage exists for both datasets. The level of P heterogeneity in D” is dependent on damping in the inversion procedure and it determines the percentage of PKP(AB-DF) data that can be explained by mantle-only structure. If the level of P heterogeneity in D” is assumed to be no larger than +/-2%, mantle structure alone can explain more than 80% of the variance in the data, including polar paths, although some unexplained large residuals remain,

For further reading:

Creager, K. C., Large scale variations in inner core anisotropy, *J. Geophys. Res.*, **104**, 23,127-23,139, 1999.

McSweeney, T. J., Creager, K.C., and Merrill, R.T., Depth extent of inner-core seismic anisotropy and implications for geomagnetism, *Phys. Earth Planet. Int.*, **101**, 131-156, 1997

Megnin, C. and Romanowicz, B., The 3D shear velocity structure of the mantle from the inversion of body, surface, and higher mode waveforms, *Geophys. J. Int.*, in press, 2000.

Tkalcic, H., Romanowicz, B., and Breger, L., in preparation

Using S_{diff} Amplitudes to Examine the Vertical Velocity Structure of the Base of the Mantle

Michael Wysession, Ghassan I. Al-eqabi, Patrick J. Shore, Washington University, St. Louis
Raul Valenzuela, Instituto de Geofisica, Mexico City
Karen M. Fischer, Brown University

We determine the vertical shear wave velocity structure of D'' under a region of the east-central Pacific Ocean using a Kermadec Islands earthquake data recorded by the PASSCAL Missouri-to-Massachusetts (MOMA) experiment. The data are show at right. We model the rate at which the diffracted S wave amplitudes decay as a function of frequency as the waves propagate across the MOMA array. This decay, expressed through an exponential decay constant, is shown at the upper right (the circles show the data values). We used reflectivity synthetic seismograms to forward-model a variety of possible D'' velocity structures including (1) near-zero gradients like that of PREM, (2) a gradual decrease of the velocity throughout D'' with increasing depth, (3) a gradual velocity increase, and (4) a discontinuous velocity increase at the top of D''. Models with a discontinuous increase in velocity were initially tested because of their prevalence in other studies, but were extensively explored because they did the best job of fitting the amplitude data. To find the best match between data and synthetics we varied the following parameters: (1) the amount and style of the velocity decrease throughout D'', (2) the thickness of D'', (3) the velocity increase at the discontinuity, (4) the velocity gradient above D'' and (5) anelastic attenuation. Some of the models are shown at the lower right, and the corresponding decay constant curves are shown at the upper right. Synthetic seismograms for the best-fitting model, RJK2705, are shown at the left.

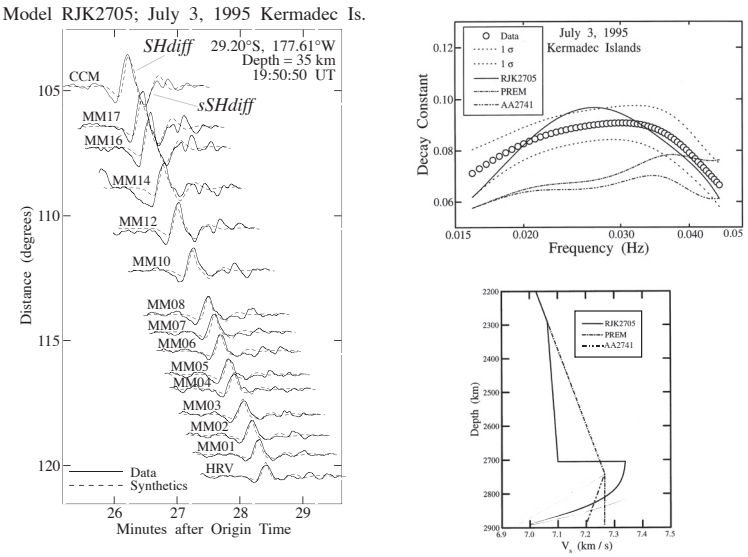

Use of the amplitude decay of core-diffracted Sdiff waves in determining the vertical velocity structure for a region of D''. Left: A profile of Sdiff waves, recorded on the PASSCAL Missouri-to-Massachusetts (MOMA) array. Also shown are synthetic seismograms from the velocity model RJK2705. Bottom right: three models shown for demonstration - PREM, a model with a negative gradient in D'' (AA2741), and a model with a discontinuity at the top of D'' (RJK2705). Top right: The decay of the Sdiff amplitudes for the data (circles) and three models, given in terms of an exponential decay constant. While the PREM and negative velocity gradient models under-predict the amplitude decay at most frequencies, the discontinuity model (RJK2705) does a reasonably good job in matching the data amplitude decay.

The basic idea behind the decay constant is that different velocity gradients will focus or defocus the seismic energy in different ways. A positive gradient will bend energy back toward the surface, generating a larger decay constant. A negative gradient will keep energy trapped near the CMB, cause large Sdiff amplitudes, and therefore smaller decay constants. So a simple D'' model with a negative velocity gradient will have low decay constant. The data decay constant curve shows the effect of both the negative gradient and the D'' discontinuity. The curve has low decay constants at high frequencies, where the waves travel closer to the CMB and strongly "feel" the negative velocity gradient. The middle part of the curve has larger decay constants due to intermediate wavelengths sampling the high velocities at the top of D''. At even lower frequencies, the decay constants are low again because waves sample the slower velocities found above the discontinuity. The resolution of this method is much better at the CMB and decreases upward, so the negative velocity gradients right at the CMB are well-constrained, but the form of the "discontinuity" is not and could be gradual rather than discontinuous.

The preferred model, RJK2705, shows a velocity increase at the top of D'' followed by a gradual decrease with increasing depth. Observation of the velocity increase atop D'' provides important independent corroboration of the results of many studies that are done with different data and techniques: triplicated PdP and SdS waves bottoming at the base of the mantle. We model the S-wave velocity increase under the east central Pacific (13N, 232E) to be ~3.4%, and 185 km above the core-mantle boundary. The amplitude decay data strongly suggest a negative gradient at the base of D''. While the D'' discontinuity likely has non-thermal contributions related to a chemical boundary layer or mineralogical phase change, the velocity decrease at the base of D'' is an expected feature of a thermal boundary layer. However, the deep extent of the negative velocity gradient found here may suggest viscosities that are higher than expected in order to support such a large thermal boundary layer.

For further reading:

Valenzuela, R.W., Wysession, M.E., Al-eqabi, G.I., Shore, P.J., Fischer, K.M., and Clarke, T.J., Using diffracted waves from the Missouri-to-Massachusetts IRIS PASSCAL array to examine the core-mantle boundary, Eos Trans. *AGU*, **77**, Fall Meeting suppl., F678, 1996.

Valenzuela, R.W., and Wysession, M.E., Illuminating the core-mantle boundary with diffracted waves, in The Core-Mantle Boundary Region, ed. by Michael Gurnis, Michael Wysession, Elise Knittle, and Bruce Buffett, *AGU*, Washington, D.C, 57-71, 1998.

Differential PKP(AB)-PKP(DF) Travel Times: the Effect of D”

Ludovic Breger, Hrvoje Tkalcic, and Barbara Romanowicz, University of California, Berkeley

We have examined the distribution of PKP(AB)-PKP(DF) differential travel time residuals for a global dataset assembled from measurements obtained by cross-correlation on broadband digital seismograms available from the IRIS DMC. These data show the well-documented trend of increasing anomaly as a function of the angle between the DF path in the inner core with respect to the rotation axis, which is generally interpreted as resulting from inner core anisotropy. There is a large scatter in the data, which we attempt to explain in terms of effects of lateral heterogeneity in D” on PKP(AB). Existing tomographic models of the mantle are too weak to explain either long wavelength trends or scatter in the differential PKP(AB)-PKP(DF) data. In a previous study of Sdiff-SKS travel times (Breger and Romanowicz, 1998), we had determined that amplifying the lateral variations of S velocity in D” while keeping the shapes of the anomalies constant was sufficient to significantly improve the fit to observed differential travel times of this type. We thus applied a similar approach here. We first considered equatorial paths for a subset of data corresponding to events in the Fiji Islands. We considered the tomographic S model of Grand (1997), converted to P velocity assuming dln(Vs)/dln(Vp)=2, and 1) saturated low velocities to -2% wherever they were originally larger than -0.8% and 2) added ULVZ in places where the have been documented (Garnero et al., 1998). This simple modification was indeed sufficient to explain the long wavelength trends of the Fiji data as well as the character of the local scatter. We then applied the same approach to our global dataset, and corrected the travel time residuals for the effects of the modified mantle model. By doing so, we found that the trend of the residuals as a function of angle with respect to Earth’s rotation axis practically disappeared (Figure, left). Only a few very large residuals remained at angles between 20 and 30 degrees, corresponding for the most parts to anomalous paths between the South Sandwich Islands and Alaska, which have been previously documented to be very anomalous (Creager, 1997). We note that the distribution of polar PKP paths is very non-uniform, and dominated by paths originating in the South Sandwich Islands regions. We believe that the effect of rapid lateral variations at the border of the African Plume (Figure, right), which is sampled by a large fraction of the available PKP polar paths, is considerable and competes with, or, to a large extent, mimicks the effect of inner core anisotropy. This and other D” effects need to be modelled accurately before inferring structure in the core using PKP data.

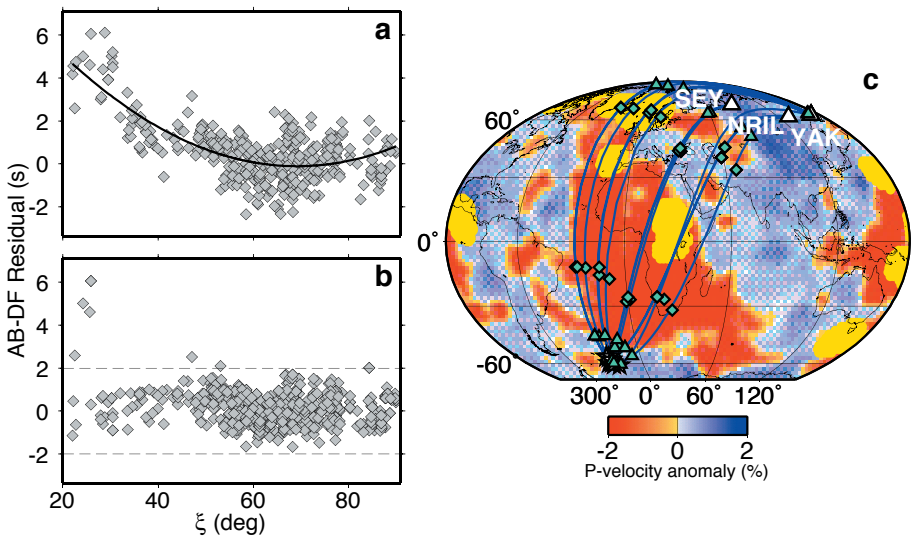

AB-DF differential travel time residuals as a function of the angle between PKP(DF) raypath in the inner core and the Earth’s rotation axis. The best fitting second degree polynomial (solid line) is shown to outline the observed trend. Such a trend is expected, at fixed distance, for models of constant cylindrical anisotropy in the inner core. (b) Same as (a) after correction for the model discussed in the text and shown in (c). Note that a few large residuals at low angle remain unexplained. These correspond to South Sandwich Islands paths to stations COL and BILL. The complexity of these particular paths has been noted previously (Creager, 1997). (c) Projections of the raypaths (blue lines) associated with stations SEY (Seymchan, Russia), NRIL (Norilsk, Russia), and YAK (Yakutsk, Russia) (white triangles), along with the corresponding events (white stars) in the South Sandwich Islands source region. Also indicated are the regions where ULVZs were detected (bright yellow regions), and the points were the AB and DF rays enter and exit the outer core (diamonds and triangles, respectively). The background P-velocity model is modified from Grand et al.’s (1997) (see text). (Adapted from Breger et al., 2000).

For further reading:

Breger, L., and Romanowicz, B., Three-Dimensional structure at the base of the mantle beneath the Central Pacific. *Science*, **382**, 718-720, 1998.

Breger, L., Tkalcic, H., and Romanowicz, B., The effect of D” on PKP(AB-DF) travel time residuals and possible implications for inner core structure, *Earth Planet. Sci. Lett.*, **175**, 133-143, 2000.

Creager, K.C., Inner core rotation rate from small-scale heterogeneity and time-varying travel times, *Science*, **278**, 1284-1288, 1997.

E.J. Garnero, Revenaugh, J., Williams, Q., Lay, T., and Kellogg, L.H., in The Core-Mantle boundary, M. Gurnis, B. A. Buffett, E. Knittle, M. E. Wysession, Eds (American Geophysical Union, Washington, DC, 1998), pp. 319-334.

Grand, S., van der Hilst, R. and Widiyantoro, S., Global seismic tomogra-

Lateral Variations in Compressional/Shear Velocities at the Base of the Mantle

Michael E. Wysession, Ghassan Al-eqabi, and Patrick J. Shore, Washington University
Amy Langenhorst, Northwestern University
Matthew J. Fouch, Karen M. Fischer, Brown University
Timothy J. Clarke, New Mexico Tech

Observations of core-diffracted P (P_{diff}) and SH (SHdiff) waves show that the ratio of compressional (P) seismic velocities to horizontal shear (SH) velocities at the base of the mantle changes abruptly from beneath the mid-Pacific (VP /VS = 1.88, also the value predicted by reference Earth models) to beneath Alaska (VP/VS = 1.83). We use data from the PASSCAL Missouri-to-Massachusetts (MOMA) array, which had 20 seismometers that spanned more than 1500 km. During the 15 months of the array, 58 profiles of P_{diff} (and/or the surface-reflected pP_{diff} and sP_{diff}) and 48 profiles of S_{diff} (and/or sS_{diff}) were obtained: 36 of the array profiles contain both. We used the slowness, or ray parameter, of the diffracted waves across the seismic array, to estimate the mean velocity at the base of the mantle, and we combined all the arrivals across the array from any one earthquake to obtain a single measurement. We find that the P and S velocities are anti-correlated beneath Alaska, with slower than average P velocities, and faster than average S velocities. This is likely to be related to the arrival at the CMB of formerly subducted lithosphere.

One possibility is chemical heterogeneity, which can affect the bulk and shear moduli differently such that VP and VS are anticorrelated. A decoupled D'' chemical boundary layer is likely to be thinnest beneath regions of downwelling, but thicker beneath upwellings. In this case, the VP/VS ratio of 1.83 beneath Alaska is representative of the anomalous paleoslab rock, and the VP/VS ratio of 1.88 beneath the Pacific is for the chemical boundary layer, which covers the majority of the CMB and is therefore obtained by global reference models. The northern part of our sample region, beneath Alaska, would appear to be "anomalous" in the sense that it is similar to the overlying mantle and therefore different from the D'' chemical boundary layer.

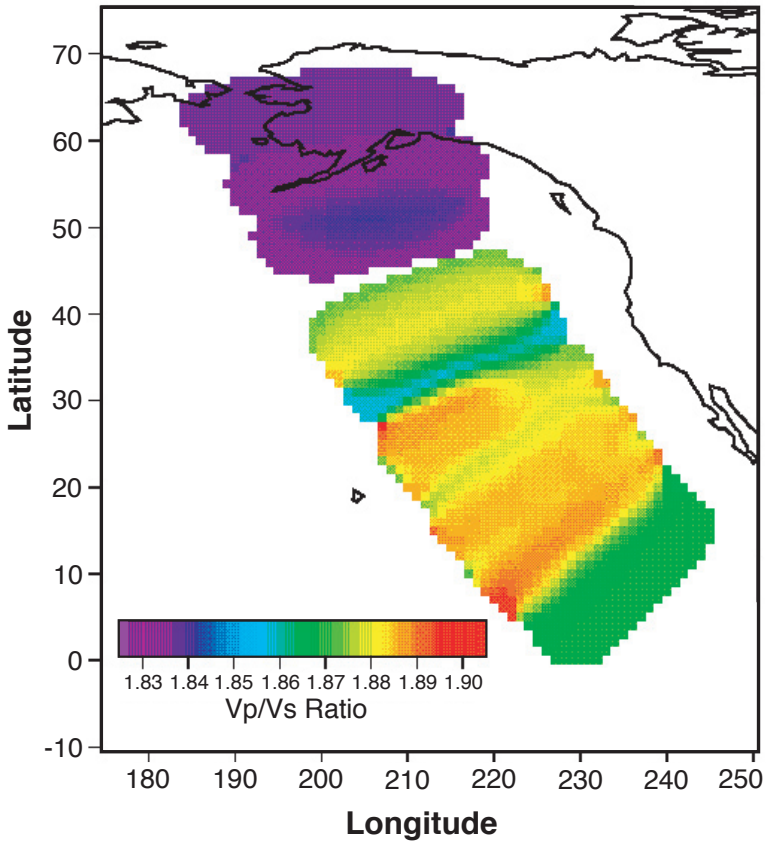

A map showing the inferred variations in VP/VS found from the combination of the P_{diff} and S_{diff} slowness residuals. The location of this anomaly correlates with the region of the CMB projected to receive the greatest amount of post-subduction paleoslab, so resulting azimuthal anisotropy would be an indication of advective flow at the CMB of the proposed paleoslab material.

Another candidate for explaining the anti-correlation of VP and VSH in D'' is that of anisotropy: our Pdiff waves are slow because they are travelling in a slow direction. Certain orientations of D'' rock fabric might provide a shape-preferred orientation (SPO) style of anisotropy that explains our seismic constraints: (A) transverse isotropy with fast inclusions, and (B) azimuthal anisotropy with either fast or slow cigar-shaped inclusions oriented perpendicular to the paleotrench. Several minerals like perovskite, periclase and columbite-structured silica are also highly anisotropic at CMB conditions, and so mineralogical anisotropy with a lattice-preferred orientation (LPO) remains a candidate. Whether the causes is chemical heterogeneity or anisotropy, or a combination of both, there is a material difference between rock at the base of the mantle beneath the interior and northern rim of the Pacific Ocean, and it is likely related to the flow pattern of the northern Pacific paleoslab as it reaches the CMB.

For further reading:

Wysession, M. E., Langenhorst, A., Fischer, K.M., Al-eqabi, G.I., Shore, P.J., Fouch, M.J., and Clarke, T.J., Mantle flow inferred from lateral variations in compressional/shear velocities at the base of the mantle, *Science*, **284**, 120-125, 1999.

Large-Scale Structure at the Core-Mantle Boundary from Diffracted P Waves

Michael E. Wysession, Washington University

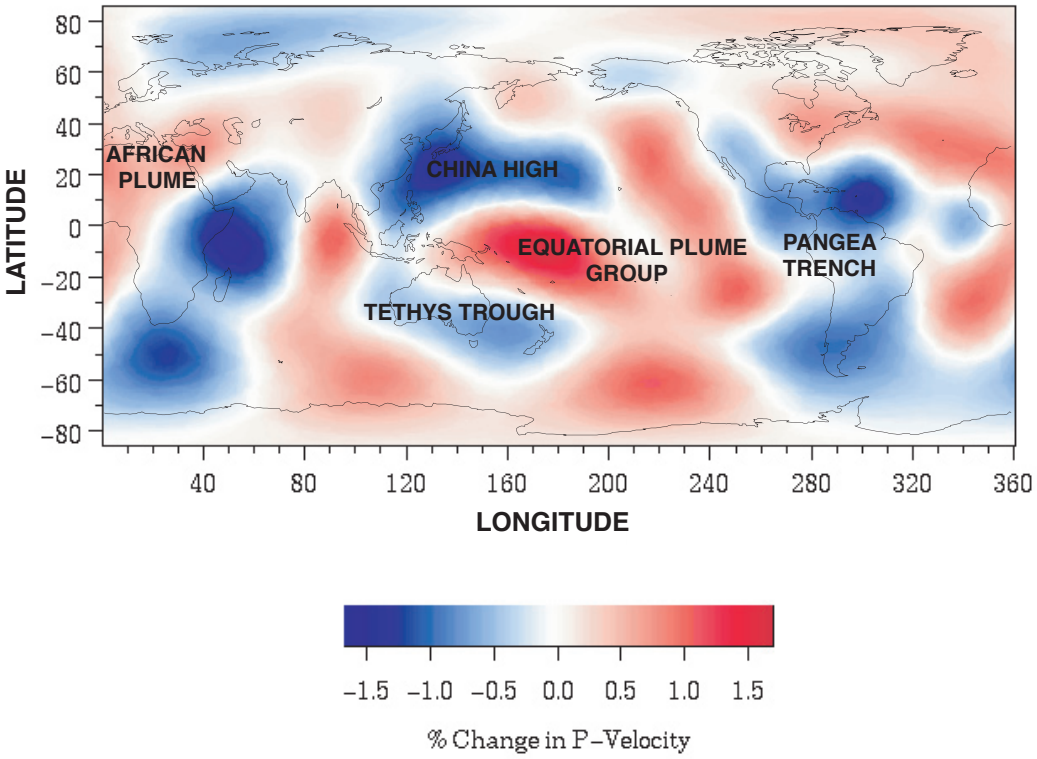

A map of the large-scale P-velocity variations at the base of the mantle, obtained from PKP-Pdiff differential travel times. The scale is from -1.5% to +1.5%. The dominant features are labelled, and correspond to either surface paleotrenches or regions at the surface with high densities of hot spot volcanoes.

We present a map of the large-scale P-velocity variations within D'' using a technique which has its greatest resolution within D''. We use the differential times of CMB-refracted PKP-DF arrivals and CMB-diffracted Pdiff arrivals. Data are primarily digital GSN records. The Pdiff waves travel extensively within D'', making them excellent probes for this layer, and the differential technique removes many effects from the ray paths outside of D''. The significance of our map of the large-scale continent-sized structure at the CMB is that it can (1) serve as a benchmark for whole-mantle tomographic P-velocity models in this region, (2) be used as a source of comparison with existing S-velocity models, and (3) that similarities between our map and projections of paleosubducted lithosphere verify previous suggestions of a strong coupling between surface plate tectonics and the dynamics of the base of the mantle.

The technique we present uses a waveform comparison between the Pdiff and PKP-DF phases and their synthetic counterparts that are computed by using a reflectivity method. The synthetic seismograms are computed with the PREM velocity structure, and deviations in the timing of the Pdiff and PKP-DF arrivals represent anomalies from this reference earth model. There is a total lateral variation of about 3% in the D'' P-velocity for the long wavelengths at which we have resolution. This is vertically averaged over the lowermost mantle for the sampling regions of the long period Pdiff waves. The wavelengths we are able to resolve are on the order of 2000 km, based on the *a priori* use of the 20 s Pdiff Fresnel zones, which have a width of this scale.

The striking similarity between the locations of fast seismic velocities in D'' and the locations of paleosubduction zones reinforces the idea that D'' may be the graveyard for subducted lithosphere. Complementary to the idea of fast D'' anomalies corresponding to cold rock brought from the upper mantle is the concept of D'' as the origin of hotspot mantle plumes. The PKP-Pdiff data suggest the locations of two large low velocity regions that correspond with the Equatorial Pacific Plume Group and Great African Plume features previously identified. The western part of the sub-Pacific low velocity region has been observed and examined by previous differential phase studies, and is one region recently found to be underlain by a narrow zone of even slower velocities. Our western African Plume extends westward beneath the northern Atlantic Ocean, though our resolution of this is poor. We also find a region of very slow velocities beneath the central Indian Ocean.

For further reading:

Wysession, M. E., Large-scale structure at the core-mantle boundary from core-diffracted waves, *Nature*, **382**, 244-248, 1996.

On the Possibility of Lateral Structure in Earth's Outer Core

Lapo Boschi and Adam M. Dziewonski, Harvard University
Antonio Piersanti, I.N.G., Rome, Italy

Lateral density structure could exist in the Earth's fluid outer core, owing to the gravitational perturbations induced by the asphericity of the mantle. We make use of the theory developed by Wahr and de Vries (1989) to obtain a quantitative estimate of the lateral density anomalies to be expected in the outer core, given a tomographic image of the core-mantle boundary (CMB) and assuming that the CMB is, to first approximation, an equipotential surface. We obtain lateral structure of long wavelength and very small (0.1%) amplitude, with a pattern closely resembling that of the assumed CMB topography; our maps do not correlate with any of the existing tomographic images of the outer core (e.g., Vasco and Johnson, 1998; Boschi and Dziewonski, 2000; Piersanti et al., 2000).

For further reading:

Boschi, L. and Dziewonski, A.M., Whole Earth tomography from delay times of P, PcP, PKP phases: lateral heterogeneities in the outer core, or radial anisotropy in the mantle? *J. Geophys. Res.*, in press, 2000.

Piersanti, A., Boschi L., and Dziewonski, A.M., On the possibility of lateral structure in the Earth's outer core, *Geophys. Res. Lett.*, submitted, 2000.

Vasco, D. W. and Johnson, L.R., Whole Earth structure estimated from seismic arrival times, *J. Geophys. Res.*, **103**, 2633-2671, 1998.

Wahr, J. H. and de Vries, D., The possibility of lateral structure inside the core and its implications for nutation and Earth tide observations, *Geophys. J. Int.*, **99**, 511-519, 1989.

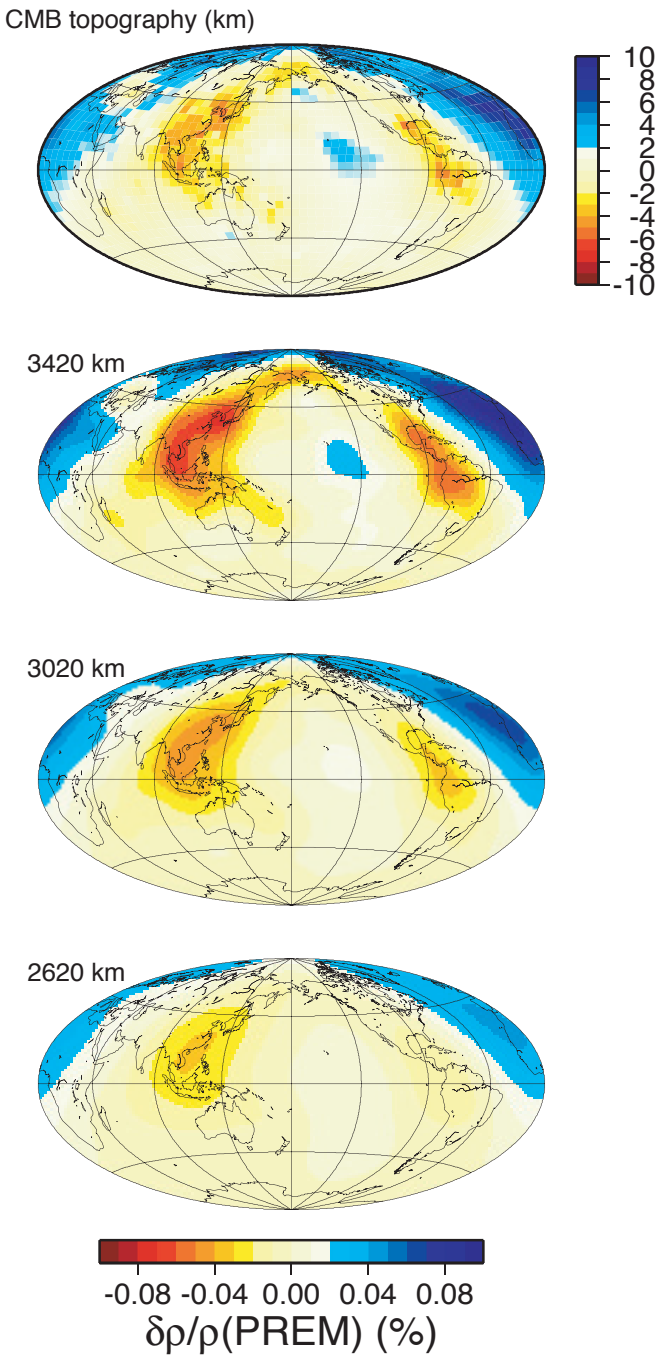

Top map: CMB topography model 1 from Boschi and Dziewonski (2000). This tomographic image is based exclusively upon measurements of the delay time of the seismic phase PcP, carrying energy that has been reflected by the CMB, and therefore not sensitive to the Earth's core. The availability of a large number of seismic measurements from the GSN, well-distributed over Earth's surface, is crucial to the correct solution of the tomographic inverse problem.Other maps: our predicted geographic distribution of percent density anomalies at three different radii in the outer core, relative to PREM, generated by such CMB undulations.

Anomalous Splitting of Free Oscillations: a Re-Evaluation of Possible Interpretations

Barbara Romanowicz and Ludovic Breger, University of California, Berkeley

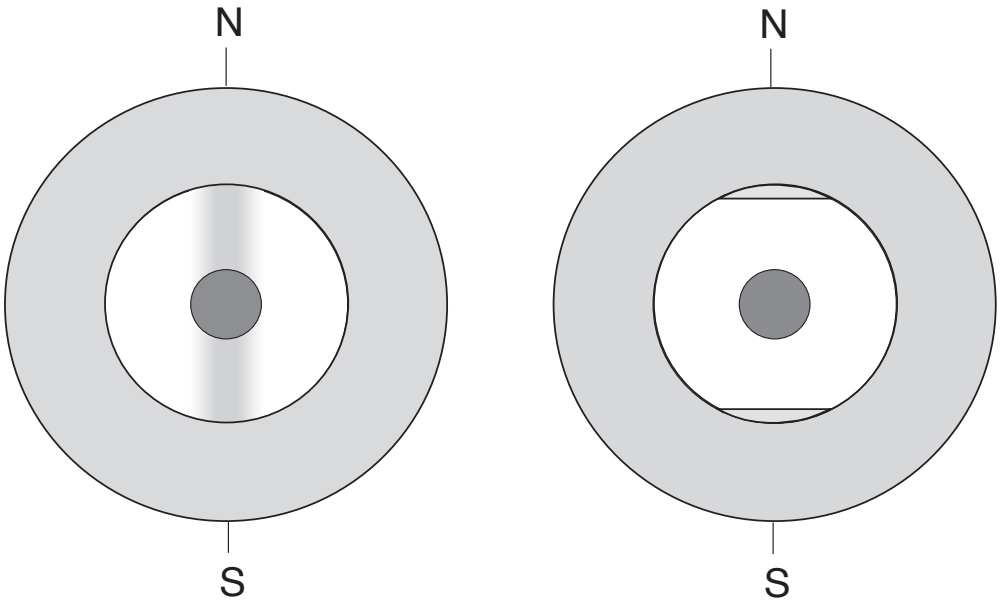

The splitting of normal modes sensitive to structure in the inner core is larger than can be explained by 3-D heterogeneity confined to the Earth's mantle. A preferred interpretation of this anomalous splitting involves inner core anisotropy, providing a unified explanation of these data and of observed trends in the travel times of PKP waves that sample the inner core. We reexamine this interpretation, as well as a previously suggested alternative one in terms of outer core structure. Our motivation comes from recent results which indicate that simple, smooth models of inner core anisotropy are in disagreement with some PKP observations. We invert a recently assembled high quality dataset, comprising modes sensitive to mantle and outermost core structure, as well as modes sensitive to mantle, outer core and inner core structure, and obtained from the unprecedented quality records of several very large earthquakes (such as the M8.2 06/09/94 deep Bolivia earthquake) at broadband stations of the GSN and Geoscope. We compare models parametrized to include either inner core anisotropy or heterogeneity in the outer core. We show the following (Romanowicz and Breger, 2000): (1) Outer core models, with fewer parameters, provide better overall fits to most modes with weak or strong sensitivity in the inner core, except for mode 3S2, the inner core mode with the strongest splitting. (2) Outer core models provide a good fit to the 4S and 5S P mantle mode branches, whereas models with inner core anisotropy, or models restricted to mantle structure, significantly overpredict the splitting of these branches. (3) Outer core models are more stable, and more consistent with each other than models with inner core anisotropy, when subsets of modes with different sensitivity to the inner core are inverted separately. (4) Lateral heterogeneity restricted to the mantle, in particular strong heterogeneity in D", fails to account consistently for the splitting of all modes.

Simple anisotropic models of the inner core therefore fail to explain the splitting of mantle P modes and core modes simultaneously, but when, alternatively, heterogeneity in P velocity is allowed in the outer core, this problem is resolved. The outer core structure obtained is consistent with concentration of light elements near the rotation axis in the outer core, either confined to the Taylor cylinder tangent to the inner core, or in polar caps at the top and bottom of the outer core. A small amount of shear within such polar caps might account for the large splitting of 3S2. Such models deserve further investigation as they should be weighted against more complex models of inner core anisotropy.

For further reading:

Romanowicz, B. and Breger, L., Anomalous splitting of free oscillations: a re-evaluation of possible interpretations, *J. Geophys. Res.*, in revision, 2000.

Regional Scale Anomaly in the Inner Core and Tilt of the Axis of Symmetry of Anisotropy

A. M. Dziewonski and W. J. Su, Harvard University

The inner core turned out to be more difficult to study than many, including these authors, have thought. In a way, it might have been anticipated that for a body occupying less than 1% of the Earth's volume and, for the surface focus, the range of incidence angles for which the inner core can be seen being less than 2°, there would be problems with obtaining adequate and evenly distributed sampling. This inadequate sampling led to oversimplifying assumptions, such as that the anisotropy of the inner core can be represented by an axially symmetric model of constant transverse isotropy, or the next simplest thing, that the axis of symmetry is slightly tilted with respect to the rotation axis. Once a departure from this simple model is allowed, and attempts are made to consider a more general case, the insufficiency of the data either leads to erroneous conclusions or no conclusions at all.

The tilt of the axis of symmetry represents a good example how such simplifying assumptions can be misleading. The top left panel of the figure shows Cylindrical Anisotropy Stack (CAS; Su and Dziewonski, 1995) of PKIKP residuals in the distance range from 150 to 153 degrees. If the symmetry axis of anisotropy coincided with the rotation axis, the patter of the fast residuals should be symmetric with respect to the pole. It clearly is not, and this result led Su and Dziewonski to postulate an 11° tilt of the symmetry axis. Stripping of the lowest spherical harmonics revealed that there is a short-wavelength signal present in this pattern: there is only one such place, and further analysis identified its source as corresponding to the paths from South Sandwich Islands to Alaska. In the map (see figure), all paths with the approximately the same ray angle are plotted and the region where the anomaly seems to originate is shown with a red circle of a radius of 15°. The CAS stack (top right) is obtained after the rays bottoming within the red circle are removed. The pattern does not require a detectable tilt of the symmetry axis. Thus a regional anomaly, interpreted as an integral part of a global field, has corrupted the interpretation.

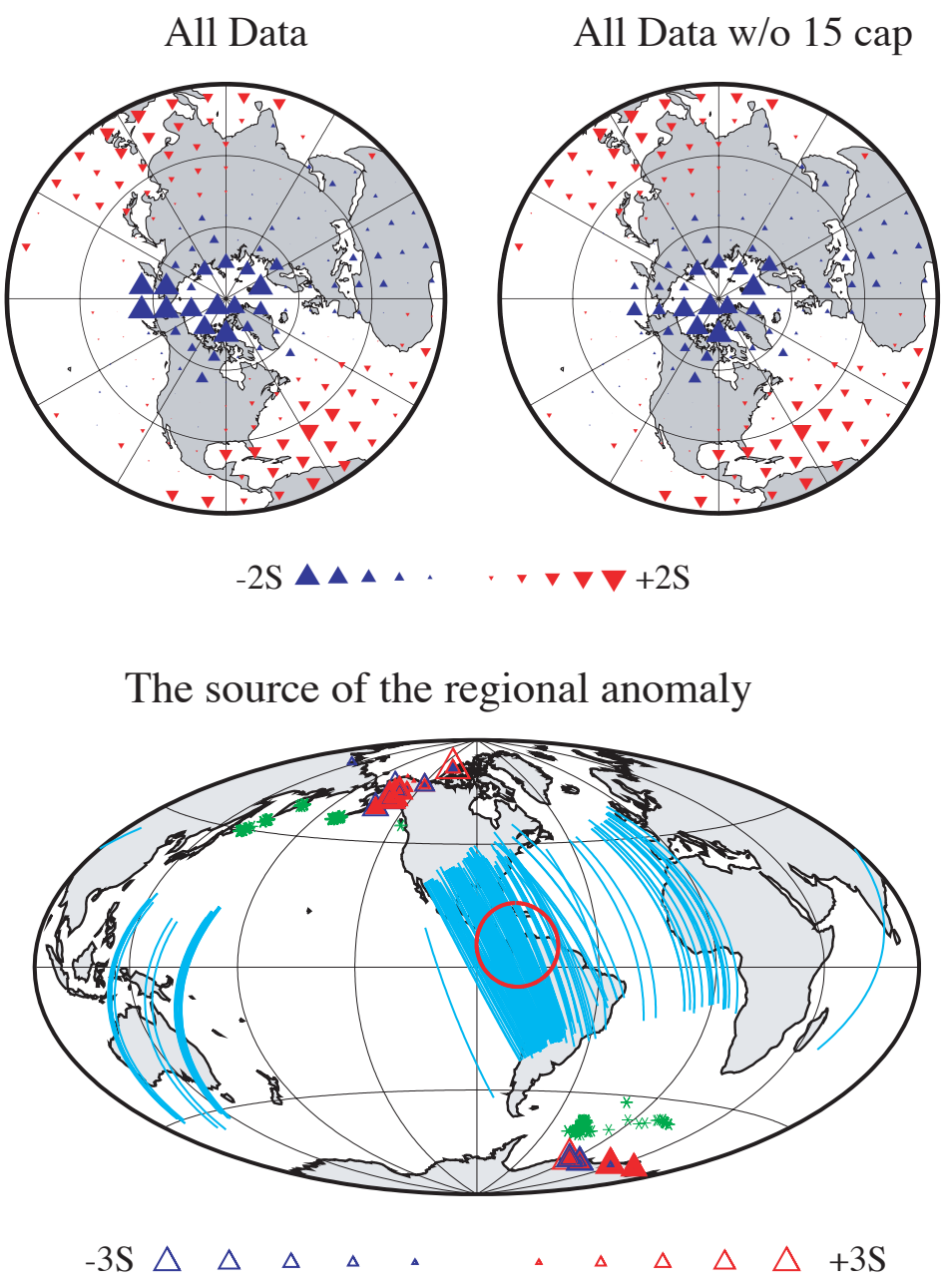

It is expected that the expansion of GSN and other IRIS-related observing systems, such as USArray, will help to elucidate the origin of the regional anomalies in the inner core.

Is There Anisotropy in the Inner Core?

A. M. Dziewonski and W.-J. Su, Harvard University

The complexities beginning to arise with the hypothesis that the inner core is anisotropic, and the difficulty with providing a plausible mechanism for its origin, led some authors to question whether the anomalies in data (travel times, splitting of normal modes) could not originate somewhere else in the Earth. For example, Romanowicz and Breger (1999) consider a possibility that the cause of the anomalies is located in the outer core. Most of the travel time studies are based on differences between the BC and DF arrivals. This allows for an accurate measurement but includes the ambiguity which phase (or both) is anomalous. We consider the absolute travel time residuals of BC and DF phases extracted from the ISC bulletins 1964-1996. Even though the accuracy of individual observations is worse, it is more than made up by the number of observations and distribution of source-receiver paths.

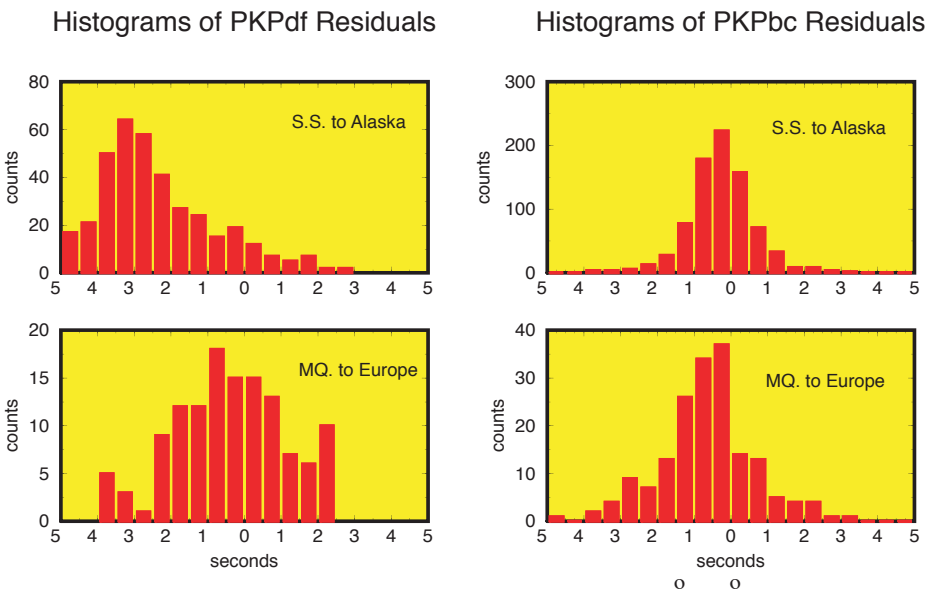

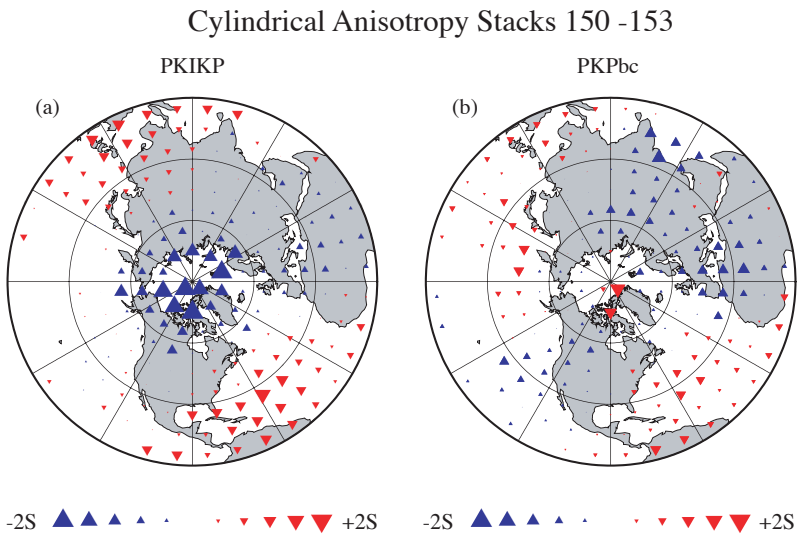

In the upper part of the figure we compare the residuals of BC and DF branches in the distance range from 150 to 153 degrees for two groups of rays, with approximately the same ray angle with respect to the rotation axis. One group is dominated by paths from South Sandwich Islands to Alaska and its DF residuals are strongly anomalous (about -3 sec), while the BC histogram is indicates normal arrival times. From this we may conclude that it is indeed a patch in the inner core under Bolivia-Venezuela that is anomalous. For the other path, from Mcquarie Island to northern Europe, both BC and DF are normal. This indicates that the inner core under southeastern Asia is less anisotropic than average. But specific examples may be misleading; one can still introduce an anomaly in the outer core of such a geometry that would satisfy both sets of observations. For this reason, we wish to compare the global Cylindrical Anisotropy Stacks (CAS) for both the BC and DF phases. The 'ray-angle' for BC corresponds to the direction of the tangential at the ray's bottoming point. The CAS for the DF phase (with the influence of the South Sandwich to Alaska path removed) shows a distinct set of negative residuals, with the maximum roughly coinciding with the position of the pole. In the CAS for the BC phase there is no indication of anomalously fast travel times associated with rays parallel to the rotation axis. The observation is valid for a range of azimuths and angles with respect to the rotation axis, and therefore the question posed in the title should be answered with "YES."

However, in the equatorial latitudes, there is a similarity between the two patterns, perhaps indicating that the mantle anomaly has not been fully accounted for. This would be important in the studies which depend on the complete stripping of the mantle effects, such as those of detecting the differential rotation of the inner core.

The continuing flow of data from IRIS's GSN and future deployments of the USArray should be essential in investigating the sources of anomalies that, with the current data set, may be projected onto the inner core.

An Inner Core Transition Zone Revealed by Broadband Data from Stations in Alaska and Canada

Xiaodong Song, University of Illinois at Urbana-Champaign
Don V. Helmberger, California Institute of Technology

We have recently observed that seismic waves traversing Earth's inner core along north-south (NS) paths produce unusually broad pulse shapes at long periods, compared with waves along east-west (EW) paths, and reflections from below the inner core boundary at short periods (Song and Helmberger, 1998). The observations provide compelling evidence for a seismic velocity discontinuity along NS paths about 200 kilometers below the inner core boundary separating an isotropic upper inner core (UIC) from an anisotropic lower inner core (LIC) (Figure 1). The triplication associated with the rapid increase of velocity at such a transition along NS paths provides a consistent explanation for the anomalously broad waveforms of the inner core PKP(DF) phases on broadband displacement records, compared with outer core arrivals PKP(BC) and PKP(AB), and the short-period reflections from within the inner core. The UIC/LIC boundary is speculated to be irregular, which may explain recent reports of large scatter in inner core travel times (Tanaka and Hamaguchi, 1997; Creager, 1999).

The most compelling differences between observations along EW versus NS paths are shown in Figure 2. From left to right are synthetics for PREM2, data from EW paths, data from NS paths, and synthetics for a model with a 4.3% P velocity jump at 250 km below the ICB. All the NS paths are earthquakes in the South Sandwich Islands (SSI) to stations in Alaska and Canada (except that labeled ARU 10, from Drake Passage west of the SSI to Arti, Russia). The ray paths sample the inner core beneath Colombia and Venezuela. The EW paths are from two events in the Tonga and Fiji Islands region to stations of the German Regional Seismic Network (GRSN) except the bottom trace (event 11 in the SSI recorded at INCN, Korea). The waveforms of the DF phases from

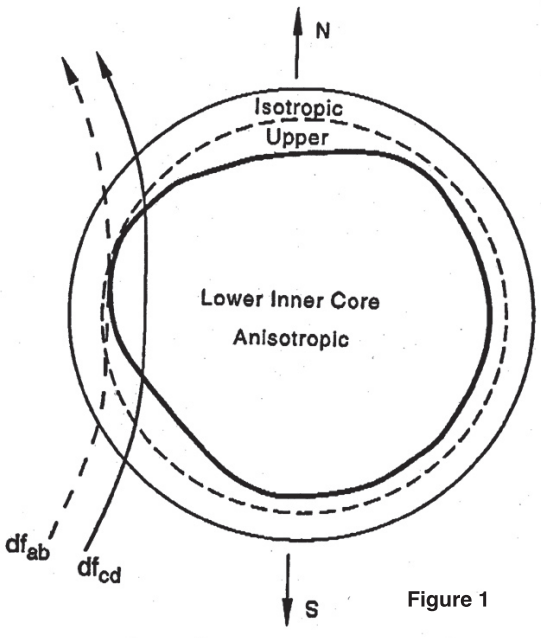

Figure 1

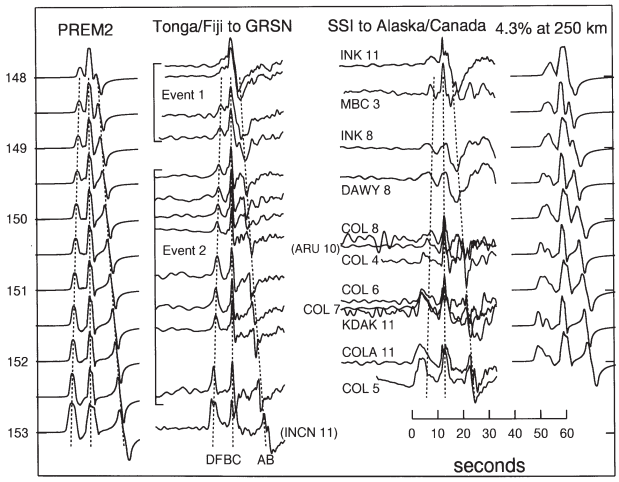

Figure 2

the EW paths are similar to the corresponding BC waveforms with the exception of a slight broadening and less high requency content in the DF waveforms due to inner core attenuation. The difference in time of the DF versus the BC arrivals is well predicted by the reference model PREM2 (Song and Helmberger, 1995), which was based on a modification of the Preliminary Reference Earth Model (PREM) (Dziewonski and Anderson, 1981) and was proposed to provide a better fit to the averages of PKP differential travel times and waveforms from EW paths. In contrast, the DF phases from the NS paths arrive earlier than predicted by the reference model, as attributed to the inner core anisotropy, and have much broader waveforms than the corresponding BC and AB phases. Note the sharp contrast in DF wave-forms and BC to DF differential times between the EW path from the SSI event 11 to station INCN in Korea and the NS paths from the same event to KDAK and COLA in Alaska and to INK in Canada. The broad DF waveforms from the NS paths are reasonably reproduced in the synthetics for the model with a velocity jump inside the inner core. Most of NS data in this study were from GSN stations, and almost all data were obtained through the IRIS DMC.

For further reading:

Creager, K.C. Large-scale variations in inner core anisotropy, *J. Geophys. Res.*, **104**, 23127-23139, 1999.

Dziewonski, A.M., and Anderson, D.L., Preliminary reference Earth model, *Phys. Earth Planet. Inter.*, **25**, 297-356, 1981.

Song, X.D., and Helmberger, D.V., A P-wave velocity model of the Earth's core, *J. Geophys. Res.*, **100**, 9817-9830, 1995.

Song, X.D., and Helmberger, D.V., Seismic evidence for an inner core transition zone, *Science*, **282**, 924-927, 1998.

Tanaka, S., and Hamaguchi, H., Degree one heterogeneity and hemispherical variation of anisotropy in the inner core from PKP(BC)-PKP(DF) times, J. Geophys. Res., 102, 2925-2938, 1997.

Differential Rotation of the Inner Core Suggested by Time-Dependent Observations

Xiaodong Song, University of Illinois at Urbana-Champaign
Paul G. Richards, Lamont-Doherty Earth Observatory of Columbia University

The idea that the solid inner core, separated from the mantle by a liquid outer core, may move differently from the once-a-day rotation of the mantle and crust was proposed 20 years ago (Gubbins, 1981). A more recent study of numerical simulation of Earth's dynamo (Glatzmaier and Roberts, 1995) predicted that electromagnetic torque would drive the inner core to rotate a few degrees per year faster than the crust and the mantle.

In 1996, we reported evidence for differential rotation of the inner core (Song and Richards, 1996). We used a simple approach to detect inner core motions — by comparing seismic waves that travel through the inner core recorded at the same monitoring station from earthquakes at the same location but several years apart. We used relative measurements between the inner core arrival, PKP(DF), and the outer core arrival, PKP(BC), because these two ray paths are very close in the mantle, and such measurements reduce biases from mantle heterogeneity and source mislocations. Our basic observation is that such inner core waves show systematic changes in wave speed over a few decades. In particular, using earthquakes in South Sandwich Islands recorded over 28 years at an Alaskan station, we found that seismic waves have taken progressively faster paths in the inner core so that the most recent waves have a travel time that is shorter by 0.3 s than the very early ones (Figure 1).

The travel-time change is explained by an inner core rotation that reorients the anisotropic inner core. Assuming that the fast axis of the inner core anisotropy is tilted from the spin axis, we interpreted the gradual travel time increase as evidence that the inner core is rotating eastwards around the spin axis so that the fast axis moves progressively closer to the PKP(DF) ray path (Figure 2). We estimated a rotation rate of about 1 degree per year. Subsequently, Creager (1997) suggested that the lateral velocity gradient is steep in this part of inner core, and reinterpreted the temporal change at COL as a shift of the lateral velocity gradient with a much smaller differential rotation rate of 0.2-0.3 degrees per year. Our current best estimate of the rate ranges from 0.3 to 1.1 deg/yr (Song, 2000).

These estimates of the rotation rate are remarkably fast for geological processes — several tens of thousands faster than the fastest relative plate motion. The rotation has implications for the geodynamo and core dynamics and adds a new dimension - time - to traditional seismological studies of the deep interior structure of our planet. The College, Alaska GSN station provided critical data for this study. The work benefitted from easy access to data from the IRIS DMC.

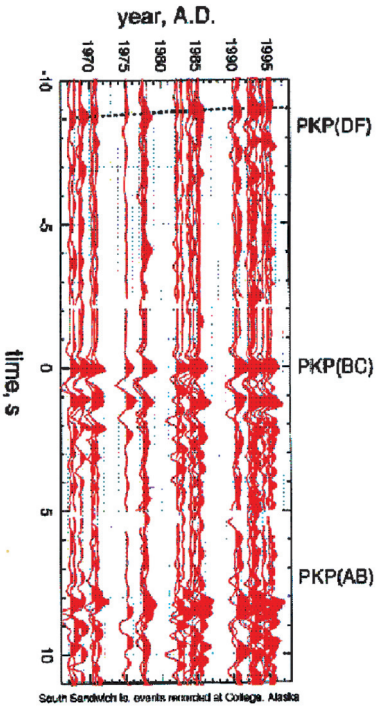

Figure 1. All 38 seismograms recorded at station College, Alaska used by Song and Richards (1996) to infer a differential rotation of the inner core. The records are plotted with respect to earthquake origin times and are aligned with PKP(BC). The PKP(DF) waveforms are windowed out and corrected to a standard distance of 151°. The PKP(DF) amplitudes are enlarged by 5 times. The PKP(AB) arrivals are corrected for 90° phase shift and are referenced to the standard distance. The dashed line shows the predictions for the best-fitting model of inner core rotation of Song and Richards (1996).

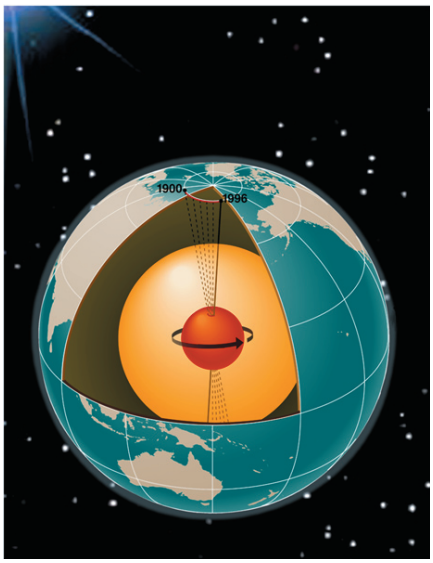

Figure 2. A representation of the original interpretation by Song and Richards (1996) that the anisotropic symmetry axis of the inner core is moving due to inner core rotation. As the solid core and its symmetry axis rotates, there is a change in the angle between the symmetry axis and the inner core leg of a ray for a fixed source and fixed station, resulting in the systematic shift we see in the total time taken to travel along the ray. We show the motion of the symmetry axis since the turn of the century, according to the estimate of a 1.1 deg/yr eastward rotation about the N-S axis.

For further reading:

Creager, K.C., Inner core rotation rate from small-scale heterogeneity and time-varying travel times, *Science*, **278**, 1284-1288, 1997.

Glatzmaier, G.A., and Roberts, P.H., A three-dimensional convective dynamo solution with rotating and finitely conducting inner core and mantle, Phys. Earth Planet. Inter., 91, 63-75, 1995.

Gubbins, D., Rotation of the inner core, *J. Geophys. Res.*, **86,** 11695-11699, 1981.

Song, X.D., Joint inversion for inner core rotation, inner core anisotropy, and mantle heterogeneity, *J. Geophys. Res.*, **105**, 7931-7943, 2000.

Song, X.D., and Richards, P.G., Observational evidence for differential rotation of the Earth's inner core, *Nature*, **382**, 221-224, 1996.

Imaging Inner Core Structure and Rotation using Alaska Stations

Xiaodong Song, University of Illinois at Urbana-Champaign

Observational evidence for a differential rotation of the inner core was reported a few years ago from time-dependent differential travel times between the inner core arrival PKP(DF) and the outer core arrival PKP(BC) (Song and Richards, 1996). In particular, using earthquakes in the South Sandwich Islands (SSI) recorded over 28 years at COL (College, Alaska), we found that the seismic waves have taken progressively faster paths in the inner core so that travel times of the most recent waves are 0.3 s shorter than those of the very early ones. However, inference of the rotation rate from the observed travel time changes depends on the inference of local lateral velocity structure in the part of the inner core sampled by the paths (Creager, 1997), which in turn may be affected by mantle heterogeneity.

The long operating histories of the COL station and other stations of the dense Alaska Seismic Network (ASN) prove to be very useful in attacking this problem (Song, 2000). We obtained 611 measurements of PKP(BC)-PKP(DF) differential travel times from 92 SSI earthquakes over the past nearly half a century recorded at the Alaskan stations. Because mantle structure does not move as the inner core rotates, the dense sampling of the SSI-Alaska pathway at different time periods allows us to invert simultaneously for the inner core rotation, inner core structure, and mantle structure. Surprisingly, the inner core rotation seems resolvable even from digital data observed at ASN in the 1990s (spanning over eight years) alone in such a joint inversion. The figure shows snapshots of the anisotropy of the sampling region beneath Colombia in the inner core at three time periods in 1990s. The lateral velocity gradients obtained separately from the three periods are very similar, confirming that the gradients are robust. The results clearly show that the image in 1996-1998 (bottom map) has shifted to the east relative to the image in 1993-1995 (middle map), which in turn has shifted to the east relative to the image in 1990-1992 (top map).

The inferred rotation rate from the Alaska data ranges from 0.3 to 1.1 per year faster than the mantle. The combination of the steady decrease of the PKP(DF) travel times through the inner core and the steep negative lateral velocity gradient from the west to the east in this part of the inner core rules out a westward inner core rotation.

The data at Collage, Alaska for 1980 to the 1990's were obtained from the IRIS DMC. I thank Douglas Christensen, Guy Tytgat, Kent Lindquist, Mitch Robinson, Jim Taggart, Jack Townshend, Waverly Person, Willie Lee, Lowell Whiteside, and Harley Benz for assistance with data acquisition.

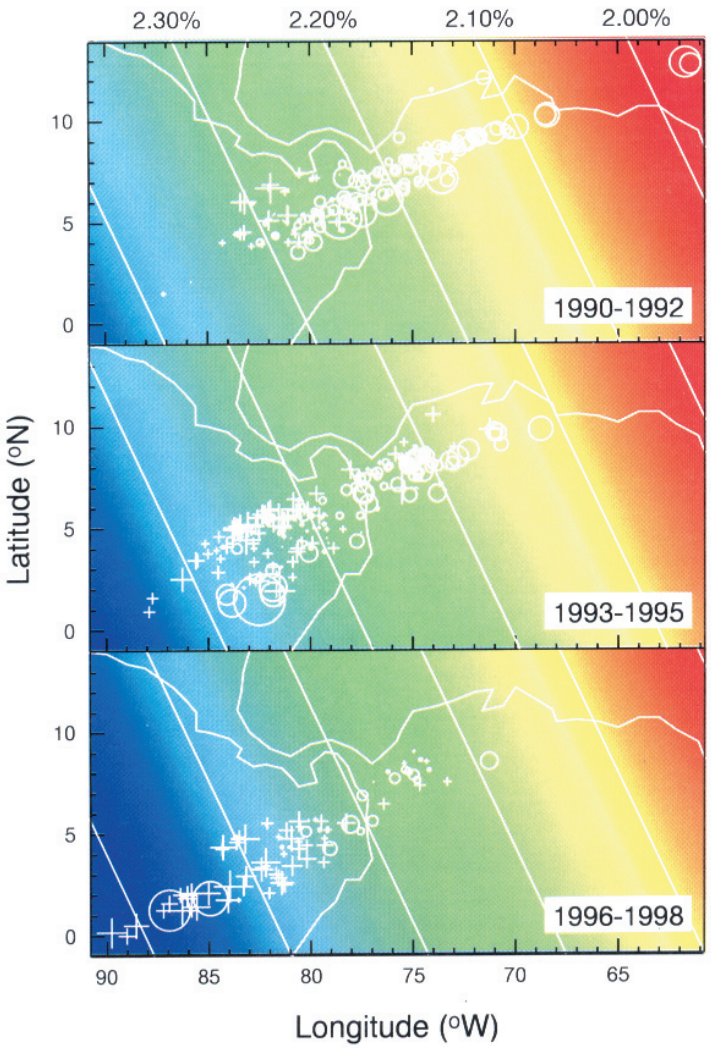

Maps of differential PKP(BC)-PKP(DF) travel time residuals (as a percentage of PKP(DF) travel times in the inner core) observed at College, Alaska station and Alaska Seismic Network from South Sandwich Islands earthquakes in (top) 1990-1992, (middle) 1993-1995, and (bottom) 1996-1998. The residuals have been corrected for mantle structure obtained in a joint inversion for inner core rotation, inner core structure, and mantle structure (Song, 2000). The velocity perturbations are plotted at the bottoming points of the PKP(DF) rays in the inner core (symbols). The circles indicate values smaller than the average of all the perturbations (1990-1998) after the corrections; the crosses indicate values larger than the average. The size of the symbols is proportional to the departures from the average. The colors and the parallel lines represent the linear regressions of the corrected velocity perturbations on the distances along the sampling profile. Note the eastward shifts of the color patterns, indicating inner core super rotation.

For further reading:

Creager, K.C., Inner core rotation rate from small-scale heterogeneity and time-varying travel times, *Science*, **278**, 1284-1288, 1997.

Song, X.D., and Richards, P.G., Observational evidence for differential rotation of the Earth's inner core, *Nature,* **382**, 221-224, 1996.

Song, X.D., Joint inversion for inner core rotation, inner core anisotropy, and mantle heterogeneity, *J. Geophys. Res.*, in press, 2000.

Rotation of the Inner Core: Constraints from Normal Modes

Gabi Laske, Guy Masters, and Freeman Gilbert, University of California, San Diego

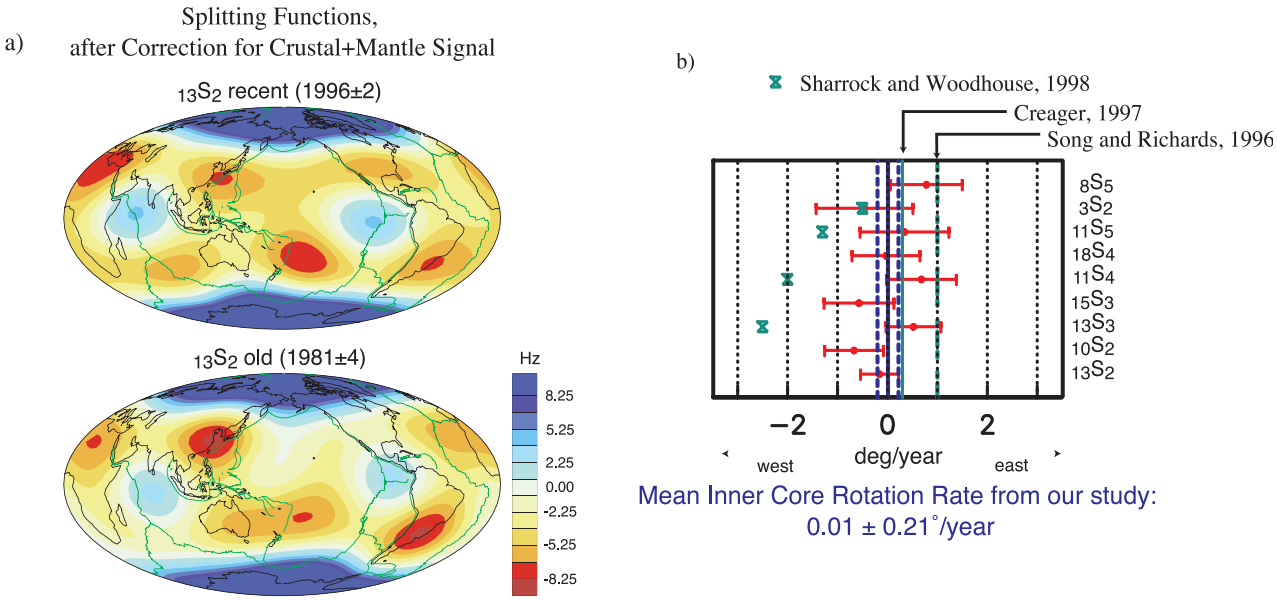

a) Recent and past splitting functions for mode 13S2. The past splitting function is not accurate enough to reliably constrain inner core rotation. b) Inner-core rotation rates obtained for nine core-sensitive modes. Hour-glass symbols mark the results of a recent mode study, and two green lines those of recent body-wave studies. Our data are marginally consistent with a superrotation of 0.3 deg/yr, but a superrotation of 1 deg/yr is clearly inconsistent for most of the modes.

Differential rotation of the inner core (IC) has recently been inferred by several body-wave studies with most agreeing that a superrotation may exist with a rate between 0 and 3 degrees per year. The wide range of inferred rotation rate is caused by the sensitivity of such studies to local complexities in structure which have now conclusively been demonstrated to exist. Free-oscillation "splitting functions" are insensitive to local structure and are therefore better candidates for estimating differential rotation.

We have used a new technique to determine splitting functions that allows us to solve for the most general form of the splitting matrix without knowledge of the earthquake sources. This technique is based on the autoregressive property of combinations of seismograms for each event allowing the splitting matrix to be estimated in a non-iterative, one-step process. We have applied this technique to recordings of recent "great" earthquakes and get extremely reliable estimates of splitting functions for modes which are sensitive to the inner core. Unfortunately, the data volume and quality for earthquakes 20 years ago is insufficient to allow a similar determination for that time with the same fidelity. We are therefore currently restricted to use a hypothesis test as an indirect method to obtain the inner core rotation rate: for each inner-core sensitive mode, the "recent" splitting function is used to compute a theoretical one for past earthquakes assuming different relative rotation rates for the inner core. We then investigate which rotation rate best fits the data of past "great" earthquakes. Our current estimate is that IC differential rotation has been essentially zero over the last 20 years, though a small relative rotation of up to 0.3 deg/yr is possible.

Clearly, we would like to be able to significantly decrease the uncertainty of our estimate. This is possible if we can determine splitting functions for different time periods with high fidelity. A comprehensive database of future very long-period data from global seismic broad-band networks such as the GSN is the essential tool to accomplish this task.

For further reading:

G. Laske, and Masters, G., Limits on differential rotation of the inner core from an analysis of the Earth's free oscillations, *Nature*, **402**, 66-68, 1999.

The Unique Anisotropy of the Pacific Upper Mantle

Göran Ekström and Adam M. Dziewonski, Harvard University

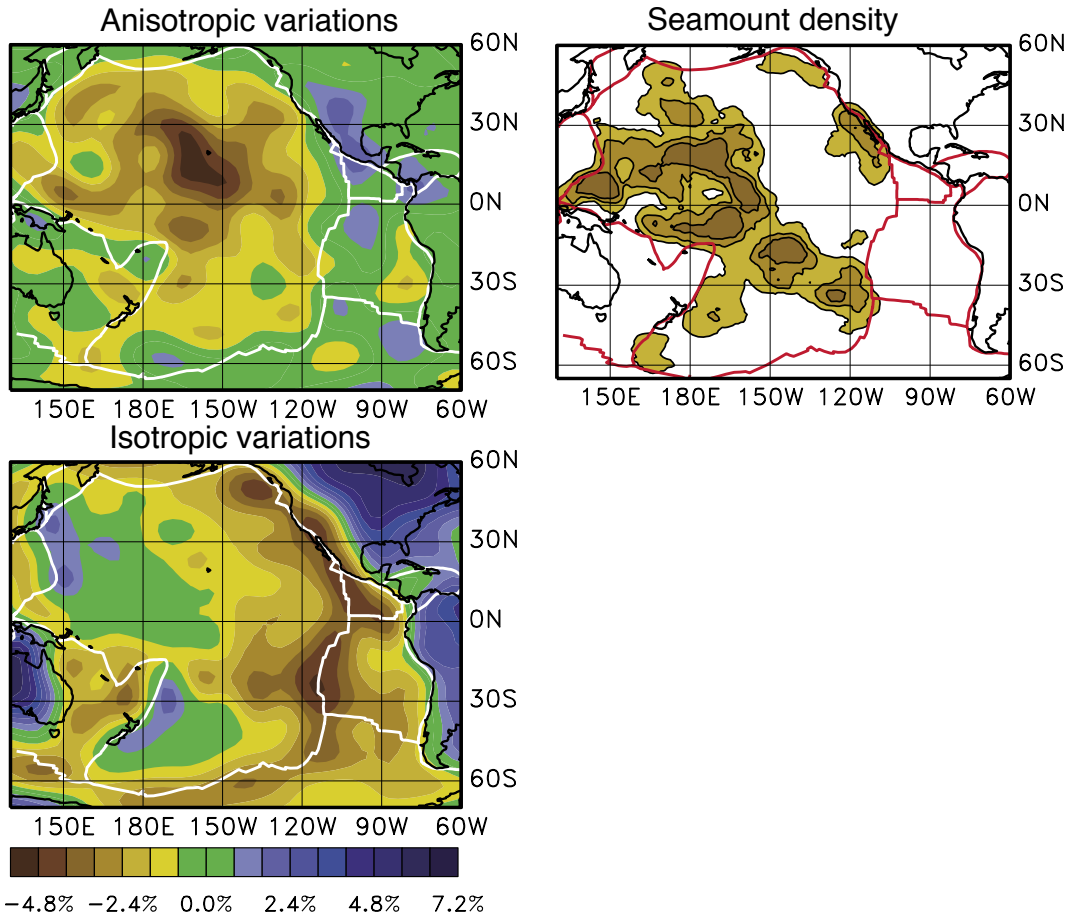

Data from the Global Seismographic Network (GSN) have been used extensively to map seismic wave velocites in the Earth. Three-dimensional variations in seismic velocities depend on both temperature, which produces isotropic changes in velocity, and material fabric, which can produce elastic anisotropy. Until recently, most global tomographic efforts have focused on imaging isotropic (presumed thermal) variations. In a recent study of global surface wave dispersion, a three-dimensional S-velocity model of the Earth has revealed very large regional variations in radial anisotropy. With a peak at 150 km depth, the upper mantle beneath the central Pacific shows a very large regional anomaly, with V_{SH} as much as 7% faster than V_{SV}. The top left panel shows the geometry and magnitude of the anisotropic anomaly at 150 km depth. The location of the anomaly is not correlated with the age of the seafloor. This is in striking contrast with the lateral variations in isotropic *S* velocities, which at the same depth (150 km) show a correlation of the anisotropic anomaly with seamount density (upper right panel) in the Pacific Basin (Wessel and Lyons, 1997) may provide a clue to the underlying physical processes responsible for the anisotropic anomalies. Because seismic anisotropy often is an indicator of strain in Earth materials, one can speculate that asthenospheric flow associated with Pacific intraplate volcanism is organized in such a way as to generate the fabric that we are now beginning to map out in three dimensions.

For further reading:

Wessel, P., and Lyons, S., Distribution of large Pacific seamounts from Geosat/ERS-1: Implications for history of intraplate volcanism, *JGR*, **102**, 22,459-22,475, 1997.

Ekström, G., and Dziewonski, A.M., The unique anisotropy of the Pacific upper mantle, *Nature*, **394**, 168-172, 1998.

Constraining Locations of Mid-Ocean Ridge Earthquakes

Jianfeng Pan and Adam M. Dziewonski, Harvard University

Earthquakes associated with the creation of new ocean crust are difficult to locate precisely because most often they are far away from seismic stations. Displays of epicenters determined by the ISC, for example, often show large and systematic deviations from the bathymetric features associated with the sea floor spreading such as mid-ocean ridges and transform faults. With the improvement in resolution and accuracy of the bathymetry, it is possible to use this information to constrain location of the events. If the ocean floor bathymetry for a particular plate boundary is displayed in the coordinate system whose pole corresponds to the pole of rotation between the two plates, then a transform fault should be a parallel in this system and the mid-ocean ridge a meridian. Using the CMT catalog we can choose earthquakes that clearly correspond to ridge activity (normal faults) or transform fault (strike-slip). The longitude of the former (in the plate rotation coordinate system) can be fixed, and only the latitude allowed to vary and the opposite can be done in the latter case. This should improve the accuracy of at least one of the coordinates. In this way, we are able develop a set of master events, or station corrections, which can be used to relocate other events, either of smaller magnitude than required for a CMT solution or predating the CMT catalog. We have applied this concept to the earthquakes on the Romanche Fracture Zone (RFZ). The top panel in the figure shows the ISC locations at the center of a particular beach-ball for earthquakes on the RFZ and its vicinity. The middle panel shows the locations obtained using the procedure outlined above only for the strike-slip earthquakes that can be associated with the RFZ. The bottom panel shows the change in the location, magnified by a factor of 1.5. It is clear that the ISC locations are systematically south of the RFZ and that these mislocations can be as large as 40 km.

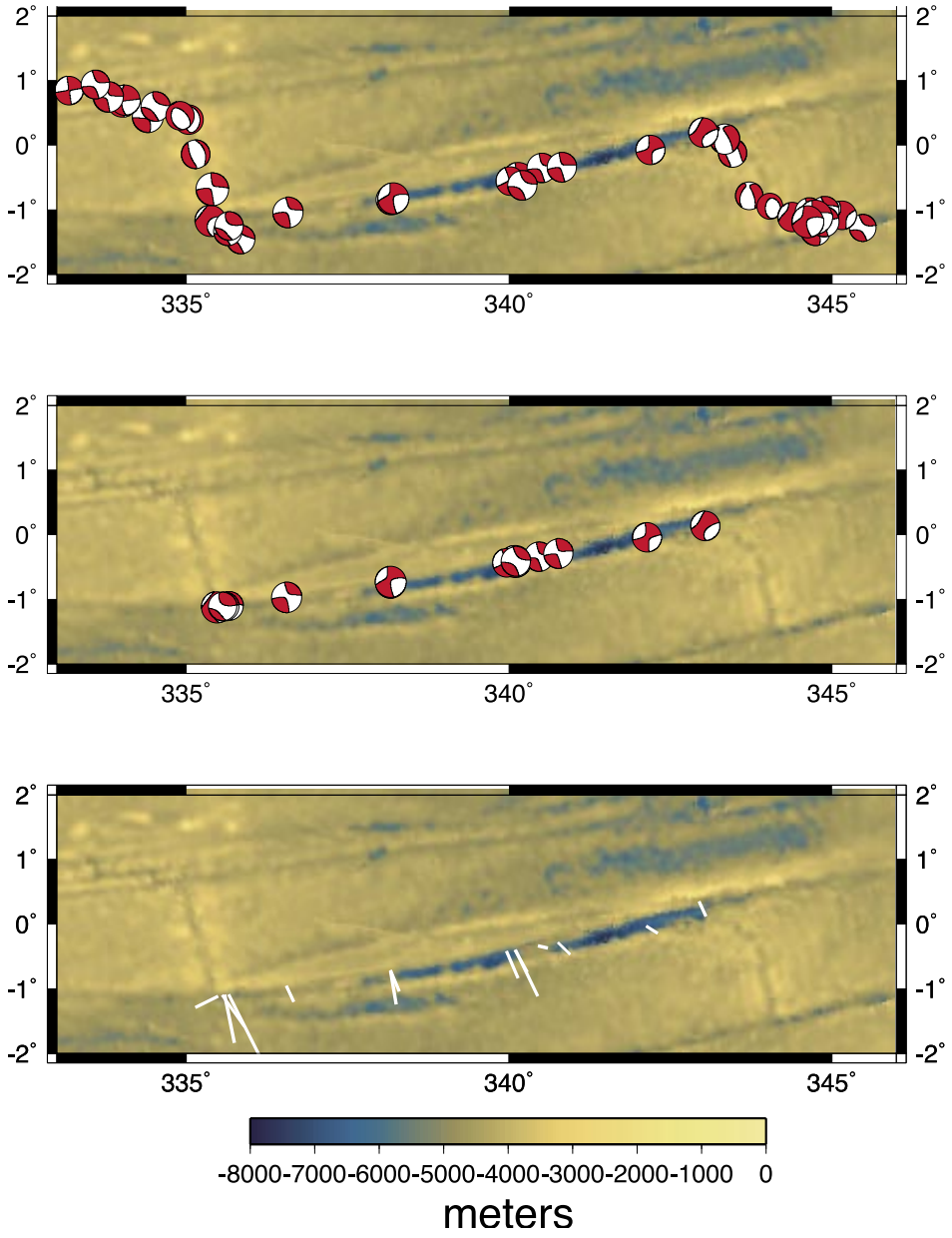

All of the CMT solutions that are used to determine whether an earthquake happened on the ridge or a transform fault have been obtained by waveform analysis of Global Seismographic Network

Earthquakes on Oceanic Transform Faults

Rachel Abercrombie and Göran Ekström, Harvard University

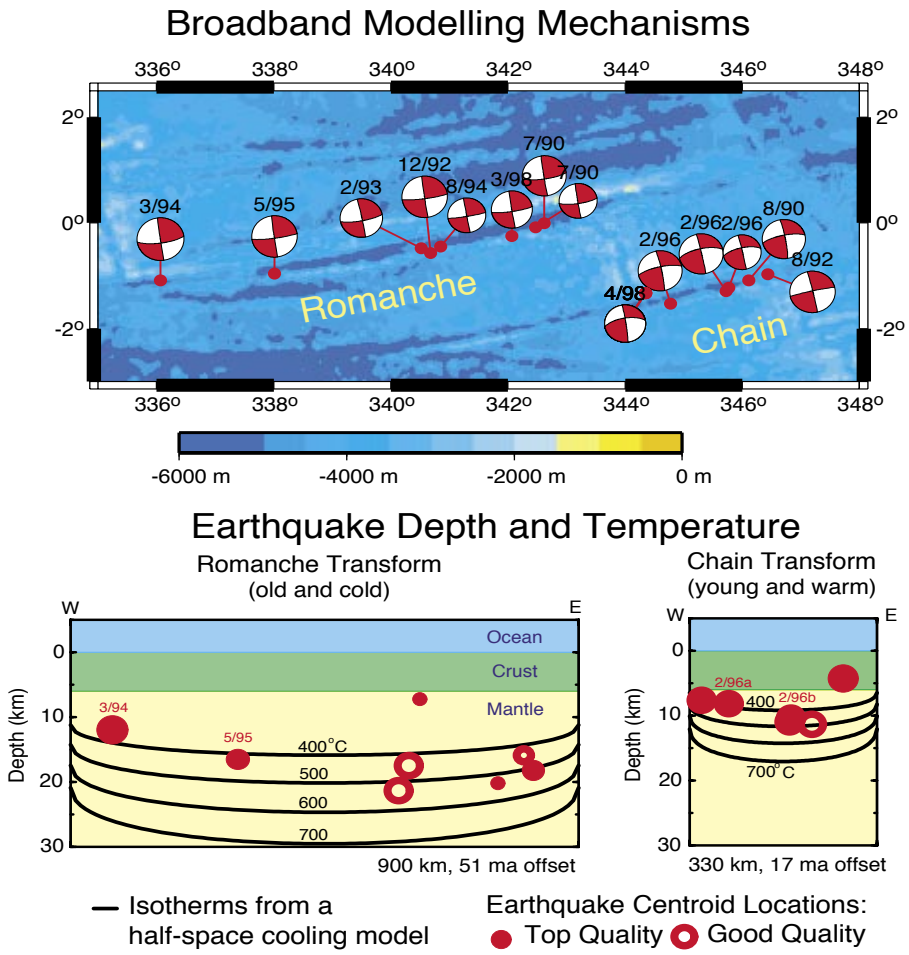

Oceanic transform faults are one of the three principal types of plate boundaries, yet the manner in which they slip is poorly understood. The depths of earthquakes on these faults are not well-constrained. Therefore, the width of the seismic zone, and the ratio of seismic to aseismic slip on the faults are also unknown. Within the last decade, broadband recordings of earthquakes at GSN and other stations have sufficient resolution to obtain reliable depths and mechanisms for oceanic transform earthquakes. Early studies of oceanic transform earthquakes have suggested that relatively slow earthquake rupture may be common. More recently it has been proposed that very slow slip may precede the more normal rupture in many oceanic transform earthquakes, including the 1994 Romanche earthquake. If precursory slip could be detected in real time it could prove useful for earthquake prediction. The observations remain controversial, however, partly because of their small amplitude, and partly because of uncertainties in the source parameters (depth, orientation, structure) assumed in the modelling.

Here we model broadband body wave seismograms to obtain well-resolved depths and mechanisms for fourteen earthquakes on the Romanche and Chain transform faults in the equatorial Atlantic ocean. The earthquake mechanisms on the individual transforms are extremely consistent, suggesting that the faults are planar and parallel to the plate motion. The Romanche transform dips steeply to the south and the Chain transform to the north. Earthquakes on the longer Romanche transform are systematically deeper than those on the neighboring Chain transform. The predicted isotherms are also deeper on the Romanche transform as it offsets older, colder lithosphere. These earthquake depths indicate that the maximum depth of brittle failure is at a temperature of ~600ºC in oceanic lithosphere. We find that the body waves from the Romanche 1994 earthquake can be well modelled with slip on a single fault. We use the mechanism and depth of this earthquake to recalculate its source spectrum. The previously reported slow precursor can be explained as an artifact of uncertainties in the assumed model parameters, principally the depth and Earth structure of the source.

Structure of the Iceland Crust and Plume Resolved with the PASSCAL-HOTSPOT Broadband Network

Richard Allen, Guust Nolet, Jason Morgan, Princeton University
HOTSPOT team

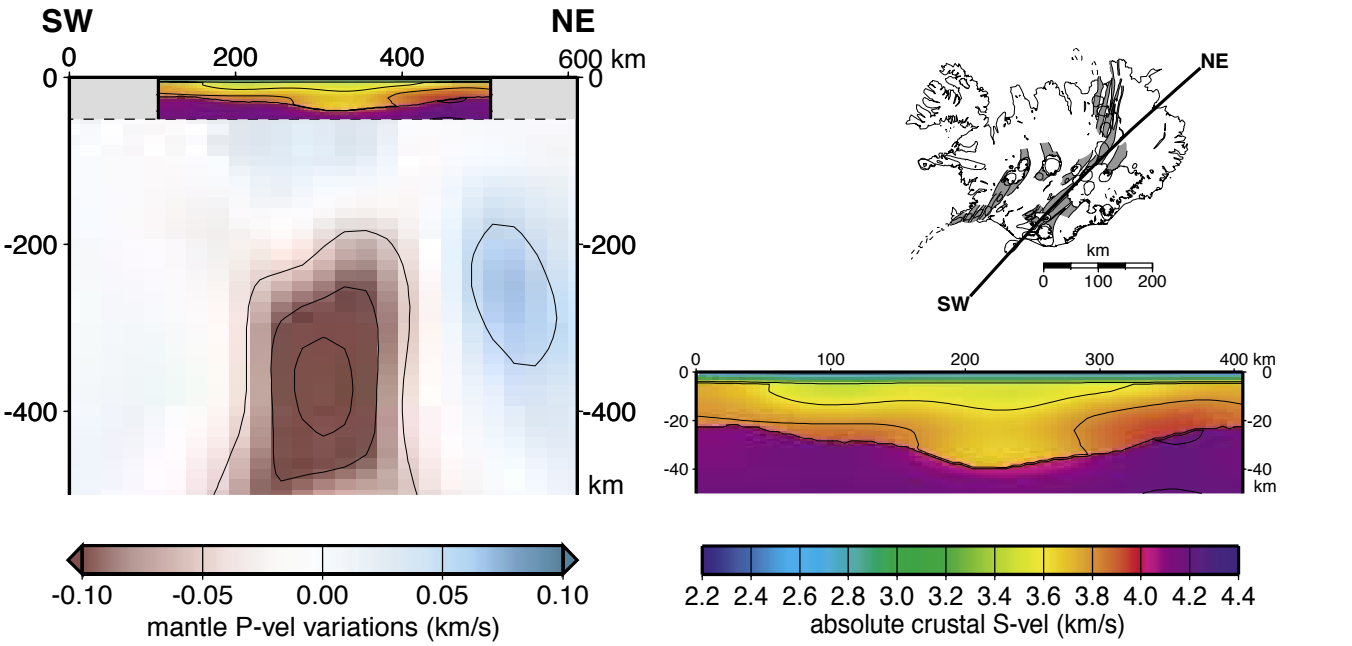

Left: Vertical slice parallel to the eastern neovolcanic zone (line on the insert map). Mantle P-velocity variations reveal a low-velocity anomaly extending from 500 to 200 km depth. The crustal S-velocity has been superimposed in the upper 50 km. Bottom right: enlargement of thecrustal model along the same slice. Absolute S-velocity is shown revealing the transition from crust to mantle (orange to purple). Note the thicker crust above the center of the plume and the plume-like low velocities anomaly in the lower crust which then extends along the neovolcanic zone in the upper crust.

Since the 1970s it has been hypothesized that Iceland is the product of a plume of hot rock rising up from hundreds of kilometers depth and impinging on the surface. The PASSCAL-HOTSPOT experiment was designed to produce a high resolution image of the velocity structure beneath Iceland from the surface to 500 km depth that would be able to conclusively prove or disprove this hypothesis. 30+ PASSCAL broadband instruments were deployed from June 1996 to August 1998 to record local, regional, and teleseismic earthquakes; the results to date are summarized by the figure. The high density of stations allowed a surface wave study to determine the 3D S-velocity structure of the crust beneath Iceland. A slice through the neovolcanic zone (the Mid-Atlantic Ridge) is shown. The crustal velocity structure shows a transition from ridge-like, elongated low velocity anomalies near the surface, to plume-like, circular anomalies, in the lower crust. Knowing the crustal structure also allows better imaging of the mantle structure beneath.

Two approaches have been taken to imaging the mantle structure to date. Firstly, the frequency dependence of focusing of S wave amplitudes was used to estimate the size and amplitude of the plume velocity anomaly. We determined that the plume has a radius of about 100 km with a peak S-velocity anomaly of -12%. This amplitude of the anomaly is considerably larger and the plume is considered much narrower than deduced from previous estimates using classical travel time tomography.

In the second approach we now return to more classical travel-time tomography. Knowledge of the crustal structure allows accurate correction for near-surface variations which cannot be resolved using teleseismic data. The slice through the 3D model shown in the figure shows a plume-like low velocity anomaly extending from 500 km up to ~200 km and confirms the narrow width of the plume. The velocity anomaly below the crust is not yet known in absolute value, but from this preliminary image we may conclude that lateral variations are small and the plume seems to spread out at least over the full width of the island.

For further reading:

Allen, R.M., Nolet, G., Morgan, W.J., Vogfjord, K., Bergsson, B.H., Erlendsson, P., Foulger, G.R., Jakobsdottir, S., Julian, B.R., Pritchard, M., Ragnarsson, S., Stefansson, R., The thin hot plume beneath Iceland, *Geophys. J. Int.*, **137**, 51-63, 1999.

The Hawaiian SWELL Experiment: An Example for the Need of Ocean Bottom Seismograms

G. Laske, J. Orcutt and J. Phipps Morgan, University of California, San Diego

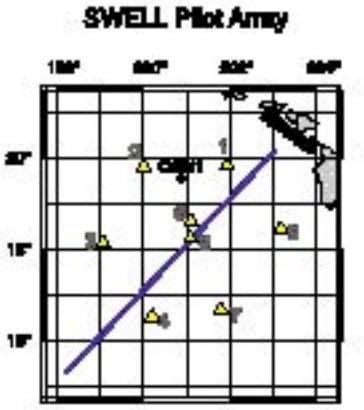

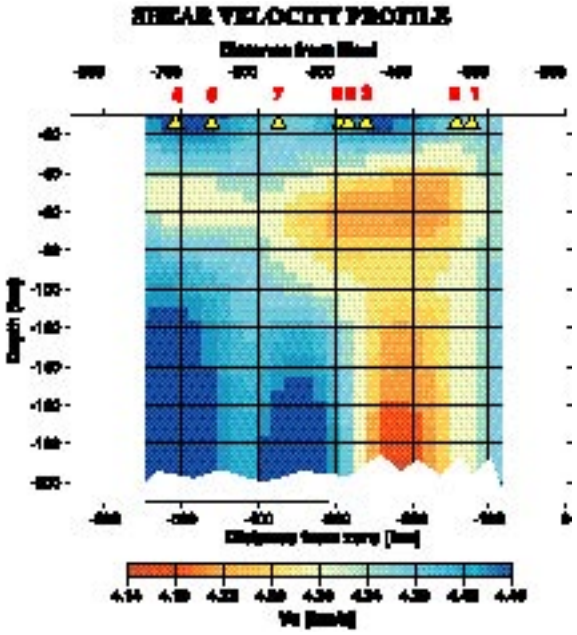

Until recently, seismic tomographic studies of the Hawaiian plume have been restricted to using land-based recordings. The limitation of such studies is obvious: the data coverage is inadequate to image the proposed plume conduit and details of the seismic structure around Hawaii on scale-lengths less than several hundreds of kilometers. Hence, it is not too surprising that even the location of the plume conduit currently is not known.

Several years ago, we proposed a "PASSCAL experiment in the Ocean," a regional surface wave study using ocean bottom instruments. In 1997, we received NSF funding for a proof-of-concept pilot deployment between April 1997 and May 1998 to the southwest of the Hawaiian Islands. We used the SIO L-CHEAPO dataloggers (Low-Cost Hardware for Earth Applications and Physical Oceanography) with differential pressure sensors. Such instruments enable us to record teleseismic intermediate-period Rayleigh waves between 15 and 70 seconds. The pilot experiment was successful in many respects and resolved important issues: (1) the equipment is adequate for deployment in long-term experiments, (2) the equipment is adequate for recording surface waves in the required period band, (3) we are able to record enough high-quality seismograms in a year-long deployment, and (4) surface wave dispersion can be measured with a precision high enough to reliably constrain the seismic structure in the study area. We analyzed over 70 events and found significant heterogeneity in seismic structure across the array. Seismic velocities are clearly reduced within roughly 300 km of the island chain and the extent of the anomalous region reaches at least into the lower lithosphere.

The results of this experiment demonstrate that the time is ripe to extend passive regional seismic experiments into the oceans. For example, it is important to recall that the North American continent does not extend to the tidal mean high water mark, but extends well out to sea on the continental margin and slope. Planning for USArray must therefore include an ocean component to understand the structure of the continents. Discussions with both Earth Sciences and Ocean Sciences are ongoing on this matter.

For further reading:

G. Laske, Phipps Morgan, J., and Orcutt, J.A., First results from the Hawaiian SWELL Pilot Experiment, *Geophys. Res. Let.*, **26**, 3397-3400, 1999.

Broadband Seismology in the Oceans: Lessons from the Ocean Seismic Network Pilot Experiment

John Collins and Ralph Stephen, Woods Hole Oceanographic Institution
Frank Vernon and John Orcutt, Scripps Institution of Oceanography

The fundamental objective of the Ocean Seismic Network Pilot Experiment (OSNPE) was to learn how to make sustained, high-quality, broadband seismic measurements in the deep oceans. The experiment was carried out at Ocean Drilling Program Site 843B (OSN-1) 225 km southwest of Oahu, Hawaii from late January to early June 1998. At site OSN-1, three broadband seismographs were deployed adjacent to each other. The seismometers were: (i) a Teledyne GeoTech KS-54000 deployed at the sediment-basement interface 242.5 m beneath the seafloor in a borehole, (ii) a Guralp CMG-3T deployed on the seafloor, and (iii) a Guralp CMG-3T buried just beneath the seafloor.

The OSNPE demonstrated that broadband seismic data of a quality similar to that achievable with land instruments can be recorded in the deep ocean. However, the location of the seismometer – whether it be on the seafloor, surficially buried in the seabed, or in a deep borehole – has a profound effect on data quality. The two most striking results of the OSNPE were the low ambient noise levels of the surficially-buried seismometer (station OSN1B) in the long-period band (< 0.1 Hz; Figure) and of the borehole seismometer (station OSN1) in the short-period (> 0.1 Hz) band. For station OSN1B, the high signal-to-noise of the long-period data on all three components – comparable to that of a good PASSCAL station - is attributable to the fact that the seismometer was buried in the seabed, and hence was not subjected to tilt accelerations generated by seafloor currents pushing on the seismometer. Over 202 teleseisms were observed on station OSN1B, ranging in size from an M_s 3.6 at 35° epicentral distance to the 8.1 M_w Balleny Island earthquake at 91° epicentral distance. Remarkably, all of these events were well-recorded on all three seismometer components. The most distant event detected was a m_b 4.8, M_s 5.8 earthquake near Price Edward Island on the Southwest Indian Ridge at 150° epicentral distance. In the short-period band, the location of the borehole seismometer well below the seafloor interface means that the amplitude of evanescent interface waves is reduced. Consequently, the short-period, teleseismic detection limit for station OSN1 is significantly less than for the seafloor and near-seafloor stations.

The OSNPE was jointly funded by NSF-OCE, IRIS, WHOI, and SIO.

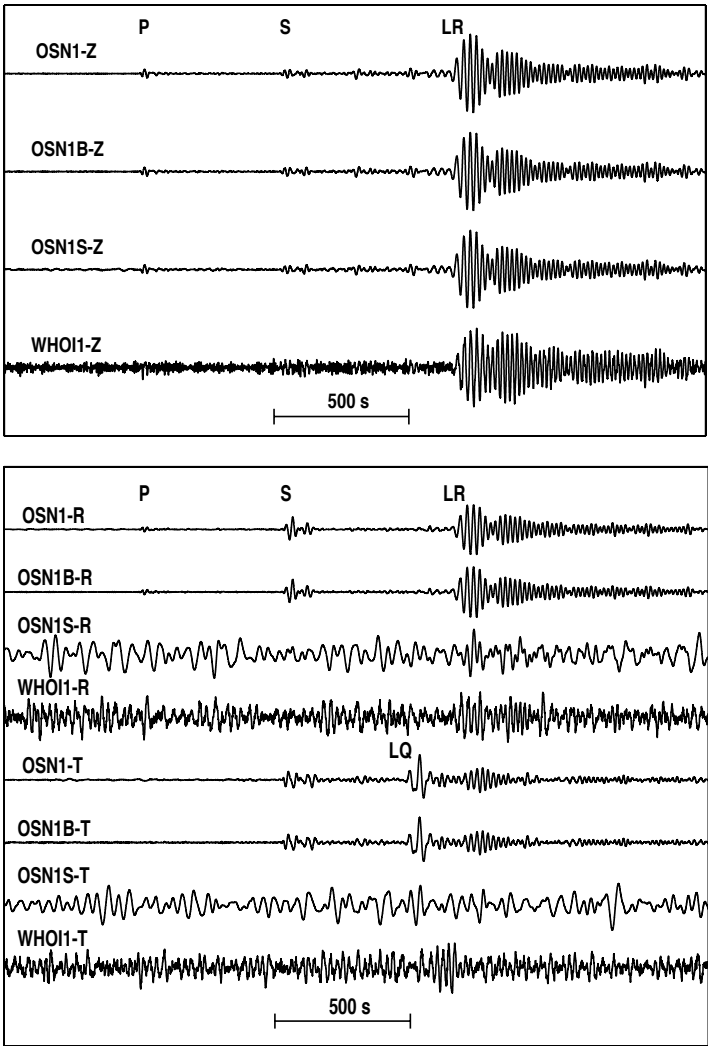

OSNPE seismograms of the 05/10/1998 m_b 5.8 (IDC REB), M_s 6.0 (IDC REB) earthquake offshore Guatemala. Focal depth is 34 km, and the epicentral distance is 65°. The seismometer for station OSN1 was installed ~240 m below the seafloor at the sediment-basalt interface, that for station OSN1B was buried surficially in the seabed, while the seismometers for station OSN1S and WHOI1 sat on the seafloor. Stations OSN1, OSN1B, and OSN1S were equipped with broadband seismometers; station WHOI1 had a short-period (1 Hz) seismometer only. Data are filtered 20-50 s. (top) Vertical components. (bottom) Horizontal components. Stations OSN1 and OSN1B show clear P, S, LR and LQ phases. These phases are not seen on the horizontal-component data from stations OSN1S and WHOI1.

The Time Dependence of Ambient Noise Beneath the Deep Sea Floor

R A Stephen, S T Bolmer, J A Collins, K R Peal, Woods Hole Oceanographic Institution
J A Hildebrand, J A Orcutt, F N Spiess, F L Vernon, Scripps Institution of Oceanography

Between February and May 1998, the Ocean Seismic Network Pilot Experiment (OSNPE) acquired over 115 days of broadband borehole seismic data at ODP Site 843B in 4407m water depth off Oahu. The borehole seismometer was clamped in casing within the upper 6m of igneous basement beneath 242 m of sediment. In addition to over 50 earthquake events that were observed, ranging from a 4.5 Mb event at 44° epicentral distance to the 7.9 Mw Balleny Islands earthquake at 91° epicentral distance, this data set provides an opportunity to study the time dependence of ambient noise in a borehole in the deep sea over a four month duration. The ambient noise behavior falls into four distinct frequency bands. In the infra-gravity band, 1-10mHz, where ambient noise levels are greater than levels on the co-located buried sensor, there is a strong tidal frequency dependence indicating that water flow in the hole, past the instrument, may be exciting installation noise. The largest amplitude changes occur in the noise notch, 10-50 mHz, where vertical component noise varies from the quietest levels observed world-wide [-185dB re: 1$(m/s^2)^2$/Hz] to levels above -120dB re: 1$(m/s^2)^2$/Hz after the Balleny Islands earthquake. The microseism band, 50-300mHz, is characterized by three peaks. Levels of the single frequency micro-seism peak at 60 mHz can increase 60 dB after a large earthquake. The levels of the two double frequency micro-seism peaks, one each from distant and local sources, is much less variable (less than 20dB) and is related to sea state. The short period band (or HOLU spectrum), 300 mHz to 7.5 Hz, consists of a set of peaks that correspond to shear modes in the seafloor which are excited by local sea state. Above 5 Hz there is a weak tidal dependent effect, primarily on the vertical component, which could be related to bottom currents washing against the re-entry cone.

All of the broadband data are available through the IRIS Data Management Center. This work was sponsored by the National Science Foundation, IRIS, Joint Oceanographic Institutions, Scripps Institution of Oceanography and Woods Hole Oceanographic Institution.

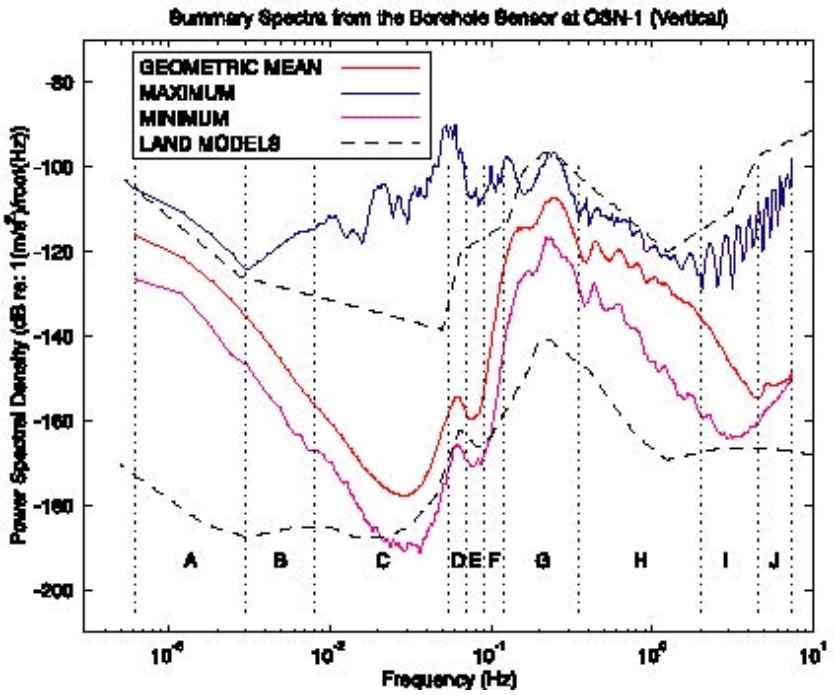

Power spectral densities in the band 0.6mHz to 7.5Hz were computed in approximately two hour windows for the whole data set acquired on the Ocean Seismic Network Pilot Experiment. The geometrical mean of all of the spectra and the largest and least spectral values at each frequency are shown in this figure for the vertical component data. The USGS high- and low-noise models, which are based on a synthesis of data from land and island stations, are also shown for comparison. The labels indicate frequency bands in which the time dependence of ambient noise has similar behavior. The very high levels in bands B through F are arrivals from the large (Mw=7.9) Balleny Islands earthquake on Julian Day 84. In bands C through F and I the borehole sensor on the seafloor was as quiet as the quietest land stations. At the microseism peak, band G, where the source of the ambient noise is loading by surface swell, the seafloor sensor has high noise levels.

For further reading:

Collins, J.A., Vernon, F.L., Orcutt, J.A., Stephen, R.A., Peal, K.R., Wooding, F.B., Spiess, F.N. and Hildebrand, J.A., Broadband seismology in the oceans: lessons from the Ocean Seismic Network Pilot Experiment, *Geophys. Res. Lett.,* submitted, 2000.

Stephen, R.A., Collins, J.A., Peal, K.R., Hildebrand, J.A., Orcutt, J.A., Spiess, F.N., and Vernon, F.L., Seafloor seismic stations perform well in study. *Trans. AGU* (EOS), **80**, 592, 1999.

Repeating Deep Earthquakes in the Tonga Subduction Zone

Douglas Wiens, Washington University

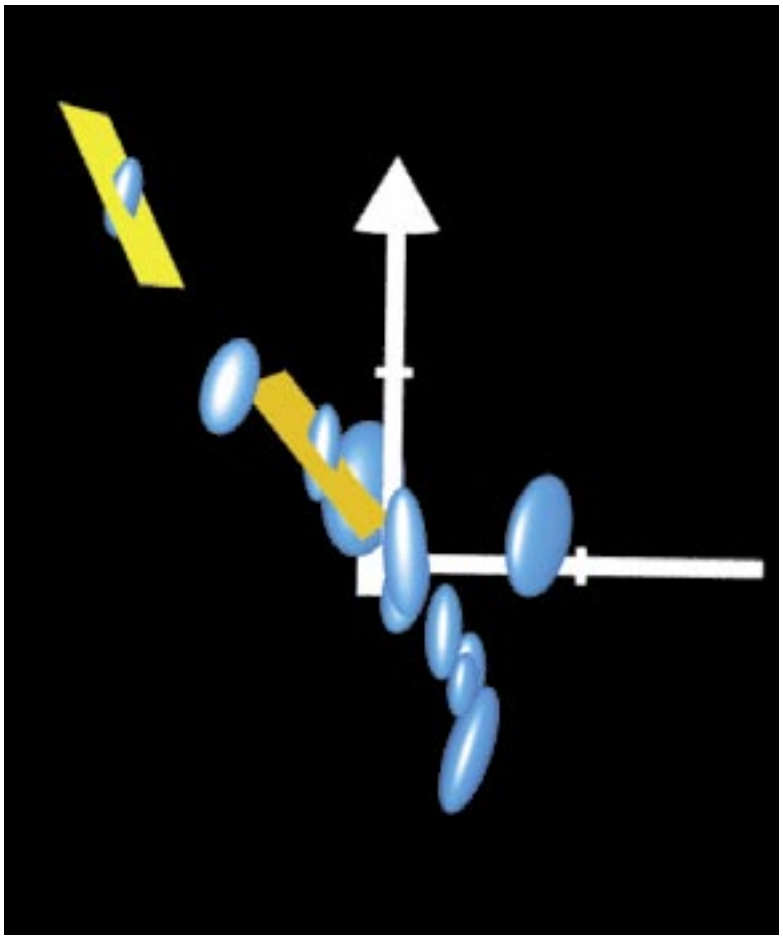

Visualization of a dense region of deep earthquake epicenters in Tonga observed during the PASSCAL SPASE seismic experiment. Earthquakes show similar waveforms and are located using a cross correlation technique. Ellipsoids show 95% uncertainty regions, and yellow planes denote fault planes obtained from CMT solutions of the larger events. Coordinate axes point north and east, and tic mark spacing is 10 km. Some of the earthquakes are co-located to within 1-2 km, such that their rupture zones overlap. These events demonstrate repeated slip along the same fault plane at great depth.

Waveforms from some deep earthquakes in highly seismic regions of the deep Tonga slab show exceptional similarity at stations of the Southwest Pacific Seismic Experiment (SPASE); the waveforms are often similar down to the smallest details of the scattered coda waves. We locate the earthquakes using a cross-correlation relative location scheme. This method allows us to locate the rupture centroids with maximum relative travel time residuals of about 0.1 s. The earthquakes show a planar alignment that is coincident with fault planes of the larger earthquakes obtained from CMT solutions. The maximum width of these fault-like structures is on the order of 3 km. The relative relocation shows that some of the larger events are co-located to within 1-2 km. Since seismic scaling laws predict fault dimensions of about 7 km for earthquakes of this moment (Mw 5.5), this observation suggests that rupture can reoccur along deep earthquake faults.

This observation poses difficulties for models of deep earthquakes that rely on nonreversible and non-repeatable mechanisms, such as phase transformations. For example, the transformational faulting hypothesis suggests that deep earthquakes are associated with the metastable transformation of olivine to spinel, a process that could not reoccur on the same fault. The observation that deep earthquakes can reoccur along the same fault suggests that the main process of deep earthquake rupture propagation must involve some process other than transformational faulting, such as melting, ductile shear instabilities, or fluid-induced weakening.

For further reading:

Wiens, D.A., and Snider, N.O., Repeating deep earthquakes: Evidence for fault reactivation at great depth, *EOS Trans. Am. Geophys. Un.*, **80**, 667, 1999.

Earthquake Distribution in the Kermadec Forearc

Meredith Nettles and Göran Ekström, Harvard University
Richard Von Harzen, Woods Hole Oceanographic Institution
Seiichi Nagihara, University of Houston

Earthquakes occur frequently on the plate-bounding thrust fault of the Kermadec subduction zone, but their depths are often poorly constrained. We have modeled broadband P waves from earthquakes recorded at IRIS GSN stations between 1988 and mid-1993 in order to obtain better depth estimates for these events and to constrain more accurately the dip of the plate interface. Harvard CMT focal mechanisms for the 20 earthquakes analyzed are shown in the map, in lower hemisphere projection, and in the cross-section, in back hemisphere projection. The cross-section location is indicated in the map by the solid yellow bar, and each event is plotted at the depth determined in our study. A best-fit line through the hypocenters gives a dip of ~17° for the plate interface. The earthquakes studied were chosen to lie close to heat flow measurement profiles taken during cruise TT025 of the R/V *T. Thompson* in 1993; the approximate profile locations are indicated in the map as dashed yellow lines. The geometrical constraints provided by the seismological analysis have been utilized by Von Herzen et al. (1999) in a model of 2-D thermal conduction, based on steady-state subduction and heat generation along the thrust fault as a result of shear stress, to predict heat flow along these profiles. Comparison with the predicted values shows that the heat flow measurements are consistent with either a uniform shear stress on the fault of 50 ± 25 MPa or a linearly increasing stress with distance from the trench of 0.5± 0.25 MPa/km. The estimated shear stress on the fault is thus at least one order of magnitude smaller than the overburden stress.

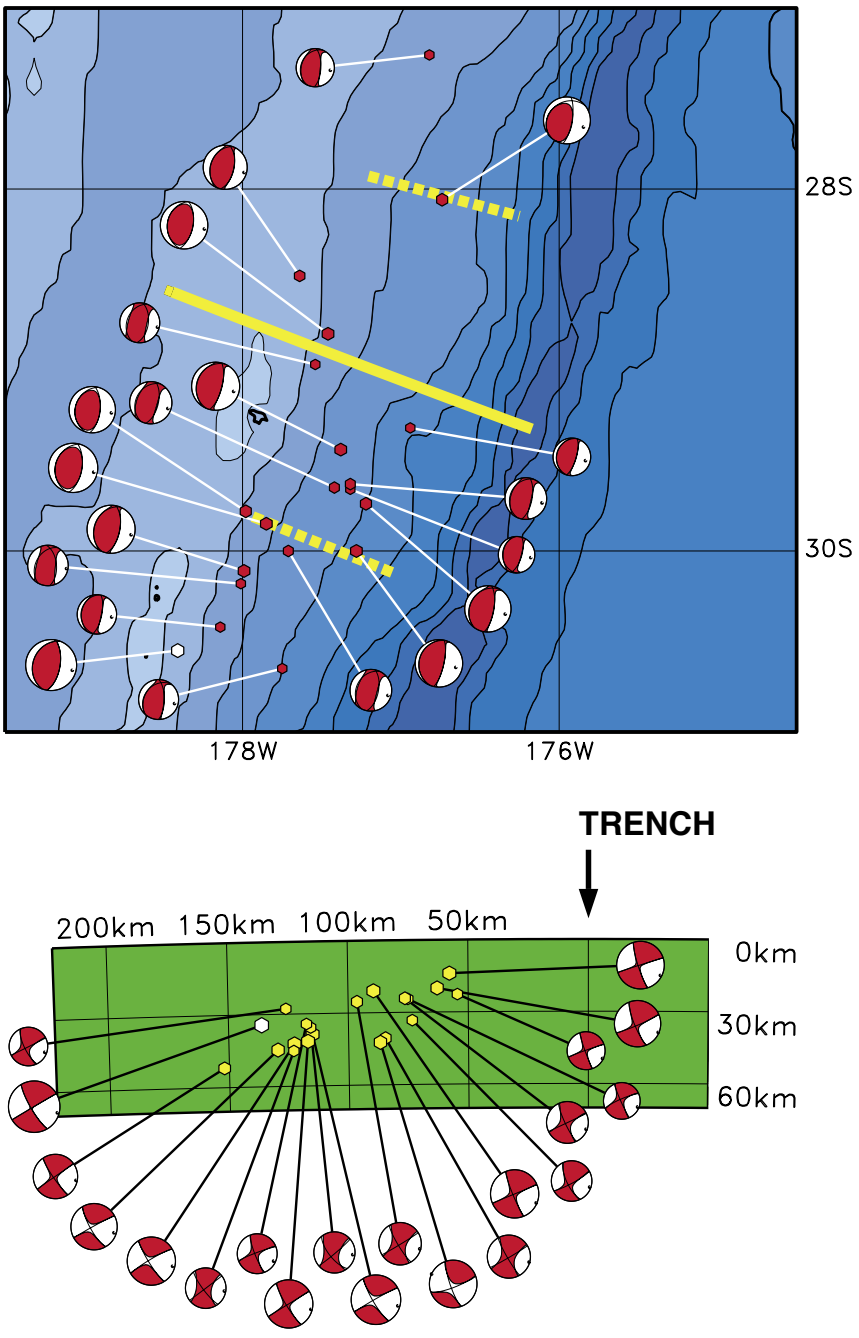

For further reading:

Von Herzen, R. P., Molnar, P., Ruppel, C., Nagihara, S., Nettles M., and Ekström, G., Geothermal and earthquake data from the Kermadec forearc: Implications for shear stress on the thrust fault, *Eos Trans. AGU*, **80**, F920, 1999.

The 2 June, 1994 Java Earthquake: Rupture Over a Subducted Seamount

Michael Antolik, Rachel E. Abercrombie, Karen Felzer, and Göran Ekström, Harvard University

Earthquakes that excite anomalously large tsunamis compared with their seismic moment are widely believed to result from rupture in low-rigidity subducted sediments close to the trench axis. These "tsunami earthquakes" commonly exhibit low energy release in the frequency range 0.1-1 Hz, presumably because of a slow rupture speed in these sediments (Newman and Okal, 1998). A large tsunami results from the confinement of rupture to very shallow depths and corresponding large deformation of the seafloor (Kanamori and Kikuchi, 1993; Satake and Tanioka, 1999).

An interesting tsunami earthquake occurred south of Java, Indonesia in June, 1994. Tsunami runup heights reached as large as 14 m on the south coast of the island. Although the mainshock (Mw 7.8) occurred on the thrust interface between the Australian and Eurasian plates, all of the aftershocks listed in the Harvard CMT catalog have extensional focal mechanisms. The mainshock represents the only large thrust earthquake to occur along this part of the Java trench since 1977. We used broadband and long-period body waves recorded by GSN stations to determine the spatial and temporal history of moment release in the mainshock. We also examined the long-period source spectrum to search for a slow component of rupture.

Using geometrical constraints and the fit to teleseismic body waves, we obtain an accurate estimate of 16 km for the depth of the hypocenter. Rupture proceeded downdip and eastward from the hypocenter along the thrust interface. The seismic data indicate that the main energy release was confined to a depth of 20-25 km below the seafloor, and we find no evidence for shallow slip near the trench. The location of the main energy release corresponds well with a large bathymetric high. This feature, located 50-100 km from the deepest part of the trench, is probably a result of deformation in the overriding plate caused by a seamount that has been subducted (Masson et al., 1990). The source spectrum shape shows no evidence for slow rupture and is well fit using a low stress drop model of about 3 bars.

Based on these observations, we propose that the age of the subducting lithosphere and predominance of normal-faulting earthquakes point to the nearly complete decoupling of the two plates except for the region over the subducted seamount. This area is completely coupled as a result of its differing frictional properties. The low stress drop in the mainshock can be explained by partial extension of the main rupture into the surrounding decoupled region. Instead of rupture near the trench we propose that the larger than expected tsunami resulted from displacement of water by the bathymetric high (Tanioka and Satake, 1996) slumping on its slopes, or generation closer to shore than previously believed. Either the 1994 Java earthquake is not typical of most tsunami earthquakes, or the presumed source model for tsunami earthquakes needs to be modified.

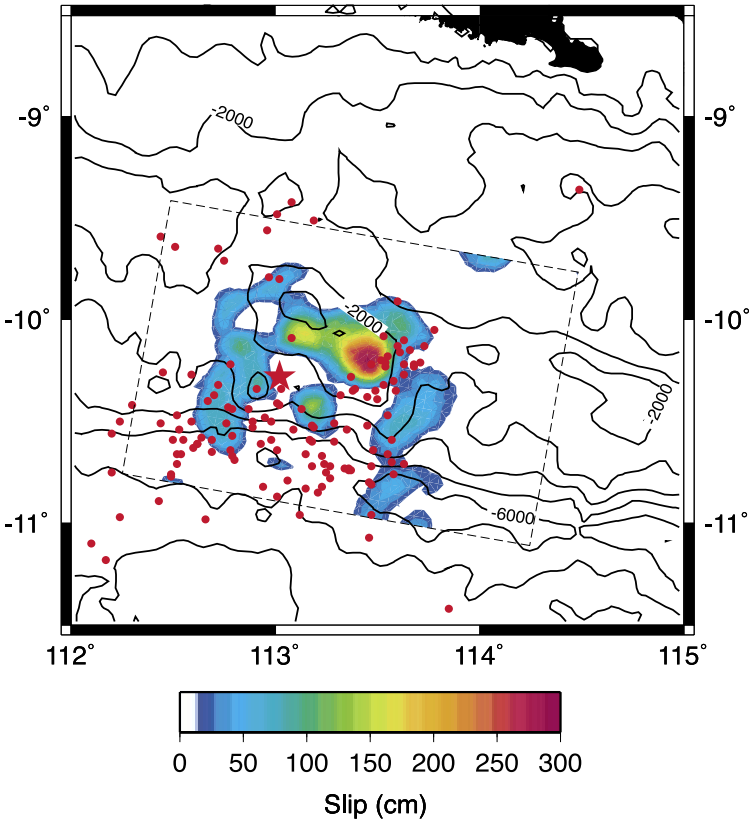

from inversion of teleseismic body waves. Red dots indicate aftershocks relocated in this study using a three-dimensional velocity model. The hypocenter is indicated by the star. Solid black lines are contours of bathymetry at 1000 m intervals. The largest asperity ruptured in the earthquake is located under a broad bathymetric high located shoreward of the Java trench. This feature probably lies over a seamount on the subducting plate. The black area at top is the coast of Java.

For further reading:

Kanamori, H., and M. Kikuchi, The 1992 Nicaragua earthquake: A slow tsunami earthquake associated with subducted sediment, *Nature*, **361**, 714-715, 1993.

Masson, D. G., Parson, L.M., Milsom, J., Nichols, G., Sikumbang, N., Dwiyanto, B., and Kallagher, H., Subduction of seamounts at the Java Trench: A view with long-range sidescan sonar, *Tectonophysics*, **185**, 51-65, 1990.

Newman, A. V., and E. A. Okal, Teleseismic estimates of radiated seismic energy: The E/Mo discriminant for tsunami earthquakes, *J. Geophys. Res.*, **103**, 26,885-26,898, 1998.

Satake, K., and Y. Tanioka, Sources of tsunami and tsunamigenic earthquakes in subduction zones, *Pure and Applied Geophys.*, **154**, 467-483, 1999.

Tanioka, Y., and K. Satake, Tsunami generation by horizontal displacement of ocean bottom, *Geophys. Res. Lett.*, **23**, 861-864, 1996.

Noncharacteristic Behavior and Complex Recurrence of Large Subduction Zone Earthquakes

Susan Y. Schwartz, University of California, Santa Cruz

The last five years have been remarkable with respect to the number of large underthrusting earthquakes in subduction zones that reruptured plate boundary segments that failed in previous great events. Availability of seismic data from the GSN has made it possible to compare the spatial distribution of moment release for two consecutive large earthquakes rupturing the same portion of the plate interface. Such comparisons have been made for the plate boundary segments that failed in: (1) the 1957 (Mw=8.6), 1986 (Mw=8.0), and 1996 (Mw=7.9) Aleutian Islands earthquakes; (2) the 1963 (Mw=8.5) and 1995 (Mw=7.9) Kuril Islands earthquakes; (3) the 1971 (Mw=8.0) and 1995 (Mw=7.7) Solomon Islands earthquakes; and (4) the 1968 (Mw=8.2) and 1994 (Mw=7.7) northern Honshu earthquakes. The spatial distribution of moment release for all four of the initial great earthquakes and two of the repeat events has been determined in previous studies. I have determined slip distributions for the three most recent events from inversion of source time functions, derived by empirical Greens function analysis of GSN long-period surface waves and broadband body waves. Comparisons of the spatial distribution of moment release for sequential earthquake ruptures reveal considerable differences in the pattern of recurrent fault slip. The 1994 northern Honshu and 1995 Solomon Islands earthquakes primarily fill in areas of slip deficit left by their preceding events rather than rerupture identical asperities. The 1995 Kuril Islands and the 1996 Aleutian Islands earthquakes both rerupture portions of an asperity distribution defined by preceding events but with variable amounts of slip. This study provides the first direct evidence that recurrence of large circum-Pacific plate boundary events is more complex than repeat rupture of dominant asperities. Recurrent fault slip for the four plate boundary segments studied does not support characteristic slip models either where failure on an entire fault segment occurs repeatedly in events with nearly identical rupture lengths, locations, and slip magnitudes or where failure of individual asperities occurs with identical slip functions through consecutive earthquake cycles. These sequential slip patterns are not consistent with physical models of earthquake rupture where slip complexity is exclusively controlled by invariant geometric and/or material heterogeneity but suggest that dynamic considerations are also important.

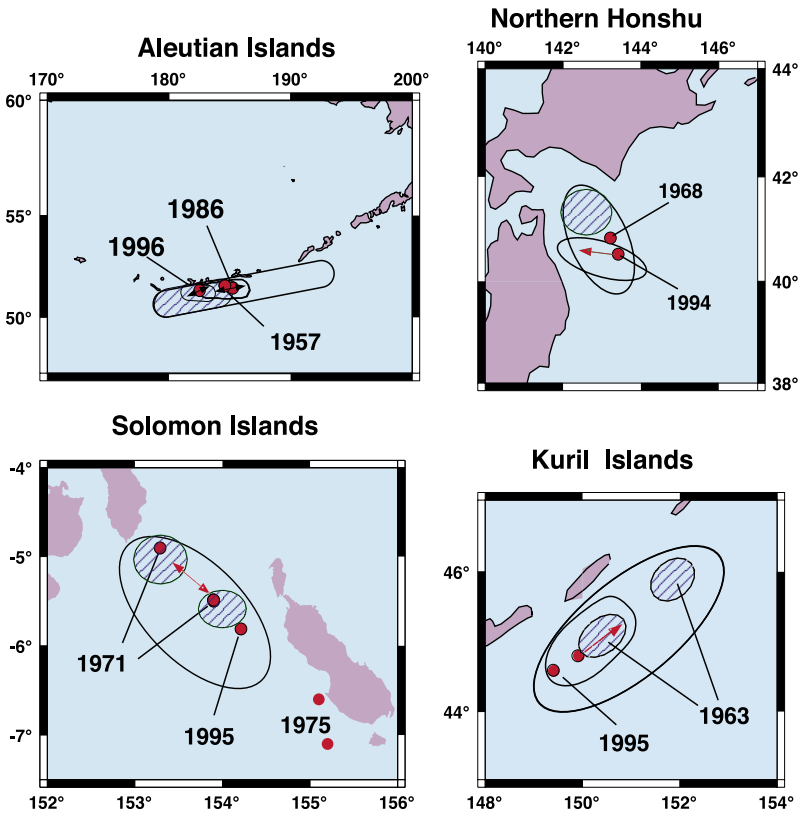

Comparisons of recurrent slip in four subduction zones. Blue hatchured regions show asperity locations for the initial great earthquakes and the arrows show locations of concentrated slip in the subsequent events.

For further reading:

Schwartz, S.Y., Noncharacteristic behavior and complex recurrence of large subduction zone earthquakes, *J. Geophys. Res.*, **104**, 23,111-23,125, 1999.

Mining Subducting Plates with Seismograms

Geoffrey Abers, Boston University

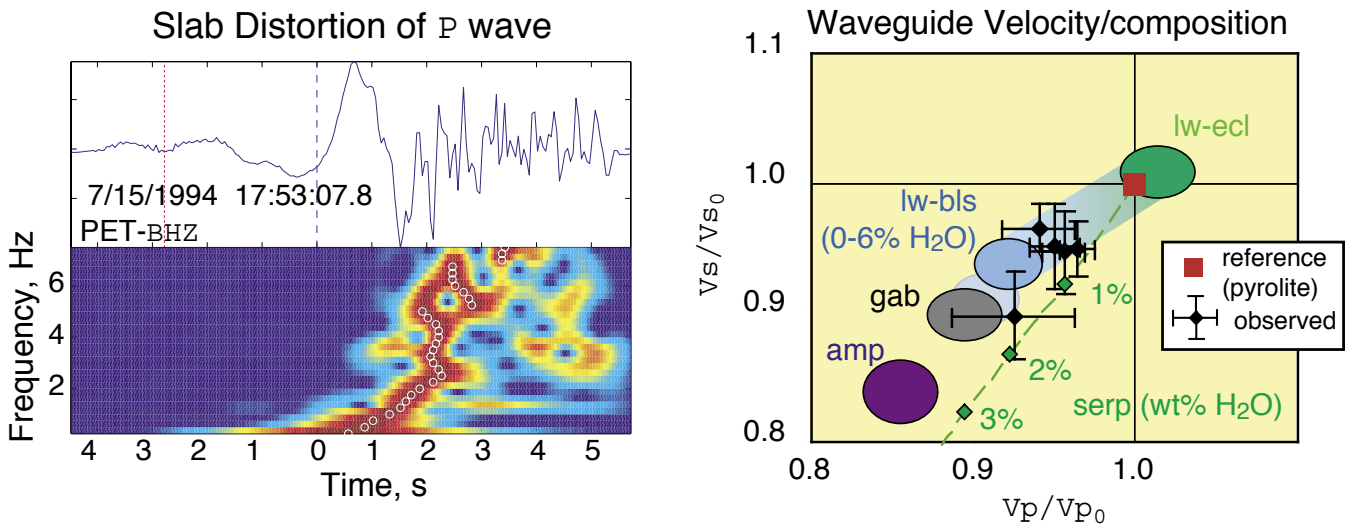

Body waves, distorted by subducting slabs, place constraints on their water content. (Left) Distorted P wave recorded at GSN station PET, Kamchatka and corresponding spectrogram (frequency-time plot). Signal propagates 500 km along the slab surface from event 118 km deep, and high frequencies are delayed 1.5 - 2 sec relative to the low-frequency arrival. (Right) summary of velocities inferred for five arcs from similar analyses (Alaska, Aleutian, Kurile, Japan, Mariana). Mineral P and S velocities calculated for various assemblages at 4 GPa and 650°C, the approximate conditions sampled by the seismic signals at top of slabs. Observed Vp and Vs are that of waveguide relative to surrounding medium; petrologic estimates are relative to nominal dry mantle.

As oceanic crust subducts, it is thought to undergo a series of transformations through blueschist to eclogite facies, becoming both denser and seismically faster. These transformations should release water along the way. Depending upon their sequencing, the release may provide a good explanation for the volcanic front (where, generally, slabs reach 100 km depth) and for the generation of intermediate-depth earthquakes. Still, basic observational constraints had been contradictory, even in the sign of the relevant seismic anomalies.

Tremendous growth of the GSN has greatly increased the seismic sampling of subduction zones. Numerous GSN stations lie atop arcs and sample wave propagation in subucting plates. Such recording at regional distances (<1000 km) has unexpectedly provided a wealth of information on subduction structure. Many of the most interesting slab-related seismic effects come from interaction between high-frequency (>0.5 Hz) seismic waves and the very top of the subducting plate, where oceanic crust is descending into the mantle.

Utilizing several GSN stations at north Pacific arcs, we observe systematic distortion of seismic body waves that travel along the top of subducted slabs (Abers, 2000). These signals (Figure) show characteristic and strong dispersion, which in all cases results in the delay of high-frequency energy relative to the dominant low-frequency first arrival. Such dispersion of P and S waves can be simply explained as a consequence of a low-velocity waveguide atop subducting plates, a few km thick, that is 5-8% slower than surrounding mantle. Not only are all north-Pacific slabs similarly slow, all show similar degrees of dispersion for waves traversing the slab at 100-200 km depth. (The one apparent exception, signals from Tonga earthquakes recorded in New Zealand, occur only on a single path that is considerably deeper, so may reflect local path effects or deeper structure.) If these layers indeed represent oceanic crust, as they appear to, their presence suggests that oceanic crust persists as a slow, probably hydrated layer well past the volcanic front, and that eclogite formation is suppressed. One petrologically consistent scenario is for the persistence of some slow hydrous phases well below the blueschist stability field, for example some amphiboles or chlorites, although to date little experimental work has been done at relevant temperatures (Figure). Continued analysis of these GSN data, coupled with focused PASSCAL (and PASSCAL + OBS) experiments, is beginning to provide the data needed to image these remote regions at scales relevant to the processes that operate there.

For further reading:

Abers, G.A., Hydrated subducted crust at 100-250 km depth, *Earth and Planet. Sci. Lett.*, **176**, 323-330, 2000.

Transition Zone Anisotropy Below the Tonga-Fiji Subduction Zone

Renate Hartog, University of Wisconsin-Madison
Susan Y. Schwartz, University of California at Santa Cruz

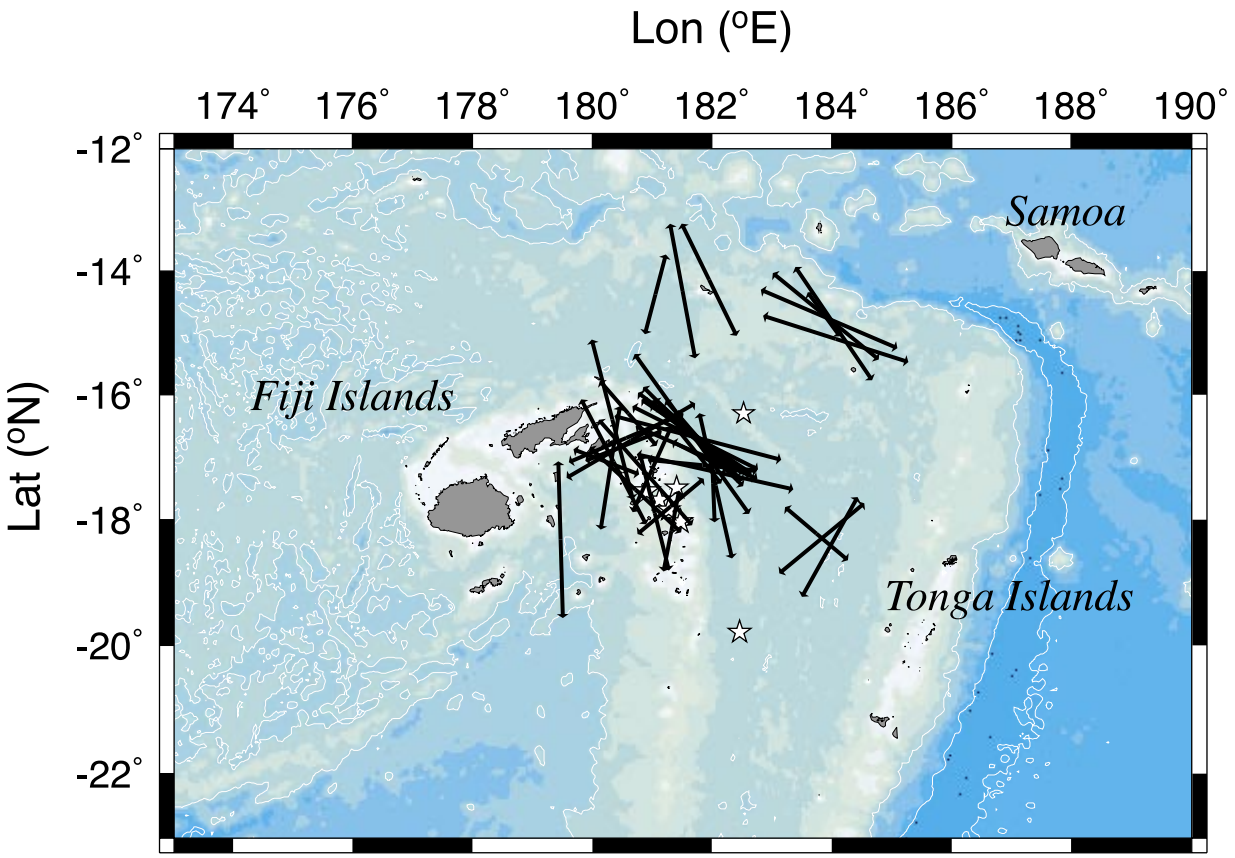

Bathymetry map of the study region with individual splitting parameters (arrows, orientation is parallel to the fast polarization direction, length is proportional to the delay time between fast and slow shear wave) shown at the intercept of each teleseismic ray with a depth of 700 km. Earthquake locations are indicated by white stars.

The IRIS Data Management Center facilitates easy access to seismic data from a global network of digital broadband stations, which has allowed us to study the anisotropic properties of the transition zone beneath the Tonga-Fiji subduction zone. Although the transition zone between Earth's upper and lower mantle may signify a boundary layer between two partly decoupled convective regions where strain may localize, seismic evidence for anisotropy within the transition zone is scarce and inconclusive.

We present teleseismic observations of shear waves generated by several deep-focus (h≥400 km) earthquakes in the Tonga-Fiji subduction zone that show strong evidence for anisotropy beneath the source, i.e. in the lower transition zone. After correction for receiver-side anisotropy, residual splitting is observed at seismic stations at various azimuths from the earthquakes. In all cases, the S-phases turn above the D" region and the splitting can therefore not result from anisotropy in the lowermost mantle. We assume that most of the lower mantle is isotropic and attribute the splitting to anisotropy near the source region. The splitting parameters obtained show variability, however, the fast polarization directions are predominantly NW-SE and the delay times are large, 1.15-2.50s. In the study region the Tonga-Fiji slab is deflected sub-horizontally within the transition zone and its geometry shows along strike variations. A plausible cause of the anisotropy is the alignment of anisotropic minerals within the subducted slab due to the strain associated with the distortion of the slab. However, elastic anisotropy of the uppermost lower mantle cannot be ruled out. Continued investigation of spatial variations of the observed splitting will allow us to determine exactly where the anisotropy is located and therefore teach us about the mineralogical properties and dynamics of the lower transition zone and/or uppermost lower mantle.

Outboard Earthquakes Disassociated With Fast Seismic Wave Speeds in the Transition Zone Beneath the Tonga Back-Arc: Metastable Olivine or Melt?

Michael R. Brudzinski and Wang-Ping Chen, University of Illinois

In the transition zone of the mantle, a narrow, sub-horizontal swath of "outboard" earthquakes extends nearly 800 km to the west of the inclined Tonga Wadati-Benioff zone. In a previous study, we reported that the seismogenic region itself is surprisingly NOT associated with high P-wave speeds (Vp), even though an adjacent region of fast Vp (+3%) exists immediately to the south of the outboard earthquakes. This observation is now corroborated by a similar distribution of shear-wave speeds (Vs), established by modeling 150 broadband SH waveforms.

The association of deep earthquakes with cold temperature in subducted lithosphere is well established. Furthermore, cold temperature is expected to raise both Vp and Vs. Thus it appears that the effect of cold temperature, as implied by the presence of large deep-focus earthquakes, must have been counteracted by other factors such as pronounced variations in composition or mineralogy.

Two obvious candidates for triggering earthquakes and lowering both Vp and Vs in the mantle transition zone are: (1) a small amount of melt induced by volatiles, or (2) metastable olivine in the cold core of subducted lithosphere. Combining measurements for both Vs and Vp provides a potential diagnostic to differentiate the two candidates: The fractional reduction in shear-wave speed by a moderate amount of melt (~5%) is expected to be twice as large as that in P-wave speed. Contrary to this scenario, however, our results show that fractional reductions in Vs and Vp are comparable in the source region of outboard earthquakes. Meanwhile, metastable olivine remains a viable candidate to account for the curious absence of fast P- and S-wave speeds in the source zone of deep earthquakes.

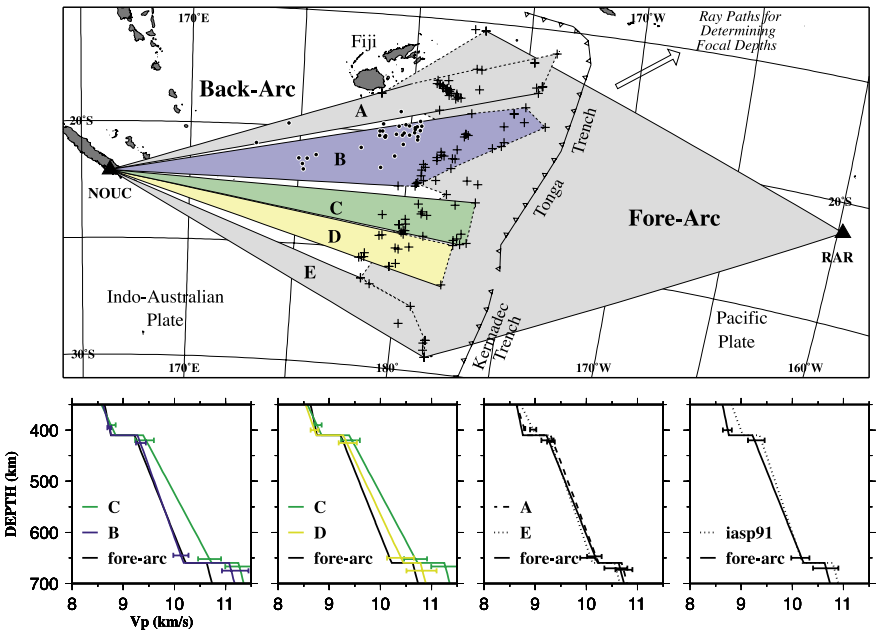

(Top panel) Map showing azimuthal sectors (A–E and fore-arc) used to delineate lateral variations in Vp. Solid circles indicate an unusual, sub-horizontal region of "outboard" earthquakes that occur in the transition zone of the mantle but are removed from the inclined Wadati-Benioff zone. Crosses indicate epicenters of intermediate- and deep-earthquakes (>50 km) within the Wadati-Benioff zone whose waveforms recorded at broadband stations NOUC and RAR are used in this study (solid triangles). For each event used, its focal depth is estimated from the timing of the pP phase recorded at teleseismic stations along azimuths (large arrow) that span the fore- arc where Vp is laterally homogeneous. Labels A–E mark the approximate locations where most ray paths used in our experiment bottom near the mantle transition zone. As such, models shown in bottom panel are most sensitive to Vp near these locations. (bottom panel) Comparisons of Vp among sectors. For each horizontal error bar, its width indicates the range of acceptable Vp, and its vertical position marks a bound on the depths of seismic discontinuities. Vp beneath the fore-arc differs only slightly from that of the iasp91 average earth model. Lateral variations in the back-arc are limited by sectors A and E where Vp is similar to that of the fore-arc at depths below 410 km. In the transition zone, fast Vp occurs in sectors C and D, but not in sector B where outboard earthquakes occur. In the lower mantle, fast Vp is most prominent in sectors B and C. In sector C, the two fast Vp anomalies clearly overlap.

Anisotropy within an Active Back-Arc Basin System

Gideon P. Smith and Douglas A. Wiens, Washington University
Leroy Dorman and Spahr Webb, Scripps Institution of Oceanography
Karen Fischer, Brown University

We have made observations of seismic anisotropy in the Lau backarc basin using shear wave splitting analysis of local S waves from events within the subducted slab. These data were from a temporary deployment of PASSCAL instruments called the Southwest Pacific Seismic Experiment (SPaSE) and ocean bottom seismographs of the 1994 Lau Basin Ocean Bottom seismograph survey (LaBattS). Results of the splitting analysis are shown in Figure 1. Fast directions sub-parallel to the absolute plate motion are indicated in the western part of the basin and island arc. However, closer to the plate boundary readings become more trench parallel. This is not easily explained by simple models of mantle strain resulting from flow coupled to the downgoing plate. Instead, it indicates complexity, as suggested by the modelling of Buttles and Olson (1999), where the flow patterns depend on the angle of convergence. The observations at the western end of the OBS line are consistent with the modelling of Fischer et al (1999). Although large (1s) splitting times are observed at the western and eastern ends of the basin, much smaller measurements are recorded in the center of the basin. We infer that this effect is due to vertical flow associated with the spreading center, consistent with the modelling of Blackman et al (1996). Our anisotropic mapping is also consistent with the regional mantle flow recently indicated using geochemical tracers. Turner and Hawkesworth (1998) report helium isotope data indicating the Samoan plume enters the Lau Basin in the northwest through an opening tear in the Pacific plate. This inferred southward flow of Pacific mantle is consistent with the N-S fast directions we obtain in the central and eastern basin.

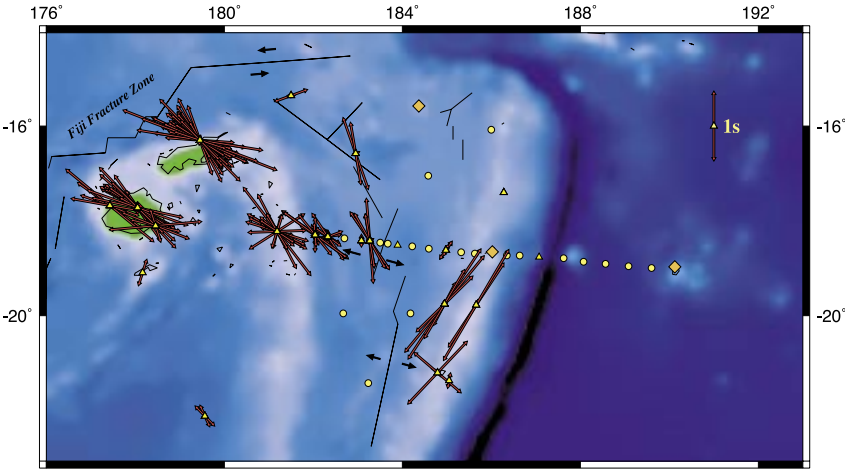

Figure 1: Splitting measurements at SPASE and LaBatts stations. Stations for which we have made positive measurements (including nulls) are shown as triangles. Splitting vectors are aligned parallel to the fast direction and their lengths are proportional to the splitting time.

We have also been examining the anisotropic signature from surface waves traversing the western end of the basin using data recorded during the same PASSCAL deployment. We used Rayleigh waves at 40 s period, which should have peak sensitivity in the range 50 to 55 km depth, and are thus relatively insensitive to crustal thickness variations. We pre-processed the data using a phase-matched filter technique (Russell et al, 1988). Application of a Wiener filter was used to estimate the Green's functions, and the interstation phase velocities then obtained from the phase spectrum of these Green's functions. Figure 2 shows that the Rayleigh wave phase velocities at 40 s period appear consistent with our splitting analysis confirming a fast direction N50W on the Fiji platform and an anisotropy of 3%.

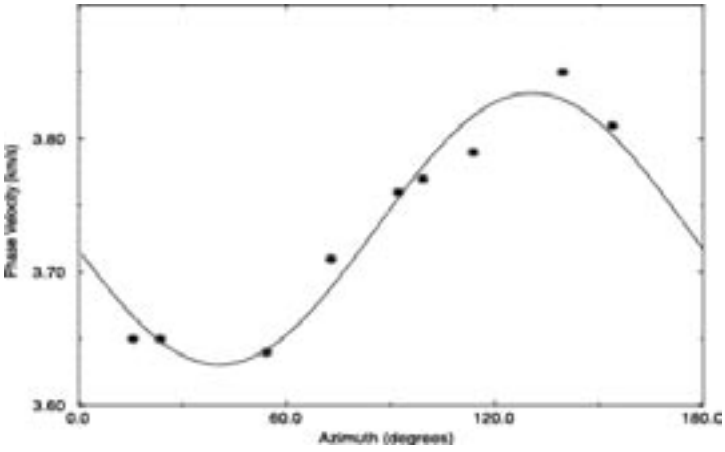

Figure 2: Rayleigh wave inter-station phase velocity estimates at 40s plotted as a function of azimuth (stars). The solid line is the best fitting function for an anisotropy with a 2-theta character.

For further reading:

Blackman, D.K., Kendall, J.-M., Dawson, P.R., Wenk, H.-R., Boyce, D., Phipps Morgan, J., Teleseismic imaging of subaxial flow at mid-ocean ridges: travel-time effects of anisotropic mineral texture in the mantle, *Geophys. J. Int.*, **127**, 415-426, 1996.

Buttles, J. and Olson, P., A laboratory model of subduction zone anisotropy, *Earth and Plan. Sci. Lett.*, **164**, 245-262, 1998.

Fischer, K.M., Parmentier, M., Stine, A.R., and Wolf, E.R., Modeling anisotropy and plate-driven flow in subduction zone back-arcs, submitted to *J. Geophys. Res.*, 1999.

Russell, D.R., Herrmann, R.B., and Hwang, H.-J., Application of frequency variable filters to surface-wave amplitude analysis, *Bull. Seis. Soc. Am.*, **78**, 339-354, 1988.

Turner, S., and Hawkesworth, C., Using geochemistry to map mantle flow beneath the Lau Basin, *Geology*, **26**, #11, 1019-1022, 1998.

Upper Mantle Structure of the Tonga Subduction Zone and Lau Back-Arc Spreading Center

Dapeng Zhao, Ehime University, Japan
Douglas Wiens, Washington University, St. Louis
Leroy Dorman, John Hildebrand, and Spahr Webb, Scripps Institution of Oceanography

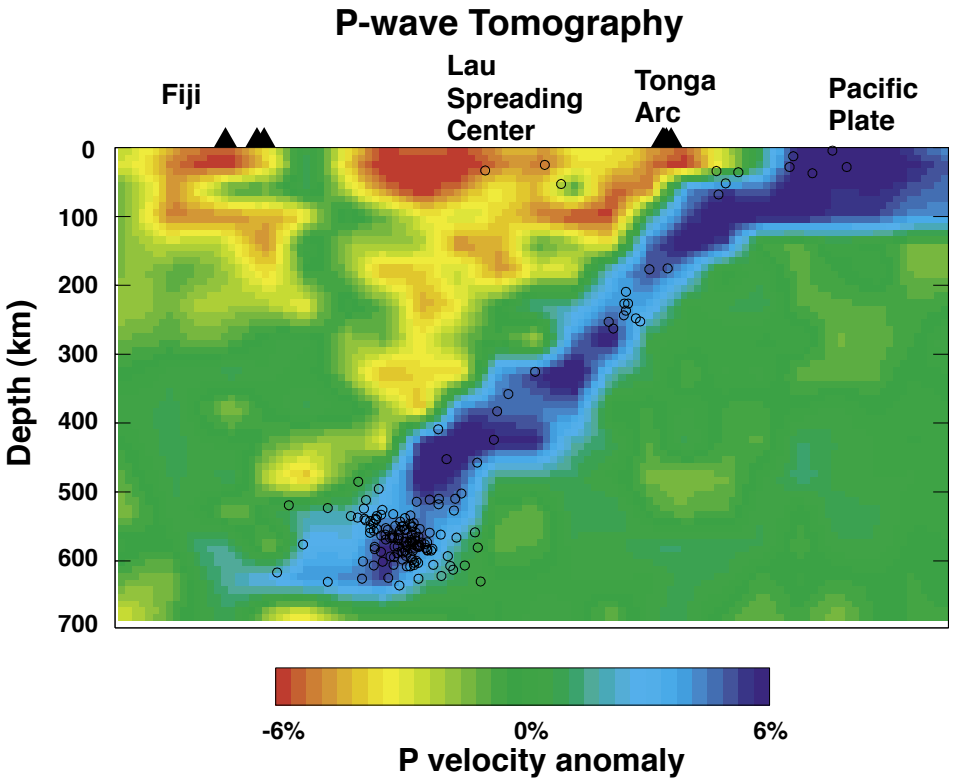

East-West cross section of the P-wave tomographic model of the Tonga-Fiji region [Zhao et al., 1997]. Red and blue colors denote slow and fast velocities, respectively. Circles denote earthquake locations, and triangles show the locations of island volcanos. Strong low velocity regions beneath the Tonga arc and Lau backarc spreading center probably represent the source regions for these lavas.

Knowledge of the seismic structure beneath island arcs and back-arc spreading centers is important for a variety of questions, including the dynamics of seafloor spreading, the geochemical source of arc and back-arc magmas, and the interaction between subducting slabs and arc and back-arc processes. A combination of a two year 12 station land PASSCAL deployment (SPASE) and a 3-month deployment of 30 ocean bottom seismographs (LABATTS) has produced this high resolution image of the velocity structure of the Tonga slab and Lau back-arc basin. A total of 41,471 P-wave arrival times from 926 earthquakes were used to construct this tomographic image. This image shows that very slow velocity anomalies (5-7%) beneath the active Lau spreading center extend to 100 km depth, and are connected to moderately slow anomalies (2-4%) in the mantle wedge to 400 km depth. This indicates that geodynamic systems associated with back-arc spreading are related to deep processes, such as the convective circulation in the mantle wedge and deep dehydration reactions in the subducting slab. The slow regions associated with the Tonga arc and the Lau back-arc are separated at the shallowest depths, but merge at depths greater than 100 km, suggesting that slab components of back-arc magmas occur through mixing at these depths.

For further reading:

Zhao, D., Xu, Y., Wiens, D.A., Dorman, L., Hildebrand, J., Webb, S., Depth extent of the Lau back-arc spreading center and its relationship to subduction processes, *Science*, **278**, 254-257 1997.

The Woodlark Rift Earthquake Seismology Transect, a PASSCAL Experiment

Geoffrey Abers and Aaron Ferris, Boston University
Mitchell Craig and Sioni Sioni, Univ. Papua New Guinea
Art Lerner-Lam, Columbia University

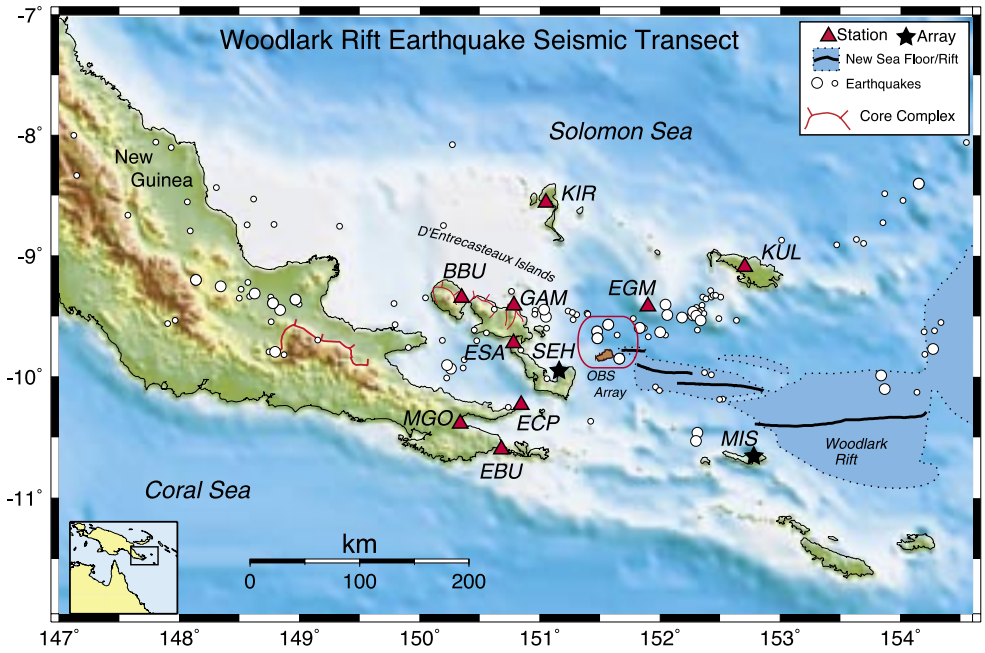

Map of the Woodlark Rift experiment, showing locations of single stations (red triangles), arrays (black), background seismicity and the young faults bounding metamorphic core complexes. Earthquakes shown are relocated from ISC catalog data for the years prior to the experiment.

Continents rift at sites that become ocean basins and passive margins. The Woodlark Rift of Papua New Guinea presents a rare opportunity to study rifting because here it is active, showing a full progression from seafloor spreading to continental extension. This site rifts rapidly: the continental segments of the Woodlark Rift show opening rates of 30-40 mm/yr concentrated on a single fault system, the fastest localized rifting anywhere on the planet. Such high strain rates have produced the youngest metamorphic core complexes on Earth, with rocks now at 2-3 km elevation exhumed from 25 km depths within the last 3-4 million years. Large earthquakes reveal that this is one of the only places where normal faults with shallow dips (< 30 degrees) generate seismicity, perhaps on the faults responsible for exhuming the core complexes. Still, this is a very remote part of the world, and little is known about fault geometry and the underlying mantle framework for rifting.

The 1999-2000 Woodlark Rift experiment is a first attempt to investigate the processes by which this extraordinary rift is developing. The experiment has two primary goals. First, by recording and identifying local earthquakes, we hope to resolve the geometry of modern faulting and test the idea that the core complexes form by low-angle slip of brittle faults. These data will also elucidate the transition in fault geometry from continental rifting, where extension is accommodated entirely by faults, to an adjacent segment where sea floor spreading predominates. Second, these data provide a host of information that should reveal the response of the upper mantle to continental breakup. In particular, we can investigate the transition from apparently asymmetric extension via normal faulting to symmetric sea floor spreading, the role of mantle upwelling in core complex formation and the relation between surface topography and mantle extension.

The Woodlark Rift presents several logistical challenges that have led to many innovative features in experimental design, being a remote tropical region of many islands and reefs. The experiment has been designed with roughly equal numbers of on- land PASSCAL instruments and Ocean Bottom Seismographs (OBS's). Many of the PASSCAL instruments are concentrated in two small arrays used to provide beamforming and slowness estimates for many seismic signals, making up for the otherwise sparse nature of the network. The PASSCAL instruments were installed in July, 1999 and removed through spring 2000. The OBS instruments were deployed in September 1999 and recovered in February 2000, giving six months of simultaneous overlapping recording.

Lithospheric Control of Plate Boundary Deformation and Evolution

Tim Melbourne, Central Washington University
Don Helmberger, California Institute of Technology

The seismic wavefield propagating along the recently instrumented Pacific-North American plate boundary (California) displays remarkable variation, with regional shear waves arriving at coastal stations up to 20 seconds earlier than equidistant stations in eastern California. Broadband modeling of this data reveals coastal paths sample fast upper mantle typical of Miocene-aged ocean plate (> 50 km thickness). Inland paths sample slower uppermost mantle, with the seismic lithosphere, or Lid, measuring less than 5 km thick, characteristic of the Basin and Range extensional province. The Lid step coincides with GPS-inferred maximum dextral strain, indicating lithospheric control of margin deformation. Expressing the juxtaposition of stronger Pacific plate lithosphere with weaker continental North America, the correlation between Lid thickness and present plate-boundary deformation indicates that buttressing at depth by the stronger Pacific plate modulates plate boundary evolution.

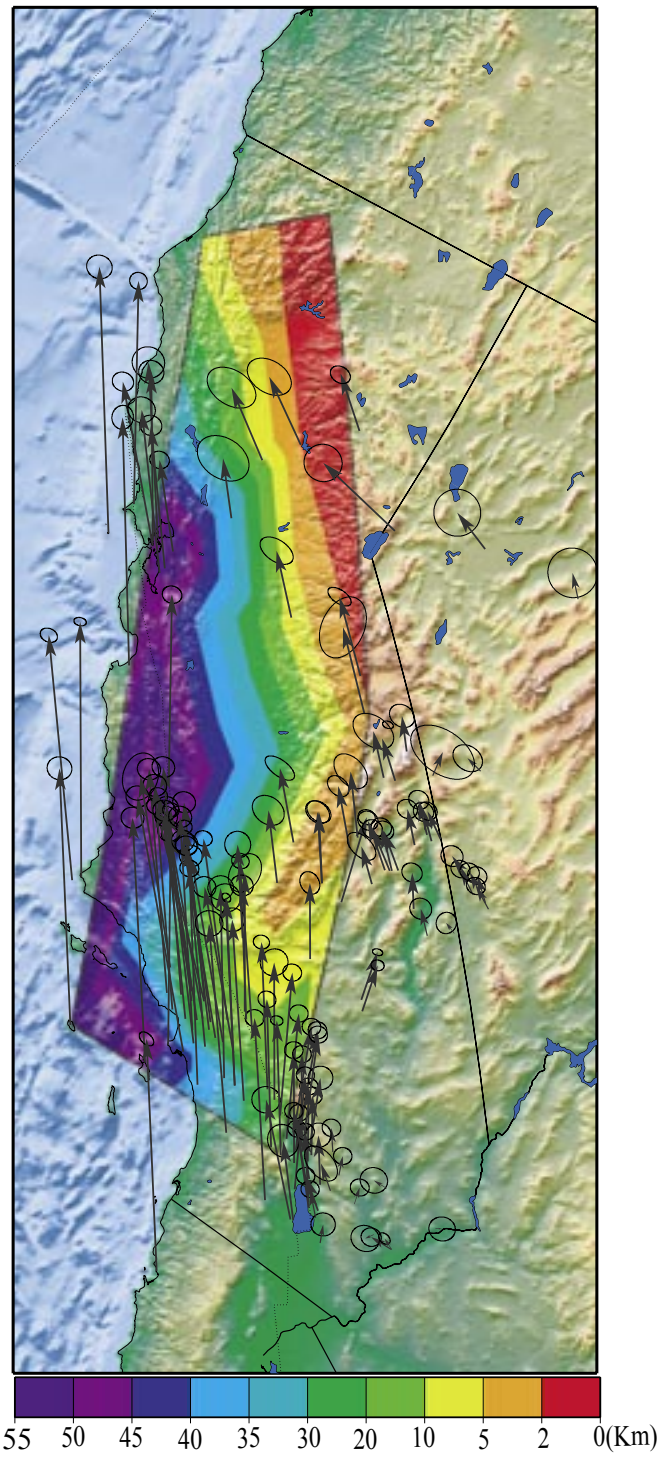

Contoured seismic lithosphere thicknesses beneath North American continental margin derived from broadband SS waveforms and S-SS travel times. Lithospheric Lid (Vs = 4.55 Km/S versus 4.3 Km/S non-Lid, TNA upper mantle) thicknesses range systematically from 55 km along margin coastal paths (Peninsular Baja-Western California), typical of Miocene-aged oceanic lithosphere and similar to that observed beneath eastern Pacific, to effectively 0 Km along Eastern California-Eastern peninsular Baja paths, typical of Basin and Range upper mantle. Intraplate dextral strain, as indicated by geodetic measurements conducted across thick lithospheric Lid regions, is substantially lower than interplate dextral strain, indicated by measurements taken across regions of high Lid thickness gradients.

The Southern Alpine Orogen of New Zealand - a Continent-Continent Collision

Tom Henyey and David Okaya, University of Southern California
Tim Stern, Victoria University, Wellington
Fred Davey, Institute of Geol. Nuclear Sci., Wellington
Donna Eberhart-Phillips, I.G.N.S., Dunedin
Tom McEvilly, University of California, Berkeley
W. Steven Holbrook, University of Wyoming

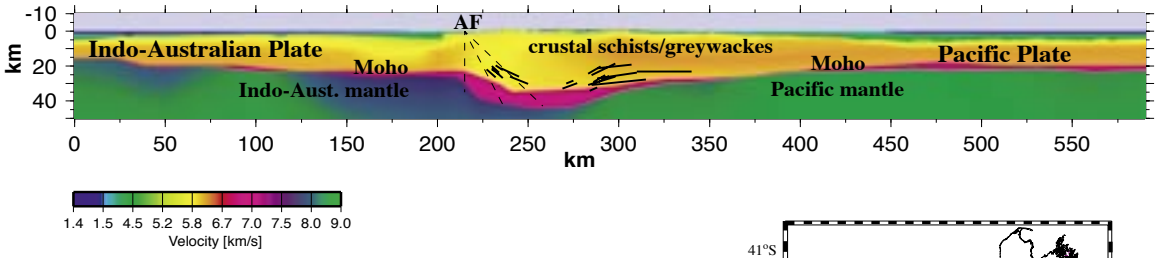

Six-hundred km-wide velocity cross-section across the Indo-Australian/ Pacific plate boundary at the Southern Alpine Orogen. Active-source seismic experiments used PASSCAL instrumentation. Deformation at plate boundary is asymmetric with respect to South Island (200-350 km); crustal deformation occurs distributed within the Pacific plate. AF is Alpine fault.

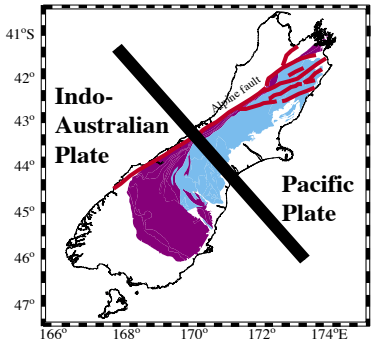

A geophysical research program to study the Pacific/Austro-Indian plate boundary across the South Island of New Zealand has involved a collaboration between U.S. and New Zealand scientists over the past five years. The boundary is characterized by active continent-continent transpressional collision, forming the Southern Alpine uplift and transcurrent Alpine fault.

The Southern Alpine orogen of New Zealand is an excellent natural laboratory in which to study continental dynamics. The rapid rates of deformation allow active processes to be studied thoroughly using Quaternary geology, geodesy, and seismology. The combination of exceptionally rapid erosion and youth of deformation allows the study of mountain building in its infancy through the simultaneous analysis of rocks deformed at the surface and those deeply exhumed in late Cenozoic time.

The U.S./New Zealand collaborative program combined a set of geophysical transects across the South Island with the rich surface geology and geodetics to study the plate boundary configuration and coupling between crust and mantle to the continental collision. Geophysical experiments included seismic reflection, explosion refraction, onshore-offshore wide-angle reflection/refraction, regional and teleseismic passive seismology, magnetotellurics, laboratory petrophysics, gravity, and rheological analyses. Funding was provided by the N.Z. Science Foundation and the U.S. National Science Foundation-Continental Dynamics programs. PASSCAL provided field equipment and logistical support for the four major seismological field efforts.

These investigations found the following: Ninety per cent of the crustal deformation resulting from the plate boundary is distributed within the South Island. The plate boundary can be traced to a depth of approximately 30 km as an east-dipping (~ 60°) Alpine Fault Zone (AF) that is 10-15 km thick. This fault zone is seismically quiet, has low seismic velocities, and below 20 km has resistivities as low as 30 ohm-m. Upper mantle shear-wave splitting exhibits fast polarization orientation parallel to the plate boundary. Teleseismic P-wave delays recorded across the South Island suggest subjacent high velocities in the mantle indicative of symmetrical downwelling of mantle lithosphere at the plate boundary.

For further reading:

Stern, T., Molnar, P., Okaya, D., and Eberhart-Phillips, D., P-wave teleseismic delays and lithospheric thickening beneath the central South Island, New Zealand, *J. Geophys. Res.*, in press, 2000.

Godfrey, N.J., Christensen, N.I., and Okaya, D.A., Anisotropy of schists: contributions of crustal anisotropy to active-source seismic experiments and shear-wave splitting observations, *J. Geophys. Res.*, submitted, 1999.

Molnar, P., Anderson, H., Audoine, E., Eberhart-Phillips, D., Gledhill, K., Klosko, E., McEvilly, T., Okaya, D., Savage, M., Stern, T., and Wu, F., Continuous deformation versus faulting through continental lithosphere: tests using New Zealand as a laboratory for the study of continental dynamics, *Science*, **286**, 516-519, 1999.

Klosko, E., Wu, F., Anderson, H., Eberhart-Phillips, D., McEvilly, T., Audoine, E., Savage, M.K., and Gledhill, K., *Geophys. Res. Lett.*, **26**, 1497-1500, 1999.

Using Dense Array Data to Image Lithospheric Roots Beneath Young Continental Collision Zones

Monica D. Kohler, University of California, Los Angeles

Evidence that young, actively deforming continental collision zones exhibit thickened lithospheric seismic high-velocity roots as part of their early development is provided by travel-time tomography of convergent plate boundary regions. We have used high-density regional seismic array data combined with existing three-dimensional network data from actively deforming orogenic belts to understand the mode of lithospheric deformation and seismicity beneath them. The existence of PASSCAL has made array studies using high quality, dense broadband instrumentation possible and highly successful.

The Transverse Ranges in Southern California are the result of recent, diffuse transpressional plate boundary tectonics. High-resolution tomographic images from the PASSCAL Los Angeles Region Seismic Experiment I array and Southern California Seismic Network teleseismic data suggest that the entire lithosphere below the San Gabriel Mountains and San Andreas fault in the Transverse Ranges has thickened in a narrow, vertical sheet. P-wave travel-time inversions of the combined data support the presence of the well-documented upper mantle high-velocity anomaly that extends ~200 km into the mantle under the northernmost Los Angeles basin and Transverse Ranges (e.g., Humphreys and Clayton, 1990). We find that the high-velocity upper mantle anomaly comprises a 60-80-km wide sheet of mantle material that lies directly below a 10-km thick crustal root in the San Gabriel Mountains (Kohler, 1999). The three-dimensional view shows that high velocities are approximately centered beneath a large region of convergence and thickened crust that includes the San Andreas fault plate boundary zone (Figure, left). Subsequent dynamic modeling of lithospheric deformation uses the tomographic results to provide constraints on deformation geometry. In our experiments, the interaction of the buoyancy-driven lithospheric downwelling with external plate boundary convergence determines the geometry of the crustal thickening and mantle downwelling (Houseman et al., 2000). When we apply our results to the Transverse Ranges, we find that both plate-driven convergence and gravitationally driven instability are significant processes that can simulate the observed thickening and downwelling in the tomographic images.

We are now testing whether thickened, compressed crust underlain by local high-velocity mantle anomalies continues into the western Transverse Ranges using teleseismic data recorded during the recently completed 1998-1999 PASSCAL Los Angeles Region Seismic Experiment II. The 100-km-long array contained 83 seismometers and crosses the San Andreas fault in southwestern Southern California. Its location makes it valuable for determining the relationship between faulting and ductile deformation in the lithosphere across the plate boundary.

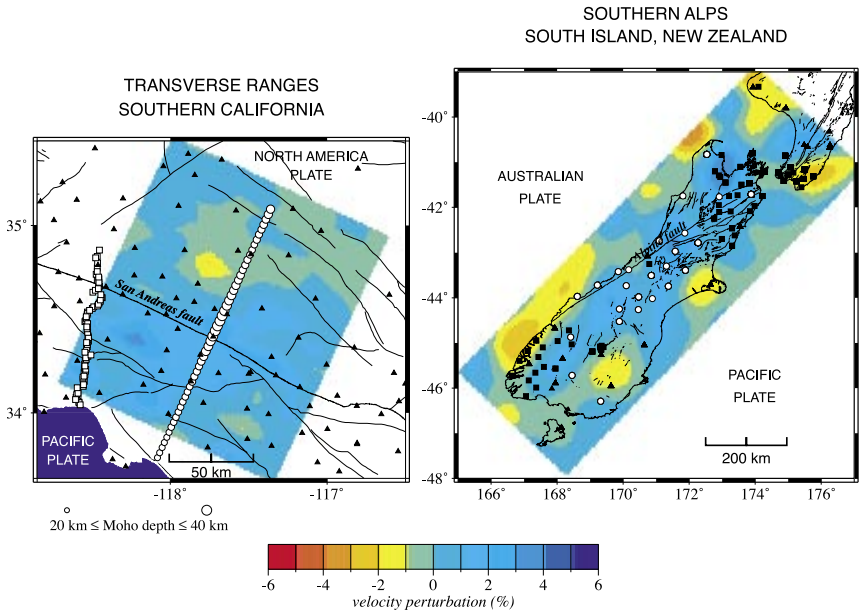

P-wave velocity variations at a depth of 60 km below the Transverse Ranges in Southern California (left) and the Southern Alps in South Island, New Zealand (right). Left image shows crustal thickness variations and station locations of the Los Angeles Region Seismic Experiment I (circles) and II (squares), and the Southern California Seismic Network (trianges). Right image shows station locations of the Southern Alps Passive Seismic Experiment (circles), other regional networks (squares), and the New Zealand National Seismograph Network (triangles).

Similar tomographic results are obtained for crustal and upper mantle structure below the young, actively uplifting Southern Alps in South Island, New Zealand by teleseismic P-wave travel-time inversion (in a collaboration with Dr. Donna Eberhart-Phillips). The data consist of teleseismic travel times recorded during the 1995-1996 PASSCAL Southern Alps Passive Seismic Experiment and by the permanent New Zealand National Seismograph Network. The three-dimensional tomographic images show a near-vertical, high-velocity (+4%) structure in the uppermost mantle that directly underlies thickened crust along the NNE-SSW axis of the Southern Alps (Figure, right). The center of the high-velocity anomaly lies to the east of the Alpine fault which separates Australian Plate rocks to the west which are obliquely colliding with Pacific Plate rocks to the east resulting in the uplift of the Southern Alps during the past 5-7 m.y.

For further reading:

Humphreys, E. D., and Clayton, R.W., Tomographic image of the southern California mantle, *J. Geophys. Res.*, **95**, 19725-19746, 1990.

Kohler, M. D., Lithospheric deformation beneath the San Gabriel Mountains in the southern California Transverse Ranges, *J. Geophys. Res.*, **104**, 15025-15041, 1999.

Houseman, G. A., Neil, E.A., and Kohler, M.D., Lithospheric instability beneath the Transverse Ranges of California, *J. Geophys. Res.*, in press, 2000.

Active Source Investigation of the Lithosphere in Europe: An International Cooperation

G. Randy Keller, University of Texas at El Paso

The POLONAISE'97 seismic refraction - wide angle reflection experiment conducted during May of 1997 was a very large cooperative effort in which PASSCAL instrumentation played a major role. It included contributions from the geophysical and geological communities in Poland, Denmark, the United States, Germany, Lithuania, Finland, Sweden and Canada and was led by the Association for Deep Geological Investigations of Poland (ADGIP) with the support of the Institute of Geophysics of the Polish Academy of Sciences and the Institute of Geophysics of the University of Warsaw. The vast majority of the funding for this ~$2,000,000 effort was provided by Polish sources. UTEP's participation in this project was funded by the National Science Foundation through a grant from International Programs.

POLONAISE'97 consisted of two deployments of over 600 individual portable recording instruments and five multi-channel seismic recording systems. These instruments were located at about 800 different positions to record sources from 63 shot points located along five profiles with a combined length of about 2000 km (Figure). The spacing between recording stations was averaged 2 km. Most of the shot points were located in Poland, but one was located in Germany and three were located in Lithuania. Distances between shot points were 15 to 35 km. The basic layout of four interlocking profiles (profiles 1-4) remained the same during both deployments with only a small percentage (<20%) of the recording stations being moved between the deployments. The multi-profile deployments led to significant three- dimensional coverage as shots along individual profiles were recorded as fans into the other profiles.

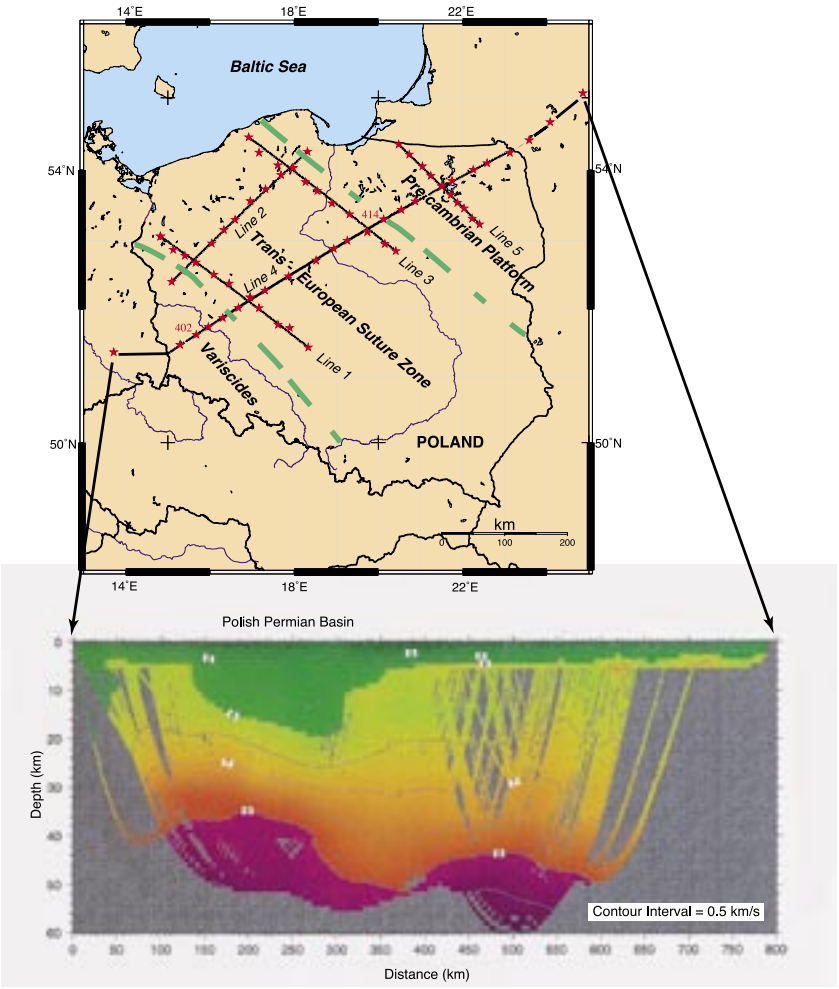

Velocity model and location map for the 1997 Polonaise experiment.

POLONAISE'97 provide a huge amount of data concerning the structure of the Trans-European Suture Zone (TESZ) in central Europe. The initial analysis of these data generally confirms the results of previous studies and allows us to formulate a few significant seismic and tectonic observations: (1) The velocity models show that the depth of the Moho, approximated by the 8 km/s velocity isoline, is 32-39 km under the Palaeozoic Platform and 43-45 km under the Precambrian Craton. The TESZ/TTZ is associated with a crustal root in which the thickness of the crust probably exceeds 50 km. (2) The depth of the 6 km/s isoline has maximum values of 16-20 km in the Polish Basin. This indicates that the sedimentary cover in the Polish Basin might be as thick as 20 km. (3) A distinct asymmetry between the maximum thickness of the sedimentary cover and the crustal root associated with TESZ/TTZ is observed along profile P4.

Seismotectonics in Central Panama

Joan Gomberg, Tom Pratt, and Eugene Schweig, U.S. Geological Survey
Hugh Cowan, New Zealand Geologic Service
Paul Bodin, University of Memphis

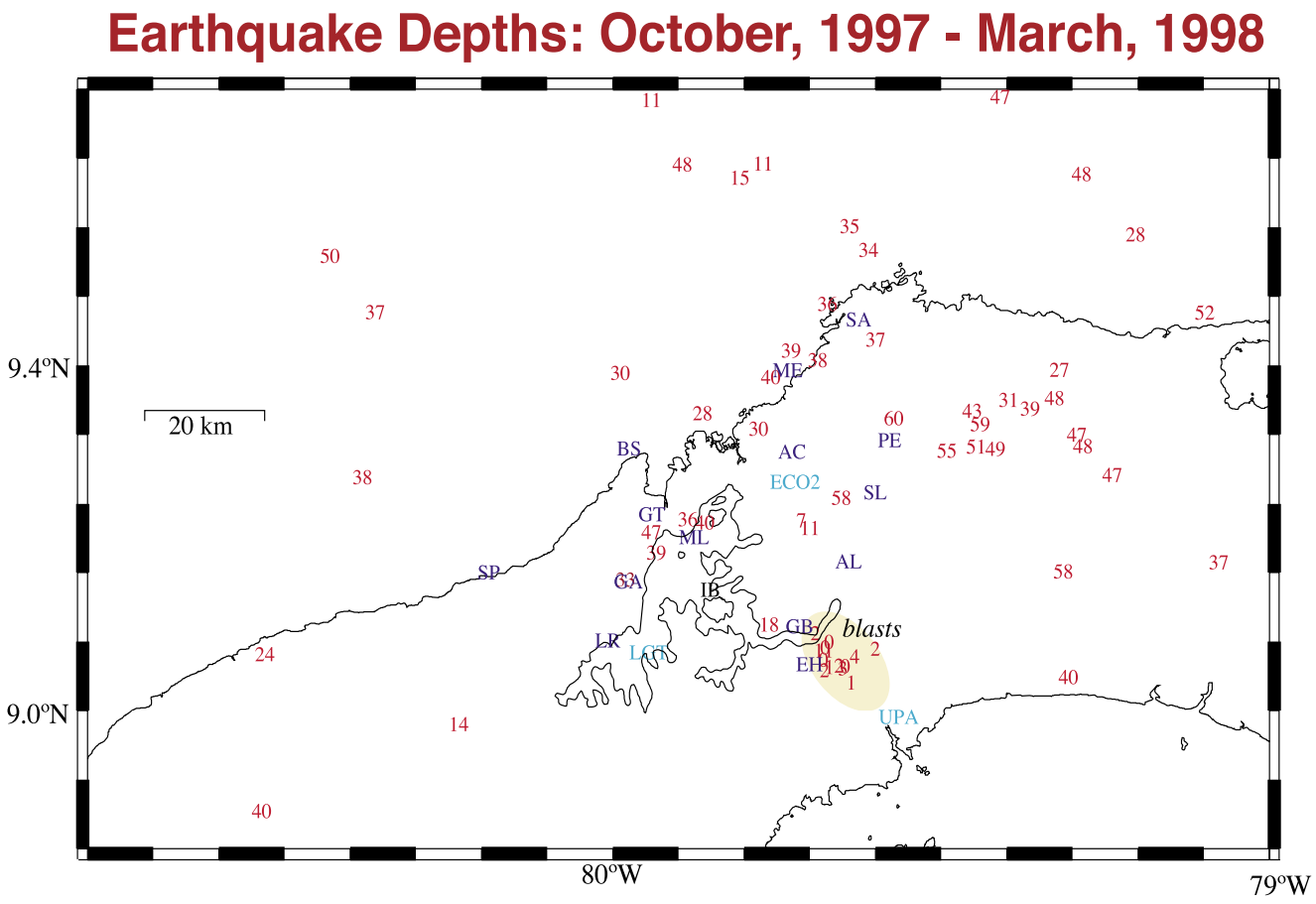

PASSCAL provided 14 instruments deployed in north central Panama from October 1997 through April 1998. PASSCAL also provided training and software. This seismic monitoring experiment was part of a collaborative project between the U.S. Geological Survey and the Panama Canal Commission with the goal of better understanding the tectonics of the region. This study was conducted in parallel with geologic and shallow seismic reflection studies. Low crustal deformation rates inferred in the latter are consistent with the observation of only three crustal earthquakes recorded inside the network, and only about five beneath all of central Panama. Most importantly, a deepening of earthquakes from the coast inland provided the first direct evidence of subduction beneath the Panamanian Isthmus. A cluster of deeper earthquakes occurred in the eastern part of the study area that correlates with the highest topography. The seismicity also suggests that if a 'Canal Discontinuity' (documented in the literature as a possible major suture zone) exists, it is not a major feature.

Geodetic Constraints on the Rigidity and Relative Motion of Eurasia and North America Using IRIS-JPL GPS Stations

Mikhail G. Kogan, Lamont-Doherty Earth Observatory
Robert W. King, Massachusetts Institute of Technolgoy

The Eurasian plate provides the most natural frame of reference for geodetic studies of a wide variety of tectonic processes along its boundary. Until recently, the Eurasian stations contributing high-quality space geodetic data have been located only in the western fifth of the plate, providing a geometrically weak definition and leaving open the question of whether there is significant relative motion between Europe and the major part of Eurasia. Since 1995, we have benefited from the IRIS/NIMA-supported project RUSEG (Russia-US Experiment in Geodynamics by GPS Technology) which is fulfilled in collaboration with RDAAC, Geophysical Survey of the Russian Academy of Sciences. GPS measurements were performed throughout Russia and Kazakhstan, including previously unsurveyed areas of the Russian Platform, Siberia, and the Kamchatka Peninsula. Between 1997 and 1999 we established continuous GPS stations at seven sites in eastern Russia (Figure). All of these stations were integrated with GSN stations in terms of collocation, facilities, data flow, and personnel (Kogan et al., 2000). JPL joined this project in 1998.

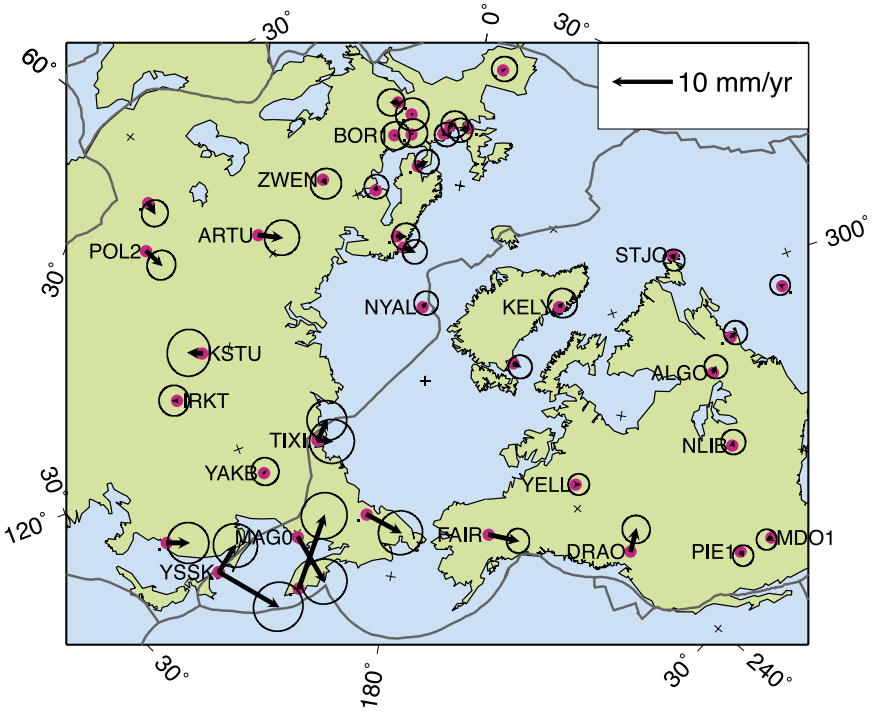

Horizontal velocities and their 95% confidence ellipses relative to the Eurasian and North American plates defined by this study. Plate boundaries shown by thick grey lines correspond to NUVEL-1A global plate model. Velocities for the two boundary-zone stations (YSSK and TIXI) are shown relative to both plates.

GPS observations in northeastern Asia, when combined with observations from the global network for the period 1992-1999, yield an angular rotation vector between Eurasia and North America consistent with and a factor of two more precise than estimates derived using GPS or VLBI data previously available from only western Eurasia. The new vector implies a pole of relative rotation 1200 km more to the northwest than predicted by the NUVEL-1A global plate model, suggesting a significant change in the relative motion of Eurasia and North America over the past 3 m.y. The standard deviations of horizontal velocities from rigid plate motion for nineteen stations in Eurasia and ten in North America are less than 1 mm/yr; the observations place an upper bound of 2 mm/yr at 95% confidence for relative motion between western and eastern Eurasia.

In 2000, we intend to install continuous GPS stations at Norilsk (northern margin of Siberian platform) and at Lovozero (Kola Peninsula) integrated with relevant GSN stations. We also started real time, 1-s sampling rate transmission of continuous GPS measurements from GSN station Yakutsk to support the tomography of the ionosphere/troposphere with Low Earth Orbiting satellites.

For further reading:

Kogan, M. G., Steblov, G.M., King, R.W., Herring, T.A., Frolov, D.I., Egorov, S.G., Levin, V.Y., Lerner-Lam, A., Jones, A., Geodetic constraints on the rigidity and relative motion of Eurasia and North America, *Geophys. Res. Lett.*, in press, 2000.

Tibetan Seismicity From Project INDEPTH III

William Langin, Larry Brown, and Eric Sandvol, Cornell University

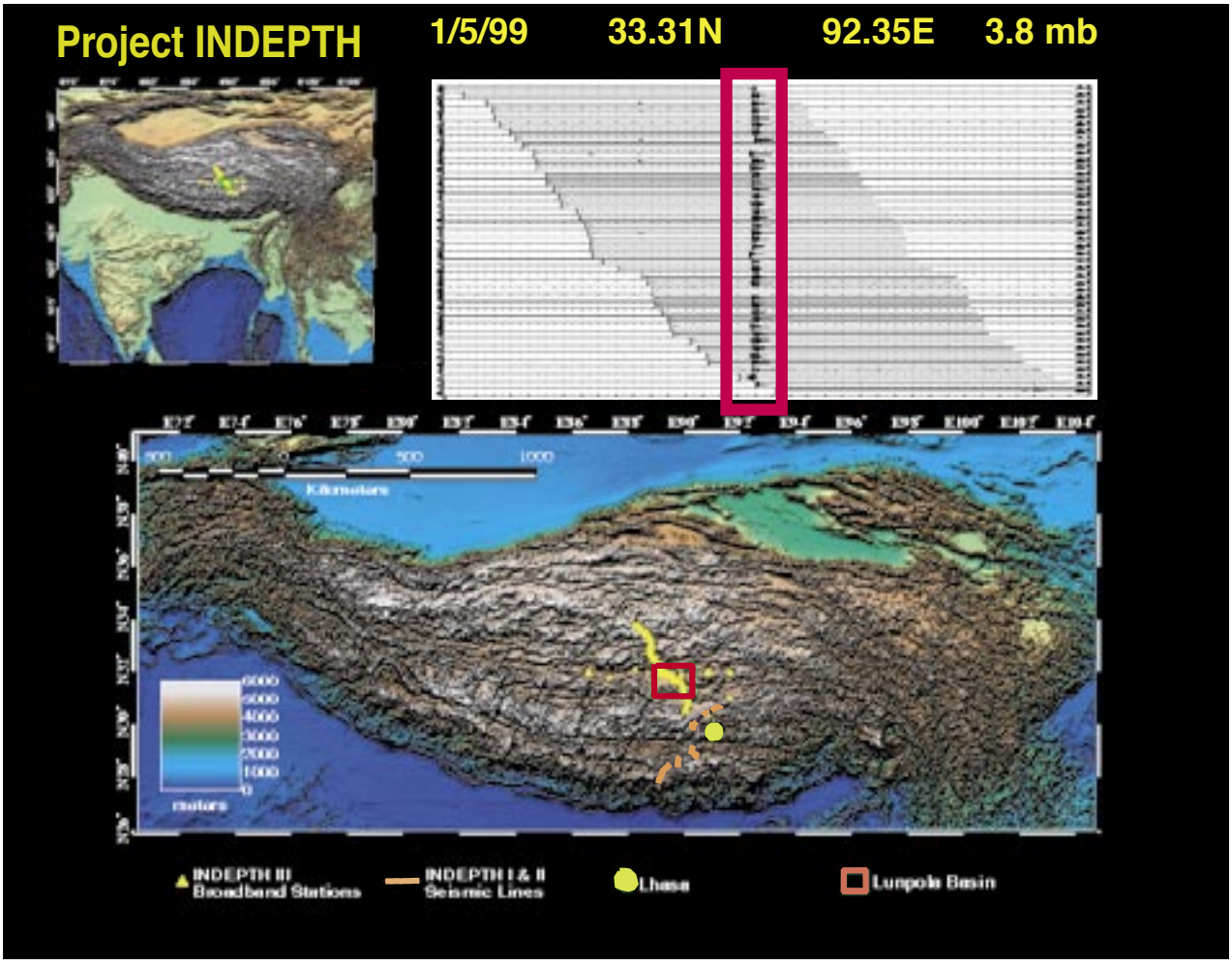

Although it is well accepted that the India-Eurasia continental collision is the driving force behind the uplift of the Tibetan Plateau, the mechanism of the uplift remains in question. The most popular current models invoke varying degrees of lithospheric underthrusting, crustal shortening and thickening, and hydraulic uplift. Project INDEPTH is a consortium of universities with members from the United States, Europe, and China dedicated to profiling the deep structure of Tibet and the Himalayas. Various members of the group are currently examining data collected from the third phase of the project to determine lithospheric structure, receiver functions, tomography, and anisotropy. As part of Phase III of Project INDEPTH, fifty-seven PASSCAL seismic instruments, including thirty-four with broadband sensors, were deployed in Tibet from August 1998 to August 1999. The seismic network consisted of a 400 km long north-south line with a cross line in the central plateau region. The network recorded continuously for one year at a sample rate of 5 milliseconds, gathering approximately 0.5 terrabyte of data. We are currently using these recordings to document seismicity within the central plateau. Accurate earthquake locations may help to constrain the extent to which Indian lithosphere underthrusts Eurasia, the depth to the brittle-ductile transition, and the mode of shortening in the upper crust, key elements in determining the mechanics that uplifted the Tibetan Plateau to an average elevation of nearly 5 km.

We intend to use the new earthquake locations and focal mechanisms to refine our knowledge of the active faulting and fault mechanisms. Along with suggestions as to the depth of the brittle-ductile transition and extent of Indian underthrusting, the relative amounts of strike slip, thrust, and normal faulting may be quantified. The detection of seismic phases such as PxP, SxS, and PxS that may represent reflections from magma chambers at mid-crustal levels would provide evidence of partial melting beneath the Tibetan Plateau. Each of these factors has specific implications toward the mechanics of uplift for the Tibetan Plateau.

Seismic Polarization Anisotropy Beneath the Central Tibetan Plateau

Wei-Chuang Huang, James Ni, Frederik Tilmann, Richard Rapine, Tom Hearn, New Mexico State University
Rainer Kind, Joachim Saul, GeoForschungsZentrum Potsdam, Germany
Wenjin Zhao, Jingru Guo, Chinese Academy of Geological Sciences, Beijing, China
Doug Nelson, Syracuse University

A consortium of institutions and universities carried out the INDEPTH-III experiment in 1998 and 1999 to image the crustal and upper mantle structure beneath the uplifted Tibetan plateau and to shed light on the details of the continental collision process. INDEPTH-III comprised the one-year deployment of a narrowly spaced array of 62 stations. The instruments were provided by the PASSCAL facility and the German instrument pool at the GFZ in Potsdam.

SKS and SKKS phases were analyzed for the direction and extent of seismic polarization anisotropy. Splitting times from one to two seconds and fast directions from E-W to NE-SW were observed for stations north of 32°N. In contrast, no detectable splitting was observed for most stations south of this latitude. The transition between zero measured splitting (implying splitting times <0.6 s) to splitting of 2 s is very abrupt and occurs ~40 km south of the BNS, approximately at the southern edge of a zone of inefficient Sn propagation (Ni and Barazangi, 1983). The magnitude of splitting decreases towards the northern stations where splitting times are between 1 and 1.5 s. The fast directions vary over short distances and also differ for ray paths from opposite backazimuths, indicating lateral heterogeneity in all directions.

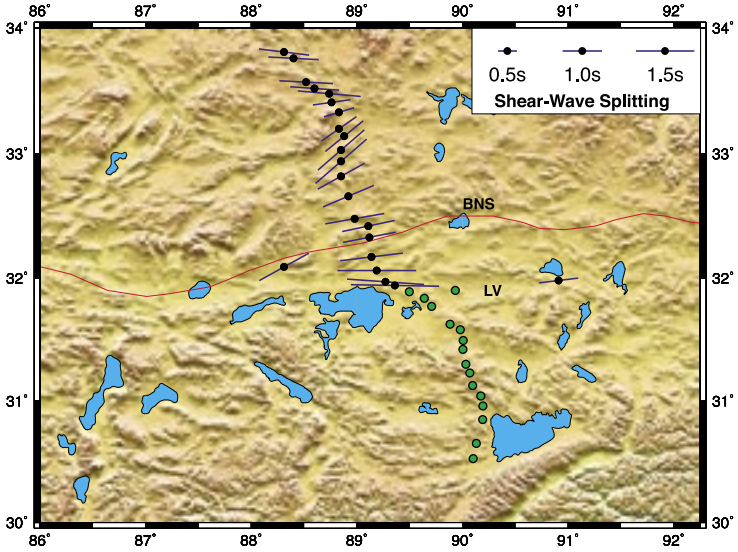

Averaged fast directions and delay times based on SKS splitting measurements. A rapid change of splitting parameters from no observed splitting to splitting of 2 s (fast direction approximately E-W) occurs at 32°N, coincident with a series of right-lateral strike-slip faults in the Lumpola Valley. Further north the fast direction rotates to NE-SW and then back to E-W; the splitting times are somewhat reduced to 1-1.5 s. BNS - Banggong-Nujiang Suture; LV -Lumpola Valley. The region to the north of the BNS is part of the Qiangtang block, the region to the south belongs to the Lhasa block.

Based on previous studies, it is thought that the Qiangtang block is underlain by hot and possibly partially melted Asian mantle. When this less viscous material is squeezed between colder lithospheres (India and Tsaidam/ Tarim, respectively), it is extruded to the east and subject to shear strain. At large strain (>150%) and typical upper mantle conditions, the seismically fast direction of olivine will align approximately parallel to the shearing direction (Zhang and Karato, 1995). The splitting measurements can hence be understood as indicators of the shear direction, where the large splitting times and E-W directions near the Lumpola Valley are obtained because shear tends to be concentrated near the edge of a region that is being extruded. The lateral variation in splitting parameters can be attributed to heterogeneity of strain and material properties in the mantle which influence the way lattice preferred orientation is developed.

Different geodynamic models had been proposed to account for previous observations of splitting in Tibet (e.g., McNamara et al., 1994; Sandvol et al., 1997). We found that neither the model which approximates the deformation of Asia as a thin-viscous sheet (England and Houseman, 1986) nor the present-day crustal strain field as determined from earthquake moment tensors and Quaternary fault slip rates (Holt and Haines, 1993) can fully explain the splitting observations.

The most remarkable result of the present study is the sharpness of the onset of measurable anisotropy and the variation of the anisotropy parameters, in particular the fast directions, over short distances. This variability which, as just mentioned, provides further constraints for geodynamic models of the Tibetan collision zone, had not been visible in previous experiments as a result of much larger station spacings and could only have been observed because of the availability of a large number of broadband instruments.

For further reading:

England, P. and Houseman, G., Finite strain calculations of continental deformation 2. Comparison with the India-Asia collision zone, *J. Geophys. Res.*, **91**, 3664-3676, 1986.

Holt, W.E., and Haines, A.J., Velocity fields in deforming Asia from the inversion of earthquake-related strains, *Tectonics*, **12,** 1-20, 1993.

McNamara, D., Owens, T., Silver, P., and Wu, F. Shear wave anisotropy beneath the Tibetan Plateau, *J. Geophys. Res.*, **99**, 13,655-13,665, 1994.

Ni, J., and Barazangi, M., High-frequency seismic wave propagation beneath the Indian Shield, Himalayan Arc, Tibetan Plateau and surrounding regions: High uppermost mantle velocities and efficient Sn propagation beneath Tibet, *Geophys. J. R. Astr. Soc.*, **72,** 665-689, 1983.

Sandvol, E., Ni, J., Kind, R., and Zhao, W., Seismic anisotropy beneath the southern Himalaya-Tibet collision zone, *J. Geophys. Res.* **102**, 17813-17823, 1997.

Zhang, S., and Karato, S., Lattice preferred orientation of olivine aggregates deformed in simple shear, *Nature*, **375**, 774-777, 1995.

Seismological Studies of the Tien Shan with a Deployment of PASSCAL Broadband Sensors

Steve Roecker, Rensselaer Polytechnic Institute
Gary Pavlis, Indiana University
Frank Vernon, University of California, San Diego

Previous seismological studies of the Kyrgyz Tien Shan have revealed unusual heterogeneity (e.g., Kosarev et al., 1993; Roecker et al., 1993; Vinnik and Saipbekova, 1984) and flow directions (Makeyeva et al., 1992; Martynov et al., 1998; Wolfe and Vernon, 1998) in the upper mantle that suggest that the concentration of shortening in this area may be a consequence of a weak or nonexistent lithosphere (e.g., Roecker et al., 1993) and that a detachment of a lithospheric root may have occurred within the past few million years (Chen et al., 1997). While intriguing, the current lack of seismic observations in much of the Tien Shan allows inferences of the state of the mantle beneath the greater part of the range only by poorly constrained extrapolation. Thus, while it is clear that the mantle beneath the Tien Shan is anomalous, the extent of such anomalies and, hence, their role in the overall deformation picture remain unclear. Similarly, while focused studies of earthquake activity (e.g., the Suusamyr aftershock zone; Mellors et al., 1997), have defined the depth and dip of one active structure in the crust, the nature of activity in most of the Tien Shan, including that within the highly active Kokshal range in the south, is poorly constrained. Finally, a key measurement needed to quantify the evolution of the Tien Shan is the total shortening that has occurred, which may be estimated from a map of crustal thickness. Although the thickness of the crust is known in a few locations (Chen et al., 1995; Bump and Sheehan, 1998; Kosarev et al., 1993) it is not well known throughout much of the range.

In the summer of 1999, we completed the deployment of 28 broadband seismographs in and near the Kyrgyz Tien Shan (Figure), in order to determine the structure of the crust and upper mantle, directions of flow in the mantle (using seismic anisotropy), and the nature of brittle failure in the crust. This temporary deployment is augmented in key areas by existing stations, most notably by KNET, and will operate for a period of about 12 months in 1999-2000. This 28-station array is designed to provide lateral resolution of mantle structure on the order of 25-30 km (the average spacing between stations) to depths of 400 km (the approximate aperture of the network), with deeper structures being imaged by converted phases. We plan to process the recorded data using a suite of techniques including shear-wave splitting, receiver functions, travel time tomography, and recently developed array processing techniques to generate images of mantle heterogeneity and anisotropy, and short-period waveform modeling to constrain hypocenters and mechanisms for local and regional earthquakes.

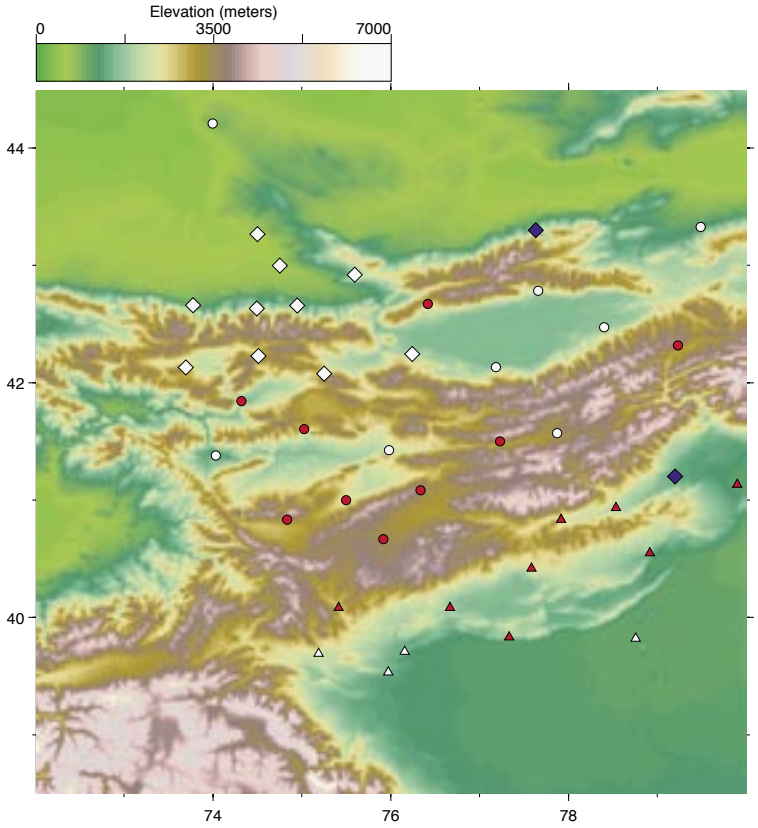

For further reading:

Bump, H. A. and Sheehan, A. F., Crustal thickness variations across the northern Tien Shan from Teleseismic receiver functions. *Geophys. Res. Lett.*, **25**, 1055-1058, 1998.

Chen, Y.H., Kosarev, G.L., and Roecker, S.W., The nature of crustal and upper mantle discontinuities determined from analysis of waveforms recorded by broad-band arrays in Pakistan and Kyrgyzstan, EOS, Trans. Amer. *Geophyys. Un.*, **75** (suppl), 464, 1994.

Chen, Y.H., Roecker, S.W., and Kosarev, G.L., Elevation of the 410 km discontinuity beneath the central Tien Shan: Evidence for a detached lithospheric root, *Geophys. Res. Lett.*, **24**, 1531-1534, 1997.

Kosarev, G.L., Petersen, N.V., Vinnik, L.P., and Roecker, S.W., Receiver functions for the Tien Shan analog broadband network: Contrasts in the evolution of the structures across the Talasso-Ferghana fault, *J. Geophys. Res.*, **98**, 4437-4448, 1993.

Makeyeva, L.I., Vinnik, L.P., and Roecker, S.W., Shear-wave splitting and small-scale convection in the continental upper mantle, *Nature*, **358**, 144-147, 1992.

Mellors, R.J., Pavlis, G.L., Ghose, S. Hamburger, M.W., Vernon, F.L., Abers, G.A., Mishatkin, V., and Iliasov, B., The Ms 7.3 1992 Suusamyr, Kyrgyzstan Earthquake in the Tien Shan: 1. Constraints on fault geometry and source parameters based on aftershocks and body wave modeling, *Bull. Seismol. Soc. Amer.*, **87**, 11-22, 1997

Roecker, S.W., Sabitova, T.M., Vinnik, L.P., Burmakov, Y.A., Golvanov, M.I., Mamatkanova, R., and Munirova, L., Three-dimensional elastic wave velocity structure of the western and central Tien Shan, *J. Geophys. Res.* **98**, 15,779-15,795, 1993.

Vinnik, L.P., and Saipbekova, A.M., Structure of the lithosphere and asthenosphere of the Tien Shan, Annal. *Geophysicae*, **2**, 621-626, 1984.

Seismic Characterization of an Active Metamorphic Massif, Nanga Parbat, Pakistan

Anne Meltzer and Golam Sarker, Lehigh University
Leonardo Seeber, Lamont-Doherty Earth Observatory of Columbia University

While a growing number of studies have improved our understanding of the subsurface structure of mountain belts at regional scales, detailed characterizations of igneous and metamorphic processes in active orogens remain relatively uncommon. Data recorded by PASSCAL instruments at Nanga Parbat, in the core of the Western Himalayan syntaxis, provide a new opportunity to assess synorogenic metamorphism and mass flow during mountain building.

At 8126 m, the summit of Nanga Parbat, sculpted from Pre-Cambrian Indian crust, stands far above the surrounding terrane (Figure 1). The world's largest relief, 7 km in 21 km horizontal distance, occurs between the peak and the Indus River running at its base. The basement gneisses of Nanga Parbat exhibit a polymetamorphic history acquired during Tertiary continental collision between India and Asia. Recent faulting, rapid exhumation, the presence of hot springs, young intrusive rocks, and young metamorphism all suggest a level of vigorous tectonic activity distinct from surrounding terranes. As part of a study to understand the active tectonic processes responsible for crustal reworking at Nanga Parbat we deployed a dense seismic array to characterize seismicity at the massif and to determine crustal structure beneath the mountain (Meltzer et al) (Figure 2a).

Microseismicity, somewhat distributed along strike beneath the massif, exhibits a sharp drop-off west of the massif and a more gentle drop-off east of the main summit ridge crest. Brittle deformation is largely restricted to depths ≤ 2 km below sea level (~5-6 km below the average topographic surface). The seismicity base forms a prominent antiformal shape beneath the massif with approximately 3 km of structural relief over a lateral distance of 12 km (Figure 2b). The apex of the antiform is offset from the topographic ridge crest and is consistent with particle paths developed in a two-sided orogen. A 3-D joint inversion for hypocenter location, Vp, and Vs reveals anomalously low velocities, up to 10%, over lateral distances of 10-20 km (Figure 2c) that extend to depth through the entire crust. Significant attenuation of both P and S waves is observed in waves travelling through the massif. This leads to the conclusion that the remarkably high topography of the massif sits above hot, thin, weak crust, dynamically supported by the continuous flow of material from depth.

Figure 1. Nanga Parbat- Haramosh Massif.

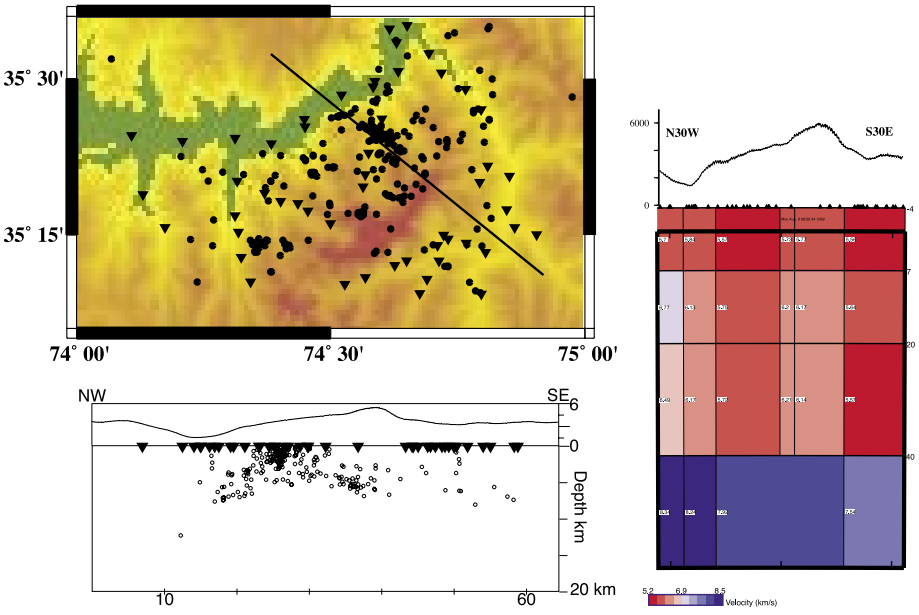

Figure 2. Top left (2a) Nagna Parbat seismic array (triangles) and microseismicity (circles) on topographic base. Bottom left (2b), hypocenters projected to a cross section (shown in 2a). Right (2c), P-wave velocities from tomographic inversion.

The main locus of seismicity and regions of low seismic velocity and high attenuation correlate with the area of most rapid exhumation, cooling ages less than 2 Ma, young granitic dikes and plutons, young migmatites formed under low-P, high-T conditions, and high crustal resistivity suggesting a genetic link between these phenomena in which hot rocks, rapidly advected from depth, are pervasively modified at shallow depths in the crust.

For further reading:

Meltzer, A., Sarker, G., Seeber, L., Armbruster, J., Beaudoin, B., Seismic Characterization of an Active Metamorphic Massif, Nanga Parbat, Pakistan Himalaya, in review.

Eastern Turkey Seismic Experiment: A Study of the Anatolian Plateau, Bitlis Suture, and Northern Arabian Platform

Eric Sandvol, Dogan Seber, and Muawia Barazangi, Cornell University
Niyazi Turkelli and Cemil Gurbuz, Bogazici University, Istanbul, Turkey

The boundary between the Anatolian and Arabian plates offers an excellent opportunity to study the early stages of continental collision. In order to fully understand this collisional terrane we must combine all available geophysical, geological, and geochemical measurements to produce a coherent picture of the geodynamic processes occurring in this complex region. The lack of geophysical measurements that would constrain the lithospheric and uppermost mantle structure in this region make Eastern Turkey an exciting region for a PASSCAL passive source broadband experiment. During late October and early November of 1999 we successfully installed 29 broadband seismometers in the eastern portion of the Anatolian Plateau. Shortly thereafter we visited each of the stations and collected approximately two to three weeks of data for most of the stations in the network. We plan to analyze the data collected, utilizing standard broadband seismological methods involving both teleseismic waveform inversion, hypocenter location inversion, and tomographic travel time inversion to resolve the rheology and structure of both the crust and upper mantle beneath the Bitlis suture and the East Anatolian plateau. Preliminary receiver functions already have revealed a potential crustal root beneath the easternmost portion of the Anatolian Plateau. Furthermore, preliminary analysis of SKS and SKKS phases for shear wave splitting have shown that there is very little change in the splitting parameters across the Eastern Anatolian Fault Zone. In the future we also plan to integrate seismic data from existing short period stations in Turkey and the surrounding area. In addition, we have also begun to integrate all of the available geophysical and geologic data into Cornell's Middle East and North Africa GIS databases. This work will place important new constraints on the geodynamic models of continent-continent collision.

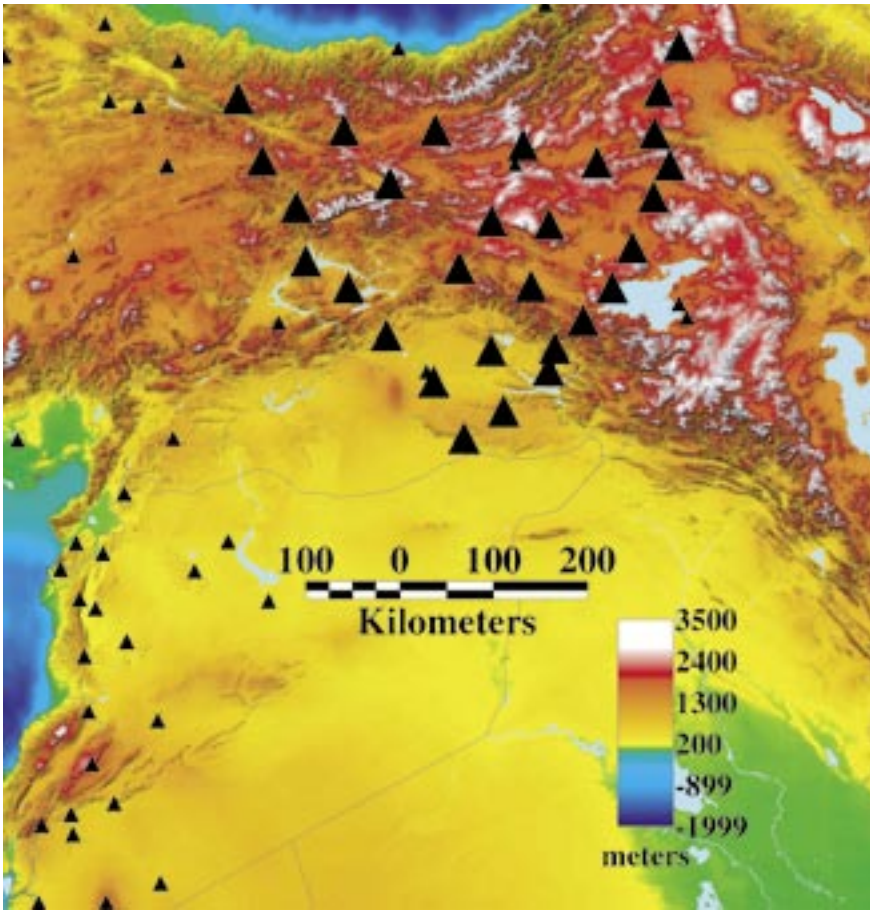

A map showing the station locations of the Eastern Turkey Seismic Array. Large triangles are sites with PASSCAL instruments. Small triangles are permanent stations in the region.

Regional Seismic Wave Propagation in the Arabian Plate and Surrounding Regions

Khaled Al-Damegh, Eric Sandvol, and Muawia Barazangi, Cornell University

Saudi Arabian National Digital Broadband Seismic Broadband Network

Continuous recordings of 17 broadband stations from a newly established seismological network in Saudi Arabia were provided by King Abdulaziz City for Science and Technology, Riyadh, Saudi Arabia. These data along with recordings from the broadband stations of the GSN, MEDNET, GEOFON and a temporary IRIS array in Saudi Arabia are used to study the lithosphere structure of the Arabian plate and surrounding regions. Tectonically, the Arabian plate is surrounded by different types of plate boundaries: continental collision (Zagros belt and Bitlis suture), continental transform (Dead Sea Fault System), sea floor spreading (Red Sea, Gulf of Aden), and oceanic transform (Owen Fracture Zone). In addition to the plate boundary processes, many intraplate Cenozoic processes such as active volcanism, faulting and folding are taking place. By studying the Pn, Sn and Lg wave propagation, the rheology and the structure of the crust and uppermost mantle can be inferred.

We are currently using these data to map zones of blockage, inefficient, and efficient propagation of the Lg and Sn phases in the Middle East and East Africa. These results will provide new information on the rheology and structure of the crust and the mantle lid in the region. Together with an estimate of Pn attenuation, these maps will provide important new information on the nature of the lithosphere in Arabia and East Africa.

A Crustal Transect on the Southeastern Arabian Margin Across the Oman Mountains

Ali I. Al-Lazki, Dogan Seber, Eric Sandvol, and Muawia Barazangi, Cornell University

The unique tectonic setting of Oman mountains, Semail ophiolite, and ongoing hydrocarbon exploration have led to extensive geological research focused on sedimentary units and ophiolite stratigraphy of Oman. Few studies investigated the crustal-scale structure of the southeastern Arabian continental margin. The aim of this study is to decipher the crustal structure of Oman mountains and nearby region.

We have constructed a NE-SW oriented crustal transect in the northern Oman mountain, across the Akhdar Mountain, covering a distance of 255 km. Within the transect the upper 3-8 km of the crust is primarily constrained by surface geology, 152 km of 2-D seismic reflection profiles, and 8 exploratory wells. For the first time, constraints on Moho depth are determined by constructing receiver functions based on waveform of teleseismic earthquakes recorded by four digital seismic stations located along the profile. Finally, Bouguer gravity modeling was used to further constrain depth to basement.

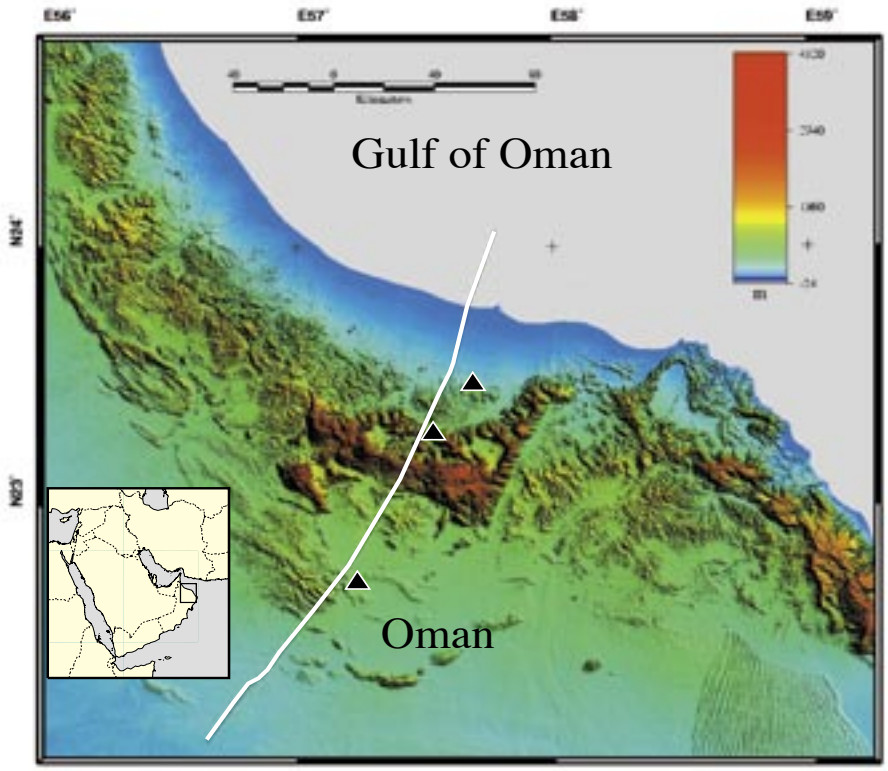

Triangles represent station locations; the line represents the transect extent.

We document in this study three principal findings. First, we infer the presence of a mountain root beneath the Akhdar Mountain with about 60 km of lateral extent at depth. A Moho depth of 48-52 km was obtained in the northeastern limb of the Akhdar Mountain. A Moho depth of 39-43 km was obtained at about 25 km to the northeast of the Akhdar Mountain in the Batinah costal plain. A Moho depth of 41-45 km was obtained about 25 km to the southwest of the Akhdar Mountain in the Hamrat Duru range. Determined Moho depth assumes 6.4-7.0 km/sec average crustal P-wave velocity.

Second, based on Bouguer gravity modeling, we infer 13-16 km depth to basement southwest of the Akhdar Mountain. An anomalously shallow basement depth of 7-8 km is found to coincide with Jabal Fitri, that aligns with the Salakh-Madmar-Qsaybah Arch coinciding with the front of emplaced Hawasina nappes. The model assumes 40 km and 44 km Moho depth for the northeastern and southwestern ends of the crustal transect, respectively.

Third, based on interpretation of seismic profiles to the south of the Akhdar mountain, we document the presence of NW-SE oriented basement involved strike-slip faults offsetting Neogene sediments. Moreover, the reflection profiles across the Batinah coastal plain clearly delineate the upper geometry of Rustaq-Nakhl ophiolite block that was important in the final Bouguer gravity modeling.

For further reading:

Colman, R. G., Tectonic setting for ophiolite obduction in Oman, *Journal of Geophysical Research*, **86**, 2497-2508, 1981.

Searle, M. P. & Cox J., Tectonic setting, origin, and obduction of the Oman ophiolite, *GSA Bulletin*, **111**, no. 1, p. 104-122, 1999.

Hanna, S. S., & Smewing J. D., *Science and Technology Journal* , Sultan Qaboos University, **1**, 1-19, 1996.

Hanna, S. S. & Nolan, S. C., *Journal of Geological Society*, London, **146**, 867-871, 1989.

Le Metour, J., Michel, J.C., Bechennec,F., Platel, J.P., and Roger, J., Geology and Mineral Wealth of the Sultanate of Oman, Dir. Gen. Of Minerals, Ministry of Petroleum and Minerals, Muscat, Oman, 1995.

Receiver Functions from Regional P waves

Vadim Levin and Jeffrey Park, Yale University

Seismic signals from earthquakes at regional distances (200-1000 km) are complex, containing considerable scattered energy. For teleseismic P waves, receiver-function (RF) analysis estimates P-to-S converted energy from buried interfaces in the shallow Earth, using vertical seismic motion to predict motion in the radial and transverse horizontal directions. Theoretically, this principle should apply to shallow-incident P waves and P waves trapped in the crustal waveguide. If so, estimates of Moho depth and of the location of major crustal interfaces, usually the target of wide-angle active-source refraction surveys, could be made from the regional phases of small earthquakes. With a new RF-estimation method based on multiple-taper spectral correlation estimates of P-to-S conversions at frequencies approaching 5 Hz can be obtained. Here we demonstrate the feasibility of using receiver-function analysis on regional P waves to investigate the crust-mantle transition.

We used data from seismic station RAYN (Ar Rayn, Saudi Arabia) that has abundant seismicity within 'regional' distances (up to 1000 km). To facilitate a search for shared features, we selected distant and regional earthquakes that lay within similar backazimuthal ranges. Seismicity within Arabia is scarce, but the Zagros active convergence zone lies at regional distances in the backazimuthal range 30° to 80°. We analyzed 128 regional events for RAYN, with M > 4.5. We also analyzed 35 teleseismic events with M > 6.3 in backazimuthal range 45° to 115°, corresponding to the southern Asian convergence zones and the subduction zones of the southwest Pacific.

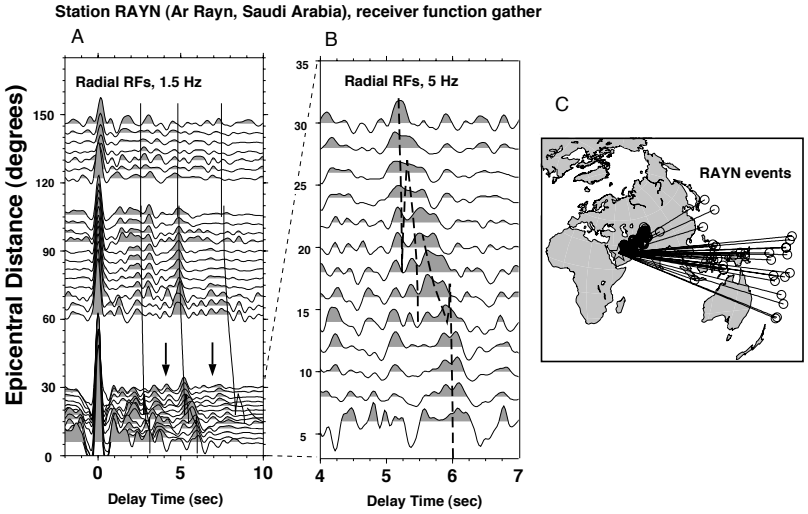

(A) RAYN receiver functions (RF), averaged in epicentral-distance bins with 50% overlap (10° bins for 60°<Δ< 160°; 4° bins for 0°<Δ <30°). Results for broadband data (20 sps) are shown for eastern backazimuths, with RF spectra limited at 1.5Hz. Superimposed delay curves are computed for the three P-S converted phases that would arise from interfaces at 21, 41 and 72 km depth in a simple velocity structure based on the model for RAYN suggested by Levin and Park (2000). The phase velocities of incoming P and P_n waves are computed for a source at 15 km depth using the IASPEI91 model and software. The hypothetical Moho head-wave conversion P_ns has a near-constant delay of 6 s for 0°<Δ< 17°. Arrows show time interval expanded in panel B. (B) Regional and near-teleseismic RAYN receiver functions, averaged in 2° epicentral-distance bins. Results for short-period data (40 sps) are shown for eastern backazimuths, with RF spectra limited at 5Hz. Dashed lines show delay curves for converted phases, as in A. (C) Map of sources used in RF analysis.

We estimated receiver functions at RAYN as a function of epicentral distance, averaging data from sources in overlapping distance intervals. Data overlap causes adjacent traces in the RF profiles to be correlated. Features in the RFs that span three or more adjacent traces are "real," not processing artifacts. Spectra of composite RFs have cutoff frequency 3 Hz, with an effective corner frequency at f=1.5-2.0 Hz. Thin lines traced over the RF profile show expected delay times of Ps converted phases from the major subsurface interfaces identified at RAYN: a midcrustal reflector at 21 km, the Moho at 41 km, and the Hales discontinuity at 72 km.

The conversion from the Moho is a positive one-sided pulse at approximately 4.75 s for teleseismic events (epicentral range 60°to 90°). By extending the RF profile to regional events, we show that the Moho conversion can be easily identified for all epicentral distances. We analyzed the same regional events at RAYN using data from the short-period channels, sampled at 40 sps. In the epicentral range 12° to 20° the Moho pulse bifurcates as a result of a P wave triplication caused by velocity gradients in the mantle transition zone. The timing of the pulse at 5.5—6.0 sec delay is appropriate for a P-to-S conversion from a whispering-gallery P_n phase.

For further reading:

V.Levin and Park, J., Shear zones in the Proterozoic lithosphere of the Arabian Shield and the nature of the Hales discontinuity, *Tectonophysics*, in press, 2000.

A Surface Wave Dispersion Study of the Middle East and North Africa

Michael E. Pasyanos and William R. Walter, Lawrence Livermore National Laboratory
Shannon E. Hazler, University of Colorado, Boulder

We have performed a large-scale study of surface wave group velocity dispersion across the Middle East, North Africa, southern Eurasia and the Mediterranean (Pasyanos et al., 2000). Our database for the region is populated with seismic data from regional events recorded at broadband, 3-component digital stations, including permanent IRIS stations and several PASSCAL deployments, as well as data from Geoscope, Mednet, and other open stations. We measured the group velocity using multiple narrow-band filters on deconvolved displacement data. Overall, we have examined more than 13,500 seismograms and made good quality dispersion measurements for 6817 Rayleigh and 3806 Love wave paths. The top panel in the figure shows the path coverage for 50- second Rayleigh waves. We use a conjugate gradient method to perform a group velocity tomography. Our current results include both Love and Rayleigh wave inversions across the region for periods from 10 to 60 seconds. The bottom panel in the figure shows the inversion results for 50-second Rayleigh wave group velocities.

Our findings indicate that short period structure is sensitive to slow velocities associated with large sedimentary features such as the Mediterranean Sea and Persian Gulf. We find our long period Rayleigh wave inversion is sensitive to crustal thickness, such as fast velocities under the oceans and slow along the relatively thick Zagros Mountains and Turkish-Iranian Plateau. We also find slow upper mantle velocities along known rift systems. We then use the group velocities to model the velocity structure of the crust and upper mantle. When we compare crustal parameters such as crustal thickness to other studies, we find that our results are comparable to other estimates, giving us confidence in our results in poorly covered regions, such as North Africa. Our high-resolution seismic velocity model should help us to better understand the tectonics of the region. This study also has applications to improving small magnitude Ms estimation and event location calculation, both important aspects of monitoring the Comprehensive Nuclear Test Ban Treaty (Pasyanos, 2000).

This work was performed under the auspices of the U.S. Department of Energy by University of California Lawrence Livermore National Laboratory under contract No. W-7405-Eng-48.

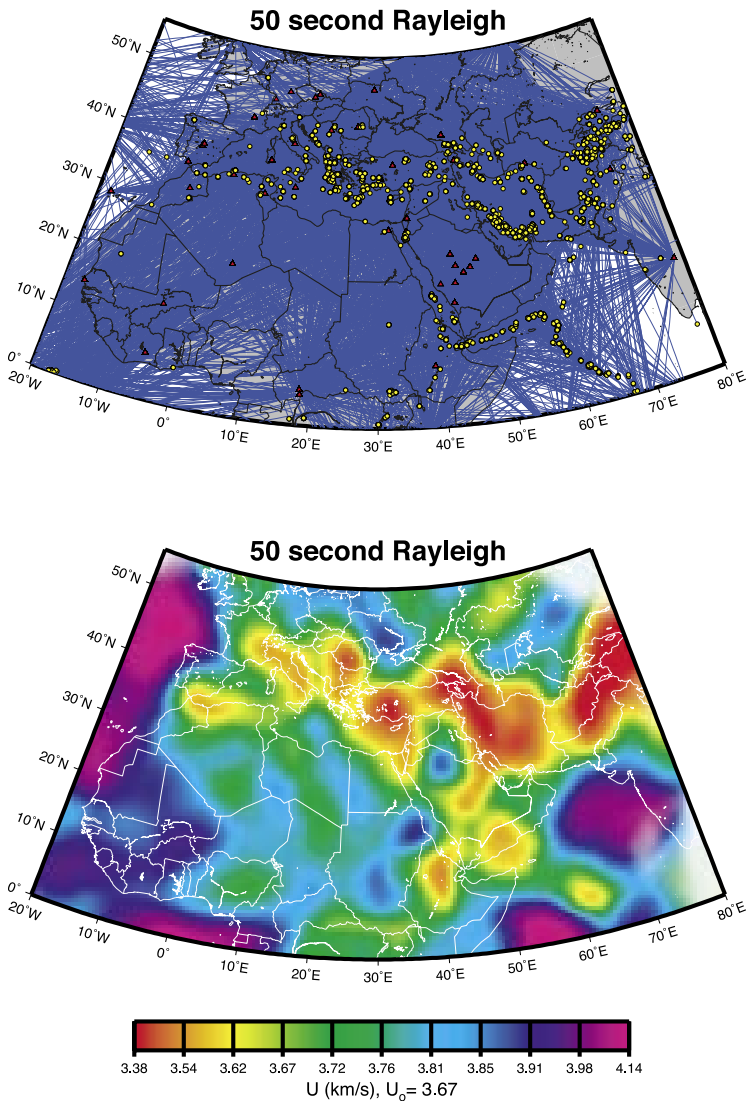

Distribution of paths for 50 second period Rayleigh waves (top) and results of group velocity inversion (bottom) of the same area. The color scheme varies from slow (red) to fast (purple).

For further reading:

Pasyanos, M.E., Predicting geophysical measurements: Testing a combined empirical and model-based approach using surface waves, in press *Bull. Seism. Soc. Amer.*, 2000.

Pasyanos, M.E, Walter,W.R., and Hazler, S.E., A surface wave dispersion study of the Middle East and North Africa for monitoring the Comprehensive Nuclear-Test-Ban Treaty, in press, *Pure App. Geophys*, 2000.

The Ethiopia PASSCAL Project

Andrew A. Nyblade, Charles A. Langston, and Margaret H. Benoit, Pennsylvania State University

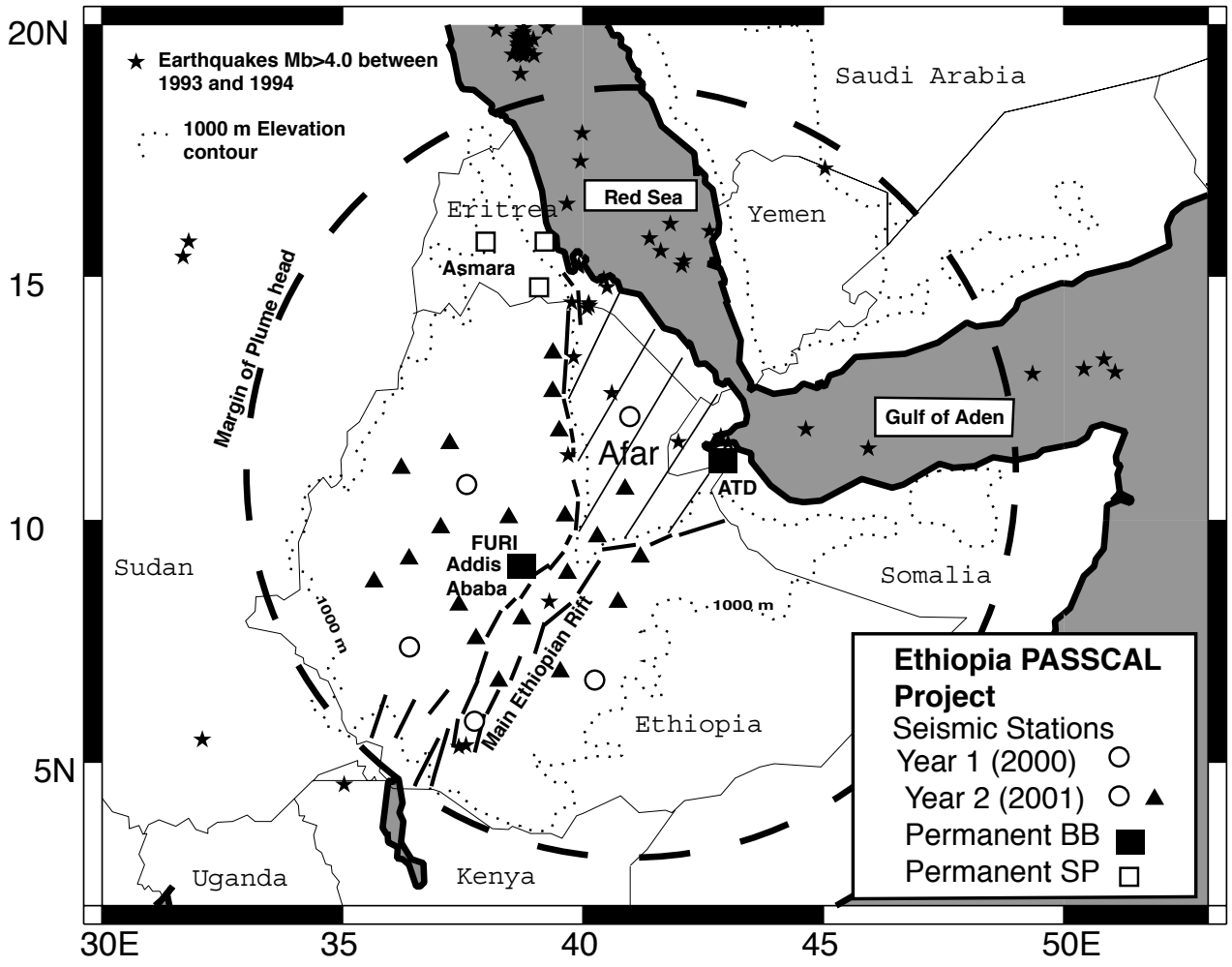

Map of Ethiopia showing the main tectonic features of the region and station locations for the Ethiopia PASSCAL project.

The Ethiopia PASSCAL project consists of a two-year-long deployment of 25 broadband seismic stations to record local, regional and teleseismic earthquakes across the Ethiopian Plateau, the Main Ethiopian Rift, and the Afar Depression. Five stations were installed in Ethiopia during February/March, 2000 and an additional 20 stations will be added to the network in early 2001. A network of up to five broadband stations will also be running in Kenya during the 2000-2001 time interval. The main scientific goal of this project is to image seismically crust and upper mantle structure beneath the Afar hotspot, and then to use our images to evaluate hypotheses for the origin of the hotspot.

Seismic Velocity Structure of the Upper Mantle Beneath Tanzania, East Africa: Evidence for a Mantle Plume?

Andrew A. Nyblade and Charles A. Langston, Pennsylvania State University
Thomas J.Owens, University of South Carolina

East Africa has long been regarded as a region of incipient continental breakup. The Archean Tanzania Craton lies within the center of the East African Plateau and is surrounded by several Proterozoic mobile belts. The Cenozoic rift valleys have developed primarily within the mobile belts. To examine upper mantle structure beneath the East African plateau, local, regional, and teleseismic earthquakes were recorded in Tanzania for one year (1994-1995) using 20 broadband PASSCAL seismographs. Tomographic inversion of teleseismic P and S wave travel times indicates that high-velocity lithosphere beneath the Tanzania Craton extends to a depth of at least 200 km and that low velocity regions beneath the East African rifts extend to depths below 400 km. The velocity contrast between upper mantle under the craton and the rifted mobile belts is about 5 to 6 percent. Results from stacking receiver functions indicate that the 410 km discontinuity is depressed by 20-30 km beneath the Eastern rift. In contrast, the 660 km discontinuity shows little relief. The upper mantle seismic velocity variations coupled with the structure of the 410 and 660 km discontinuities reveal a 200-400 km wide thermal anomaly extending into but not necessarily through the transition zone. This finding is not easily explained with models of small-scale mantle convection induced by passive stretching of the lithosphere but is consistent with the presence of a mantle plume, provided that a plume head lies beneath the eastern margin of the Tanzania Craton.

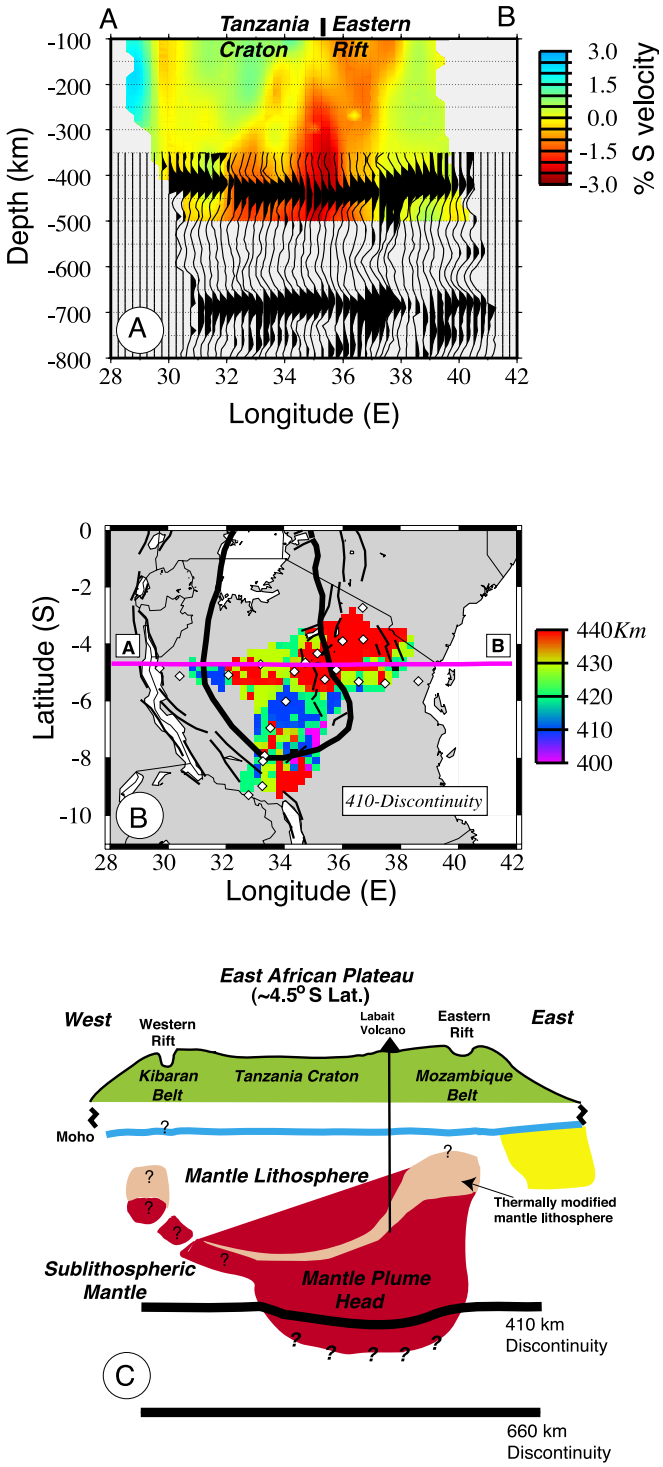

(A) West-east cross section through the S wave velocity model. Uncertainties in the horizontal and vertical dimensions of the velocity structures are ~50 and 100 km, respectively. Velocity structure above 100 km and below 500 km is poorly resolved and therefore is not shown. The location of the cross section is shown in (B). Stacked receiver functions showing the broad depression of the 410 km discontinuity and a flat 660 km discontinuity are superimposed on the S velocity model. Traces begin at 350 km depth to highlight arrivals from the 410 and 660 km discontinuities. (B) Depths to the 410 km discontinuity obtained from receiver functions stacked using a 3-D method. Uncertainties in the depth estimates shown are +/- 5 km. Diamonds give station locations, the wide black line shows the margin of the Tanzania Craton, and the narrower black lines show the major rift faults. (C) Schematic cross section at ~4.5 S showing a plume head beneath the eastern margin of the Tanzania Craton. Question marks beneath the Eastern and Western Rifts and at the bottom of the plume head indicate that the structures illustrated there are poorly constrained.

Regional Wave Propagation and Source Characterization for Earthquakes in East Africa

Charles A. Langston, University of Memphis
Andrew A. Nyblade, Penn State University
Thomas J. Owens, University of South Carolina

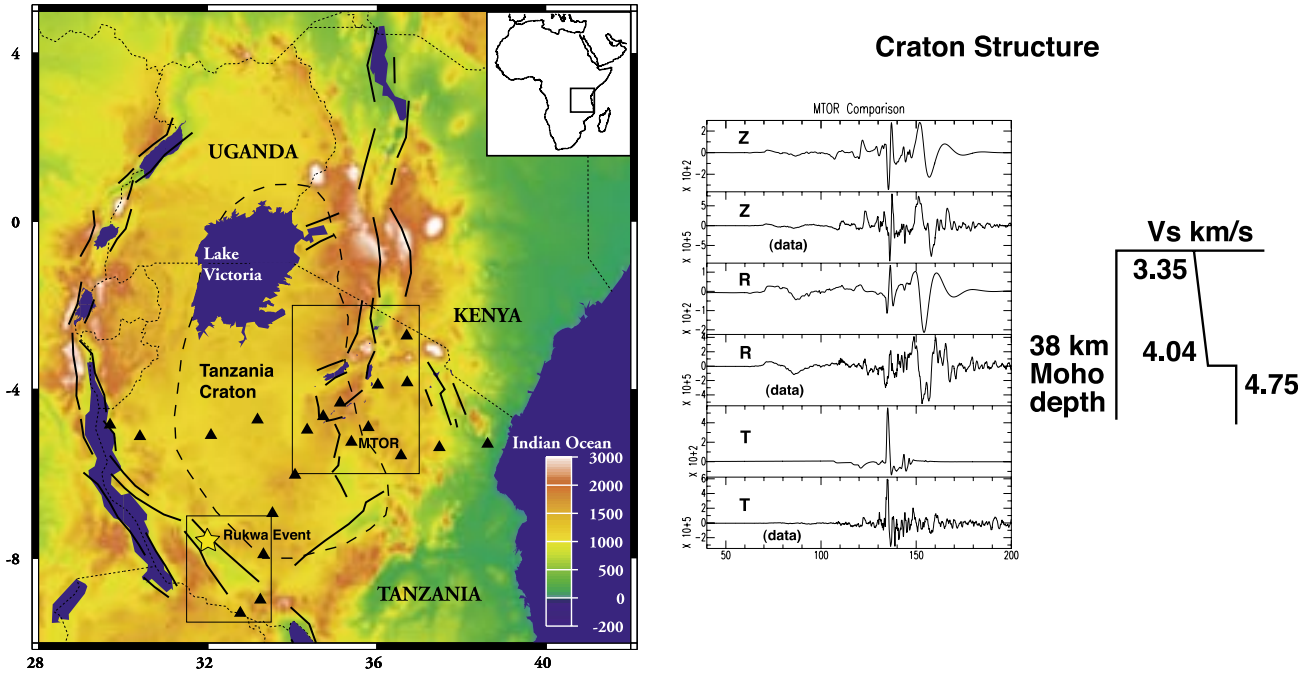

The map shows the location of stations (triangles) for the Tanzania Broadband Seismic Experiment. Topography, major lakes, rift faults and the outline of the surface expression of the Tanzania craton are also shown. The location of the M6 Rukwa graben earthquake is shown as a yellow star. The right hand side shows data from the earthquake, synthetic seismograms and the inferred crustal model for station MTOR. A very simple crustal model can reproduce the character and amplitude of the waveforms. This model has been used to model other smaller events recorded by the experiment.

The 1994-1995 Tanzania Broadband Seismic Experiment was primarily designed as a passive teleseismic array for the purpose of interrogating lithospheric structure under the Tanzania craton. Consisting of 20 continuously recording PASSCAL broadband seismographs deployed across Tanzania, East Africa, the experiment also yielded a rich harvest of data from local and regional earthquakes situated within the craton and within the East African Rift zone. Analysis of this data set has yielded fascinating insights on the nature of regional wave propagation, structure of the crust and uppermost mantle within the craton and rift zones, and earthquake source parameters with implications for the thermal/mechanical structure of the rifts. Utilizing the seismograms from a M6 earthquake in western Tanzania, the simple nature of crustal structure could be inferred directly from broadband waveform modeling in conjunction with well-controlled earthquake source parameters inferred from teleseismic waveform modeling. These constraints on structure give rise to two additional important results. First, knowledge of structure effects gives insight on important, unsolved problems in regional wave propagation such as the excitation and propagation of the Lg wave. Across the Tanzania craton, Lg is seen to be composed of deep turning S wave multiples in the crust that become critical at increasingly larger distances. Secondly, knowledge of the crustal structure allows waveform modeling of other earthquakes to obtain source parameters such as source mechanism and source depth. Modeling of a number of small earthquakes occurring within the rift zones has shown that seismicity occurs throughout the crust and possibly, into the uppermost mantle. This suggests that the lower crust and uppermost mantle in Tanzania is mostly cold and thermally unperturbed by rifting processes. Passive broadband seismic experiments are valuable sources of seismic data in that there are many uses for the data over and above the design parameters of the principal investigators. These kinds of experiments represent Earth exploration in its purest sense and offer the geophysical community numerous opportunities for performing new research years after the original experiment.

Tomographic Imaging of Mantle Structure Beneath Southern Africa

D.E. James, J.C. VanDecar, and M.J. Fouch, Carnegie Institution
S. van der Lee, ETH, Zurich

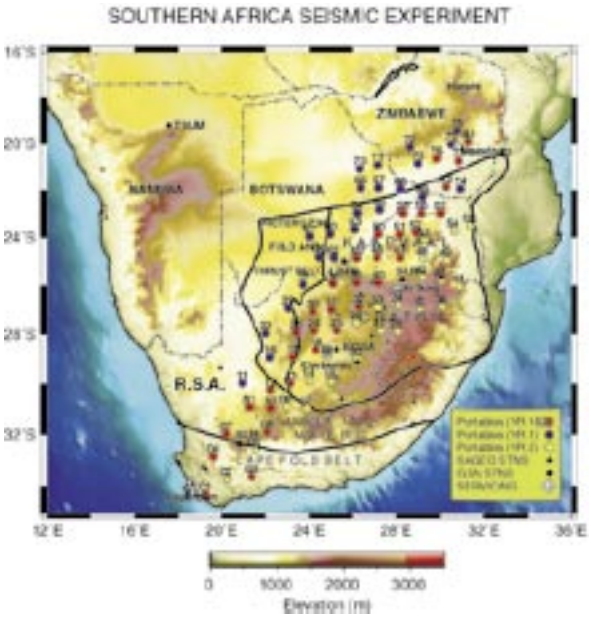

The Southern Africa Seismic Experiment, an array of 55 PASSCAL and Carnegie portable broadband seismic stations, was deployed from April 1997 to July 1999 along a NNE-SSW transect 1800 km long by 600 km wide, covering three countries of southern Africa (Figure 1). Approximately half the stations were redeployed to new sites in April/May 1998 for a total of 82 stations. The PASSCAL telemetered array of 30 REFTEK/STS2 stations was deployed in the region of Kimberley, South Africa for a period of about six months early in 1999.

This major seismic experiment was part of the multidisciplinary Kaapvaal Project undertaken jointly by Carnegie Institution, MIT, southern African academic institutions and industry collaborators to study the formation, structure, composition, and evolution of the Archean cratons and adjacent Proterozoic belts of southern Africa. Extensive geochemical and petrologic studies of an abundance of kimberlite-derived mantle xenoliths found in southern Africa complement the seismic investigations. These thoroughly studied xenoliths demonstrate that a buoyant, highly depleted, and ancient tectospheric mantle keel extends beneath the Kaapvaal and Zimbabwe cratons to all depths from which xenoliths have been derived, some in excess of 200 km (e.g., Carlson et al., 1999).

Approximately 8000 teleseismic P-wave delay times from over 200 events recorded by the broadband array were analyzed to obtain tomographic images of mantle structure beneath southern Africa to depths in excess of 1000 km (Figure 2). With a few notable exceptions, high velocity (blue) mantle material clearly defines the boundaries of the Kaapvaal and Zimbabwe cratons. The most prominent high velocity regions shown on the horizontal sections (depths 150 and 300 km) define the undisturbed (southern) core of the Kaapvaal craton. Here, as shown in vertical section A-A', the mantle root of the craton attains depths of at least 250 km and perhaps as much as 300 km. The tomographic evidence to date indicates that except for regions of disrupted craton (as in the Bushveld) the tectospheric root appears to be at least 200 km almost everywhere beneath Archean terranes, including the Limpopo Belt, an Archean collision zone wedged between the Kaapvaal and Zimbabwe cratons. Post-Archean terranes adjoining the cratons are generally characterized by distinctly lower upper mantle velocities and the Phanerozoic Cape Fold Belt by much lower velocity upper mantle.

The Bushveld province within the Kaapvaal craton is notable for the relatively lower velocities in the mantle root beneath the region. The velocity anomaly, which extends well west of the Bushveld intrusion itself, correlates well with greater crustal delay times and with a zone of null SKS splitting. The seismic results coupled with evidence of younger Re/Os model ages (Carlson et al., 1999) of mantle nodules within the region of the Bushveld suggests possible cratonic disruption during formation of the great layered Bushveld intrusive complex (about 10^6 km^3).

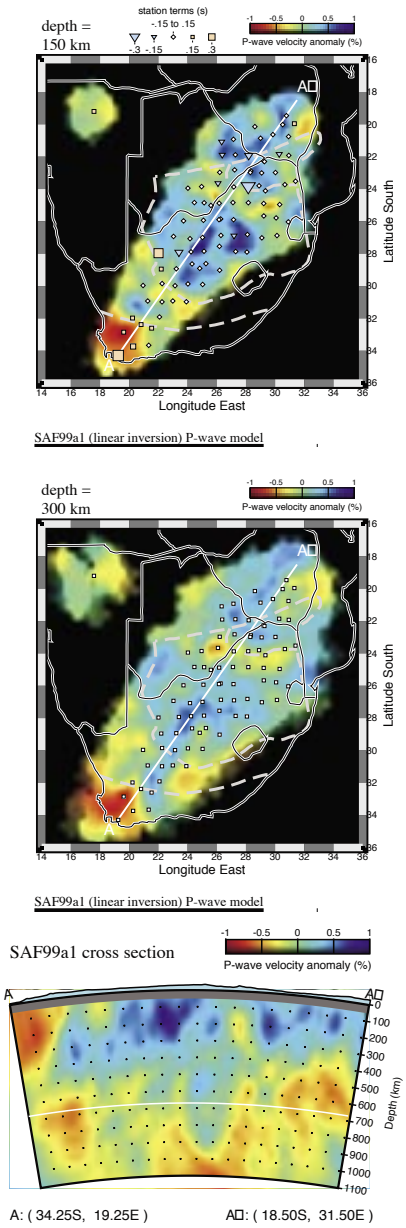

Figure 2

For further reading:

Carlson, R.W., Pearson, D.G., Boyd, F.R., Shirey, S.B., Irvine, G., Menzies, A.H., and Gurney, J.J., Re-Os systematics of lithospheric peridotites: Implications for lithosphere formation and preservation, (in) Proceedings of the 7th International Kimberlite Conference, Capetown, South Africa, edited by J.J. Gurney, J.L. Gurney, M.D. Pascoe, and S.H. Richardson, **1**, 99-108, 1999.

Crustal Structure of the Kalahari Craton and Adjacent Mobile Belts from Analysis of Broadband Teleseismic Waveforms

T. Nguuri and C. Wright, WITS, Johannesburg, RSA
J. Gore and T. Zengeni, U. Zimbabwe
J. Harvey, UCT, Capetown, RSA
D. James, Carnegie Institution

The southern Africa seismic experiment of the Kaapvaal Project provided an unprecedented opportunity to map Moho morphology over a wide region of varying geologic and topographic terranes. The experiment, carried out during a two- year period with 55 PASSCAL and Carnegie REFTEK/STS-2 seismograph units, covered nearly a million km^2 in three countries of southern Africa. A total of 82 stations were deployed for a period of at least one year. Receiver functions were computed for all stations and stacked by a phasing-depth method that corrects for moveout. No corrections were made for varying azimuth of arrivals. Results of the stacking are shown in at right, where station names and number of stacked traces are shown to the right of each trace. A map of depth to Moho based on a 1-D crustal velocity model is shown below. The stacked traces in the figure to the right are organized by terrane. Receiver functions for stations on undisturbed craton exhibit a very well defined Moho signature. For terranes off craton and in disturbed craton, Moho signatures are considerably weaker. For the highly deformed Limpopo Belt, Moho signals are either ambiguous, smeared out, or, in some cases, virtually absent.

PHASING DEPTH IMAGES

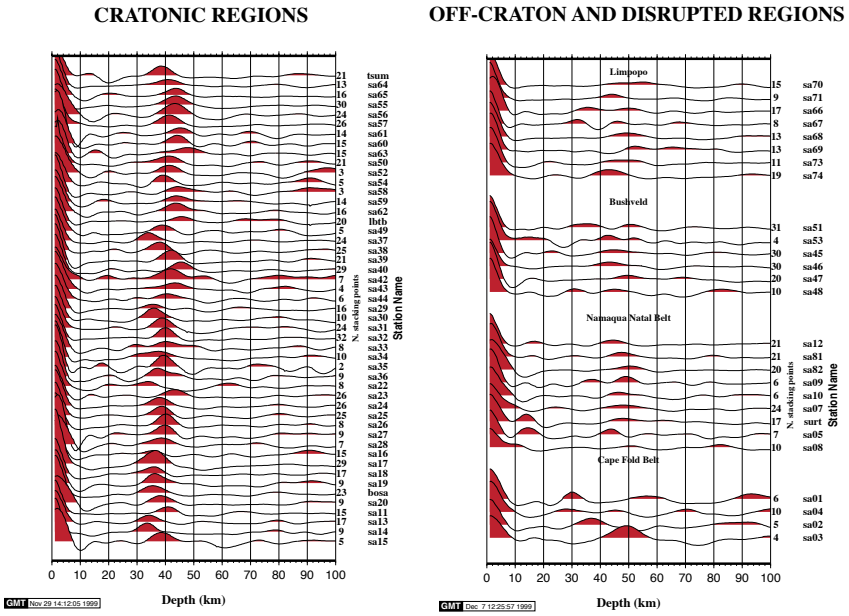

Results of the receiver function analysis show the following:

(1) Crustal thickness in southern Africa does not correlate with elevation. Regions of high elevation within the undisturbed Kalahari (Kaapvaal + Zimbabwe) craton tend to be characterized by thin crust, whereas some regions of low elevation, such as the Archean Limpopo mobile belt between Kaapvaal and Zimbabwe cratons, have notably thickened crustal sections. Absence of a correlation between crustal thickness and Bouguer gravity anomaly indicates isostatic balance is achieved by lateral density contrast in the upper mantle and/or in the crust. Both may be important.

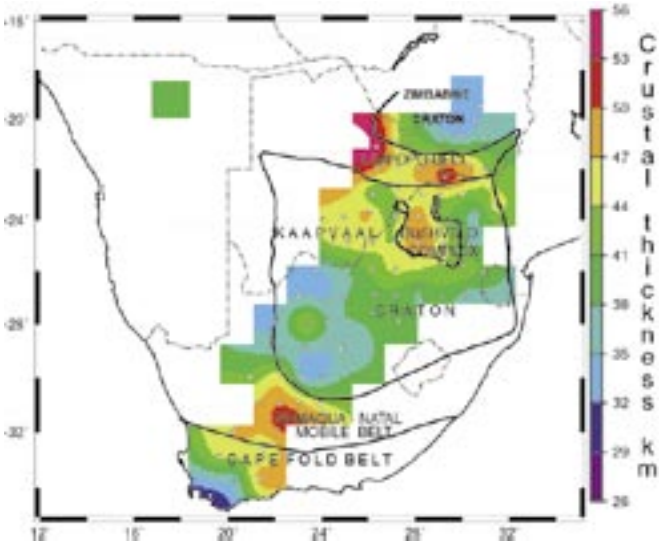

(2) In regions of undisturbed craton, the M-discontinuity is sharp with a major first order jump in velocity. Elsewhere, including off-craton and disturbed craton, the Moho is much less well defined. The remarkably clean character of the Moho beneath the craton suggests that the process of crustal formation: (i) was highly efficient in separating crust from mantle; (ii) produced a nearly planar first-order M-discontinuity; and (iii) gives no indication of magmatic underplating or other processes for accreting material to the base of the Archean crust. Such simple Moho structures are observed consistently in cratons but are not common in post-Archean continental terranes.

(3) Intermediate crustal discontinuities are rarely observed anywhere in the Kalahari craton, indicating little or no layered differentiation of the Archean crust.

Seismic Anisotropy Beneath Southern Africa

Stephen S. Gao, Kansas State University
Paul G. Silver, Carnegie Institution of Washington

Seismic anisotropy revealed from SKS and SKKS splittings measured at 79 sites in southern Africa supports the notation that in old cratonic areas, anisotropy is primarily caused by structural fabrics frozen in the lithosphere. Most of the boundaries between different tectonic units are also boundaries dividing different characteristics of the two splitting parameters, the fast polarization direction Φ and splitting time Δt, which provide constraints on the orientation and layer thickness of mantle deformation, respectively.

Values of Φ follow closely the orientation of Archean orogenic structures, suggesting that the mantle deformation is preserved as fossil anisotropy. Splitting delay times are small, averaging 0.45 s, compared to a global average of about 1 s for continents worldwide. The simplest explanation is a single layer that is either thin (about 60 km) or possesses weak (about 2%) intrinsic anisotropy. The correspondence between Φ and direction of ancient structures lends support to the vertically coherent deformation hypothesis, since the simple asthenospheric flow model cannot easily account for such small scale variations. One of the implications of the vertically coherent deformation model is that the anisotropy is early Archean in age, making it the oldest anisotropy yet detected.

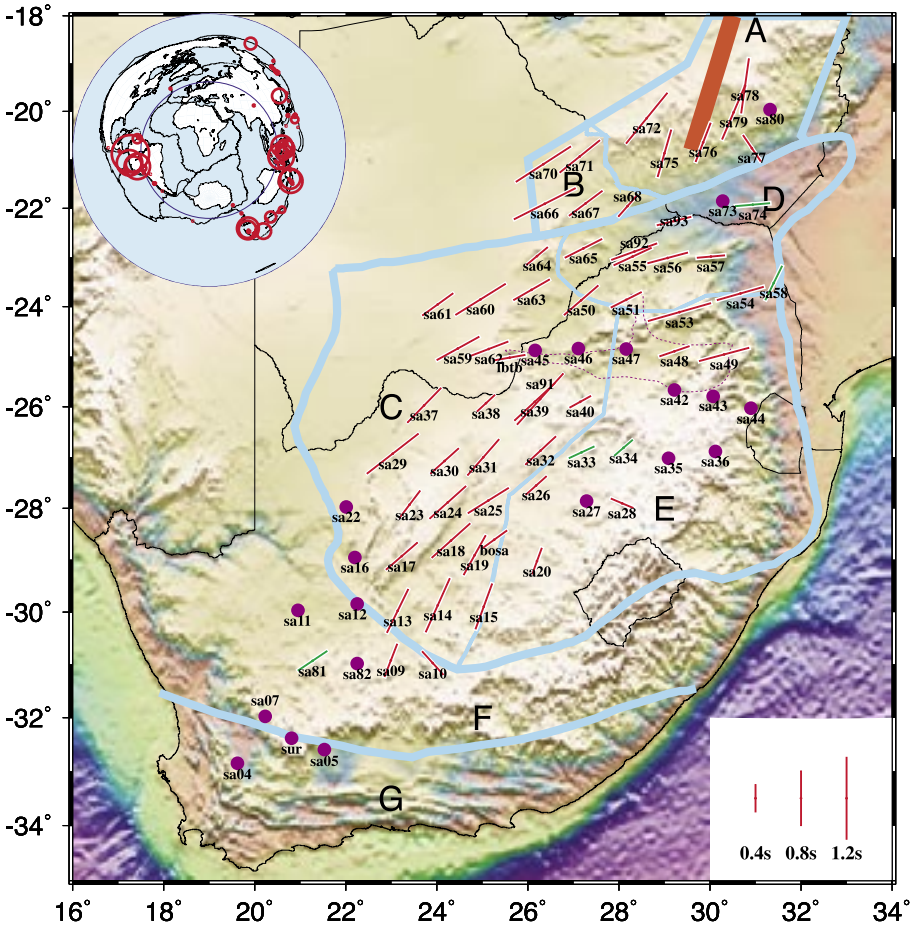

Map showing results of shear wave splitting measurements, topography, and boundaries of tectonic areas of southern Africa. Red bars are well-defined measurements with the direction being the fast polarization direction and the length being proportional to the size of the splitting. Blue bars are poorly-defined measurements, and purple dots represent measurements with zero or near-zero splitting times. The thick line in Area A represents the Great Dykes. The small inset at the top-left corner shows the location of the events used in the study. The size of the circles is proportional to the number of used SKS and SKKS records from the event.

Azimuthal Anisotropy of the Australian Upper Mantle

F.J. Simons and R.D. van der Hilst, Massachusetts Institute of Technology

Azimuthal anisotropy provides important insight into the structure and evolution of continental lithosphere. Seismic anisotropy reflects the alignment of anisotropic mantle crystals. It links the static wave speed distribution (and the parameters inferred from it, such as composition and temperature) with geodynamic aspects such as mantle shearing and lithospheric deformation.

Australia is the ideal place to investigate anisotropy in and below a continent and to investigate the relative importance of either pre-existing geological structures or upper mantle shear related to plate motion; its location amidst belts of high seismic activity allows excellent data coverage, it consists of a wide range of geological domains, and it has been involved in rapid plate motion for several tens of million years.

The SKIPPY project (Van der Hilst et al., 1994) has obtained a wealth of high-quality broadband data, which - along with data from permanent observatories of the GSN, GEOSCOPE and AGSO networks - allows a range of tomography applications. Thus far, the surface wave studies have focused on isotropic wavespeed variations (Zielhuis and Van der Hilst, 1996; Simons et al., 1999). However, the excellent data coverage also allows joint inversions for velocity heterogeneity and anisotropy; such studies are often prohibited by insufficient resolution of the isoptropic models so that the intrinsic trade-offs cannot be controlled. Our preliminary models are based on fundamental and higher mode data from a total of about 2200 wave paths, mostly from within the Australian plate, which densely sample the continent of Australia.

We invert for the relationships that exist between the elastic constants of a generally, but slightly, anisotropic medium (Montagner and Nataf, 1986). We use the isotropic path averages obtained from the waveform inversion of fundamental and higher Rayleigh modes and invert for aspherical shear wave speed heterogeneity and two azimuthal parameters which are dependent of geometric functions of the azimuth of the path.

We have investigated the influence of different tomographic inversion techniques (Simons et al., 2000). In inversions for 3-D shear-wave structure using surface waves, one of three philosophies is usually followed. The first uses a global basis, such as spherical harmonics, to represent the lateral variations of the model parameters. The second relies uses a statistical formulation to characterize the unknown parameters by an a priori covariance function (Montagner, 1986). In a third, the wavespeed variations are expanded by means of discrete blocks. For regional studies only the latter two approaches are convenient. We use different parameterizations to quantify the reliability and robustness of the models resulting from the third approach. In addition to regular grids we use grids of which the node spacing is adapted to the predicted model resolution, and grids which represent the average structure of predefined tectonic regions. Furhtermore, we investigate how the inclusion of anisotropic parameters trades off with the isotropic results. Finally, we aim to interpret the anisotropic results in the framework of the large-scale structure and evolution of the continent, and pursue ties to mineralogy and results from shear-wave splitting measurements.

The figure presents preliminary results for depths 80, 140, 200 and 300 km. While in the first two layers the anisotropic maximum direction is too variable to allow interpretation in terms of mantle flow (it may thus represent the frozen anisotropy of the complexely built continent), in the latter two the maximum directions seem much smoother and are more in agreement with the direction of absolute plate motion, which is roughly NNE. However, the magnitude of this deeper anisoptropy is relatively small considering the fast northward motion of the Australian plate. In contrast to the isotropic component, the depth variation of the magnitude of anisotropy appears poorly correlated with the age of the crust or the main tectonic units. The shear wave splitting directions predicted by interpreting our model in terms of horizontal axes of anisotropy are not readily in accord with observed SKS-splitting measurements (Clitheroe and Van der Hilst, 1998; Ozalaybey and Chen, 1999). However, this depth-integrated measure of anisotropy seems to divide the continent into major structural units of homogeneous anisotropic directions, varying on length scales of less than one thousand kilometers.

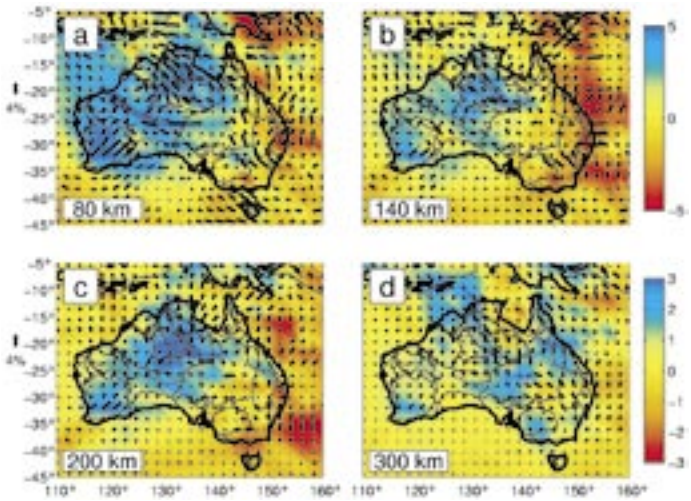

For further reading:

Montagner, J.-P., Regional three-dimensional structures using long-period surface waves, *Ann. Geophys.*, **4**, 283-294, 1986.

Montagner, J.-P., and H.-C. Nataf, A simple method for inverting the azimuthal anisotropy of surface waves, J. Geophys. Res., 91, 511-520, 1986.

Ozalaybey, S., and Chen, W.P., Frequency-dependent analysis of SKS-SKKS waveforms observed in Australia: Evidence for null birefringence, *Phys. Earth Planet. Inter.*, **114**, 197-210, 1999.

Simons, F. J., Zielhuis, A., and van der Hilst, R.D., The deep structure of the Australian continent from surface-wave tomography, *Lithos*, **48**, 17-43, 1999.

Simons, F. J., van der Hilst, R.D., Montagner, J.-P., and Zielhuis, A., Shear-wave speed heterogeneity and azimuthal anisotropy of the Australian upper mantle from fundamental and higher-mode Rayleigh-wave tomography, *Geophys. J. Int.*, in preparation, 2000.

van der Hilst, R. D., Kennett, B.L.N., Christie, D. and Grant, J., Project Skippy explores the lithosphere and mantle beneath Australia, *Eos Trans. AGU*, **75**, 177-181, 1994.

Zielhuis, A., and van der Hilst, R.D., Upper-mantle shear velocity beneath eastern Australia from inversion of waveforms from Skippy portable arrays, *Geophys. J. Int.* **127**, 1-16, 1996.

Antarctic Network of Unattended Broadband Seismometers

Sridhar Anandakrishnan, University of Alabama

The Antarctic is a gaping hole in the rapidly improving field of global seismic imaging and tomography. On this huge continent (surface area of 14 million square km) there are only eight broadband seismic observatories. Furthermore, all of those stations are along the margins of the continent (except for SPA at the South Pole) and none are in the West Antarctic. We have deployed seismic stations in the interior of the continent and successfully operated them through the Antarctic winter using wind generators to produce power. This five-year experiment, funded by the NSF Office of Polar Programs, is aimed at understanding the local and regional seismicity of Antarctica, the crustal thickness and properties, and to image upper mantle velocities, all of which are poorly known. The ice that covers 98% of the continent prevents much of the traditional geologic interpretation, so seismic methods are particularly valuable.

To adequately answer these questions, year-round data is needed, which is a difficult technical problem in the cold and dark Antarctic winter from April to September. For that reason we developed custom power, heating, and data-logging devices that power the PASSCAL equipment through the winter. Satellite telemetry is used for State-Of-Health information, and seismic data are stored onsite. The current status of the system can be monitored in real time at http://ice.geo.ua.edu/~sak/Anubis. Six stations are deployed in a sparse network in W. Antarctica, and four more are deployed in East Antarctica.

For further reading:

Anandakrishnan, S., Penguins everywhere: GNU/Linux in Antarctica, *IEEE Software*, **16**, 90–98, 1999.

Anandakrishnan, S., Voigt, D.E., Burkett, P.G., Long, B.R., and Henry, R.C., Deployment of a broadband seismic network in West Antarctica, *Geophysical Research Letters*, in press.

Shear Wave Splitting from the MOMA and NOMAD PASSCAL Seismometer Arrays

Matthew J. Fouch, Carnegie Institution of Washington
Karen M. Fischer, E. Marc Parmentier, Brown University
Michael E. Wysession, Washington University
Timothy J. Clarke, New Mexico Institute of Mining and Technology

The Missouri-Massachusetts broadband seismometer deployment (MOMA) and the North American Mantle Anisotropy and Discontinuity experiment (NOMAD) are two PASSCAL arrays that were deployed in the eastern U.S (Figure). MOMA is a 20-station array that extended across the eastern U.S. from January 1995 to March 1996, and NOMAD is a 6-station array that was located in central NY state and areas of CT state from June 1997 to March 1999. Both arrays were complemented by nearby permanent GSN stations, and were uniquely positioned to seismically probe the crust, mantle, and core-mantle boundary from a variety of earthquake sources.

To examine the structure of the lithosphere and deeper mantle beneath eastern North America, we performed shear wave splitting analysis of SKS, SKKS, and PKS waveforms from these arrays (Fouch et al., 2000). This study documented short spatial scale variations in upper mantle anisotropy across the eastern United States. Specifically, fast directions for stations located within the continental keel (blue and green regions, Figure) are roughly parallel to absolute plate motion, while fast directions for the eastern third of the array (orange and red regions, Figure) exhibit rapid variations in fast directions. Splitting times average ~1.0 s at most stations. No variation of splitting parameters with respect to backazimuth is observed, but while dipping layers of anisotropy or multiple layers of anisotropy are not required, they also cannot be ruled out with our data set.

We developed models of mantle flow around a complex lithospheric keel to evaluate the potential contribution of sublithospheric mantle flow to the shear wave splitting pattern from eastern North America. These calculations indicate that a combination of lithospheric and sublithospheric anisotropy is a viable model for the origin of shear wave splitting in this region. This hypothesis is corroborated for a sub-region at the edge of the keel, where inversions of Rayleigh wave phase and amplitude data coupled with SKS splitting results require significant anisotropy at depths of 200 km or more (Li et al., 1999; box in Figure). Our results, combined with other studies of shear wave splitting for eastern North America, strongly suggest that both past lithospheric deformation and recent sublithospheric mantle flow make a significant contribution to the observed shear wave splitting pattern.

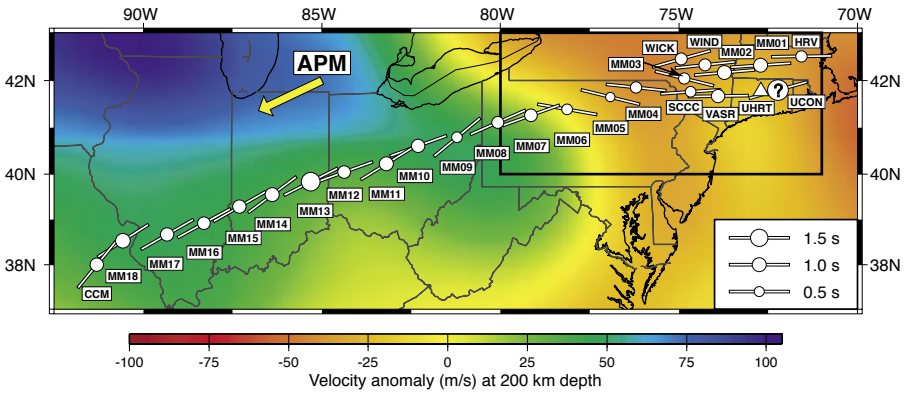

Station locations and shear wave splitting parameters for GSN stations CCM and HRV, the Missouri to Massachusetts broadband seismometer array (MOMA), and the North American Mantle Anisotropy and Discontinuity experiment (NOMAD). Background velocity image is from Van der Lee and Nolet (1997). Keel is demarcated by fast (blue and green) regions. APM, absolute plate motion. Splitting time at station UCON is questionable and is marked with a question mark; we did not retrieve well-constrained splitting parameters at station UHRT (open triangle). The stacking method of Wolfe and Silver (1998) was used to compute average station parameters. Splitting parameters for HRV are taken from Barruol et al. (1997). Fast directions are denoted by azimuth of solid bar; open circles are scaled to splitting time. Splitting times average ~1.0 s at most stations. Fast directions are roughly parallel to APM from station MM07 to the west, but rotate to a more E-W fast direction from station MM06 to the east. The rapid rotation in fast directions may be explained by variations in lithospheric anisotropy, mantle flow-induced sublithospheric anisotropy, or a combination of both factors.

For further reading:

Barruol, G., Silver, P.G., and Vauchez, A., Seismic anisotropy in the eastern United States: Deep structure of a complex continental plate, *J. Geophys. Res.*, **102**, 8329-8348, 1997.

Fouch, M. J., Fischer, K.M., Parmentier, E.M., Wysession, M.E., and Clarke, T.J., Shear wave splitting, continental keels, and patterns of mantle flow, *J. Geophys. Res.*, **105**, 6255-6275, 2000.

Li, A., Forsyth, D.W., and Fischer, K.M., Evidence for azimuthal anisotropy in lithosphere and asthenosphere beneath eastern North America, *Eos Trans. AGU*, **80**(46), Fall Meet. Suppl., F730, 1999.

Van der Lee, S., and G. Nolet, Upper mantle S velocity structure of North America, *J. Geophys. Res.*, **102**, 22,815-22,838, 1997.

Wolfe, C. J., and Silver, P.G., Seismic anisotropy of oceanic upper mantle: Shear wave splitting methodologies and observations, *J. Geophys. Res.*, **103**, 749-771, 1998.

Velocity Structure Beneath Central and Northeastern United States from Surface Waves Recorded by the Missouri-to-Massachusetts (MOMA) IRIS PASSCAL Broadband Deployment

G. I. Al-Eqabi, M. E., Wysession, and P. J., Shore, Washington University
K. Koper, University of Arizona
K. M. Fischer, Brown University
T. J. Clarke, New Mexico Institute of Mining and Technology

The Missouri-to-Massachusetts (MOMA) Broadband Seismometer Deployment array stations provide an opportunity to investigate the lateral variations in the crust and upper-mantle structure of the central and northeastern United States. Fundamental mode Rayleigh and Love waveforms observed across the array show resolvable dispersion up to 50 MHz (Figure, top section). Earthquakes in western North America (Texas and the Gulf of California) have occurred nearly along the strike of the array, providing an opportunity to construct a two dimensional image through the crust and mantle. For example, for the April 4, 1995 Western Texas earthquake and the August 28, 1995 Gulf of California earthquakes both Rayleigh and Love waves have resolvable dispersion and show similar moveouts. The effect of lateral heterogeneity along the array has been quantified by mapping the surface wave moveouts as lateral variations in the waveguide. In this study, we applied a genetic algorithm-based inversion method to search for an optimal laterally varying shear wave structure beneath the array. The objective of the modeling is to have the surface wave recorded at the nearest station match the observed surface wave at the farthest station after it has been propagated through the derived 2-dimensional structure. To achieve this, the interstation velocity models were improved by a sequence of comparison between observed surface waves and analytically propagated surface waves. The interstation one-dimensional velocity models are combined to produce a two-dimensional laterally-varying velocity structure beneath the MOMA array (Figure, bottom section).

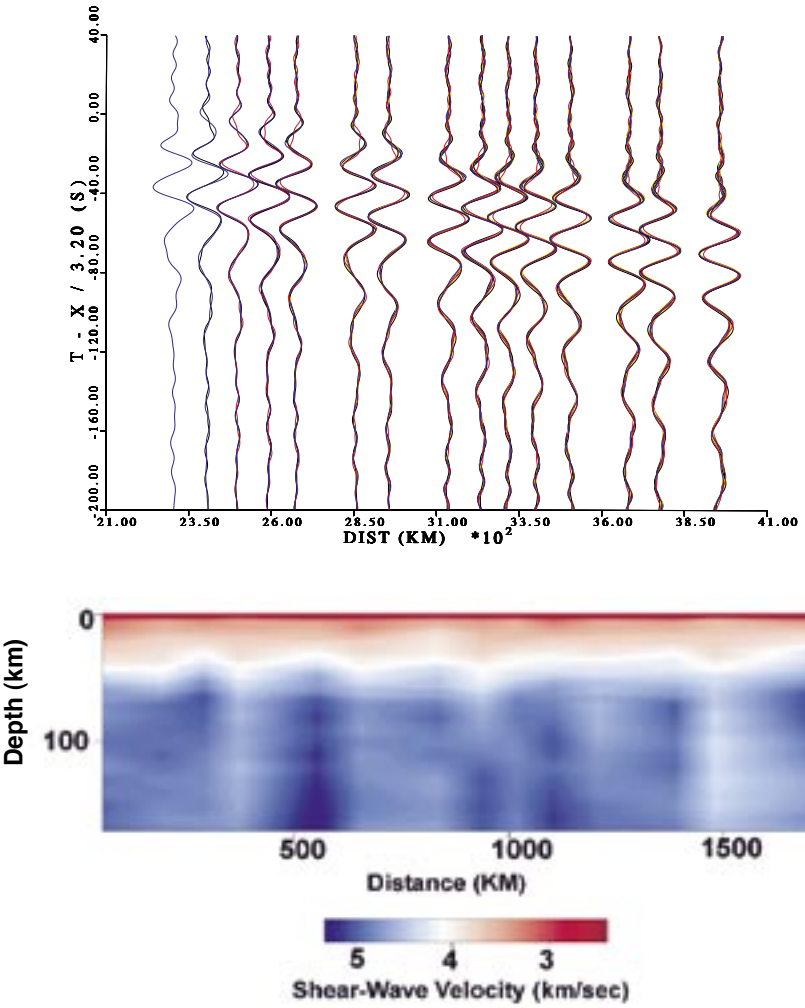

Top section: Shows an excellent match between the observed fundamental mode Love wave and the analytically propagated Love wave waveforms.

Bottom section: Shear wave velocity structure beneath the MOMA array derived from Love wave inversion using genetic algorithm.

Imaging the Eastern Edge of the North American Keel

Karen M. Fischer and Aibing Li, Brown University
Matthew J. Fouch, Carnegie Institution of Washington
Michael E. Wysession, Washington University
Donald W. Forsyth, Brown University
Timothy J. Clarke, New Mexico Institute of Mining and Technology

Keels of seismically fast, cold, lithospheric mantle extend to depths of 200 km or more beneath the stable interiors of most continents. By determining how mantle velocity gradients, anisotropy and radial discontinuities vary across keel margins, we can better understand keel properties and how the keels interact with surrounding mantle flow. These questions have been studied in eastern North America using data from the 1995-1996 MOMA Seismometer Experiment that reached from Missouri to Massachusetts, the 1997-1999 NOMAD Seismometer Experiment in New York and New England, and PASSCAL deployments conducted by other institutions (ABBA, New England Broadband Experiment, ABITIBI). The denser station spacing of these portable arrays provides much higher resolution of mantle structure than was previously possible. However, the longer term history of the GSN and USNSN stations has proven critical in providing a common baseline that ties together data from non-simultaneous portable deployments.

A key question is whether cold temperatures associated with the keel extend through the upper mantle into the transition zone, perturbing the depths of the mineral phase changes responsible for the mantle velocity discontinuities at ~410 km and ~660 km. Ps conversions recorded across the MOMA array indicate that no significant long wavelength topography exists on the "410" velocity discontinuity across the keel's eastern margin. This result implies that broad thermal anomalies of more than 100°C-150°C do not impinge on the transition zone, and that the keel does not produce large-scale cold downwelling that extends into the transition zone. Depression of the "660" to the southwest of the MOMA array may reflect its intersection with the subducted Farallon lithospheric slab.

To obtain better constraints on the distribution of azimuthal anisotropy with depth, we combined the unique vertical resolution provided by surface waves with the excellent lateral resolution afforded by SKS shear-wave splitting measurements. Specifically, variations in Rayleigh wave phase and amplitude data between array stations were used to solve for wavefield parameters and azimuthally varying phase velocities, and phase velocities were then jointly interpreted with SKS splitting observations. Application of this method to broadband stations in the northeastern United States and southeastern Canada reveals the presence of significant anisotropy at depths of 200 km or more. This result implies that, at least immediately outside the keel margin, the deeper mantle is mechanically decoupled from lithospheric plate motion.

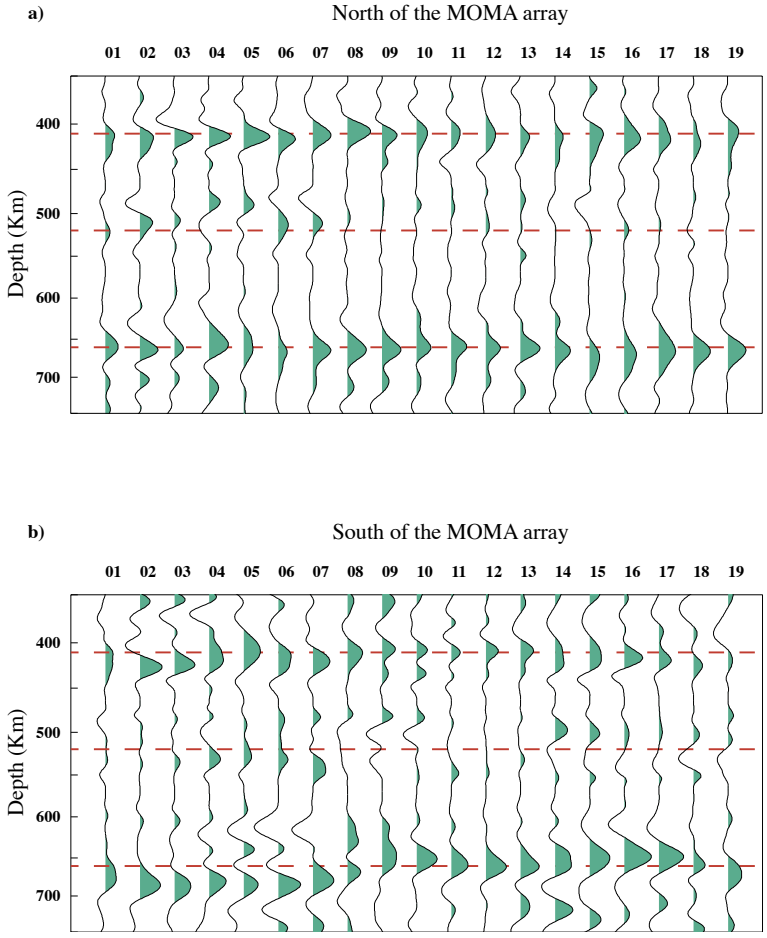

For further reading:

Fischer, K. M., van der Hilst, R.D., A seismic look under the continents, *Science*, **285**, 1365-1366, 1999.

Fouch, M. J., Fischer, K.M., Parmentier, E.M., Wysession, M.E., and Clarke, T.J., Shear-wave splitting, continental keels, and patterns of mantle flow, *J. Geophys. Res.*, **105**, 6255-6275, 2000.

Li, A., Fischer, K.M., Wysession, M.E., Clarke, T.J., Mantle discontinuities and temperature under the North American continental keel, *Nature*, **395**, 160-163, 1998.

Li, A., Fischer, K.M., van der Lee, S., Wysession, M.E., Crust and upper mantle discontinuity structure beneath eastern North America, *J. Geophys. Res.*, submitted, 2000.

No Regional Anisotropic Domains in the Northeastern US Appalachians

Vadim Levin, Jeffrey Park and Mark Brandon, Yale University
William Menke, LDEO/Columbia University

The purpose of this research was to test the proposition that the mantle beneath northeastern North America is divided into several "anisotropic domains" that are the seismic expression of the plate tectonic process of "terrain accretion." Were such the case, we would expect different directions of the shear wave fast direction and different mean shear wave velocities in each of the several terrains (whose existence has been established geologically). Thus we assembled shear wave travel-time and splitting databases for all the broadband seismic stations that were operated - even only temporarily - in northeastern North America for the past five years. These data included observations by permanent stations whose data is archived at the DMC, and data from a number of PASSCAL arrays (MOMA, ABBA and NEWE). See http://www.iris.washington.edu/PASSCAL/EasternUS.htm for detailed descriptions.

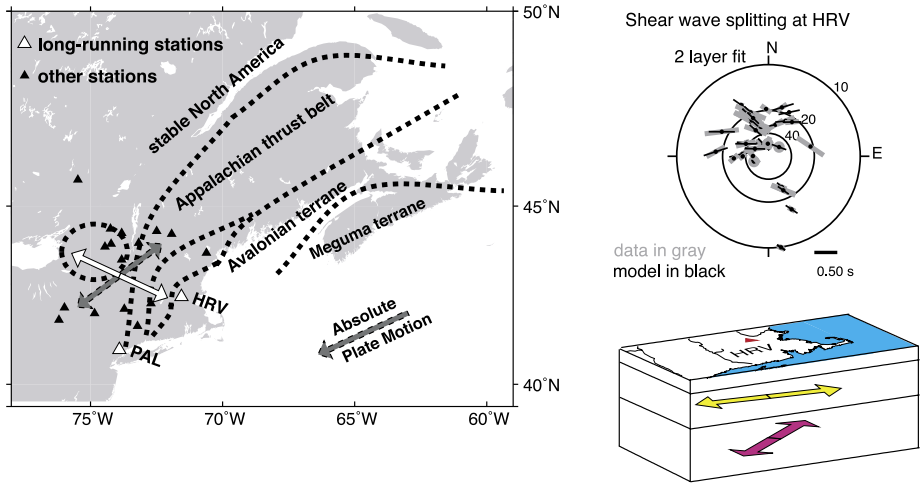

(left) Map of station network. Major tectonic boundaries for the Northern Appalachian orogen are indicated. Horizontal projections of our best-fit anisotropic fast-axis directions are indicated with double-headed arrows within the cluster of station locations (triangles). The light arrow represents the top layer. The shaded arrow represents the bottom layer. The dashed ellipse within stable North America indicates the Adirondack Mountains. (right) Shear-wave fast direction and delay for SKS waves received at GSN station HRV between 1990 and 1997. Data are shown as a gray bar centered on the nominal back azimuth and apparent velocity, with the bar's orientation parallel to the azimuth of the the fast direction, and its length proportional to the delay. Near-zero delays are plotted with open circles. SKS splitting values predicted for a two-layer anisotropic model (see schematic and Levin et al, 1999) are plotted as solid bars.

We analyzed the splitting data by comparing it to synthetic measurements drawn from synthetic seismograms computed for anisotropic models. We tomographically inverted the traveltime data. Much of the data analysis and modeling code was custom-written (by us) for this project. The results are quite suprising, and show:

- The pattern of shear wave fast directions across northeastern North America is very homogeneous. No anisotropic domains occur.
- At a given station, the pattern of shear-wave fast directions varies rapidly with the back-azimuthal angle to the earthquake epicenter. This pattern has a strong "four-theta" component that can be explained in a most excellent manner by postulating two layers of mantle anisotropy.
- These layers are laterally homogeneous across northeastern North America.
- The top layer has a shear wave fast direction oriented toward/away from the center of the craton. We believe it to be unrelated to the dynamics of the Precambrian craton, and instead to be related to a period of intense strain experienced by all the terrains during a lithospheric delamination, likely to have occurred during the during the Appalachian orogeny.
- The bottom layer has a shear wave fast direction oriented parallel to the edge of the craton. We believe it to be related to asthenospheric flow.
- Shear wave velocities at 100 km depth are quite heterogeneous, with the western Adirondacks being particularly slow. We postulate that this is a chemical heterogeneity that is unrelated to the strain-induced anisotropy.

For further reading:

Levin, V., Menke W., and Park, J., Shear wave splitting in the Appalachians and the Urals: A case for multilayered anisotropy, *J. Geophys. Res.*, **104**, B8, 17,975-17,987, 1999.

Levin, V., Park, J., Brandon M., and Menke, W., Thinning of the upper mantle during the late Paleozoic Appalachian orogenesis, *Geology*, **29**, 239-242, 2000.

Levin, V., Menke W., and Park, J., No Regional Anisotropic Domains in Northeastern US Appalachians, *J. Geophys. Res.*, in press, 2000.

Thermal Structure of the Shallow Mantle Under North America

Saskia Goes, Inst. of Geophysics, ETH Zurich, Switzerland
Suzan van der Lee, Inst. of Geophysics, ETH Zurich, Switzerland

We use S-wave velocity structure of the upper mantle under North America to derive estimates of the thermal and physical state of the uppermost mantle. The S-wave model used, NA00 (van der Lee et al., 2000), is an upgrade of NA95 (van der Lee and Nolet, 1997). This model is based on wavetrains containing S and surface waves from about 700 vertical component seismograms from IRIS and some additional data from the IRIS-PASSCAL program. Moho depth from CRUST5.1 (Mooney et al.,1998) is used.

Because temperature is the dominant parameter influencing seismicvelocities at depths of 50-200 km, we invert velocities for thermal structure (Goes et al. 2000). The velocity-temperature relations (dVs/dT) are based on experimental results from the mineral physics literature and include the effect of composition. dVs/dT at shallow mantle depths depends significantly on the degree of anelasticity. We take into account the non-linear dependence of anelasticity on temperature, which specifically at high temperatures influences the temperature estimates.

The thermal signature of the North American craton persists to about 200 km depth. Temperature estimates for the craton between 50 and 100 km reach a minimum of 300-500 degrees C regionally. This low estimate can be increased by about 100 degrees if the effect of basalt-depleted composition on S-velocity is taken into account. For the western US,the extremely low S-velocities require high mantle temperatures which approach the dry solidus, making the presence of melt plausiblealthough not necessary to explain the velocity anomalies. Our uppermost mantle temperature estimates are generally consistent with surface heat flow data (Pollack et al., 1993).

For further reading:

Goes, S., Govers, R., and Vacher, P., *J. Geophys. Res.*, **105**, 11,153-11,170, 2000.

Mooney, W.D., Laske, G., and Masters, T.G., *J. Geophys. Res.,* **103**, 727-747, 1998.

Pollack, H.N., Hurter S.J., and Johnson, J.R., *Rev. Geophys.,* **31**, 267-280, 1993.

van der Lee, S and Nolet, G., *J. Geophys. Res.*, **102**, 22,815-22,838,1997.

van der Lee, S., Goes, S. and Nolet, G., *EOS Trans. Am. Geophys. Un.,* **81**,S319, 2000.

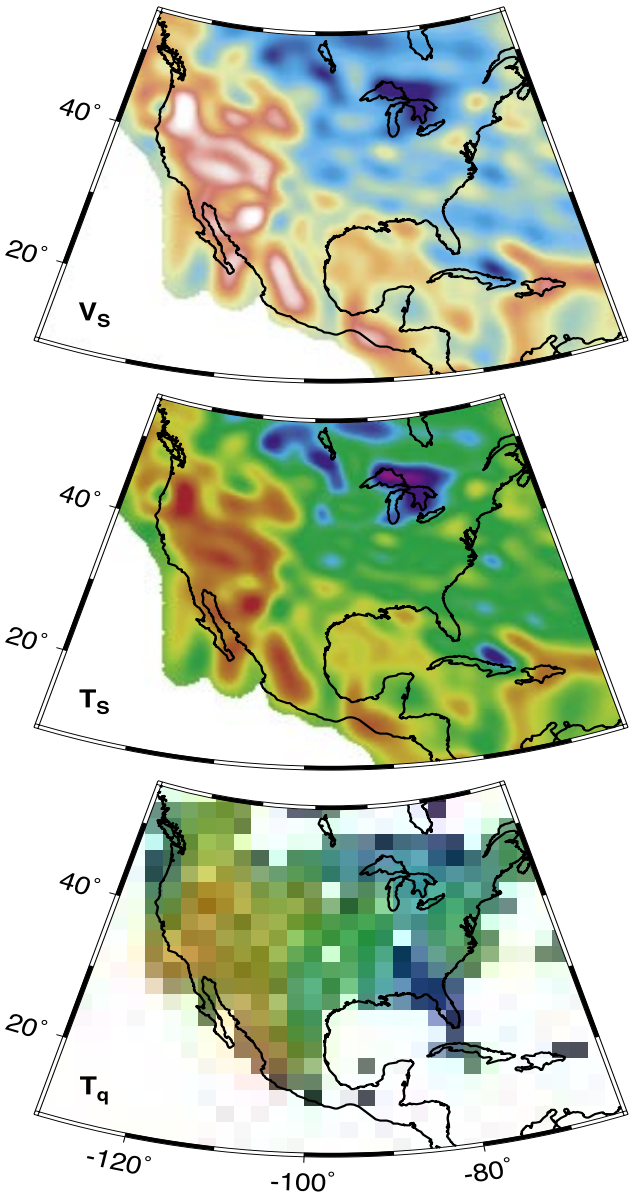

North American upper mantle structure at 70 km depth. Top: absolute S wave velocities from NA00. Middle: temperatures inferred from S velocities. Bottom: temperatures inferred from surface heatflow assuming a steady state conductive geotherm until the mantle adiabat is reached.

Seismic Anisotropy and Mantle Flow Beneath the Western United States

Martha Savage, Victoria University, Wellington, New Zealand
Anne Sheehan, University of Colorado at Boulder

Teleseismic shear wave splitting can be used to obtain estimates of mantle anisotropy, which in turn can provide information on strain history and mantle flow. Shear wave splitting and P, SKS, and S travel time residuals have been calculated for teleseismic arrivals recorded on the Colorado Plateau-Great Basin Program for Array Seismic Studies of the Continental Lithosphere (PASSCAL) portable broadband seismic deployment and for permanent stations in the western United States. Little shear wave splitting is observed for broadband recordings in the northern Colorado Plateau, the Rocky Mountains, or the central Great Basin. The transition between the Colorado Plateau and the Great Basin is marked by moderate shear wave splitting (1.0 s) and unusually late teleseismic phase arrivals. This suggests material with a higher content of mantle melt or volatiles than regions to either side. Splitting in the transition between the Colorado Plateau and Great Basin is part of a pattern of fast polarizations that align in a semicircle, surrounding a central Great Basin region of null (no splitting) measurements. Away from the California plate boundary, splitting to the north and south of our study region aligns roughly parallel to the absolute plate motion of the North American plate. No simple spatial relation of splitting with geological and geophysical features such as mountain ranges, velocity anomalies, gravity, magnetics, or heat flow is evident in most of the western United States, however, splitting in the Great Basin is compatible with asthenospheric flow. The smallest shear wave splitting delay times coincide with the Eureka Low in heat flow, also having low S velocity at 300 km depth. We suggest that the circumferential pattern of fast polarization directions ringing a central region of nulls in the Great Basin is caused by mantle flow, by the interaction of mantle upwelling and the absolute motion of the North American plate.

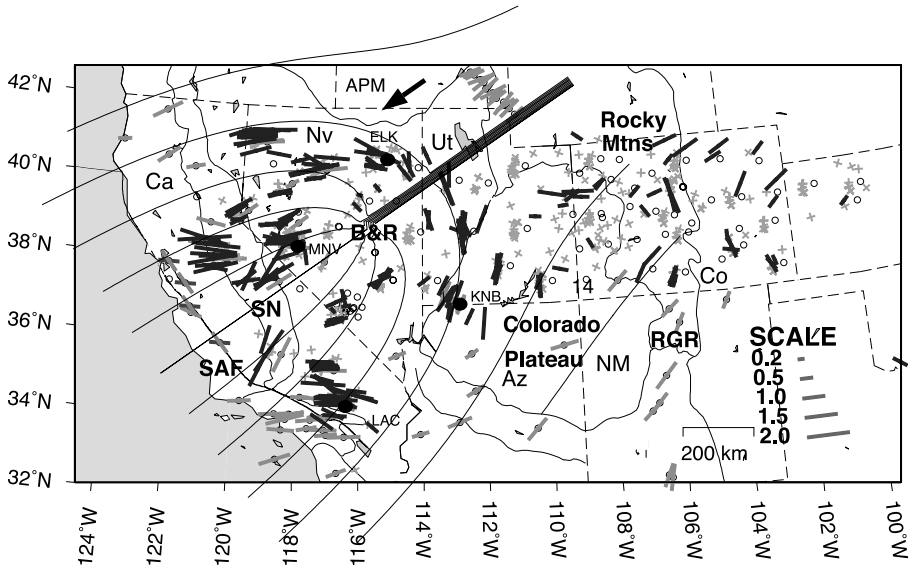

Fluid flow streamlines for a simple source into a moving fluid, superimposed on map of S wave splitting measurements for the western United States. A positive splitting measurement is represented by a single solid line oriented parallel to the fast polarization, with length proportional to the delay time. APM is absolute plate motion vector of the North American plate in the hotspot reference frame.

For further reading:

Savage, M. K., and Sheehan, A.F., Seismic anisotropy and mantle flow from the Great Basin to the Great Plains, western United States, *J. Geophys. Res.*, **105**, 13715-13734, 2000.

Sheehan, A. F., Jones, C.H., Savage, M.K., Ozalaybey, S., and Schneider, J.M., Contrasting lithospheric structure beneath the Colorado Plateau and Great Basin: Initial results from Colorado Plateau - Great Basin PASSCAL experiment, *Geophys. Res. Lett.*, **24**, 2609-2612, 1997.

Probing the Archean and Proterozoic Lithosphere of Western North America

Timothy J. Henstock and Alan Levander, Rice University
Catherine M. Snelson, G. Randy Keller, Kate C. Miller, and Steven H. Harder, University of Texas at El Paso
Andrew R. Gorman and Ron M. Clowes, University of British Columbia, Vancouver
Michael J.A. Burianyk, University of Alberta, Edmonton
Eugene D. Humphreys, University of Oregon

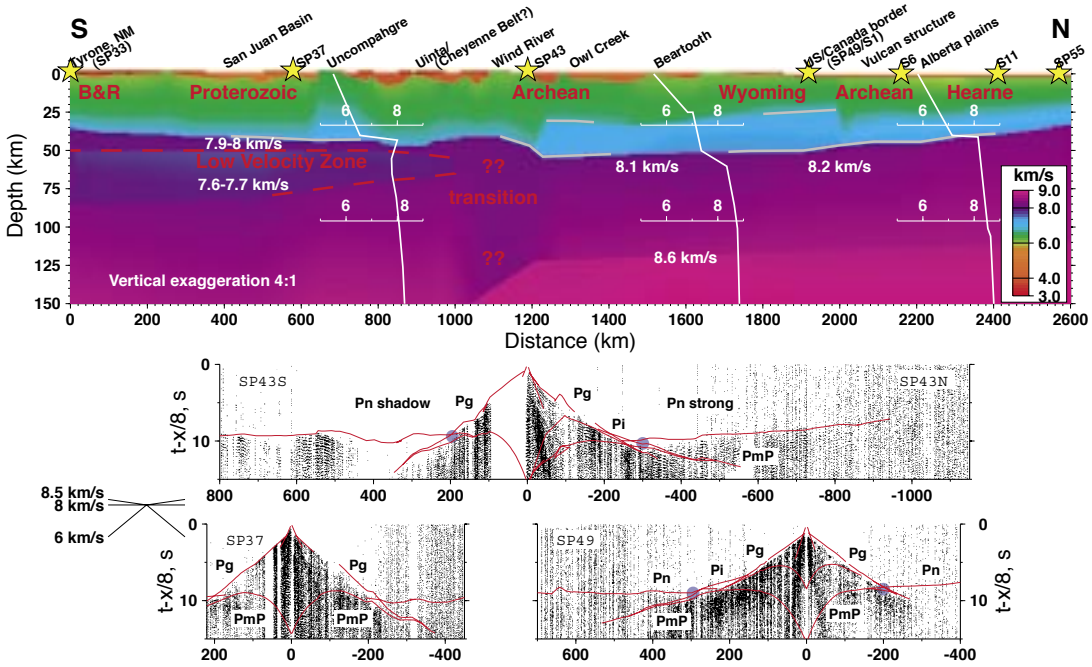

Lithospheric P-wave velocity model along the Deep Probe corridor extending from southern New Mexico to Edmonton, Alberta. Three crustal domains and two mantle domains have distinct seismic velocity structure. The mantle structure beneath the Proterozoic terranes of the southern Rocky Mountains/Colorado plateau has low velocities similar to that of a spreading ridge, whereas the mantle beneath the Archean Wyoming and Hearne Provinces is somewhat faster than that of the North American craton as a whole. The transition from slow to fast velocity occurs over a distance less than 250 km in the vicinity of the surface contact separating Archean cratonic from Proterozoic island arc terranes at the Cheyenne Belt. The two Archean provinces have distincly different crustal thicknesses and velocities. In particular the Wyoming province is characterized by a thick (~20-25 km) high-velocity (>7.0 km/s) lower crust.

The 1995 Deep Probe active source seismic experiment, a continental-scale long-range refraction investigation, extended from the North American orogenic plateau into the Archean Laurentian craton. Over 750 instruments were used in the experiment, including recorders from IRIS/PASSCAL, the GSC and the USGS. The seismic profile crossed Proterozoic terranes of the southern Rocky Mountains and Colorado Plateau and the southern part of the Archean Wyoming province, both modified by Phanerozoic tectonism, as well as the northern Wyoming province and the Archean Hearne province, both relatively stable since Archean time. The results suggest that present day seismic structure is as much controlled by initial terrane accretion as by recent tectonism. Each province is associated with a distinct crustal type, with the Wyoming province crust being thickest and fastest. The data show that the change from low to high upper mantle seismic velocity passing from the orogenic plateau to the shield seen in teleseismic tomography images occurs abruptly in the vicinity of the Cheyenne Belt, which separates the Proterozoic Rocky Mountain terranes from the Archean Wyoming province. The Phanerozoic upper mantle beneath the southern Rocky Mountains has a well developed P-wave low velocity channel similar to that found beneath the Gulf of California spreading system. The upper mantle beneath the Archean provinces has no low-velocity zone, but resembles the teleseismic average for the Canadian shield.

For further reading:

Henstock, T.J., Levander, A., Snelson, C.M., Keller, G.R., Miller, K.C., Harder, S.H., Gorman, A.R., Clowes, R.M., Burianyk, M.J.A., and Humphreys, E.D., Probing the Archean and Proterozoic lithosphere of western North America, *GSA Today*, **8**, 1-5 & 16-17, 1998.

Snelson C.M., Henstock, T.J., Keller, G.R., Miller, K.C., and Levander, A., Crust and uppermost mantle structure along the Deep Probe seismic profile, *Rocky Mountain Geology*, **33**, 181-198, 1998.

Continental Dynamics - Rocky Mountain Project (CDROM)

G. Randy Keller, Karl Karlstrom, and Gene Humphreys, Correspondents for the CD-ROM working group

The Rocky Mountain region of the western U.S. has experienced a complex geologic history that can only be unraveled by the integration of a broad range of geoscience data. This region is of great fundamental interest to studies of the dynamics and evolution of the North American continent. It is also an area where a better understanding of the scarce water resources, natural resources, and earthquake hazards depends on knowledge of the geologic structures present. Thus, the Continental Dynamics Program of the National Science Foundation (NSF) provided the major funding for a large collaborative geological and geophysical effort to study the area of southern Wyoming, Colorado, and northern New Mexico. The German counterpart to NSF and NASA are also supporting the project. This project involves 19 investigators at 14 institutions and a wide variety of research topics. The ultimate objective of CD- ROM is to understand the growth, stabilization, and reactivation of the lithosphere of the Rocky Mountain region. CD-ROM is based on a series of PASSCAL supported seismic experiments to image the structure of the lithosphere and upper mantle along a transect that obliquely crosses the Rocky Mountain region from central Wyoming to central New Mexico. The project features the acquisition of about 500 km of deep seismic reflection data. In order to achieve the differing goals of tying to geological structures exposed at the surface while also studying structures deep in the mantle, additional active and passive source seismic experiments are included. The resulting diverse seismic data set is being analyzed in a coordinated fashion, and these data will in turn be integrated with the broad spectrum of geological, geochemical, and geophysical data that are being gathered along this transect. Satellite data, image processing, digital terrain models, GIS technology, and modern visualization schemes are being employed to create a database suitable for integrated analysis and to view it in creative ways. For geologic control, the transect was chosen to coincide with exposures of Proterozoic basement. Thus by combining geophysical data with geological studies of Proterozoic shear zones, crustal xenoliths, Laramide structures, thermochronology and denudation history, CD-ROM will provide new images of the structure and new insights into the tectonic evolution of the Rocky Mountain region.

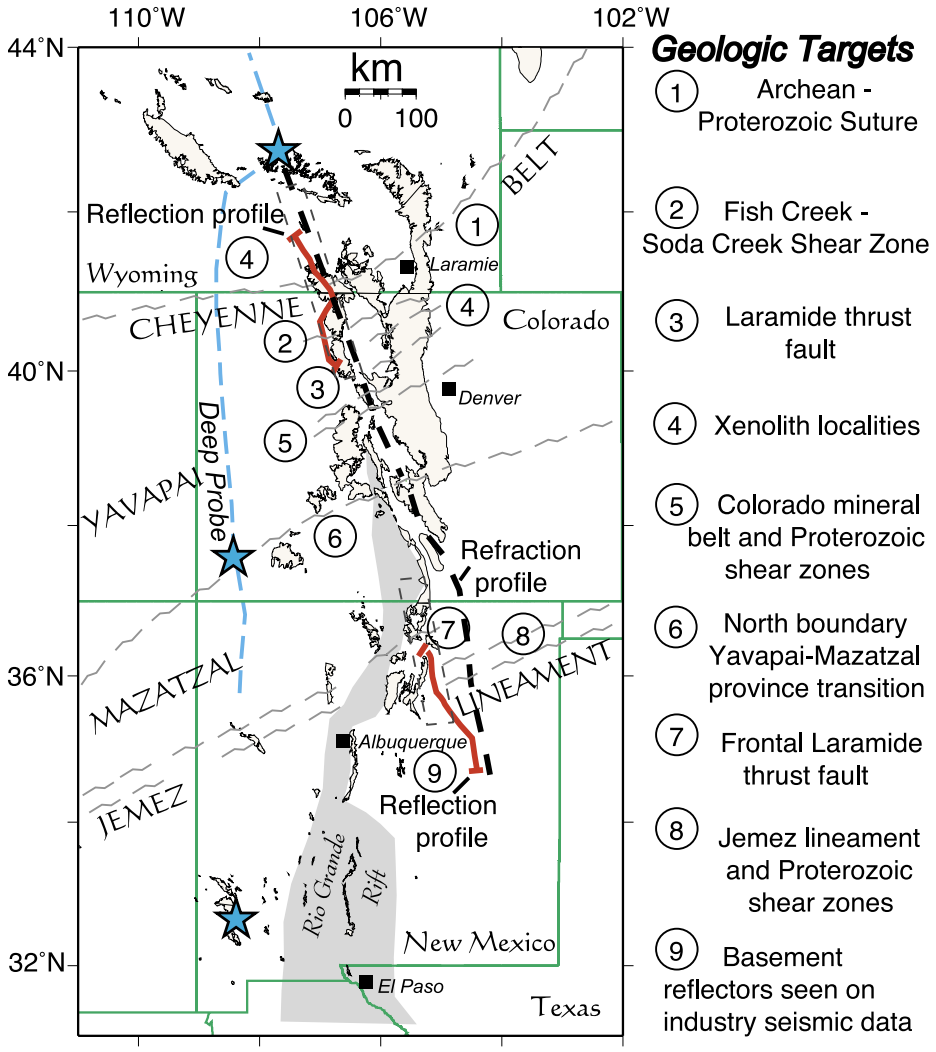

Rio Grande Rift Seismic Transect (RISTRA)

Rick Aster, John Schlue, and Joe Leon, New Mexico Institute of Mining and Technology
Jim Ni, Richard Rapine, Frederik Tilmann, and Wei-Chuang Huang, New Mexico State University
Steve Grand and Eric Matzel, University of Texas
Scott Baldridge, Los Alamos National Laboratory
Steve Semken, Alfred Blackhorse, and Laurencita Luna, Dine College

RIo grande rift Seismic TRAnsect (RISTRA)

RISTRA is a presently operating (fall, 1999 to summer, 2001) passive, approximately 1000 km-long, 20-km interstation spacing, NW-SE line of 60 PASSCAL broadband seismometers deployed along a near-great circle path from the Great Plains in west Texas to the Colorado Plateau in Utah. The experiment is designed to elucidate mantle and crustal structure, evolution, and present processes near the extreme eastern edge of deformed western North America to mantle transition zone depths. Fundamental questions to be addressed include the cause and/or maintenance of high elevation and non-extension in the Colorado Plateau, depths of surface tectonic associated mantle processes, coupling between mantle and crustal strain in the Rio Grande rift, the nature of the Jemez lineament, and the existence or nonexistence of mantle remnants from pre-extension (Farallon Plate convergence) western North America tectonics. Planned stations include off-line elements to provide lateral control on anisotropic and other structure, especially in the vicinity of the Rio Grande rift and Socorro mid-crustal magma body. The relatively large size of the experiment and a very diverse group of instrument hosts (Private, State, Bureau of Land Management, National Forest, Native American Nations) also makes RISTRA a testbed for exploring siting, permitting, deployment, and other fundamental logistical issues associated with USArray and other possible very large future IRIS deployments.

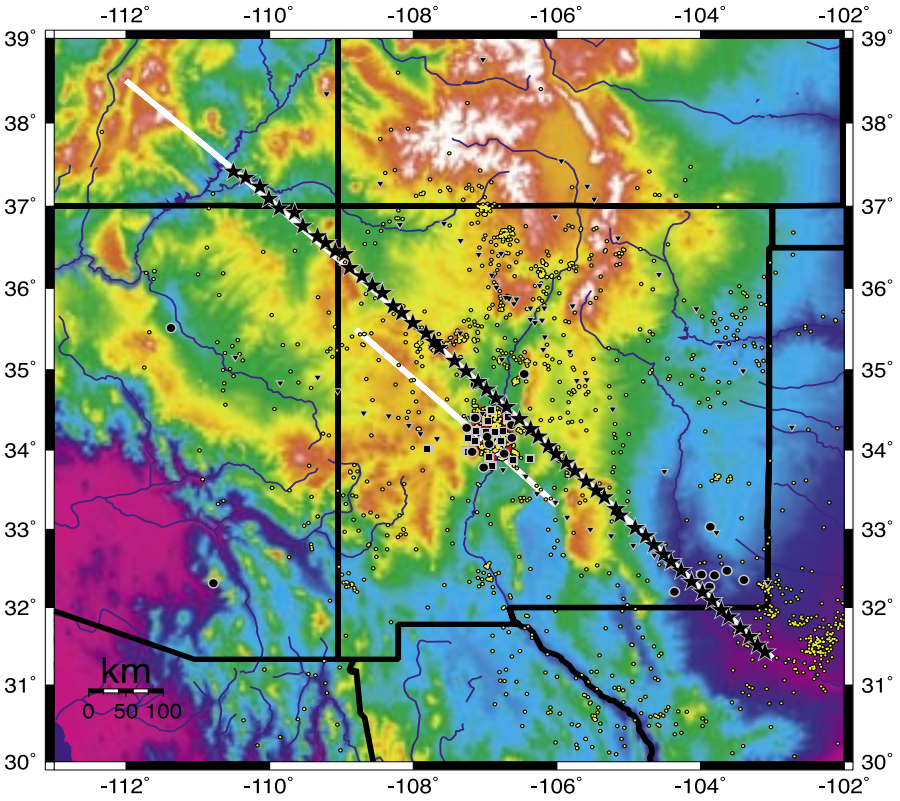

Topographic map of the southwestern United States in the vicinity of the RISTRA experiment. Stars: Presently (3/00) operating STS-2/CMG3-T RISTRA stations. Triangles: Previously deployed short/intermediate period stations to be analyzed jointly with RISTRA data. Albuquerque line; Taos line (1985), Socorro line (1987; Slack et al., 1996). Black Circles: NM Tech Earthworm System broadband and short period stations. Black Squares: NM Tech/UW short-period teleseismic stations near the Socorro magma body (1993-1994; Schlue et al., 1996; Balch et al., 1997). White Swaths: Target Ristra Primary and Secondary Great Circles. 15 additional STS-2 stations remain to be installed in along the primary line in Utah and along the secondary line. Yellow Circles: Earthquakes (local magnitude >= 1.3; 1962-1998; Allan Sanford and Kuo-wan Lin, pers. communication).

For further reading:

Balch, R.S., Hartse, H.E., Sanford, A.R. and Lin, K.W., A new map of the geophysical extent of the Socorro midcrustal magma body, *Bull. Seismol. Soc. Amer.*, **87**, 174-182, 1997.

Schlue, J., Aster, R., Meyer, R., A lower-crustal extension to a mid-crustal magma body in the Rio Grande rift, New Mexico, *J. Geophys. Res.*, **101**, 25,283-25,291, 1996.

Slack, P.D., Davis, P.M., Baldridge, W.S., Olsen, K.H., Glahn, A., Achauer, U., Spence, W., The upper mantle structure of the central Rio Grande rift region from teleseismic P and S wave travel time delays and attenuation, *J. Geophys. Res.*, **101,** 16003-16023, 1996.

Stress Field at Yellowstone National Park From Earthquake Focal Mechanisms

Greg Waite and Robert B. Smith, University of Utah

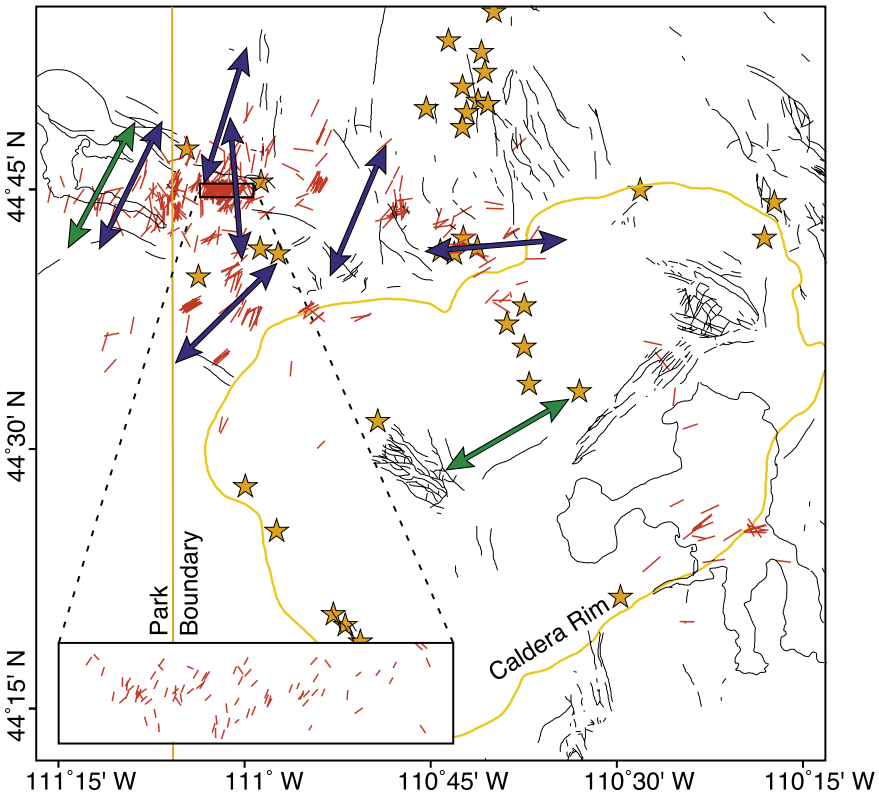

Surface projections of T-axes from focal mechanisms shown as thin red lines. Direction of maximum extensional strain from GPS measurements shown as green double arrows. Quaternary volcanic vents shown as stars. Direction of minimum principal stress from focal mechanism stress inversions shown as blue double arrows. Orientation of T-axes near Hebgen Lake parallel to extension from strain measurements and Hebgen Lake earthquake focal mechanisms. T-axes within or adjacent to the caldera oriented perpendicular to the trend of swarms and alignment of volcanic vents.

The historic seismicity of the Yellowstone volcanic field is characterized by extensive swarms of small magnitude events and by the largest historic earthquake in the Rocky Mountains, the Ms 7.5 1959 Hebgen Lake event. A catalog of 12,300 hypocenters recorded in part with PASSCAL instrumentation from 1973-1997 was relocated with a new 3-D velocity model and used to determine focal mechanisms as input for stress inversions. The focal mechanisms are dominantly oblique, normal-faulting solutions. Horizontal T-axes reveal a well-resolved, near-90° rotation from N-S extension northwest of the caldera to E-W extension across the caldera to the southeast. Swarm earthquake hypocenters often define steeply-dipping planes that appear to be small fractures 0.5 to 5 km long. Within and adjacent to the caldera, these planes trend N-NW. To the north of the caldera, where most of the swarm activity is concentrated, the majority of the swarm planes trend E-W. The E-W trending swarms north of the caldera suggest a highly fractured crust and coincide with a topographic boundary that may reflect the northern extent of the 2.0 Ma caldera. The largest swarm in Yellowstone's history, autumn 1985, was coincident with a reversal in caldera deformation from uplift to subsidence. At the onset of that swarm, earthquake activity migrated away from the caldera at ~500 m/day. Stress axes inversions from the swarm show the minimum compressive stress was horizontal and perpendicular to the plane of the swarm and the maximum compressive stress near horizontal and parallel to the swarm plane. The observations of this swarm are consistent with earthquakes induced by lateral propagation of a vertical dike. These results illustrate that Yellowstone seismicity is due to a combination of tectonic and volcanically related stress release.

Intermountain Seismic Internet Surveyer to Investigate the Yellowstone Hotspot

Greg Waite and Robert B. Smith, University of Utah
Ken Dueker, CIRES
Eugene D. Humphreys, University of Oregon

A digitally telemetered network of 31 IRIS-PASSCAL Guralp 40-T seismometers was installed in September and October, 1999 near Yellowstone National Park as part of the NSF-funded Continental Dynamics Project, "Geodynamics of the Yellowstone Hotspot." Objectives of this multi-institution collaborative experiment are to investigate the dynamics and structure of the Yellowstone Hotspot including plume-plate interaction. The network was located such that incoming waves from teleseismic earthquakes to the southwest (Tonga, Fiji, Kermadec regions) would pass through the upper mantle beneath Yellowstone. Continuously streamed digital data (sampled at 40 Hz) from the three-component broadband seismometers are transmitted to two collection towers via spread-spectrum radios and relayed to a collection site in Billings, MT using a 2.2 GHz microwave radio. The data are linked to the Internet and are fed into our primary object ring buffer (ORB) at the University of Utah supplied by the Antelope software system. Data from four additional networks in the intermountain west, spanning an area ~1,100 km north-south and ~500 km east-west, are being collected along with the Montana broadband data including all or part of the following: the University of Utah Seismograph Stations, the Montana Bureau of Mines, the Idaho National Environmental Engineering Laboratory, and the U.S. National Seismic Network. We will soon be recording stations within the U.S. Bureau of Reclamation's Teton Network as well as stations operated by the University of Nevada-Reno. Currently more than 250 seismograph stations with over 700 total channels are being fed into the ORB and recorded in real time. This amounts to almost 30kb/sec or ~2.5Gb/day of compressed data. The use of Antelope's automated triggering, locating, associating, and parsing capabilities enables us to manage this volume of data. Between October 1999 and April 2000 we have recorded 6 events of M>7, 65 events M>6 and 264 events of M>5. The size and scope of this project are prototypical of the planned USArray.

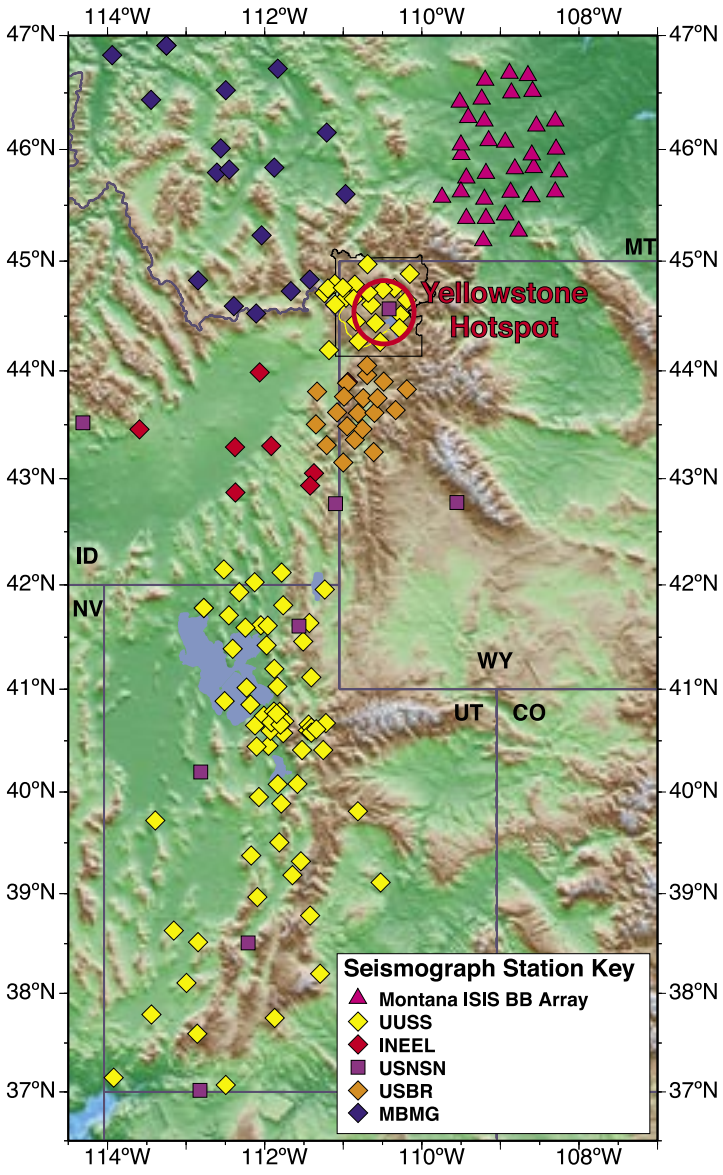

This map shows the current configuration of the ISIS network being recorded at the University of Utah. The approximate location of the Yellowstone Hotspot is shown with a red circle.

High-Resolution Imaging of Deep Mantle Discontinuities Using PASSCAL Data

Anne Sheehan, Hersh Gilbert, Ken Dueker, University of Colorado at Boulder
Peter Shearer, Scripps Institution of Oceanography, University of California, San Diego

Data sets from dense deployments of broadband seismometers, made possible through the PASSCAL program, have led to images of deep crust and mantle structure with unprecedented resolution. The wide array of signal processing techniques long used in the seismic reflection industry, such as velocity spectrum stacks, common depth point or common conversion point stacking, and seismic migration, can now be applied to these data sets. Common conversion point (CCP) stacking of records of P-SV converted phases (receiver functions) has become a widespread technique for high resolution imaging of deep mantle velocity discontinuities (e.g., Dueker and Sheehan, 1997, 1998; Li et al., 1998; Shen et al., 1998). These velocity discontinuities provide important information about the thermal and physical state of the mantle. Through the high-resolution mapping of discontinuity structure it is now possible to track the lateral variations in mantle thermal structure and its link to surface tectonics. By stacking many receiver functions which sample the same subsurface point, signal to noise is dramatically improved and small amplitude features can be resolved. These techniques have led to high-resolution images of mantle discontinuity topography, and have shown that discontinuity topography can be significant (20-30 km) over wavelengths of a few hundred kilometers. The CMP technique implicitly assumes that all P-SV conversions are produced by flat-lying, laterally continuous structures, and does not take into account diffraction effects and focussing produced by curved or laterally discontinuous interfaces. The seismic reflection community has long recognized the importance of migrating reflected phases back to their appropriate origin point. Seismic migration eliminates artifacts produced by inappropriate assumptions of horizontal planar structure, and produces dramatic improvements in reflection image quality (e.g., Claerbout, 1992). Synthetic experiments show that dramatic improvement over simple CCP stacking can be achieved through backprojection migration processing applied to receiver functions. We have now applied back-projection migration techniques to receiver functions, including data from the 1993 Snake River Plain (SRP) PASSCAL seismic experiment (Dueker et al., 1993).

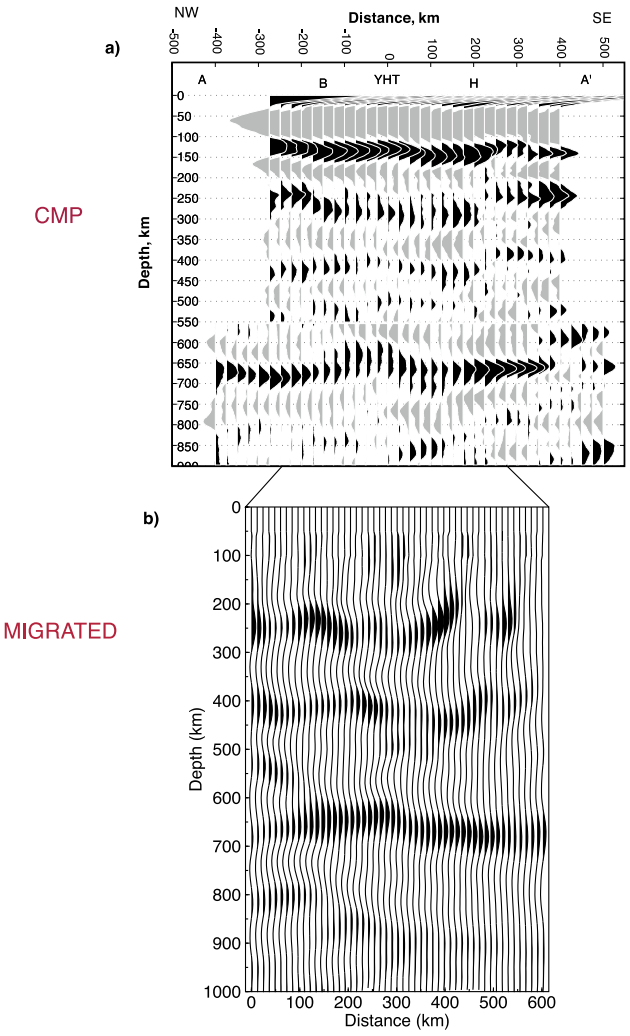

(a) Discontinuity image from Snake River Plain PASSCAL experiment data (Dueker and Sheehan, 1997). Each trace shown represents a common conversion point stack (CCP or CMP) of all receiver functions within a 75-km-wide bin stacked along appropriate normal move-out curves. Positive and negative polarity energy are plotted in solid and shaded, respectively. (b) Migrated Snake River Plain discontinuity image.

For further reading:

Claerbout, J. F., Earth Soundings Anaysis: Processing Versus Inversion, Blackwell Sci., Malden, Mass., 1992.

Dueker, K. G., and Humphreys, E. Relationships between upper mantle velocity structure and the tectonic parabola along the Yellowstone volcanic trend, *Eos Trans. AGU*, **74**(43), Fall Meet. Suppl., F602, 1993.

Dueker, K.G., and Sheehan, A.F., Mantle discontinuity structure from midpoint stacks of converted P to S waves across the Yellowstone hotspot track, *J. Geophys. Res.,* **102**, 8313-8327, 1997.

Dueker, K. G., and Sheehan, A.F., Mantle discontinuity structure beneath the Colorado Rocky Mountains and High Plains, *J. Geophys. Res.*, **103**, 7153-7169, 1998.

Li, A., Fischer, K.M., Wysession, M.E., and Clarke, T.J., Mantle discontinuities and temperature under the North American continental keel, *Nature*, **395**, 160-163, 1998.

Sheehan, A.F., Shearer, P.M., Gilbert, H., and Dueker, K.G., Seismic migration processing of P-SV converted phases for mantle discontinuity structure beneath the Snake River Plain, western United States, *J. Geophys. Res.*, in press, 2000.

Shen, Y., Solomon, S.C., Bjarnason, I.T. and Wolfe, C.J., Seismic evidence for a lower-mantle origin of the Iceland Plume, *Nature*, **395**, 62-65, 1998.

Imaging P-to-S Conversions in the Mantle Using Multichannel Deconvolution and Plane Wave Migration

Christian Poppeliers and Gary L. Pavlis, Indiana University

One of the most promising methods by which to image the lower crust and upper mantle is to extract P-to-S converted phases out of the incident wavefield. The so called "receiver function" method utilizes teleseismic earthquake data recorded by passive seismic arrays to illuminate portions of the Earth that are generally too deep to be practically accessed by reflection seismology.

Incoherent scattered energy is one of the largest sources of "noise" when using receiver functions to determine Earth structure. By using large, areal, passive seismic array data available through PASSCAL, seismologists are able to exploit the redundancy of multiple recordings of a seismic wavefield. By summing the contributions of many recording channels and/or earthquake events, random noise caused by incoherent scattered phases are canceled and coherent P to S converted modes are enhanced. The result is that more accurate images of P to S conversion horizons can be constructed which ultimately leads to a better understanding of the Earth's lower crust and upper mantle structure. We introduce a powerful tool by which to mitigate the effects of incoherent scattered energy produced by near surface effects and diffractions at depth. By applying this method to data obtained from areal passive arrays, we are able to greatly improve upon the resolution of receiver function images.

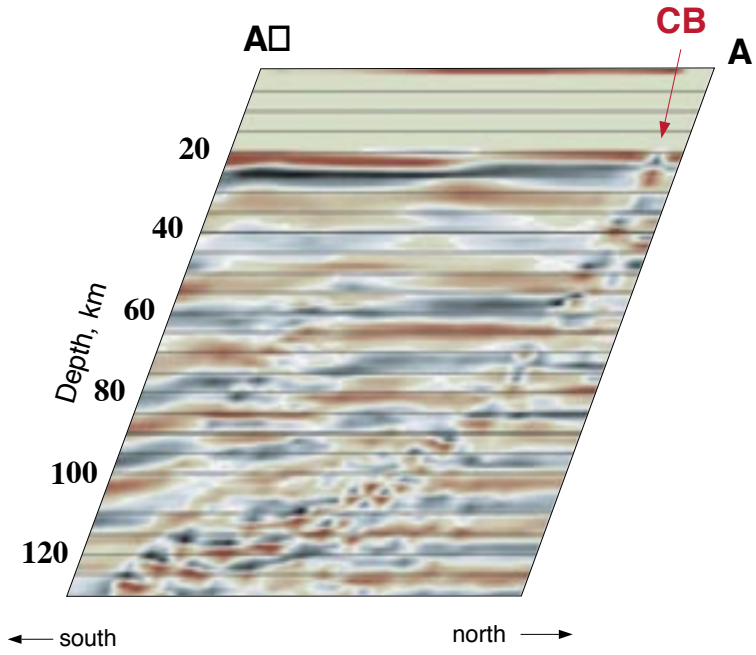

To reduce the effects of incoherent scattered energy, we use a combination of pseudostation stacking and plane wave migration. Pseudostation stacking is best thought of as a way to interpolate the observed wavefield between recording stations (see Neal and Pavlis, 1999). The technique utilizes a weighted, plane-wave stack to estimate the wavefield on a regular grid with a prescribed wavenumber cutoff. The result is that incoherent, near surface scattered energy is canceled while coherent modes are enhanced by coherent stacking.

Additionally, we have developed an innovative plane wave depth migration technique which incorporates pseudostation stacking. The migration scheme is based on producing a series of pseudostation slant-stacks by aiming the seismic array through a range of ray parameters centered about the incident wavefield's ray parameter. We then apply a downward continuation operator to place the data in the spatial domain and stack all of the resulting data volumes. The downward continuation operator incorporates the difference between P and S modes according to a 3-D velocity model and the ray parameter of a series of slant stacks.

By using these two ideas in tandem, we effectively enhance both dipping layers and point scatterers and place them in the proper spatial position on the final image. Because this algorithm is applied to single events, this algorithm is a type of 3-D prestack migration appropriate for P-to-S converted phases. We are finding that this greatly enhances the resolution of our images of the lower crust and upper mantle.

To illustrate the value of this approach, we applied this algorithm to a single, 6.3 mb South American subduction zone event recorded by the Lodore array in northwestern Colorado. The Lodore array traverses the Cheyenne belt, which is interpreted to be an ancient suture between the Archean rocks of the Wyoming province to the north and the Proterozoic rocks to the south. For the figure shown, we reduced the problem to two dimensions because of the greatly reduced computational load and for easier visualization of the final data. The most striking features of this image are the steeply dipping discontinuities seen in the image. We hypothesize that these features are associated with the suture, however definite interpretations are difficult because this image was created from only one event. The point is that by applying this migration algorithm as a prestack imaging condition, we will be able to greatly enhance the resolution of three dimensional receiver function images by combining this migration technique with multisource stacking.

For further reading:

Neal, S.L. and Pavlis, G.L., Imaging P-to-S conversions with multichannel receiver function, *Geophys. Res. Lett.*, **26,** 2581-2584, 1999.

New Techniques for Interpretation of Broadband Images of Lithospheric Structure

S.J. Rondenay, J. Shragge, and M.G. Bostock, University of British Columbia

Images of velocity structure across the Cascadia subduction zone, central Oregon (Rondenay et al., 2000). Top and bottom panels show P- and S-velocity perturbations derived through simultaneous inversion of scattered teleseismic P-waves from 30 earthquakes. The images clearly reveal the low velocity (red) subducting oceanic crust of the Juan de Fuca plate dipping to the right below the North American plate. Eastward bifurcation of the oceanic crustal anomaly may indicate delamination or, alternatively, entrapment of fluids expelled upwards from dehydration reactions in the subducting plate. The continental Moho becomes apparent east of ~150 km at approximately 35 km depth as a boundary separating low-velocity (red) crust from higher velocity (blue) mantle. The data were recorded during an IRIS-PASSCAL experiment by John Nabelek and Xiao-Qing Li in 1993-1994. Triangles at the surface represent station locations, and superimposed lines show original interpretation based on forward modelling of receiver functions (Li, 1996).

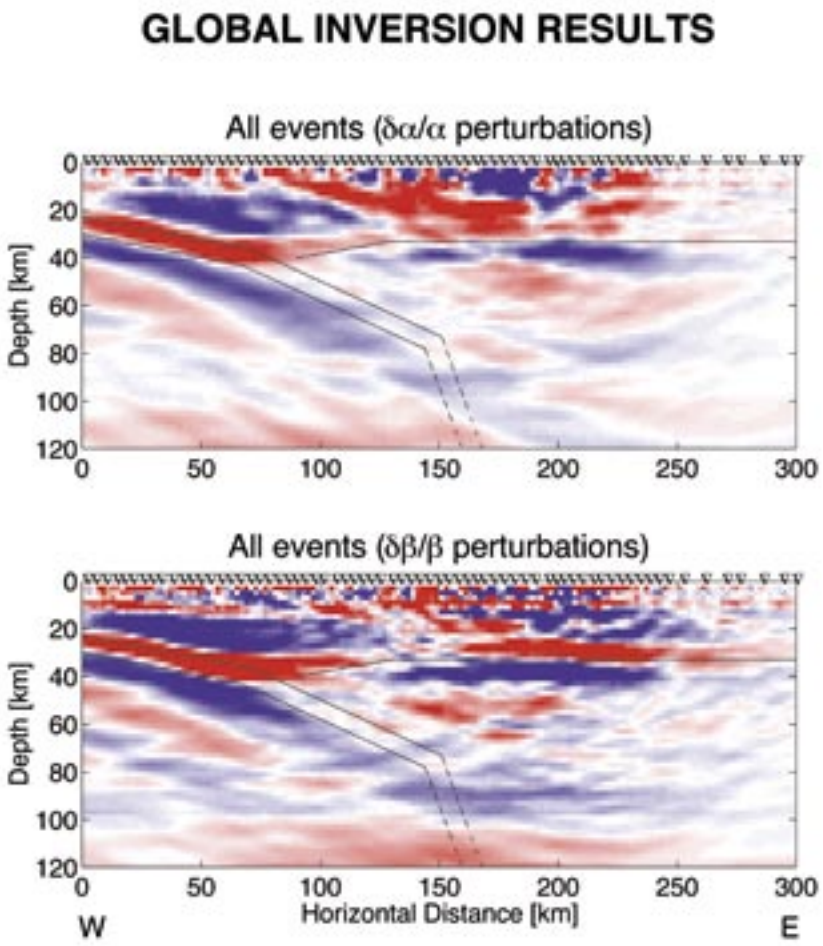

For further reading:

Rondenay S.J., Shragge J., and Bostock M.G., Imaging complex lithospheric structures using the teleseismic body wave coda II - Numerical and data examples, *EOS Trans. Am. Geophys. Un.*, **81**, S51A-03, 2000.

Li, X-Q., Deconvolving orbital surface waves for the source duration of large earthquakes and modelling the receiver function for the earth structure beneath a broadband seismometer array in the Cascadia subduction zone, Ph.D. Thesis, Oregon State University, Corvallis, Oregon, 1996.

Crustal Structure Across the Bering Strait, Alaska: Onshore Recordings of a Marine Multichannel Seismic Survey

Lorraine W. Wolf, Auburn University
Robert C. McCaleb, Kazuya Fujita, Michigan State University
David B. Stone, University ofAlaska
Thomas M. Brocher, U.S. Geological Survey
Simon Klemperer, Stanford University

The Bering Strait region links the Chukchi Shelf to the north and the Bering Shelf to the south, which together form an area of shallowly submerged continental crust (Figure). Although on strike with the trend of Brooks Range, the Bering Strait and adjacent parts of the Chukchi Sea have an inferred tectonic history distinct from that of the range in northern central Alaska, where a thick crust and elevated topography presently exist (Fuis et al, 1997; Wissinger et al, 1997). A complex history of contraction, extension, and transtension in the Bering Strait region has produced the structural features that characterize this bridge between the Asian and North American continents (Miller and Hudson, 1991). In 1994, two deep crustal marine seismic profiles and accompanying wide-angle refraction data, constituting the Bering-Chukchi Crustal Transect (BCCT), were acquired in the Bering Strait region (Brocher et al, 1995). The combination of multichannel and wide-angle coverage provides detailed images of the crust and its general attributes, such as reflectivity, crustal thickness, possible rock composition, and the deep subsurface expression of structural boundaries. Raypaths from the ship to onshore receivers crossed several geologically significant features, including Herald Arch, Hanna Trough, and a region of crustal extension and orogenic collapse in the northern Bering Shelf (Miller and Hudson, 1991). Of particular interest in the refraction experiment were: (1) the deep structure of Cape Lisburne, Hope Basin and Herald Arch, (2) the crustal thickness and velocity structure between Chukotka and Alaska, (3) the deep structure of a magmatic belt that crosses Bering Strait, and (4) the location of the western extension of the northern Brooks Range, if it exists beyond the Lisburne peninsula. Each of these items has important implications for reconstructing the structural evolution of northwestern Alaska. Our collaborative study (Wolf et al, in press) derives a refraction model constrained by multichannel reflection data (Klemperer et al, in press) and gravity data for the Bering Strait region. Results indicate present-day crustal thicknesses of 32 to 35 km, average velocities of 6.4 km/s in the middle to lower crust, and upper mantle velocities of 7.6 to 7.9 km/s. These observations are consistent with global averages for continental crust. Data observations support models of widespread extension in the portion of the Bering Sea underlain by the Cretaceous magmatic belt and, when viewed in light of studies of blueschist facies rocks on the Seward Peninsula, suggest that the crust in this area may have been at least 47 km thick prior to extension. Thickness and velocity estimates for the crust between the Seward and Chukotka peninsulas support regional geologic, petrologic, geochronologic and geochemical studies that indicate continuity of crustal structure from western Alaska to eastern Russia. Finally, the lack of compelling evidence in the seismic and gravity data for a crustal root west of the Lisburne peninsula suggests that if the Brooks Range once continued beyond the peninsula, its roots have been subsequently removed by extensional processes.

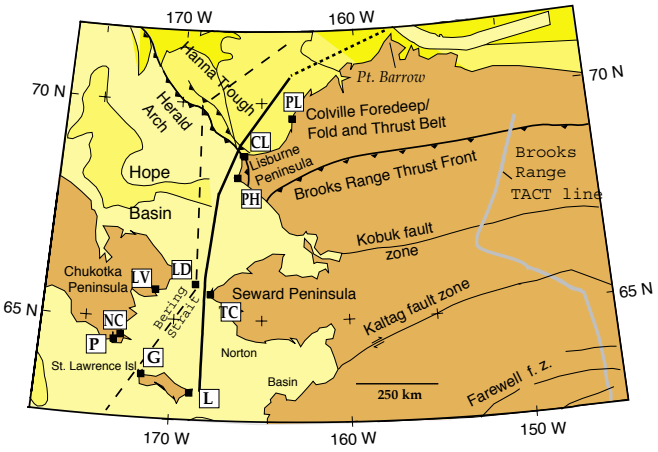

Tectonic map of western Alaska and eastern Russia showing key structural and geographic features (modified from Brocher et al.,1995). Also shown are shiptracks of the Bering-Chukchi Crustal Transect, the location of onshore portable seismic stations provided by the IRIS PASSCAL program and the University of Alaska Fairbanks. **Support for the study was provided by the USGS Deep Continental Studies program, the W. M. Keck Foundation, the Petroleum Research Fund of American Chemical Society, NATO, NSF OPP, and Shell and Exxon Oil companies. Data reduction assistance was provided by the IRIS PASSCAL instrument center.**

For further reading:

Brocher, T.M., Allen, R.M., Stone, D.B., Wolf, L.W., and Galloway, B.K., Data report for onshore-offshore wide-angle seismic recordings in the Bering-Chukchi sea, western Alaska and eastern Siberia, *U. S. Geol Surv Open File Report 95-650*, 57 p., 1995

Fuis, G.S., Murphy, J.M., Lutter, W.J., Moore, T.E., and Bird, K.J., Deep seismic structure and tectonics of northern Alaska: Crustal-scale duplexing with deformation extending into the upper mantle, *J Geophy Res*., **102**, 20,873-20,896, 1997.

Klemperer, S. L. and the Bering-Chukchi Working Group, Crustal structure of the Bering and Chukchi Shelves: deep seismic reflection profiles across the North American continent between Alaska and Russia, in: "Tectonic evolution of the Bering Shelf-Chukchi Sea-Arctic Margin and adjacent landmasses," eds. E.L. Miller, A.Grantz and S.L. Klemperer, *Geol. Soc. Am. Spec. Paper*, in press.

Miller, E.L. and Hudson, T., Mid-Cretaceous extensional fragmentation of a Jurassic-Early Cretaceous compressional orogen, *Tectonics*, **10**, 781-796, 1991.

Wissinger, E.S., Levander, A., and Christensen, N.I., Seismic images of crustal duplexing and continental subduction in the Brooks Range: *J. Geophys. Res*., **102**, 20,847-20,871, 1997.

Wolf, L.W., McCaleb, R.C., Stone, D.B., Brocher, T.M., Fujita, K., Klemperer, S., and the Bering-Chukchi Working Group, Crustal structure across the Bering Strait: onshore recordings of a marine multichannel seismic survey, in: "Tectonic evolution of the Bering Shelf-Chukchi Sea-Arctic Margin and adjacent landmasses," eds. E.L. Miller, A. Grantz and S.L. Klemperer, *Geol. Soc. Am. Spec. Paper*, in press.

A New View into the Cascadia Subduction Zone and Volcanic Arc: Implications for Earthquake Hazards Along the Washington Margin

Tom Parsons, James H. Luetgert, Ray E. Wells, Michael A. Fisher, and Uri S. ten Brink, US Gelological Survey
Anne M. Trehu, Oregon State University
Kate Miller and Fiona Kilbride, University of Texas, El Paso
Ernst Flueh, GEOMAR
Nikolas I. Christensen, University of Wisconsin

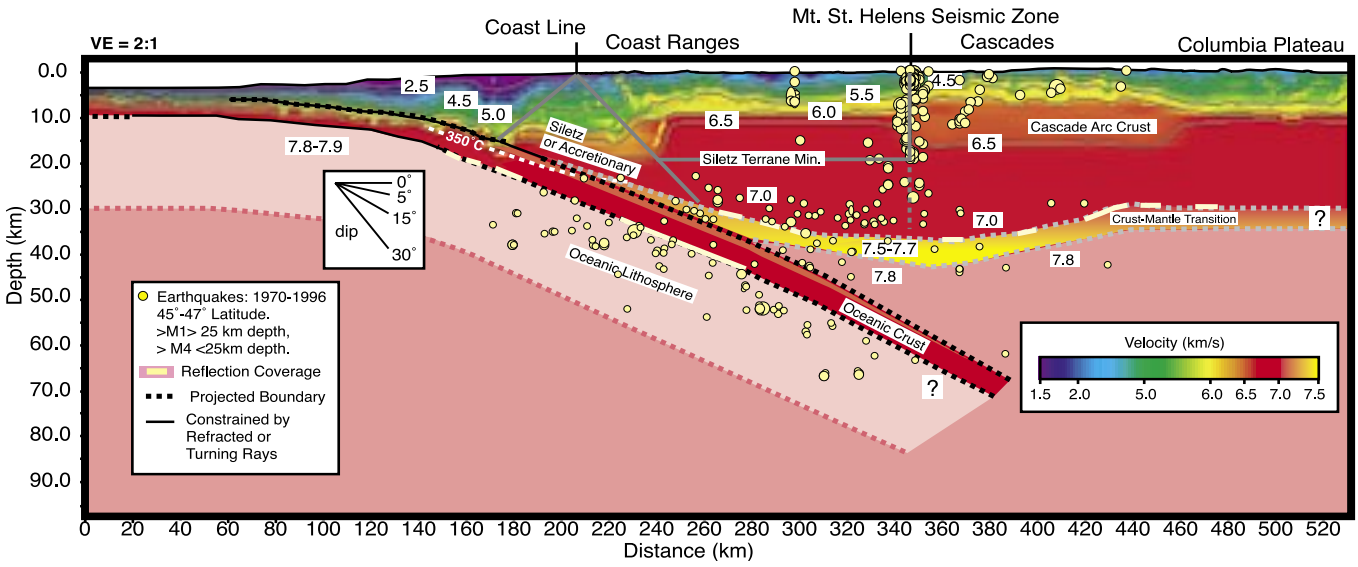

The image of the subduction process emerging from this model is one of a young (~10 m.y. old) and buoyant, shallow-dipping (12°) Juan de Fuca Plate that appears to bend as a result of overriding contact with rocks accreted to the North American plate. This observed subduction geometry concentrates the potential locked interplate contact offshore; the shallow dip broadens the zone out to the deformation front (~120 km offshore), and the steeper part of the slab encounters 350 °C temperatures at about 25-30 km depth (350 °C is thought to be the temperature where stable sliding begins).

In light of suggestions that the Cascadia subduction margin may pose a significant seismic hazard for the highly populated Pacific Northwest region of the United States, the U. S. Geological Survey (USGS), the Research Center for Marine Geosciences (GEOMAR), and university collaborators collected and interpreted a 530-km-long wide-angle onshore-offshore seismic transect using PASSCAL instruments across the subduction zone and volcanic arc to study the major structures that contribute to seismogenic deformation. We observed: (1) an increase in the dip of the Juan de Fuca slab from 2°-7° to 12° where it encounters a 20-km-thick block of the Siletz terrane or other accreted oceanic crust, (2) a distinct transition from Siletz crust into Cascade arc crust that coincides with the Mount St. Helens seismic zone, supporting the idea that the mafic Siletz block focuses seismic deformation at its edges, and (3) a crustal root (35-45 km deep) beneath the Cascade Range, with thinner crust (30-35 km) east of the volcanic arc beneath the Columbia Plateau flood basalt province. From the measured crustal structure and subduction geometry, we identify two zones that may concentrate future seismic activity: (1) a broad (because of the shallow dip), possibly locked part of the interplate contact that extends from ~25 km depth beneath the coastline to perhaps as far west as the deformation front ~120 km offshore and (2) a crustal zone at the eastern boundary between the Siletz terrane and the Cascade Range.

For further reading:

Parsons, T., Trehu, A.M., Luetgert, J.H., Miller, K., Killbride, F., Wells, R.E., Fisher, M.A., Flueh, E., ten Brink, U.S., and Christensen, N.I., A new view into the Cascadia subduction zone and volcanic arc: Implications for earthquake hazards along the Washington margin, *Geology*, **26**, 199-201, 1998.

Imaging Crustal Faults in Puget Lowland - Results From Wet SHIPS

Thomas M. Brocher, Tom Parsons, Richard E. Blakely, Michael A. Fisher, Ray E. Wells, Uri S. ten Brink, Thomas L. Pratt, Victoria E. Langenheim, Roy A. Hyndman, and Craig S. Weaver, U.S. Geological Survey
Nicolas I. Christensen, University of Wisconsin
Robert S. Crosson and Kenneth C. Creager, University of Washington
Kate C. Miller, University Texas El Paso
Anne M. Tréhu, Oregon State University
George D. Spence, University of Victoria

We present a three-dimensional seismic velocity model for the Puget Lowland to a depth of 11 km based on a tomographic inversion of nearly one million first-arrival travel times recorded during the 1998 Seismic Hazards Investigation in Puget Sound (SHIPS). The velocity model reveals that the crustal faults in Puget Lowland exhibit pronounced along-strike variations in structural relief, and indicates that structures previously thought to represent minor folds become much larger structures along strike. Structural relief on the Narrows structure (renamed here informally as the Tacoma Narrows fault) increases dramatically west of Tacoma where it is imaged as a north- dipping, south-vergent fault overthrusting the north-dipping Tacoma basin. In contrast, structural relief on the Seattle fault decreases dramatically west of Seattle. Paleoseismic evidence for uplift of tidal marsh deposits just north of the Tacoma Narrows fault and its 50- km length suggests that it is an active fault capable of a M7 earthquake.

The tomography model reveals a 2-km-deep, apparently fault-bounded, basin in the eastern Strait of Juan de Fuca located at the convergence of the Leech River, Hood Canal, Darrington-Devil Mountain, and Southern Whidbey Island faults. The southern boundary of this newly discovered "Port Townsend" basin is formed by a young E-W trending, south-dipping thrust fault previously identified near Sequim, Washington, and imaged by industry seismic reflection lines. The 50-km-length and 1-km-thick Quaternary deposits north of the Sequim fault suggest that it is also an active crustal fault capable of a M7 earthquake.

The wide-angle data analysed in this study were acquired using Refteks made available by the IRIS PASSCAL facility.

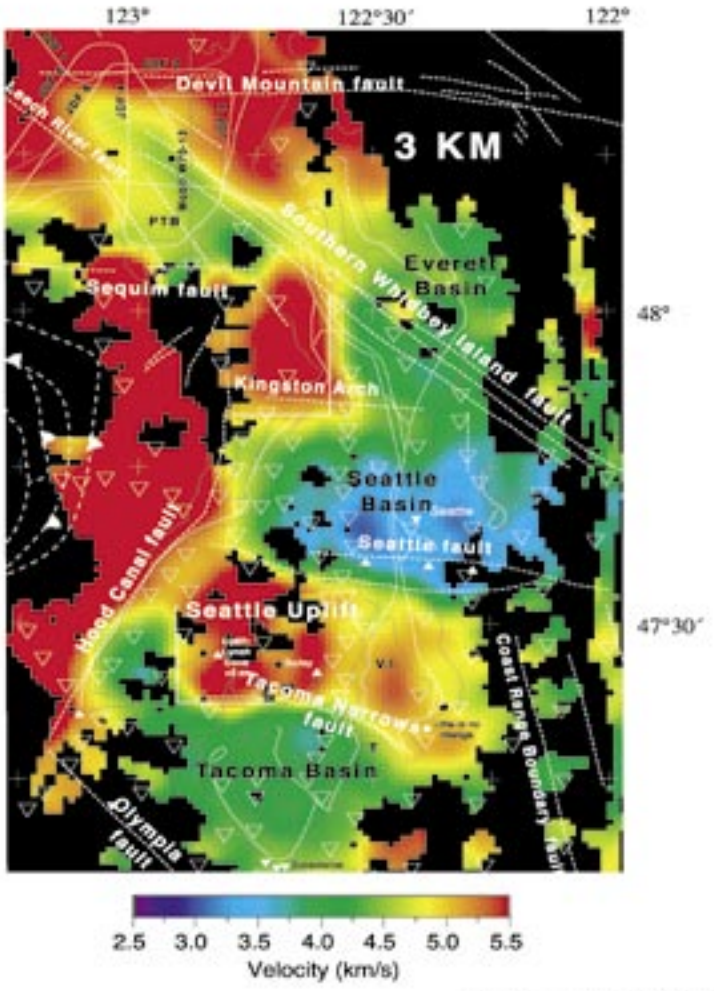

Tomography model for the Tacoma, Seattle, and Port Townsend basins at 3-km depth. White lines show the mapped faults of Gower et al. (1985). Black lines show shorelines. Thin solid white lines show locations of seismic reflection sections discussed in text. Note 90° bend in the Tacoma Narrows fault forming the northern boundary of the Tacoma basin. Various symbols show sites having evidence of uplift (solid triangles), subsidence (solid inverted triangle), and no vertical motion (filled circle) in an inferred earthquake or earthquakes dated at 1000-1100 ybp (Bucknam et al., 1992; Sherrod, 1998).

For further reading:

Bucknam, R.C., Hemphill-Haley, E., and Leopold, E.B., Abrupt uplift within the past 1700 years at southern Puget Sound, Washington, *Science*, **258**, 1611-1614, 1992.

Gower, H.D., Yount, J.C., and Crosson, R.S., Seismotectonic map of the Puget Sound region, Washington, *U.S. Geological Survey Misc. Invest. Series Map*, I-1613, scale 1:250,000, 1985.

Sherrod, B.L., Late Holocene environments and earthquakes in southern Puget Sound, Ph. D. thesis, University of Washington, 159 p., 1998.

Three-Dimensional Velocity Structure of Siletzia and Other Accreted Terranes in the Cascadia Fore Arc of Washington

Tom Parsons, Ray Wells, Mike Fisher, and Uri ten Brink, US Geological Survey
Ernst Flue, GEOMAR

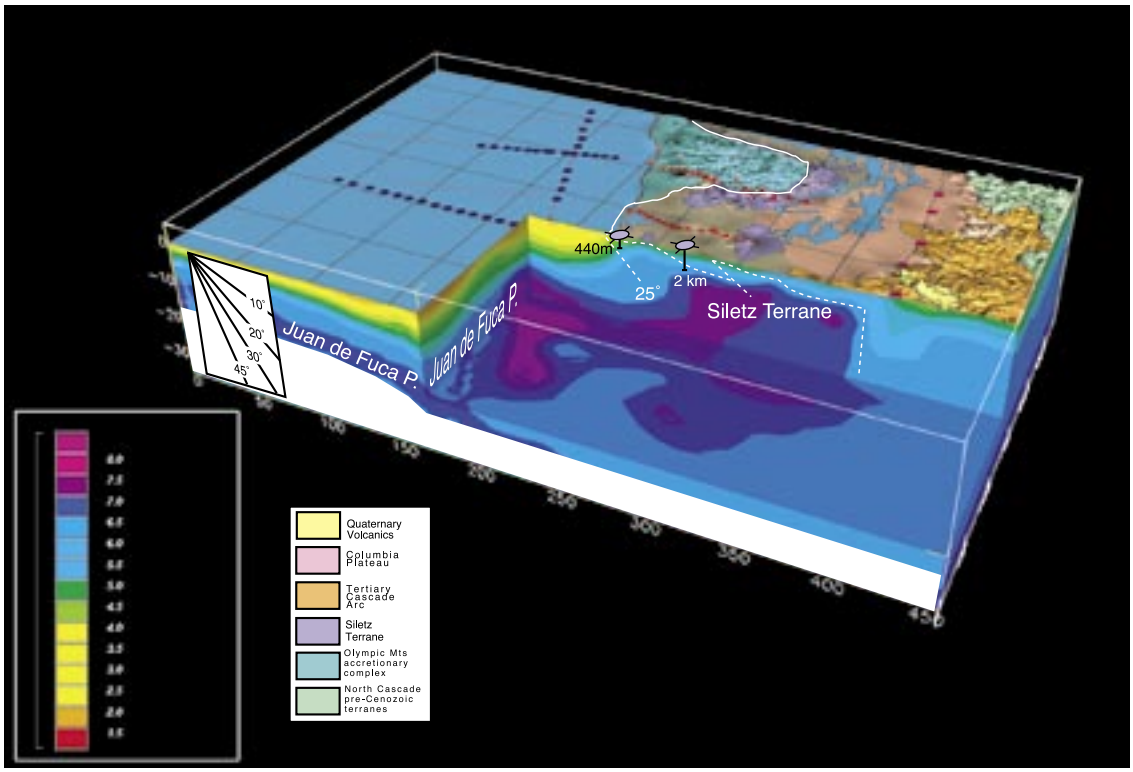

A 3-D velocity model for coastal Washington shown with the topography and generalized geology draped above.

Eocene mafic crust with high seismic velocities underlies much of the Oregon and Washington forearc and acts as a backstop for accretion of marine sedimentary rocks from the obliquely subducting Juan de Fuca slab. Arc-parallel migration of relatively strong blocks of this terrane, known as Siletzia, focuses upper crustal deformation and seismicity along block boundaries, which are potential sources of earthquakes. In a three-dimensional velocity model of coastal Washington, we have combined surface geology, well data, and travel-times from earthquakes and controlled source seismic experiments recorded on PASSCAL instruments to resolve the major boundaries of the Siletz terrane with the adjacent accreted sedimentary prism and volcanic arc. In southern Washington and northern Oregon, the Siletz terrane appears to be a thick block (~20 km) that extends west of the coastline and makes a high-angle contact with the offshore accreted sedimentary prism. On its east flank, the high velocity Siletz terrane boundary coincides with an en echelon zone of seismicity in the arc. In northern Washington, the western edge of Siletzia makes a lower-angled, fault-bound contact with the accretionary prism. In addition, alternating, east-west-trending uplifts and downwarps of the Siletz terrane centered on the antiformal Olympic Mountains may reflect focusing of north-south compression in the northern part of the Siletz terrane. This compressional strain may result from northward transport and clockwise rotation of Siletz terrane into the relatively fixed Canadian Coast Mountains restraining bend along the coast.

For further reading:

Parsons, T., Wells, R.E., E. Flueh, ten Brink, U.S., and M. A. Fisher, M.A., Three-dimensional velocity structure of Siletzia and other accreted terranes in the Cascadia fore arc of Washington, *Journal of Geophysical Research*, **104**, 18,015-18,039, 1999.

Moho Offsets in the San Andreas Fault in Mendocino Triple Junction Region

T.J. Henstock and A. Levander, Rice University
J.A. Hole, Virginia Tech

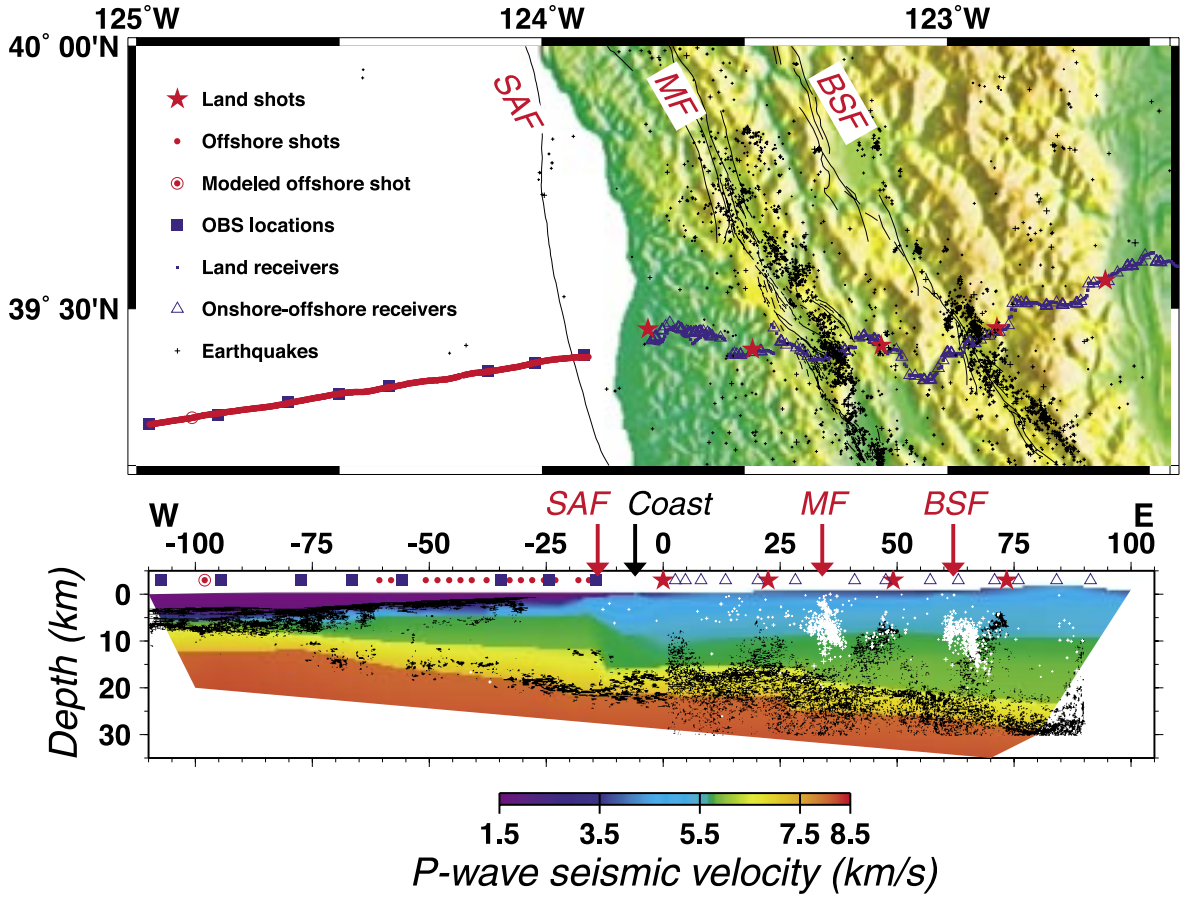

Seismic velocity-reflectivity cross section at about 39.4 degrees north across the the San Andreas transform system. Red indicates mantle velocities. The red-yellow contact is the Moho, the yellow green boundary separates overlying Franciscan accretionary rocks from the lower crustal mafic layer. Black is seismic reflectivity, white is seismicity. The top and bottom of the lower crust is offset near the San Andreas (SAF) and Macaama Faults (MF). At this latitude the San Andreas system is about 2 million years old.

A combined land-marine seismic campaign in the Mendocino Triple Junction region in northern California has produced high-resolution crustal images across the major faults of the San Andreas system. Marine reflection, OBS, onshore-offshore, and land refraction data were recorded using instruments from IRIS/PASSCAL, the GSC and the USGS. The data have been used to develop a crustal velocity model and depth migrated reflectivity image along a profile at about 39.4 degrees north extending from the Pacific Ocean Basin, across the San Andreas, Macaama, and Barlett Springs Faults to the western edge of the Great Valley.

Both the velocity model and the seismic reflectivity show offsets in the top and bottom of the mafic lower crustal layer beneath the surface expression of the strike-slip faults, evidence that the faults of the transform system cut through the entire crustal column to the mantle.

For further reading:

Henstock, T.J., Levander, A. and Hole, J.A., Deformation of the lower crust in the San Andreas Fault system, northern California, *Science*, **278**, 650-653, 1997.

Henstock T.J., and Levander, A., Lithospheric evolution in the wake of Mendocino triple junction: The San Andreas Fault system at 2 Ma, *Geophysical Journal International*, **140**, 233-247, 2000.

LARSE - The Los Angeles Region Seismic Experiment

Gary Fuis, U.S. Geological Survey
Tom Henyey and David Okaya, University of Southern California
Rob Clayton, California Institute of Technology
Paul Davis, University of California, Los Angeles
Trond Ryberg, GeoForschungsZentrum, Potsdam

The Los Angeles region is underlain by a network of active faults, including many that are deep and do not break Earth's surface. These hidden faults include the previously unknown one responsible for the devastating January, 1994 Northridge earthquake, the costliest quake in U.S. history. LARSE, conducted jointly by the Southern California Earthquake Center and the U.S. Geological Survey, investigated the subsurface fault and velocity structure of the Los Angeles metropolitan region, with a special emphasis on blind and unmapped structures. For example, knowing the configuration of buried faults is crucial to understanding how the earthquake-producing "machinery" works in the Los Angeles region, and information on the thickness and shape of the region's sedimentary basins is essential for simulating ground motions from future events. LARSE consisted of two crustal-scale seismic transects across the Los Angeles and San Fernando basins and San Gabriel Mountains using land explosions and onshore-offshore wide-angle refraction/reflection imaging using PASSCAL and other available instrumentation.

Images of the sedimentary basin beneath the San Gabriel Valley show that its depth reaches 3 miles, 50% more than earlier estimates. Because deeper sedimentary basins have greater shaking potential, earthquake hazards in the San Gabriel Valley need to be reevaluated. North of the Los Angeles basin, a strongly reflective zone was located deep beneath the San Gabriel Mountains. This zone begins at about 12 miles depth near the vertical San Andreas Fault and rises in a ramp-like fashion southward toward the Los Angeles Basin. It appears to connect to the fault system responsible for the 1987 magnitude 5.9 Whittier Narrows earthquake, which occurred on a blind thrust fault. This reflective zone is interpreted as a "master" blind thrust fault that transfers stress and strain upward and southward to a network of faults in the San Gabriel Valley and Los Angeles Basin.

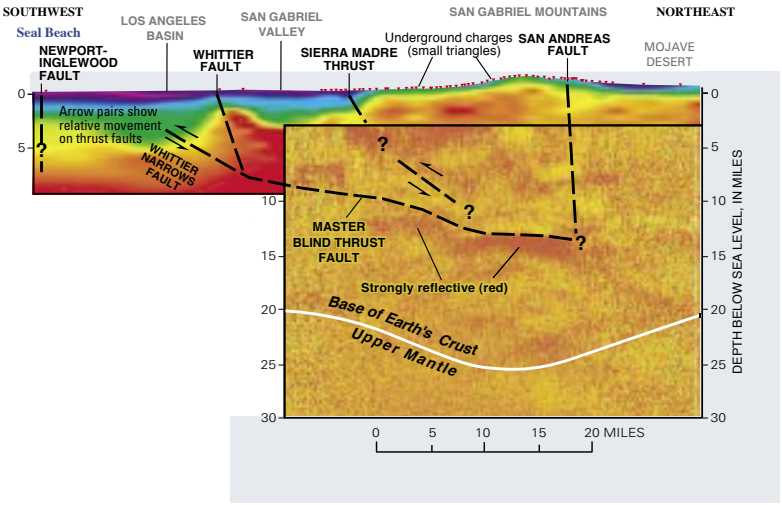

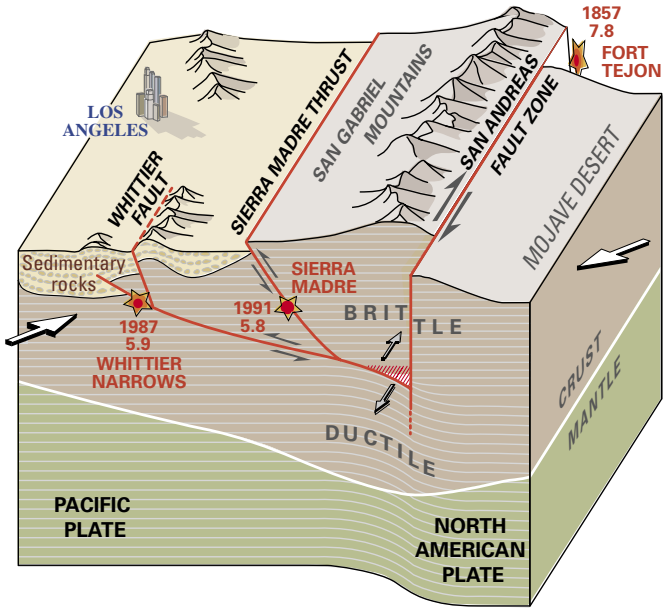

For further reading:

Godfrey, N.J., Fuis, G.S. and Okaya, D. Lower-crustal deformation beneath the central Transverse Ranges, southern California: results from the Los Angeles Region Seismic Experiment, *J. Geophys. Res.*, submitted, 1999.

Lutter, W.J., Fuis, G.S., Thurber, C., and Murphy, J., Tomographic images of the upper crust from the Los Angeles basin to the Mojave desert, California: results from the Los Angeles Region Seismic Experiment, *J. Geophys. Res.*, **104**, 25543-25565, 1999.

Ryberg, T., and Fuis, G., The San Gabriel Mountains bright reflective zone: possible evidence of young mid-crustal thrust faulting in southern California, *Tectonophysics*, **286**, 31-46, 1998.

ten Brink, U., Zhang, J., Brocher, T., Okaya, D., Klitgord, K., and Fuis, G., Geophysical evidence for the evolution of the California Inner Borderland as a metamorphic core complex, *J. Geophys. Res.*, **105**, 5835-5857, 2000.

PASSCAL Instruments and Los Angeles Region (High Resolution) Seismic Survey

Paul Davis, University of Clalifornia, Los Angeles

Immediately after the Northridge earthquake in 1994, 98 PASSCAL instruments were installed to study why Santa Monica was so badly damaged, although it was 20 km from the epicenter, while closer regions were less damaged. As a result of comparing relative amplitudes it was hypothesized that basin-edge focusing was involved (Gao et al., 1996). The figure compares aftershock amplitudes with a simple focusing model.

As part of the LARSE 1999 experiment, 75 Reftek stations were installed in the region. The stations recorded 100 shots. It was possible to set the stations to continuously record data because many of them had massive storage (1 G byte). The Hector mine earthquake occurred after installing 49 stations. We thus have a remarkable data set of over 400 aftershocks, explosions and regional earthquakes. Our objectives are to use travel time tomography to obtain the structure of the northern edge of the LA basin and to compare relative amplitudes of direct and coda waves with predictions of the model to understand geological amplification. Accurate timing on well-calibrated PASSCAL instruments of high dynamic range has been essential to this experiment, the results of which may have practical utility.

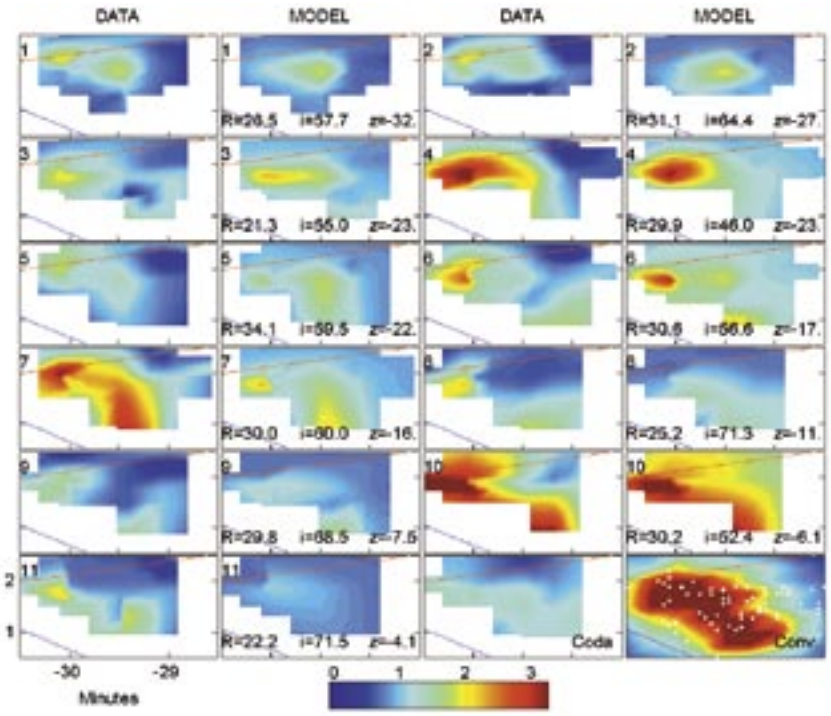

Observed and modeled amplitudes of 11 of the 22 Northridge aftershocks. Those on the left hand side are measured amplitudes corrected for site effects, while those on the right hand give the theoretical images. R is the radial distance in km to each aftershock, i the angle of incidence at the bedrock interface, z the azimuth measured clockwise from north. We observed a number of aftershocks for which the peak amplification after correction for site effects is over a factor of 4. The figures are arranged in order of increasing back azimuths to the aftershocks, northwest to north. The panel labeled 'Coda' is an image of the coda, a measure of site effects. The lower right panel labeled 'Conv' is the convolved effect of waves from the Northridge earthquake after passing through our model. The white dots correspond to condemned buildings. The buried trace of the inactive Santa Monica Fault is depicted by the ENE line. The blue line corresponds to the coastline. Latitude and longitude coordinates are in minutes of arc at N34° - W118°.

For further reading:

Gao, S., Liu, H., Davis, P.M. and Knopoff, L., Localized amplification of seismic waves and correlation with damage due to the Northridge earthquake, *BSSA,* **86**, No. 1B, S209-S230, 1996.

Seismicity of Monterey Bay and the San Gregorio Fault Region

Gerry Simila, CSU Northridge
Karen McNally, University of California Santa Cruz
Debra Stakes, Monterey Bay Aquarium Research Institute

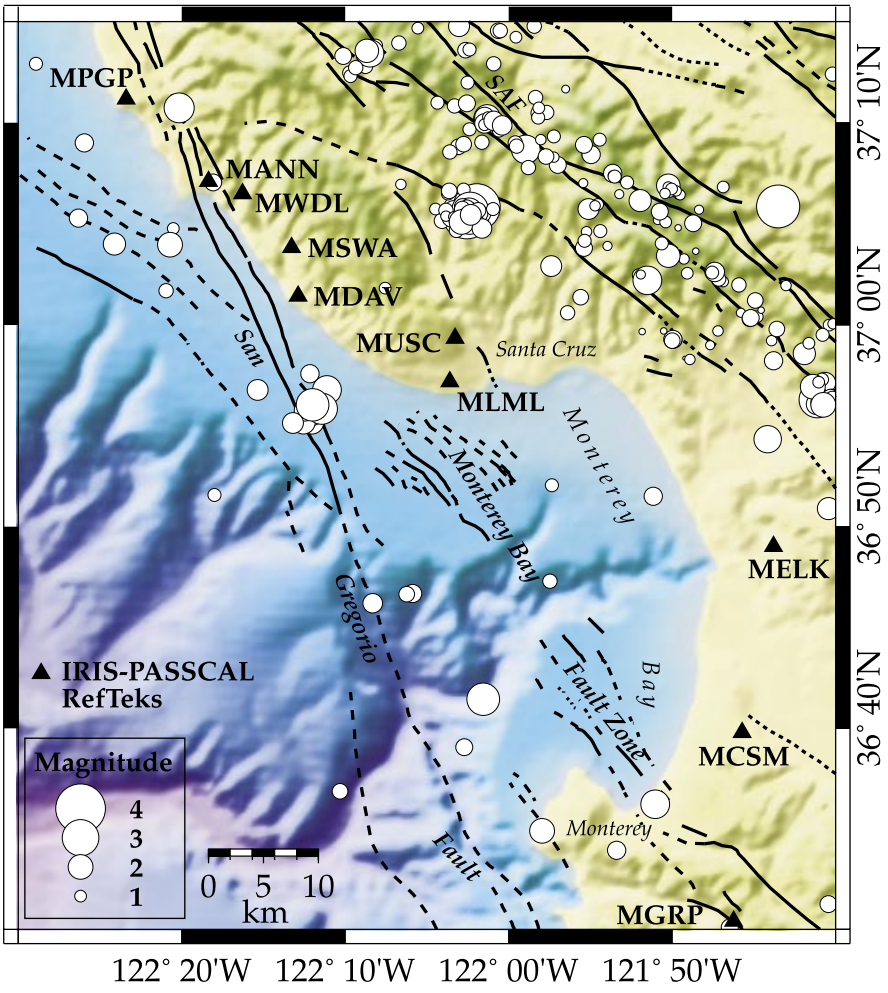

Epicenter Data (January 1998 - September 1999): Northern California Earthquake Data Center

A network of nine PASSCAL stations was operated from January, 1998 to August, 1999 to investigate the seismicity of the Monterey Bay and San Gregorio fault region. Also, four OBS instruments were deployed by MBARI on the seafloor. In addition, data from the USGS network were incorporated into the processing. Approximately 50-75 microseismic events were located, and focal mechanisms were determined. In addition, hundreds of events were detected from the San Andreas fault. The PASSCAL instruments provided critical data for fault-plane solutions and velocity modeling. Results showed three regions of seismicity along the San Gregorio fault which exhibited both right-lateral strike slip and reverse faulting mechanisms. These results are now being used for relocation of the: two 1926 (M=6.0) main shocks and associated aftershocks, and M=4.0+ events during 1930-79 for hazard evaluation of the San Gregorio and Monterey Bay faults.

For further reading:

Simila, G., McNally, K., Gallardo, V., Stakes, D., Begnaud, M., New investigation of significant Monterey Bay earthquakes (M>4.0, 1926-79) using a deployment of PASSCAL instruments, *EOS*, **79**, F589, 1998.

Seismic-Reflection Evidence that the Hayward Fault Extends into the Lower Crust of the San Francisco Bay Area

Tom Parsons and Pat Hart, US Geological Survey

PASSCAL instruments were used to gather deep seismic reflection data across San Francisco Peninsula in 1995 using large (125-500 kg) explosive sources. Shot gathers show a mostly non-reflective upper crust in both the Franciscan and Salinian terranes (juxtaposed across the San Andreas fault), an onset of weak lower-crustal reflectivity beginning at about 6 s two-way travel time (twtt), and bright southwest dipping reflections between 11 and 13 s twtt. Previous studies have shown that the Moho in this area is no deeper than 25 km (~8-9 s twtt). Three-dimensional reflection travel time modeling of the 11-13 s events from the shot gathers indicates that the bright events may be explained by reflectors 15-20 km into the upper mantle, northeast of the San Andreas fault. However, upper mantle reflections from these depths were not observed on marine reflection profiles collected in San Francisco Bay, nor reported from a refraction profile on San Francisco Peninsula. The most consistent interpretation of these events from 2-D raytracing and 3-D travel time modeling is that they are out-of-plane reflections from a high-angle (dipping ~70° to the southwest) impedance contrast in the lower crust that corresponds with the surface trace of the Hayward fault. These results suggest that the Hayward fault truncates the horizontal detachment fault suggested to be active beneath San Francisco Bay.

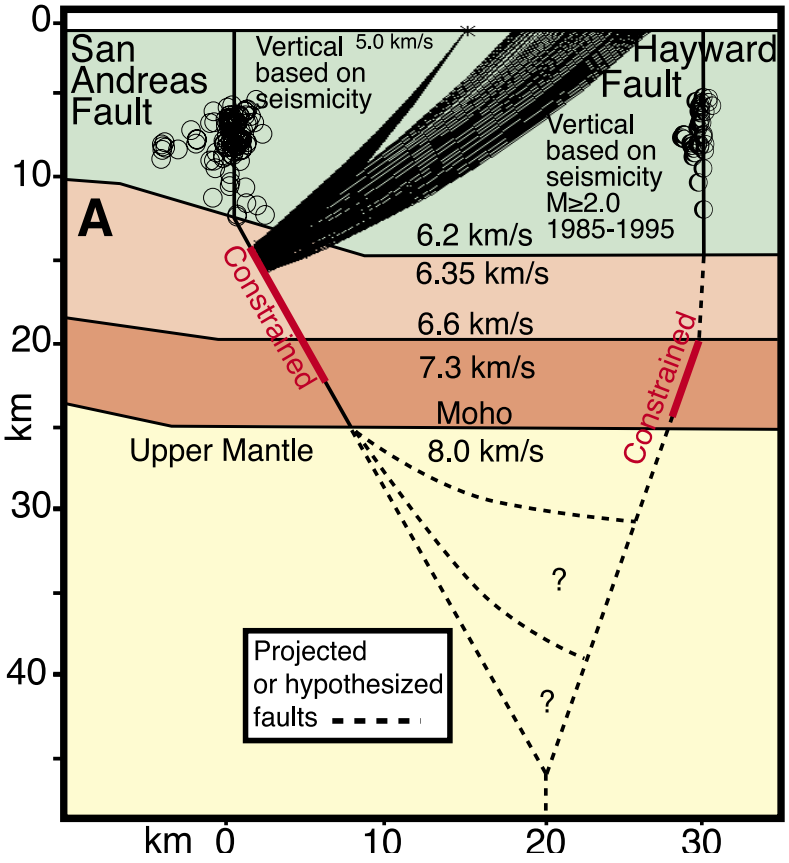

Cross-section view of San Andreas and Hayward faults as modeled from reflections. Earthquake hypocenters show that faults are near vertical in upper ~12 km. Fault planes colored red show depth extent that reflections from them are modeled. Dashed lines show projected and conjectural relationships between the two faults in upper mantle.

For further reading:

Parsons, T., Seismic-reflection evidence that the Hayward fault extends into the lower crust of the San Francisco Bay area, California, *Bull. Seis. Soc. Amer.*, **88**, 1212-1223, 1998.

Parsons, T., and Hart, P.E., Dipping San Andreas and Hayward faults revealed beneath San Francisco Bay, California, *Geology*, **27**, 839-842, 1999.

Seismic Investigation of the East Rift Zone and South Flank of Kilauea Volcano, Hawaii

C. Thurber, F. Haslinger, M. Mandernach, University of Wisconsin, Madison
Paul Okubo, USGS, Hawaiian Volcano Observatory

Starting in November 1999, we deployed a dense temporary network of 29 three-component short period PASSCAL seismographs across Kilauea volcano's East Rift Zone (ERZ) and South Flank (SF) to record local earthquake activity (Figure 1). The instruments are deployed along one long profile oriented NNW-SSE and in a combination of a shorter profile oriented N-S to the south of the ERZ plus a mini-array north of the ERZ. This array will be in operation until June 2000. We will use the data from this network in combination with data from the Hawaiian Volcano Observatory (HVO) network to investigate some fundamental questions regarding the nature of Kilauea's active rift-flank system.

A preliminary analysis of the data from the first ten weeks of network operation indicates that we record about five times more local events (triggered on five or more stations) than are located by the permanent HVO network. Most of the local seismicity occurs near the southern part of our network, beneath the SF, but some events also occur beneath the northern part of the array. We observe distinctive shear-wave splitting, previously documented for the Kilauea area by various authors, and clear shear-wave attenuation, especially for earthquakes in the south observed at northeastern stations. We have also observed clear S-to-P converted phases from deep (20 to 40 km depth) local earthquakes (Figure 2). Our long station profile was fortuitously positioned directly over a magmatic intrusion that occurred on February 23, 2000, that was accompanied by hundreds of microearthquakes.

The spatial distribution of attenuation and shear-wave splitting will provide information on the presence and extent of the proposed Deep Magma Body beneath the ERZ. The combination of accurate hypocenter determination using relative relocation techniques and observations of converted phases will provide constraints on the nature of the basal interface between the volcanic pile and the underlying oceanic crust.

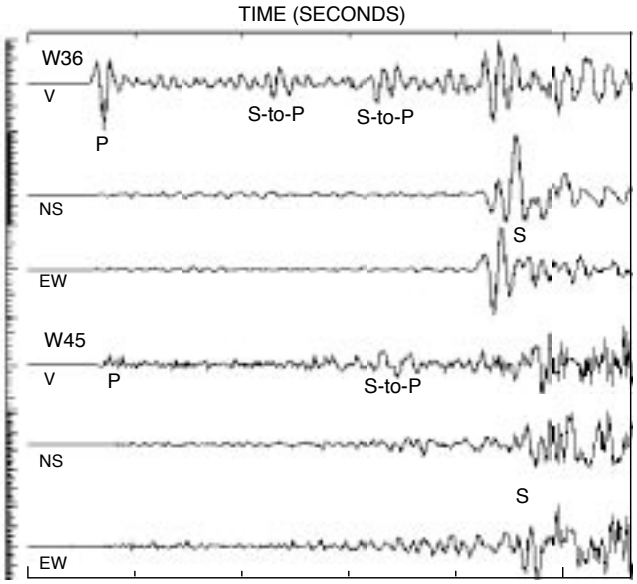

Figure 2. S-to-P converted waves, visible on the top trace between the P and S waves from a deep large (M 4.5) earthquake.

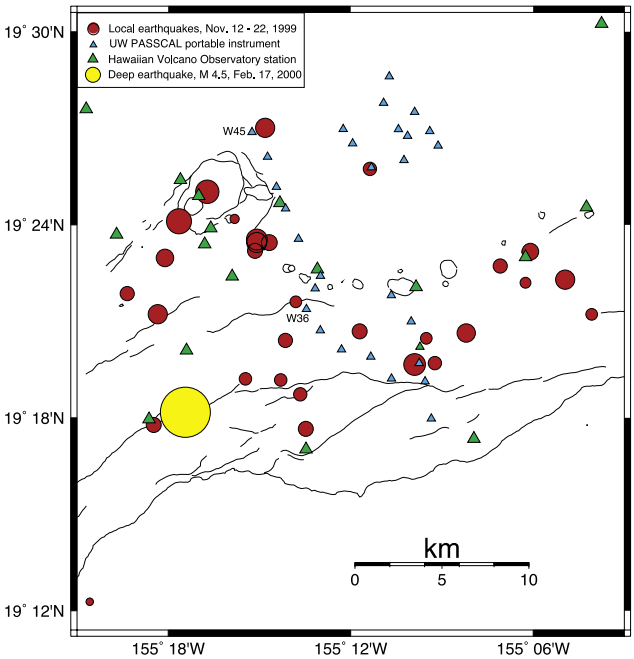

Figure 1. Array map showing geographic features of southern Hawaii, our stations (small triangles), HVO stations (large triangles), and 10 days of seismicity.

The 1975 Kalapana, Hawaii Earthquake

Meredith Nettles and Göran Ekström, Harvard University

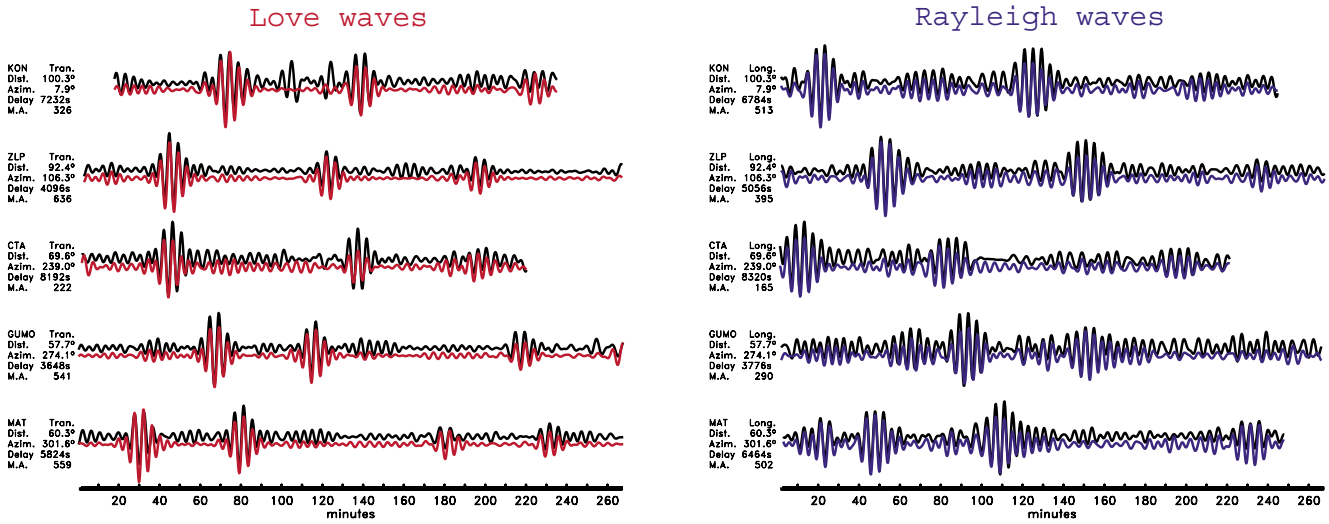

In tectonic models of the south flank of Kilauea Volcano, on the island of Hawaii, the south flank block is generally thought to be largely decoupled from the main volcanic edifice at Kilauea's east rift zone. It moves away from the island along a low-angle detachment surface as a result of stresses induced by magma injection and gravitational loading, and the slight island-ward dip of the detachment results in low-angle reverse-faulting focal mechanisms for earthquakes on this surface. The largest earthquake recorded at Kilauea in the instrumental era, the 1975 $M_S = 7.2$ Kalapana earthquake, has, however, complicated the above interpretation. Ando (1979) and Eissler and Kanamori (1987) found that predicted and observed Love wave amplitude patterns measured from WWSSN records did not agree as well as expected. Eissler and Kanamori (1987) proposed that the observed Love wave radiation pattern resulted from massive landsliding, rather than elastic faulting, at the source. Kawakatsu (1989) performed a formal inversion of the HGLP and IDA data available for the Kalapana event, and found that the variance reduction for the elastic faulting case was slightly better than that for the landsliding interpretation, but that an elastic faulting source could not explain the observed Love waves.

We have re-analyzed the digital data available for the Kalapana earthquake, using the standard Harvard CMT approach. The data included in the inversion, some of which are shown in the figure (black traces), come primarily from the stations of the digital High Gain Long Period (HGLP) network. We have also included data from early IDA and SRO stations. Calibration information for the HGLP stations was known only poorly during network operation, and Kawakatsu (1989) therefore used a single response function for all of the HGLP stations. We have used empirically determined response functions (Ekström and Nettles, 1997) for each station and channel, and find that both Love and Rayleigh wave data are very well fit by an elastic-faulting source with strike, dip and rake of 264°, 10° and 131°, respectively. Synthetic seismograms are shown above (red and blue traces) for selected stations, including KON and CTA, where Kawakatsu (1989) noted particularly poor fits to the Love wave data. We find that using the nominal HGLP response available for Kawakatsu's (1989) study results in anomalously small Love wave amplitudes, like those he described. We therefore believe that the Kalapana earthquake can be explained without recourse to a landsliding mechanism, and suggest that it in fact fits quite well into the tectonic model for Kilauea described above. The corrected HGLP response functions have been contributed to the IRIS DMC response database via the ASL Data Collection Center.

For further reading:

Ando, M., The Hawaii earthquake of November 29, 1975: Low dip angle faulting due to forceful injection of magma, *J. Geophys. Res.*, **84**, 7616–7626, 1979.

Eissler, H. K., and Kanamori, H., A single--force model for the 1975 Kalapana, Hawaii, earthquake, *J. Geophys. Res.*, **92**, 4827– 4836, 1987.

Ekström, G. and Nettles, M., Calibration of the HGLP seismograph network and centroid-moment tensor analysis of significant earthquakes of 1976, *Phys. Earth Plan. Inter.*, **101**, 219–243, 1997.

Kawakatsu, H., Centroid single force inversion of seismic waves generated by landslides, *J. Geophys. Res.*, **94**, 12363–12374, 1989.

P-Wave Velocity Structure in the Greater Mount Rainier Area

Seth Moran, U.S. Geological Survey
Jonathan Lees, Yale University
Steve Malone, University of Washington

Mount Rainier is potentially the most dangerous volcano in the Cascade Range. Even small eruptions could disrupt airline traffic, cause major flooding as a result of ice melt, or trigger flank collapses leading to debris flows that could reach heavily visited regions of the national park as well as nearby municipalities. We have recently completed a study of the seismicity and "seismic structure" of the greater Mount Rainier area with the goals of improving our understanding of the nature of seismicity occurring near and beneath Mount Rainier, and the nature of the magmatic system beneath Mount Rainier. During our study we collected data from a number of sources, including ~20 seismometers and dataloggers loaned to us through the PASSCAL facility. The IRIS instruments proved quite useful, as they allowed us to deploy instruments at temporary sites in very remote locations that would otherwise have been inaccessible due to logistical constraints and line-of-site telemetry limitations.

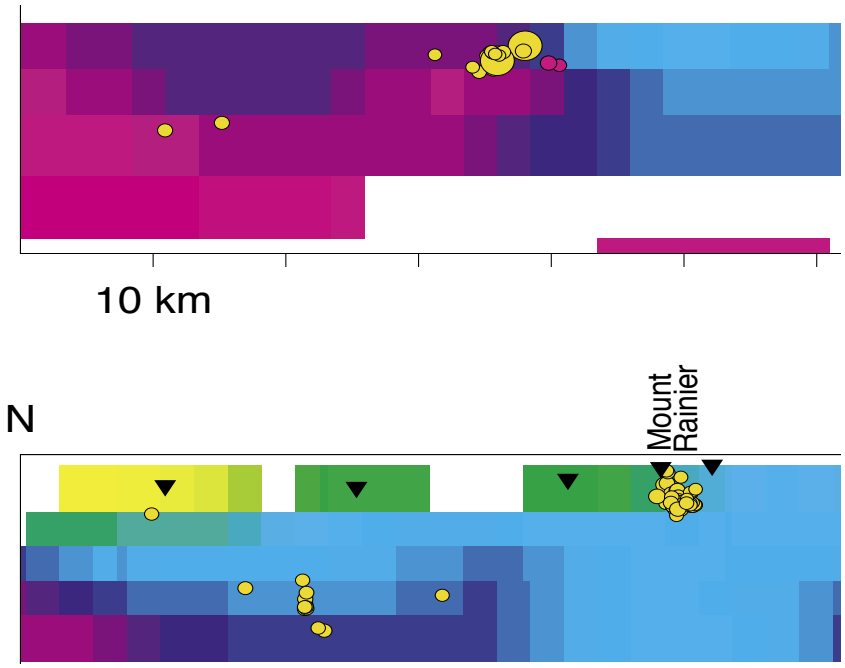

East-west and north-south cross-sections through the 3-D model determined by Moran et al. (1999). Yellow circles are "tectonic" or "VT" earthquakes, red circles are locations of deep long-period events, black triangles are locations of seismic stations. Note the lack of hypocenters within the low-velocity zone beneath Mount Rainier.

One of the most significant features in the resultant velocity model is a well-resolved, cylindrical, ~10 km-diameter low-velocity anomaly extending from 8 to 18 km directly below the summit of Mount Rainier (Figure). The amplitude of the anomaly is not large, with velocities 4-5% slower than expected. There is also no obvious attenuation of S-wave amplitudes for raypaths that traverse the anomaly. These two observations indicate that the low-velocity anomaly is not the signature of a region containing a significant amount of melt (a "magma chamber"). However, Moran et al. (1999) compared the imaged P-wave velocities to laboratory measurements of P-wave velocities for a wide variety of rock types and concluded that the anomaly could not be explained solely by lithology. The lack of any earthquakes within this anomaly (Figure) implies that the rock inside the anomaly is hot, with temperatures at some level above brittle-ductile transition temperatures. The occurrence of VT earthquakes only on top of this anomaly (Figure) and the increase of maximum earthquake depths to ~10 km on either side of the anomaly indicate a highly elevated brittle-ductile transition directly beneath the volcano. Moran et al. (1999) used these observations to infer that the low-velocity anomaly is likely caused by a volume of hot host rock containing small pockets of hot fluids and/or melt. Moran et al. (2000) speculated that the magmatic gas components and hot temperatures found in Mount Rainier's surface geothermal system are derived from the cooling of small magma bodies contained within this region. Moran et al. (2000) further speculated that deep long-period events located on the eastern edge of the Western Rainier Seismic Zone (red circles in figure) might be related to a steady trickle of minor amounts of magma from deeper sources below the WRSZ into the anomaly.

For further reading:

Moran, S. C., Lees, J.M., and Malone, S.D., P-wave velocity structure in the greater Mount Rainier area from local earthquake tomography, *J. Geophys. Res.*, **104**, 10,775-10,786, 1999.

Moran, S. C., Zimbelman, D.R., and Malone, S.D., A model for the magmatic-hydrothermal system at Mount Rainier, Washington, from seismic and geochemical observations, *Bull. Volc.*, **61**(7), 425-436, 2000.

Broadband and Acoustic Studies of Volcanic Seismicity on Mount Erebus, Antarctica

Richard Aster, Philip Kyle, Charlotte Rowe, and Noel Barstow, New Mexico Institute of Mining and Technology
Jeff Johnson, University of Washington
Ray Dibble, Victoria University

We are using PASSCAL broadband instrumentation as a key component of an interdisciplinary research program to study eruption physics and volcanic geochemistry on Mount Erebus, Ross Island, Antarctica. This volcano is remarkably favorable for studies of smaller-scale eruption processes because of its persistent inner crater phonolitic lava lake, Strombolian eruptive activity, and open conduit system. During the 1999-2000 Antarctic field season, we deployed eight broadband seismometers on the summit plateau of the volcano at elevations near 3500 m, between 0.8 and 3 km from the lava lake, and across approximately 180 degrees of azimuth. Six sites were also equipped with ~1-m- aperture, four-element, zero-lag-stack electret condenser microphones to study the short-period seismoacoustic wave field.

One remarkable result from PASSCAL broadband deployments on Erebus is that effective near-field displacements are dominated by very-long period (VLP), vertical-radial polarized, highly repeatable signals with frequency content between about 25 s and 5 s. These signals are caused by an unknown resonance process in the shallow conduit system that is excited by the gas explosions at the surface of the lava lake. The figure shows: (a) Vertical and radial lava lake explosion displacement seismograms recorded with a PASSCAL Guralp 3-ESP sensor at Nausea Knob (approximately 700 meters from the lava lake and at nearly the same elevation); (b) Displacement power spectrum of the vertical component in (a), showing distinct broadened resonance peaks associated with the VLP excitation and the spectral separation of these signals from the short-period (SP) seismoacoustic energy; (c) Particle motion diagrams for the band-passed seismograms in (a), showing a steeply-dipping, radially-oriented principal axis (probably steepened by tilt effects) for the two time periods windowed in (a).

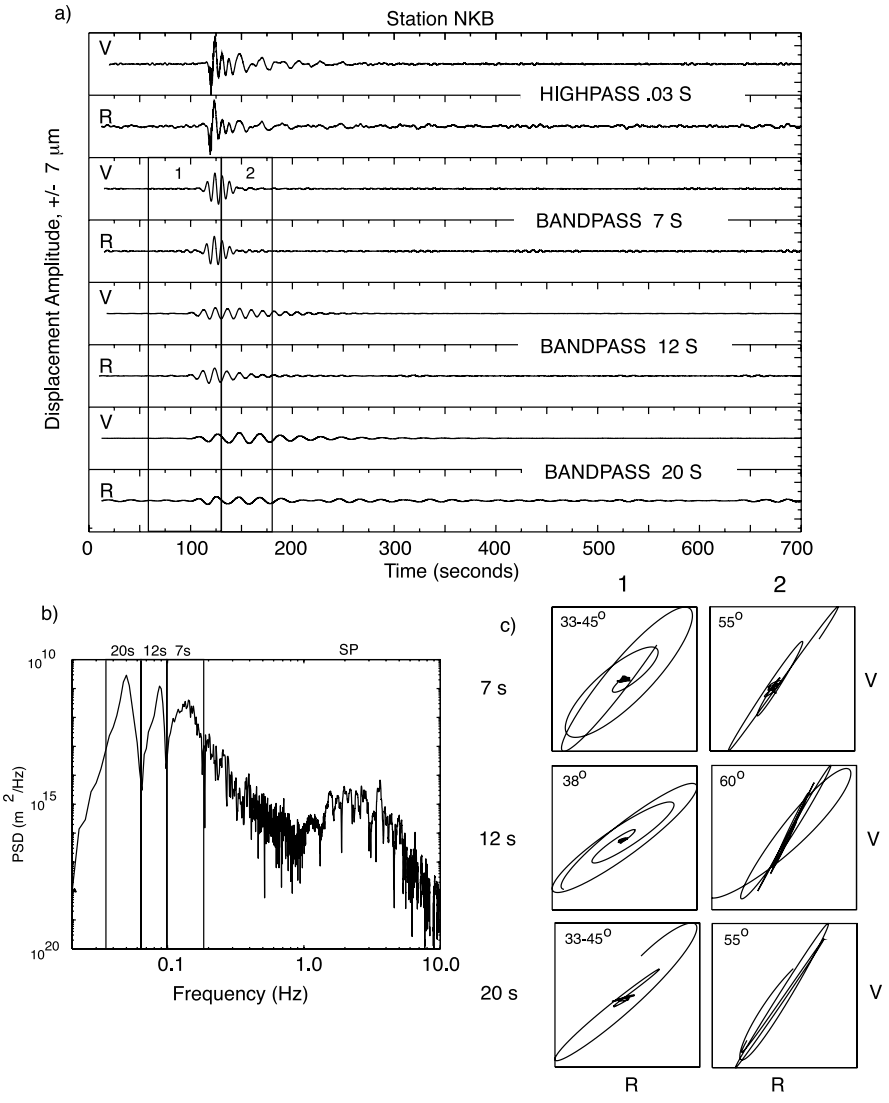

For further reading:

Rowe, C., Aster, R., Kyle, P., Schlue, J., and Dibble, R., Broadband recording of Strombolian explosions and associated very-long-period seismic signals on Mount Erebus volcano, Ross Island, Antarctica., *Geophys. Res. Lett.*, **25**, 2297-2300, 1998.

Rowe, C., Aster, R., Kyle, P., Dibble, R., Schlue, J., Seismic and acoustic observations at Mount Erebus volcano, Ross Island, Antarctica, 1994-1998., *Journal of Volcanological and Geothermal Research*, in press, 2000.

Future Directions in Seismic Instrumentation: Clues from Broadband Volcano Seismology

Charles A. Langston, University of Memphis
Dannie Hidayat and Barry Voight, Pennsylvania State University

The modern digital broadband seismometer has produced a scientific revolution in seismology and in all aspects of the Earth sciences that use seismological results. Thanks to consortia efforts like IRIS', the amazing improvement in data quality and fidelity over early analog systems is simply taken for granted by practicing seismologists. Yet, there are indications from field deployments on volcanoes that today's broadband instruments have significant, fundamental limitations that need to be addressed by future developments in instrument design. A deployment of broadband PASSCAL instruments on Merapi Volcano, Indonesia, in early 1998 yielded a fascinating data set of near-field observations of seismic events associated with a growing andesitic lava dome. The figure shows several Multiphase (MP) and Low Frequency (LF) events recorded by a station at 100 m distance from the dome. (The nomenclature for MP and LF events is based on observations of these seismic events at short-period stations more than a kilometer away.) These data show typical high frequency arrivals that probably originate in cracking of surrounding vent rock by the intruding dome magma. However, embedded in these signals is a prominent 4 second pulse. In previous studies, long-period pulses such as these have been attributed to dilatational expansion or contraction of the volcanic edifice, i.e., these waves were thought to be P waves. Particle motions seem to bear this out by showing rectilinear, horizontal motions. However, a careful analysis of these pulses on all stations of the deployment suggests that they are probably due to the tilt response of the broadband instrument. These pulses decay quite quickly with distance suggesting that they are near-field source effects. A theoretical analysis of near-field rotations from a directed point force suggests that ground tilts at 100 m distances from a seismic source should be quite large. These tilts become dominating signals through the broadband seismometer since horizontal component masses react to the acceleration of gravity. Thus, data that presumably represent vector ground motions are grossly contaminated by ground tilts. At present, there is no unique way to separate the effect of instrument tilt from instrument displacement. The effect of tilts on long-period and broadband seismic instruments has been known for many years. Point field measurements need an additional three components of instantaneous rotation in addition to the normal three components of displacement to fully characterize the seismic wave field. This seems especially important in the near field of a seismic source such as encountered in modern volcano seismic deployments. Accurate characterization of seismic sources in this near-field regime will need new developments in seismic instrumentation that can record all 6 degrees of freedom of ground motion.

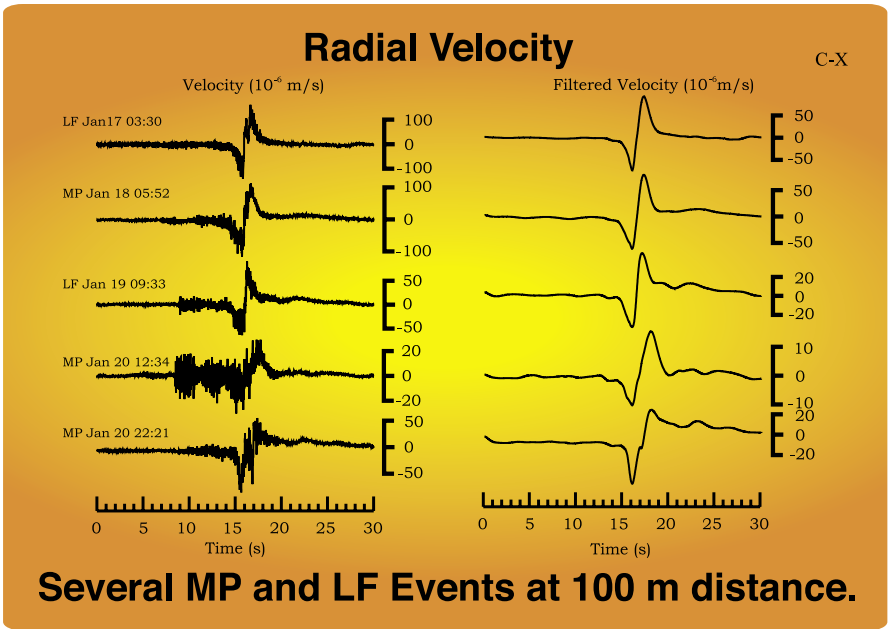

Raw radial velocity data (left) and filtered velocity data (right) for MP and LF events recorded 100 m away from a growing andesitic lava dome on Merapi Volcano. Ground tilt appears as the 4 second long-period pulse in these broadband records. New instrumentation is needed in the near-field of these sources to remove the ambiguity between displacement and rotation due to instrument design.

International Opportunities in Volcano Seismology

Clifford Thurber, University of Wisconsin-Madison
Jonathan Lees, Yale University

There are many opportunities world-wide for volcano seismology research. These opportunities include research into the internal structure and geodynamic behavior of volcanic systems, volcano monitoring, and eruption prediction. Examples of important areas of seismological research are 3-D tomographic imaging of seismic velocity structure (Figure 1), determining seismicity distribution with high precision (Figure 2), analysis of converted seismic waves, state of stress from source mechanisms and anisotropy, and the study of harmonic tremor and low-frequency seismic sources (long-period earthquakes and very-low-frequency events, up to 1000 s period).

As examples of the potential for IRIS involvement in international volcanological studies, the authors are currently involved in three major international efforts to study active volcanism: in Kamchatka, Russia; Quito, Ecuador; and Rabaul, Papua New Guinea. In the first two cases, the foreign collaborators are severely hampered and limited by the lack of high-quality instrumentation. They rely on PASSCAL instruments obtained through US collaborators for seismometers and dataloggers to monitor volcanoes. There is a great need to get high-quality equipment into these places, and various avenues for potential support are being investigated. Both Petropavlovsk (pop. 250,000) and Quito (pop. >1 million) are cities in significant danger from volcanic hazards. Societal impact related to volcano hazard mitigation is thus of immediate and great concern to these places.

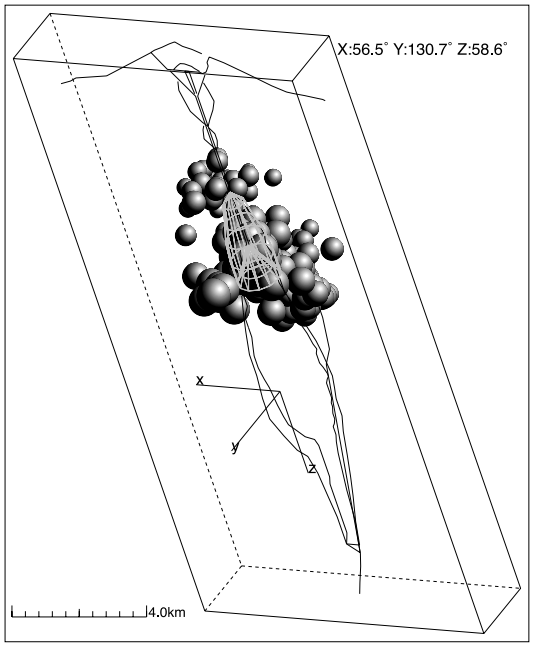

Figure 2. Spatial relationship between seismicity and the inferred magma conduit system beneath Mt. St. Helens.

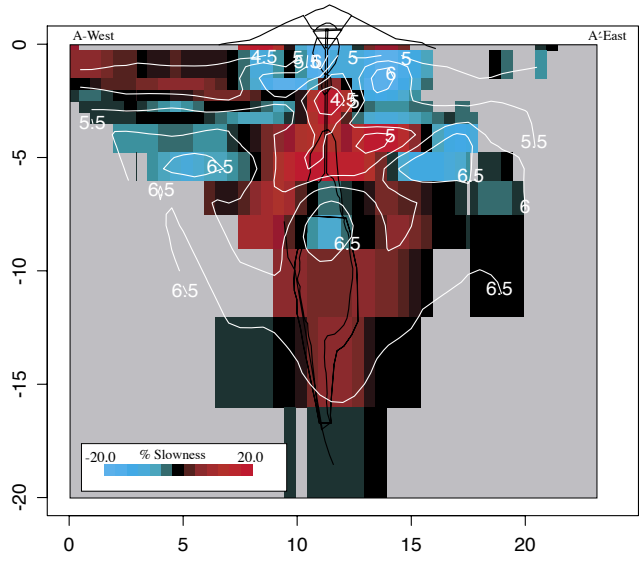

Figure 1. Cross-section of P-wave velocity anomalies beneath Mt. St. Helens, showing an upper-crustal low-velocity zone. The inferred magma conduit system is shown by the black lines here and in Figure 2.

In the case of Rabaul, UW instruments were added to a major passive-active seismic experiment in 1997 (Project RELACS) in order to double the number of three-component instruments. The three-component data will be used to look for possible converted waves and shear-wave shadowing by the presumed magma chamber beneath Rabaul Caldera.

Next-generation PASSCAL instrumentation will greatly facilitate volcano seismology studies. New data acquisition systems (DAS - smaller, lighter weight, and especially lower power) will significantly improve deployment capability in difficult volcanic terrain. We can also envision a third-generation DAS based on NASA developments that could be deployed from a helicopter in areas of significant hazard. Rugged, low-power, wide-band sensors would improve observations of low-frequency waves from long-period earthquakes and other "exotic" seismic sources. The capability for multiple data streams from a variety of sensors would be extremely valuable, permitting the recording of acoustic, temperature, wind speed and other atmospheric conditions. For volcano monitoring this is the wave of the future. Telemetry and real-time field processing is essential for monitoring for eruption prediction efforts.

Quasi-Periodic Volcanic Tremor

Jonathan M. Lees, University of North Carolina, Chapel Hill
Evgenii Gordeev, Geophysical Services, KOMSP, Russian Academy of Sciences, Petropavlovsk-Kamchatsky
Jeff Johnson, University of Washington

We have an extensive program to investigate the nature of volcanic eruptions in large, explosive andesitic systems. These include nearly all the volcanos around the Pacific Rim where heavily populated regions often are surrounded by active volcanism. Using IRIS PASSCAL portable deployments we are able to record, with high fidelity, seismic signals associated with fluid flow in volcano plumbing systems. These provide significant constraints on the physics of the magma-rock interactions that allow us to estimate eruption dynamics. In particular we have focussed investigations at Karymsky Volcano, in the Russian far east, Sangay Volcano in Ecuador, Mt. St. Helens, Mt. Rainier and Mt. Fuji in Japan.

Intensive PASSCAL deployments at Karymsky Volcano over the period 1997-1999 include the analysis of quasi-periodic tremor. Repeating pulses from exploding Karymsky volcano contain a rich variety of signals recorded on IRIS PASSCAL acoustic and seismic sensors. Several general observations regarding the pulsating train include the following facts: (1) Chugging events always follow an initial explosion, although not all explosions are followed by chugging. (2) There is almost always a lag time between the initial explosion and the commencement of intense chugging. We assume this is a preparation time where the system is building up intensity. (3) The chugging is fairly regular, with a dominant, fundamental frequency that fluctuates from 0.7 to 1.5 s. 4) Individual pulses are very uniform and are near duplicates of the initial explosive pulses. 5) A typical sequence of events has an envelope that grows rapidly in amplitude and later diminishes gradually. The pulsating sequences exhibit behavior that cannot be explained by a resonating conduit. This is clear from the correlation of amplitudes to inter-pulse time intervals. Consistent seismic arrivals appear to be keyed to the size of acoustic recording and not vice-versa, providing evidence for a shallow, oscillatory source near the vent opening. A model consisting of a sequence discrete pulses explains the data and provides a framework for understanding the dynamics of degassing at the vent.

Jonathan Lees and Jeff Johnson, 1997, installing a PASSCAL broadband station with acoustic sensors at Karymsky Volcano, Russia.

For further reading:

Johnson, J., Lees, J.M., and Gordeev, E., Degassing explosions at Karymsky Volcano, Kamchatka, Russia, *Geophys. Res. Lett.*, **25**, 3999-4002 1998.

Broadband Seismometry at Active Volcanos

Hitoshi Kawakatsu, University of Tokyo
Satoshi Kaneshima, Tokyo Institute of Technology

Seismic wavefields observed near active volcanos contain abundant information about volcanic activity in the frequency range between 0.01 Hz and 1.0 Hz where, until recently, conventional geophysical monitoring of volcanos had not paid much attention except for few rare cases. The physics operating in a volcano is extremely complex; in different frequency bands, different physical processes dominate the wavefield. This characteristic makes PASSCAL-type broadband seismic observations essential to unraveling the physical processes of volcanic activities.

We have been observing two active volcanos in Japan: Sakurajima and Aso. Two deployments of broadband instruments in Sakurajima not only convinced us of the importance of broadband seismic observation at volcanos (Kawakatsu et al., 1992), but also led us to another volcano by observing strange long period 10s wave trains apparently generated near the Aso volcano located 150km away from Sakurajima (Kawakatsu et al., 1994). Deployment of a dense network of broadband seismometers in Aso revealed a hydrothermal reservoir 1 to 1.5 kilometers beneath the crater that is continually resonating with periods as long as 15s, even when there is no apparent surface activity at the crater. During phreatic eruptions, broadband seismograms elucidate vividly the whole eruption process: gradual pressurization and long-period (about 20s) pulsations of the reservoir during the 100-200s before the initiation of the discharge, followed by gradual deflation of the reservoir concurrent with the discharging flow (Kaneshima et al., 1996, Kawakatsu et al., 1999). The observed spatial variation of the signal amplitudes reveals that the source of 15s long period tremors (LPTs) consists of an isotropic expansion (contraction) and an inflation (deflation) of an inclined tensile crack with a strike almost parallel to the chain of craters. The extension of the buried crack plane meets the crater chain including the active fumarole at the surface, suggesting that the crack has played an important role in transporting steam (gasses) and/or lava to the craters from below. This work also demonstrates a powerful usage of broadband seismometers as geodetic instruments to constrain subsurface structures at active volcanos (Yamamoto et al., 1999).

Our results so far demonstrate the high potential for PASSCAL-type broadband seismic observations near active volcanoes to add essential information missed by conventional seismometry. There is now much evidence from volcanoes of the world indicating the presence of long-period volcanic signals. We feel that volcanology should embrace state-of-the-art developments, and broadband seismometers as well as other instruments, such as infra-sonic microphones, should be installed as standard equipment for monitoring volcanic activities. PASSCAL activity is extremely important for such purposes.

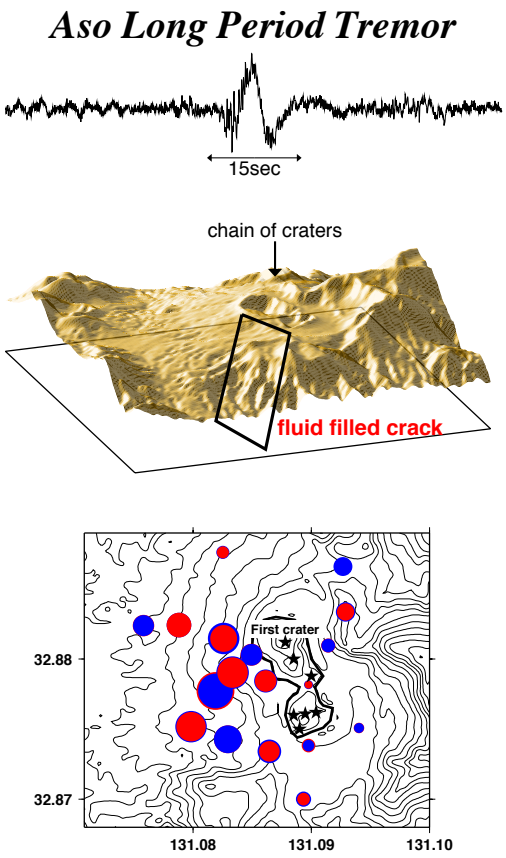

(Top) Long period tremor; (middle) Bird's-eye view of the detected crack-like conduit; (bottom) The observed and model-predicted amplitudes are respectively represented as red and blue circles whose radii are proportional to the values of the amplitudes. In this figure, a smaller circle is put onto a larger one, thus the width of the ring represents the misfit, which is very small.

For further reading:

Kawakatsu, H., Ohminato, T., Ito, H., Kuwahara, Y., Kato, T., Tsuruga, K., Honda, S., and Yomogida, K., Broadband seismic observation at the Sakurajima volcano, Japan, *Geophys. Res. Lett.*, **19**, 1959-1962, 1992.

Kawakatsu, H., Ohminato, T., and Ito, H., 10s-period volcanic tremors observed over a wide area in southwestern Japan, *Geophys. Res. Lett.*, **21**, 1963-66, 1994.

Kaneshima, S., Kawakatsu, H., Matsubayashi, H., Sudo, Y., Tutui, T., Ohminato, T., Ito, H., Uhira, K., Yamasato, H., Oikawa, J., Takeo, M., Iidaka, T., Mechanism of Phreatic Eruptions at Aso Volcano Inferred from Near-Field Broadband Seismic Observations, *Science*, **273**. 642-645, 1996.

Yamamoto, M., Kawakatsu, H., Kaneshima, S., Mori, T., Tutui, T., Sudo, Y., Morita, Y., Detection of a crack-like conduit beneath the active crater at Aso volcano, Japan, *Geophys. Res. Lett.*, **26**, 3677-3680, 1999.

Legrand, D., Kaneshima, S., Kawakatsu, H.., Moment tensor analysis of near field broadband waveforms observed at Aso volcano, *J. Vol. Geothermal Res.*, in press, 1999.

Kawakatsu, H., Kaneshima, S., Matsubayashi, H., Ohminato, T., Sudo, Y., Tutui, T., Uhira, K., Yamasato, H., Legrand, D., Aso-94: Aso seismic observation with broadband instruments, *J. Vol. Geothermal Res.*, in press, 1999.

Study of Earthquake Faults Using Fault-Zone Trapped Waves Recorded by PASSCAL Instruments

Yong-Gang Li, University of Southern California
John E. Vidale, University of California, Los Angeles

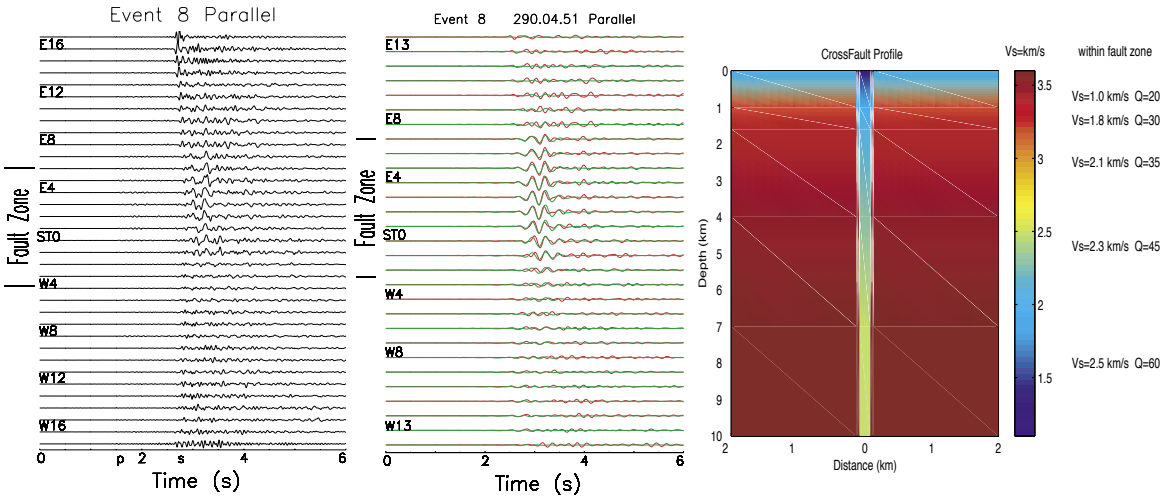

Left: Fault-zone parallel component seismograms recorded by 36 PASSCAL REFTEKs in a 3-km long line across the Landers rupture zone for an aftershock occurring within the rupture zone at 5 km depth. Middle: Low-pass filtered seismograms (red) show 3-5 Hz fault-zone trapped waves predominant at stations located within the rupture zone. 3-D finite-difference synthetic trapped waves (green) fit observations well. Right: The model used for 3-D FD synthetics, showing a depth-dependent structure of the Landers rupture zone.

In the past decade, we have used portable PASSCAL instruments (REFTEK, GEOMETRICS and other facilities) in our seismic experiments conducted in California and Japan. We recorded high-quality data using PASSCAL instruments and also used software developed by PASSCAL for data transferring, format-conversion and management. Without the use of PASSCAL facilities, it would have been impossible to achieve our scientific objects in these research projects. We greatly appreciate PASSCAL personnel for their selfless cooperation.

Since 1991, we used PASSCAL portable seismographs to record fault-zone-trapped waves from earthquakes and near-surface explosions at the San Andreas fault, San Jacinto fault, and rupture zones of the 1992 M7.4 Landers earthquake and the M7.1 Hector Mine earthquake in California as well as at the 1995 M6.9 Kobe earthquake rupture zone in Japan. In each experiment, we used 40-80 REFTEKs near the fault zone to record trapped waves for several months. These instruments always worked very well despite adverse environmental conditions, such as high summer temperatures (>130 degrees) in the Mojave Desert or heavy spring rains and wind in the mountains. These weather conditions verified the good quality of the PASSCAL instruments and good maintenance of the PASSCAL facilities. Also, the participation of PASSCAL researchers in the field experiments were key to the success of data acquisition in these experiments. For example, we acquired the unique fault-zone-trapped wave data from aftershocks and explosions at the Landers rupture zone in our repeated experiment during 1994-1998 (see figure). These data allowed us to study, with higher precision ever than before, the internal structure of the recently ruptured zones, the physical nature of fault segmentation, the relationship between fault zone structure, and the dynamic rupture process and fault healing after a major earthquake.

For further reading:

Li, Y. G., Vidale, J.E., Aki, K., Marone, C.J., Lee, W.H.K., Fine structure of the Landers fault zone; segmentation and the rupture process, *Science*, **256**, 367-370, 1994.

Li, Y. G., Aki, K., and Vernon, F.L., San Jacinto fault zone guided waves: A discrimination for recently active fault strands near Anza, California, *J. Geophys. Res.*, **102**, 11,689-11,701, 1997.

Li, Y. G., Ellsworth, W.L., Thurber, C.H., Malin, P.E., and Aki, K., Observations of fault-zone trapped waves excited by explosions at the San Andreas fault, central California, *Bull. Seism. Soc. Am.*, **87**, 210-221, 1997.

Li, Y. G., Vidale, J.E., Aki, K., Xu, F., and Burdette, T., Evidence of shallow fault zone strengthening after the 1992 M7.5 Landers, California, earthquake, *Science*, **279**, 217-219, 1998.

Li, Y. G., Aki, K., Vidale, J.E., and Alvarez, M.G., A delineation of the Nojima fault ruptured in the M7.2 Kobe, Japan, earthquake of 1995 using fault zone trapped waves, *J. Geophys. Res.*, **103**, 7247-7263,1998.

Li, Y. G., Aki, K., Vidale, J.E., and Xu, F., Shallow structure of the Landers fault zone using explosion-excited trapped waves, *J. Geophys. Res.*, **104**, 20,257-20,275, 1999.

Li, Y. G., Vidale, J.E., Aki, K., and Xu, F., Depth-dependent structure of the Landers fault zone using fault zone trapped waves generated by aftershocks, *J. Geophys. Res.*, **105**, 6237-6254, 2000.

Rapid Seismological Analysis for Emergency Response

Douglas Dreger and Asya Kaverina, University of California, Berkeley

There is considerable interest in developing the capability to rapidly characterize earthquake strong ground motions to help facilitate initial emergency response. Given a dense network of real-time telemetered strong motion stations it is possible to rapidly determine contour maps (shakemaps) of the observed strong ground motions in near-real-time (Wald et al., 1999). However, in areas where network coverage is sparse the available instrumentation may not be adequate to properly characterize near-source strong shaking for large earthquakes that exhibit wave amplification resulting from directivity focussing. There is no substitute for dense networks of strong and weak motion instruments to observe the wavefield in the urban areas, however the expense of installing dense networks on a regional scale is prohibitive. The risk due to earthquake strong shaking is region-wide including the urban core, rural communities, and the distributed water, power and transportation infrastructure, and complementary methods utilizing real-time telemetered regionally recorded seismograms are needed. We have developed such a method by modeling the extensive regional broadband, and near-fault strong motion data for the 1992 Landers (M7.3) and 1994 Northridge (M6.7) earthquakes (Kaverina et al., 1997). The October 16, 1999 Hector Mine earthquake (MW7.1) provided an opportunity to demonstrate the procedure (Dreger and Kaverina, 2000), as described below.

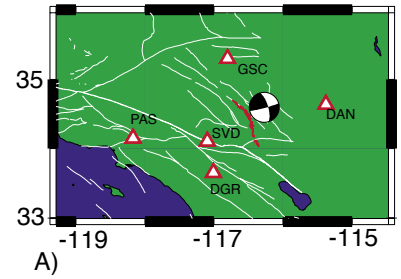

A) Map showing the locations of five three-component TERRAscope stations used in our initial analysis and a fault plane solution obtained using Berkeley Digital Seismic Network Data.

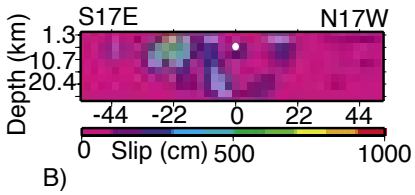

B) Fault normal projection of slip resolved on the NW striking nodal plane. Average slip is 138 cm and peak slip is 828 cm. The white circle marks the location of the hypocenter.

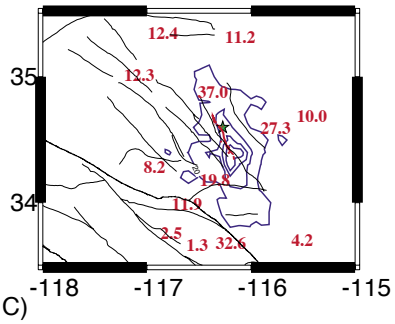

C) Peak ground velocity (PGV) derived from the slip (B) is shown as blue contours with intervals of 10 cm/s. The red numbers compare observed PGV in units of cm/s. The green star shows epicenter.

The first stage in the method is to determine a seismic moment tensor. For the Hector Mine earthquake this was accomplished using Berkeley Digital Seismic Network (BDSN) data located over 400 km from the earthquake. The second stage is to determine the causative fault (nodal) plane by inverting complete, three-component displacement waveforms recorded at five TERRAscope stations (Figure A) for a series of line source models for both possible orientations over a range of rupture velocity. This stage yielded the NNW striking nodal plane and a rupture velocity of 2.6 km/s. The third stage is to obtain, with these new constraints, the distribution of slip on a planar fault from the same broadband waveform data (Figure B). The slip model indicates a bilateral rupture with most of the slip located SE of the hypocenter. Revised models, which take fault curvature and variations in dislocation rise time, rupture velocity, and rake into account also show a bilateral rupture, but with the slip focused nearer the hypocenter (see for example http://www.seismo.berkeley.edu/~dreger/hectorweb/hectweb.htm). The final stage in the processing integrates the slip shown in Figure B over time and space using Green's functions appropriate for the near-fault region to simulate the strong motion time histories. Figure C is a contour map of peak horizontal ground velocity (PGV) derived from the synthesized time histories. The shakemap is found to agree well with near-fault observations that were not available when we performed our initial analysis and they therefore provide an affirmative test of the method. The map shown in Figure C also agrees well with the TriNet PGV ShakeMap. The Berkeley Seismological Laboratory currently estimates seismic moment tensors of events automatically within 6-9 minutes of their occurrence. The line source and planar fault inversions required 4.2 and 5 minutes respectively. It is therefore feasible that finite source information may be obtained within 15-20 minutes after the occurrence of an earthquake, and shakemaps obtained by integration of derived fault slip could be available within 30 minutes. Regional permanent networks such as BDSN and TERRAscope, the proposed ANSS, and the permanent station component of USArray provide the necessary data for implementation this method. Near-fault ground motion estimated as described above may be the only viable approach in areas where it is not practical to deploy large numbers of strong motion instruments.

For further reading:

Wald, D. J., Quitoriano, V., Heaton, T.H. Kanamori, H., Scrivner, C.W., and Worden, C.B., TriNet "ShakeMaps": Rapid generation of instrumental ground motion and intensity maps for earthquakes in southern California, *Earthquake Spectra*, **15**, 557-564, 1999.

Kaverina, A., Dreger, D., and Antolik, M.,Toward automating finite fault slip inversions for regional events, *EOS*, **78**, p F45, 1997.

Dreger, D. S., and Kaverina, A., Seismic remote sensing for the earthquake source process and near-source strong shaking: A case study of the October 16, 1999 Hector Mine earthquake, submitted to *Geophys. Res. Lett*, 2000.

Urban Seismic Arrays

Douglas Dreger, University of California, Berkeley
Alan Lindh, US Geological Survey

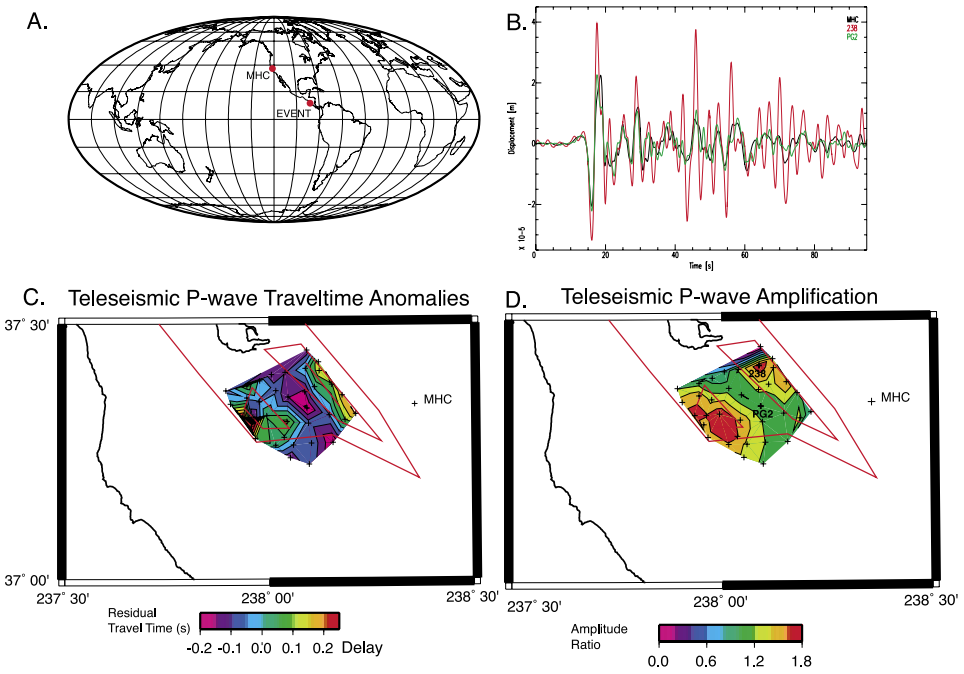

(A) Map showing the location of a M6.7 Central America earthquake and the MHC reference station. (B) Vertical component P- waveforms (0.1 to 1.0 Hz) are compared for a deep basin site (red), a shallow basin site (green), and the reference broadband station MHC (black). Note the basin generated coda, which lasts 60s at the deep basin site. (C) Traveltime delays relative to the reference site. Inner red line shows the location of the basin at 1 km depth, and the outer red line shows the edge of the basin at the surface. (D) Amplification of the first-arriving P-wave packet relative to the reference site.

During the summer of 1998 a forty-station network of three-component, short-period instruments were deployed in the Santa Clara Valley. The joint USGS/UCB/IRIS-PASSCAL experiment called the Santa Clara Valley Seismic Experiment was conducted to obtain seismic data in the heavily populated, deep sedimentary basins of the San Jose, California region. The instruments were deployed for a period of six months, and they recorded numerous local and regional events including the August 12, 1998 M5.1 San Juan Bautista earthquake. Data from this event and several other smaller events have been used to investigate the amplification of seismic waves in the Santa Clara Valley, and to constrain the velocity structure of the basins be means of finite difference modeling (e.g., Stidham, 1999; Stidham et al., 1999a). The SCVSE also recorded numerous teleseisms. Eight deep focus events produced well-recorded P-waveforms across the array. Travel time delays and relative amplification has been observed in this data set (Figure). For example, a Mw6.7 event located in Central America (Figure A) produced high quality observations at all of the stations. Figure 1b compares the vertical component velocity seismograms (0.1 to 1.0 Hz) recorded at a site with low amplification (green) and high amplification (red). The black trace compares a hard rock recording from a nearby BDSN broadband instrument (MHC). The input signal at the base of the crust is the same for all of the stations and the differences in the records are due to crustal structure. It is remarkable that there are considerable differences in amplitude of the first arriving P-wave at the two basin sites, and that the relative amplification observed across the array is seen to correlate well with the locations of the deep sedimentary basins (Figure D). A comparison of the deep basin site (red) with either MHC or the low amplification site (green) reveals that there is considerable basin-generated signal in the P-coda of the deep basin record, which is likely due to P to S mode conversions along the bottom surface of the 3D basin structure. We are presently using these data and the recordings of the local and regional recorded earthquakes to model 3D earth structure using an elastic finite difference methodology (e.g., Stidham et al., 1999b). Data from the SCVSE are providing basic information that can be used to determine 3D velocity structure, seismic wave amplification, and the nature of basin generated waves. The best strong motion data set to date in the region is that of the 1989 Loma Prieta earthquake, which had only four stations located over the basins of Santa Clara Valley and ironically were not located over the deepest parts of the basins. From January through July 2000 a similar deployment of short-period, and broadband instruments across the Oakland-San Francisco corridor has been initiated to obtain the needed data in the most heavily populated area of the San Francisco Bay Area.

For further reading:

Stidham, C. W., Three-dimensional crustal structure influences on wave propagation and generation of strong ground motion in the greater San Francisco Bay Area, Ph.D. Thesis, University of California, Berkeley, pp 316, 1999.

Stidham, C. W., Sansorney, C., Dreger, D., Characteristics of San Francisco Bay Area strong shaking hazard since the 1989 Loma Prieta earthquake, *EOS*, **80**, F40, 1999a.

Stidham, C. W., Antolik, M., Dreger, D., Larsen, S., Romanowicz. B., Three-dimensional structure influences on the strong-motion wavefield of the 1989 Loma Prieta earthquake, *Bull. Seism. Soc. Am.*, **89**, 1184-1202, 1999b.

Near-Surface Attenuation and Site Effects from Deep Borehole Recordings

Rachel Abercrombie, University of Southern California

IRIS PASSCAL dataloggers were used to record earthquakes from some of the deepest seismometers in the USA. Seismometers were installed at depths of 0, 0.3, 1.5, 2.5 and 2.9 km in the Cajon Pass borehole, southern California. I used seismograms recorded from local earthquakes to investigate source processes (Abercrombie, 1995) and also the effect of the near-surface rocks on seismic waves (Abercrombie, 1997). Near-surface and site effects are important in seismic hazard studies as they can cause large amplification and attenuation of seismic waves. Previous studies of site response have either had to compare a number of surface recordings, or else use shallower borehole recordings where the surface reflection interferes with the up-going wave, and the deepest instrument is not itself deep enough to be uncontaminated by near-surface effects. The Cajon Pass borehole penetrates 500 m of Miocene sandstone and then crystalline, granitic basement. The deepest seismometers are thus in bedrock, well beneath the near-surface layers. The distortion suffered by seismic waves travelling through the near-surface rocks can clearly be seen in the figure. Notice how simple and high frequency the recordings are at the 2.9 km instrument. As the waves travel shallower, they lose high-frequency energy and become more scattered. Also as these shallower instruments are further from the earthquake source, the time delay between the P and S arrivals is longer. The wellhead seismometer is on sediments, and the waves are amplified, of longer duration, and of lower frequency than the deepest recordings. The amplification at 1 Hz is about a factor of ten. The granite site was on basement rock about 1 km from the wellhead. Waves travelling through granite are less amplified and distorted than those travelling through sediments. Significant attenuation is observed at this site, however. Analysis of seventeen earthquakes using spectral ratio methods found that attenuation increases rapidly towards the surface, with the corresponding Q values decreasing from about 1000 at > 3 km to ~100 between 1 and 3 km, and only ~20 in the upper 300 m. The low Q values at very shallow depths appear to be independent of the rock type, although the amplification varies significantly.

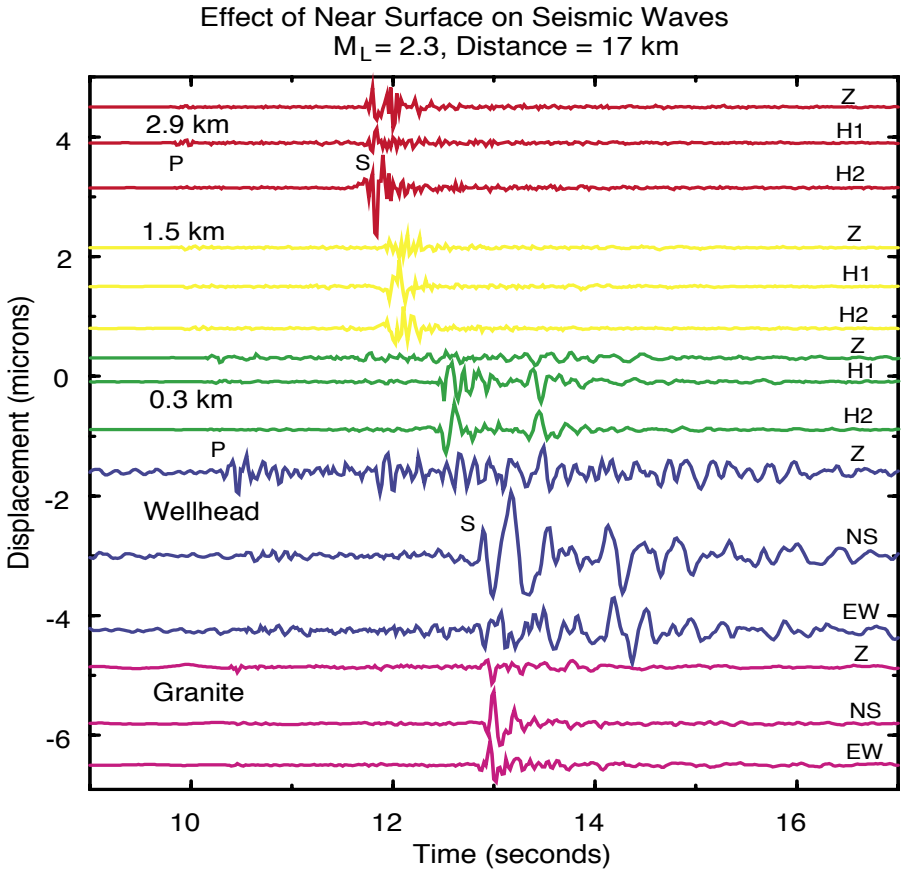

For further reading:

Abercrombie, R. E., Earthquake source scaling relationships from -1 to 5 ML, using seismograms recorded at 2.5 km depth, *J. Geophys. Res.*, **100**,
Abercrombie, R. E., Near surface attenuation and site effects from comparison of surface and deep borehole recordings, *Bull. Seism. Soc. Am.*, **87**, 731-744, 1997.

Joint Collection and Interpretation of Seismic Refraction and Surface Wave Data

Diane Doser, Deren Yuan, and Jaime Hincaip, University of Texas at El Paso

We are simultaneously recording surface waves and refracted compressional waves on the "Texan" seismographs and standard 24-channel recording units with the goal of developing new methods to characterize site variability in the shallow (<10 m) subsurface. The refracted arrivals are used to constrain P-wave velocity structure and depth to interfaces, while the surface waves provide shear velocity profiles and the ability to detect low velocity zones. Our study area comprises two sites along the Rio Grande, one "simple" site of medium to coarse grained channel sands, and one more complex site consisting of interfingered flood plain and crevasse splay deposits. We have also examined optimum sources, geophone frequencies, and recording parameters for the simultaneous collection scheme, and the use of other geological/ geophysical constraints to help speed the interpretation process. Our results suggest the technique will be an important new tool for geotechnical and environmental studies.

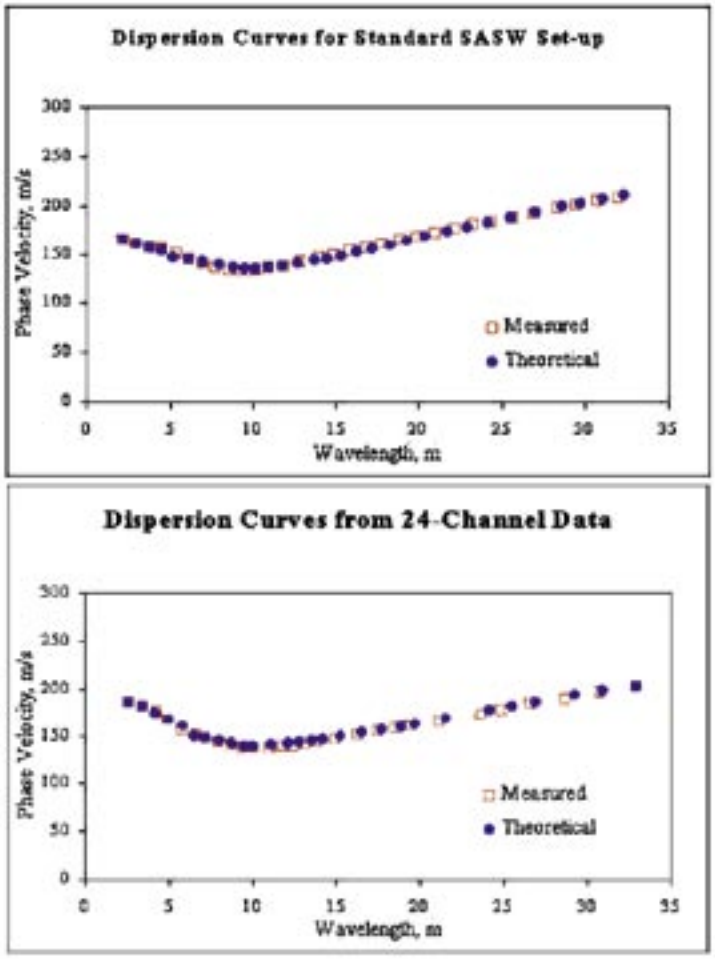

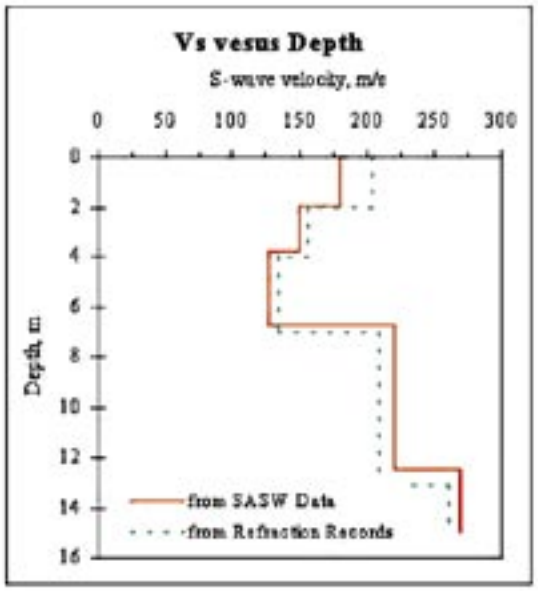

Dispersion curves (left) and shear wave velocity versus depth (above) obtained from 24-channel refraction unit and standard SASW (spectral analysis of surface waves) set up at the same site.

High Resolution Seismic Imaging at a Groundwater Contamination Site

Diana Dana, Alan Levander, Igor Morozov, Colin Zelt, Kidane Araya,William Symes, Rice University

In August 1998 Rice University acquired three high-resolution seismic profiles at a groundwater contamination site at Hill Air Force Base, Utah. The site is contaminated by a dense non-aqueous phase liquid (DNAPL) solvent that resides at the base of a shallow (<15m) aquifer consisting of Quaternary gravels, sands, and silty clays. The seismic imaging problem is to map out variations in the depth to a clay aquiclude at the base of the aquifer. The DNAPL contaminant is concentrated in a paleo-channel cut in the clay aquiclude. The buried streambed channels groundwater flow and served as a trap for the DNAPLs. Groundwater remediation efforts based on subsurface characterization derived from the 400 wells and cone penetrometer measurements at the remediation site had failed to reduce the pollutant to the desired levels due to irregularities in the paleo-channel.

Seismic data were aquired using a 60 channel IRIS Geometrics and a 60 channel Rice Bison portable seismograph. Geophones were spaced at 30cm intervals along each profile. We tested three sources: an 8 gauge shotgun, a 22 caliber rifle, and an accelerated weight drop. The 22 caliber rifle produced the broadest bandwidth pulse (60-400 Hz) and was easiest to use.

Pre-stack depth migration and depth focusing analysis produced very clear images of the channel on all three seismic lines, providing a robust estimate of channel morphology that was in good agreement with well data from the remediation site. The seismic data confirmed that the channel morphology changes rapidly over very short distances. The three 2-D profiles provided the necessary tests for design of a 3-D survey to be conducted in July 2000.

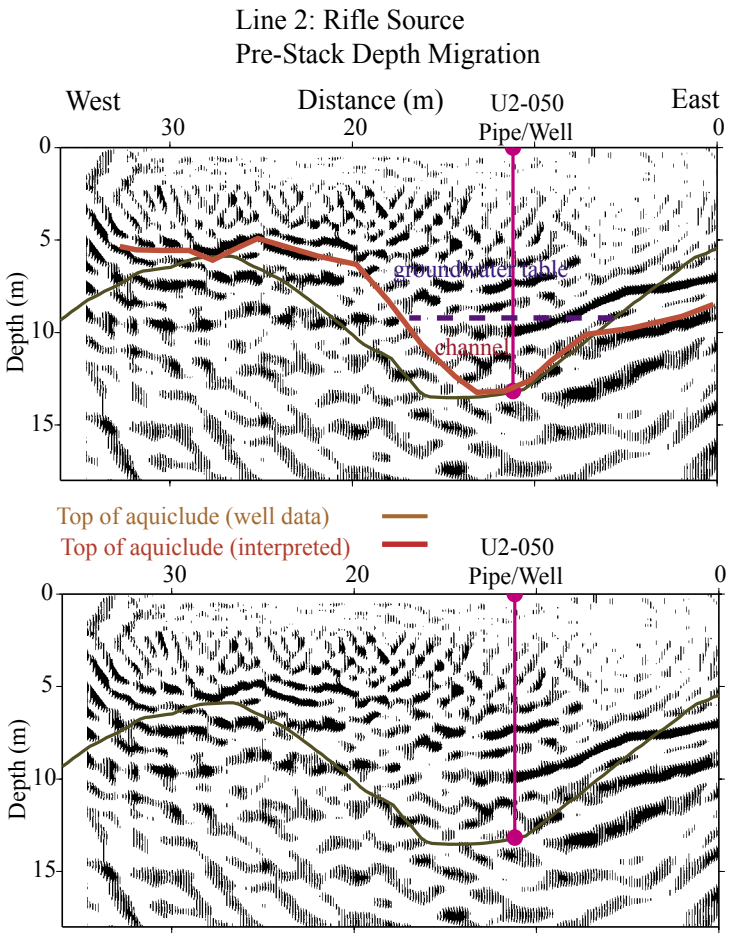

Interpreted and uninterpreted seismic sections of Line 2 at Hill AFB. The line is shown at 1:1 scale. The solid red line is our interpretation of the shape of the paleochannel. The dashed line is the estimate of channel morphology interpolated from well data. The seismic interpretation differs from the interpolated well data by meters in places.

High-Resolution Seismic Reflection Images of the San Bernardino Basin, California

William Stephenson, Robert Williams, and Jack Odum, US Geological Survey

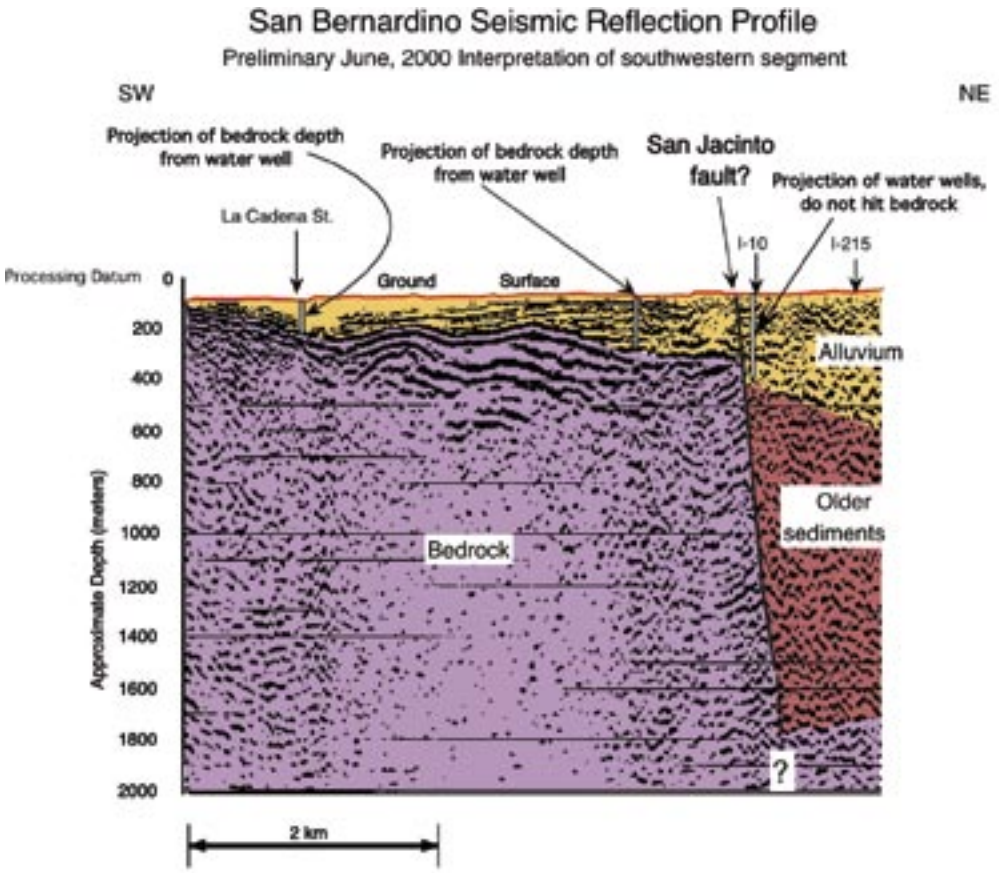

Southwestern segment of 14-km-long seismic reflection profile acquired through urbanized San Bernardino Valley

An IRIS RX-60 seismograph was used in a master-slave configuration with a second RX-60 seismograph to acquire 120 channels of high-resolution seismic reflection data across the southern 3/4 of the San Bernardino Valley, California. Approximately 14 km of these data were acquired northeast to southwest through the city of San Bernardino, from Perris Hill to La Loma Hills, using a 5 m CMP interval. We used a mini-vibe vibrational seismic source (manufactured by Industrial Vehicles, Incorporated) in this experiment with the IRIS seismograph because it was more portable than conventional industry vibroseis trucks and was capable of sweeping to frequencies as high as 500 Hz. Preliminary analysis suggests these data yield new evidence for the presence of the Loma Linda fault crossing through urban areas of the San Bernardino Valley, as well as other previously undetected faults within the valley northeast of the San Jacinto fault. The data also apparently image the top of the basement complex (mostly gneiss, granite, and schist) across 90 percent of the profile length, and suggest basement is at least as deep as 1.5 km near the San Jacinto fault. In addition to delineating young faults, these data will help constrain: (1) finite-difference modeling of earthquake ground motions in the basin, (2) groundwater modeling studies, and (3) gravity modeling of this seismically active region adjacent to the San Andreas fault.

In addition to the seismic reflection investigation, the IRIS RX-60 seismograph was also used in an engineering site response study around a 5-story office building in San Bernardino. The instrument recorded an S-wave refraction profile (about 200 m penetration) using the mini-vibe as an S-wave source. Additionally, ground motions transmitted to and from this building were recorded on the IRIS instrument simultaneously with portable seismometers installed at several key locations within the building. No preliminary results are currently available from either of these data sets.

PASSCAL High-Resolution Active-Source Recording: Evidence for Seismogenic Low-Angle Normal Faulting

Roy A. Johnson, University of Arizona

Although seismic reflection techniques have enjoyed very wide and enormously successful application in petroleum exploration and development, use of high-resolution near-surface seismic reflection techniques in detailed structural, environmental and groundwater analyses have been relatively recent applications. Moreover, systematic application of 2-D profiling, vertical seismic profiling (VSP), 3-component acquisition and 3-D data analysis to the near surface has been rare, but these techniques provide the best opportunity to characterize relevant velocity and density variations and unequivocally link these parameters directly to subsurface geology and groundwater saturation. PASSCAL multichannel systems have opened new opportunities for researchers and have made such analyses possible. Adding immeasurably to their impact, these systems also are used frequently in demonstrations and exercises associated with university and even K-12 classes. Some applications are extremely small-scale and of very short duration; others are more systematic, cover relatively large areas, and may involve significant field efforts. In most, however, important data are collected and students are exposed to modern high-resolution seismic techniques that otherwise would be relegated to a few arcane paragraphs in a textbook.

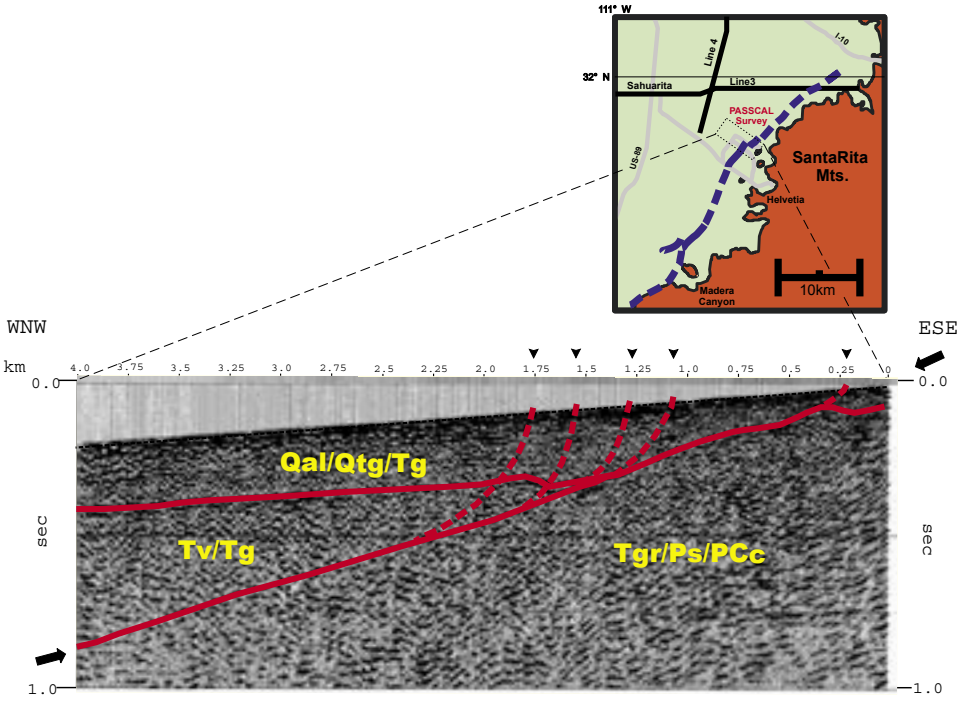

Generalized interpretation of near-surface reflection data across a series of fault scarps linked to slip on a low-angle normal fault in SE Arizona.

As one example, a relatively recent, student-staffed "near-surface" PASSCAL imaging experiment developed new data that addresses the problem of whether low-angle normal faults can cause large-magnitude (surface-rupturing) earthquakes. Old industry seismic reflection data that cross the trend of a late Quaternary, basin-bounding fault scarp in southeastern Arizona recorded reflections from an apparent low-angle (~15-20°) fault plane. The fault plane can be traced from a depth of at least 6 km to fairly near the surface, but data quality prevented an unequivocal tie to the scarps. However, projection of the fault plane reflection appears to be coincident with the surface trace of the late Quaternary fault scarps within ~300 m of the surface. These relationships suggest a genetic connection between the surface scarps and the low-angle fault plane imaged on the reflection seismic data.

To evaluate the geometry of the fault zone in the shallow subsurface and along strike, two sixty-channel PASSCAL recording systems were used to acquire densely sampled 3-D subsurface data above two mapped fault scarps, and additional high-resolution 2-D data were acquired along a 4.5-km profile using a vibrator source. The new reflection data acquired during the PASSCAL experiment show the basin-bounding fault plane to have a dip of about 15 degrees in consolidated sedimentary and crystalline rocks. Where the fault reaches unconsolidated alluvial-fan deposits in the upper 100 m, it forms a wide zone of apparently steeply dipping splays. Although subsurface relations suggest that the basin-bounding fault has been active for 10 Ma or more, the late Quaternary large-magnitude scarp-forming events indeed appear directly associated with low-angle slip on the fault.

Possible Cause for an Improbable Earthquake: The 1997, Mw 4.9 Southern Alabama Earthquake and Hydrocarbon Recovery

Joan Gomberg, University of Memphis
Lorraine Wolf, Auburn University

On October 24, 1997, an unprecedented Mw 4.9 earthquake shook southern Alabama. This event, preceded on May 4, 1997, by a magnitude 3.1 foreshock and followed by >17 aftershocks in the subsequent 3 months, occurred in the nearly aseismic Gulf Coastal Plain. The main shock normal fault mechanism (Chang et al., 1998) is consistent with a regional north-south extensional stress field (Nunn, 1985). A system of Miocene and older faults in the epicentral region is associated with the development of major salt deposits and hydrocarbon traps (Tew et al., 1993; Montgomery et al., 1997).

Our study explores circumstantial and physical evidence relevant to the hypothesis that the 1997 Mw 4.9, southern Alabama earthquake was causally related to hydrocarbon recovery. Hydrocarbon recovery activities are reported to the Alabama State Oil and Gas Board as monthly volumes of oil, gas, and water extracted, and as monthly average injection wellhead pressures and volumes of water and brine.

The characteristics of the earthquakes examined in the study were derived from main shock seismograms recorded at regional distances (Chang et al., 1998), aftershock seismograms recorded on portable seismographs deployed in the epicentral region from October 25, 1997, to January 15, 1998, and intensity surveys. Epicenters of this earthquake and its aftershocks were located within a few kilometers of active oil and gas extraction wells and two pressurized injection wells. Main shock and aftershock focal depths (2-6 km) are within a few kilometers of the injection and withdrawal depths. Although the normal fault main shock mechanism is consistent with reactivation of preexisting faults in the regional tectonic stress field, a purely tectonic origin is difficult to reconcile with strain accumulation at geologic rates in shallow sedimentary units above the basement, where M > 3 aftershocks and possibly the Mw 4.9 main shock were located. A tectonic origin also implies an uncommon frequency-magnitude relationship, given the paucity of smaller earthquakes prior to October 24, 1997. Despite this evidence, however, no clear temporal correlation between hydrocarbon recovery and the 1997 sequence has been established.

More definitive constraints on the causes of this unusual earthquake sequence will require additional detail about the local material properties and stresses, and modeling of the media response to recovery activities. However, the normal fault mechanism, extensional regional stress regime, fluid and gas volumetric data, and the previous work of others provide constraints. If injection is responsible, either by raising the pore pressure or by elastic volumetric straining, it must act very locally because extracted volumes exceed those injected by orders of magnitude. If extraction is responsible, the normal fault source may be consistent with models that account for poroelastic stresses.

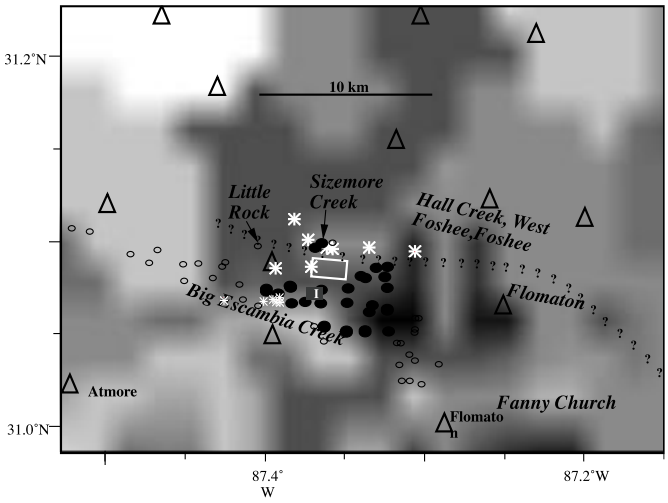

Figure 2

Map of epicentral region showing spatial relationship between earthquake epicenters and wells. Aftershock study was conducted using portable seismographs supplied from the USGS and the IRIS RAMP program. Large white asterisks = aftershocks located with data from three or more stations; small white asterisks = aftershocks located with data from only two stations and fixed surface depth; rectangle = projection of approximate main shock rupture area; ovals = locations of producing wells; square with I = two injection wells within ~5 km of probable main shock; triangles = portable seismic stations installed after main shock. Question marks indicate probable location of main fault in region (part of Miocene Pollard-Foshee fault system). Shaded background shows smoothed, interpolated intensity estimates (black = modified Mercalli intensity [MMI] VIII, white = MMI III; modified from data compiled by D. Raymond, personal comm., 1997). Although absolute intensity values may be somewhat uncertain, they reliably indicate relative severity of earthquake effects. Main shock location, although uncertain by several kilometers, is consistent with intensity data, aftershocks, and location of major preexisting fault system. Italicized names denote active production fields in region. Atmore and Flomaton are towns.

For further reading:

Chang, T. M., Ammon, C. J., and Herrmann, R.B., Faulting parameters of the October 24, 1997 southern Alabama earthquake: *Seis Res Lett*, **69**, 175-176, 1998.

Montgomery, S.L., Baria, L. R., and Handford, C. R., Frisco City sandstone: Upper Jurassic play in southern Alabama, *AAPG Bull*, **81**, 1595-1611, 1997.

Nunn, J. A., State of stress in the northern Gulf Coast, *Geology*, **13**, 429-432, 1985.

Tew, B.H., Mink, R. M., Mancini, E. A., Mann, S. D. and Kopaska-Merkel, D. C., Regional geologic framework and petroleum geology of the Smackover formation, Alabama and Panhandle Florida coastal waters area and adjacent federal waters area, *Geol Surv of Alabama Bull,* **154**, 60 p, 1993.

High Resolution Depth and Source Mechanism Estimation Using a Combination of Regional and Teleseismic data

Peter Goldstein, Doug Dodge, Gene Ichinose, Arthur Rodgers, Lawrence Livermore National Laboratory

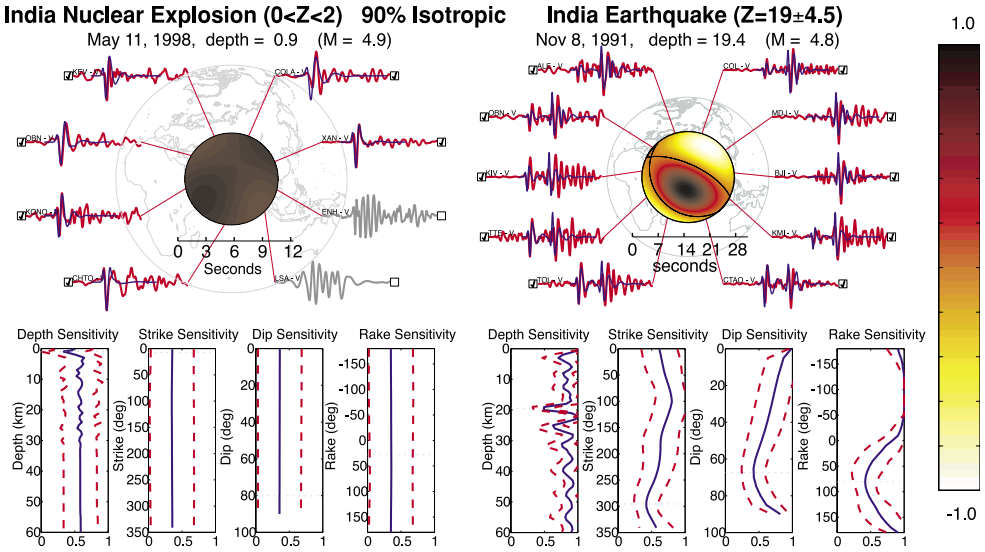

We are developing tools and techniques for regional calibration and ground truth source parameter estimation. We are combining regional and teleseismic techniques for better constraints on source and structure. Far-regional and teleseismic data (above) provide high-resolution estimates of depth. Regional data help constrain the mechanism and structure.

We present an overview of methods for estimating depth and mechanism and summarize our recent efforts to use waveform modeling based depth and mechanism estimates for special event analysis, event screening and regional calibration. We summarize the strengths and limitations of a variety of techniques and describe our on-going efforts to develop accurate high-resolution depth and mechanism estimates by extending existing techniques and integrating methods that use different types of seismic data.

We illustrate the advantage of combining different techniques for estimating depth and mechanism by combining broadband (0-2Hz) far-regional and to teleseismic body waveform modeling estimates of depth and mechanism with those obtained using intermediate to long period estimates based on regional data. We show that the broadband body waves provide strong constraints on source depth and that the broadband body waves and the intermediate to long period regional waves can constrain complementary aspects of the source mechanism.

We describe a new tool that we have developed and validated that provides fast and accurate estimates of depth and mechanism based on far-regional to teleseismic (20^0 to 90^0) P-waveform modeling. Significant features of this tool include its ability to provide accurate, high-resolution depth estimates ($\delta z<2$km) using a small number of stations. It also works well over a large range of depths including events that are very shallow ($z<1$km). It is applicable over a broad band of frequencies ($0 \le f \le 2$ Hz) and magnitudes ($mb \ge 4.5$) and provides constraints on event mechanism including isotropic contributions. It also provides estimates of random and model errors and can be used to test hypotheses and investigate sensitivity to and trade-off between model parameters.

We illustrate the utility of this technique for regional calibration, special event analysis, and event screening by comparing estimated depths and mechanisms of events in the Middle East and North Africa with those of the NEIC and by comparing our depth and mechanism estimates for selected events such as the May 11, 1998 India nuclear explosion and a November 8, 1991 earthquake that occurred in the same region.

This work was performed under the auspices of the U.S. Department of Energy by Lawrence Livermore National Laboratory under contract No. W-7405-Eng-48 for the Office of Research and Development, NN-20, within the Office of NonProliferation and National Security, NN-1.

The May 11 and 13, 1998 India Nuclear Tests

Terry C. Wallace, University of Arizona
Mark Tinker, QTSI, Air Force Technical Applications Center

On May 11, 1998 India conducted an underground nuclear test at their Pokharan test site in northwestern India. At a press conference on May 17 the Indian government gave details of the test: three devices detonated simultaneously with a combined yield of approximately 55 kt. The Indian government announced two further tests conducted on May 13. The announced yield of these tests were subkiloton (0.6 and 0.2 kt). The Indian tests were well recorded on the GSN, and the open data provide an excellent resource to independently assess and analyze the tests.

The map (see figure) shows the locations determined by the USGS (the "dot" and corresponding formal error ellipse) and the pIDC (the REB location and corresponding error ellipse). Previous investigations of satellite photos by Gupta and Pabian (1996) identified test preparations (star), which is the presumed location of the May 11 explosions.

We used the seismic waveforms from 32 GSN stations and 19 PASSCAL instruments to calculate a yield for the explosions. We determined yield using mb, Ms, Mblg and spectral signatures. All the methods gave a yield of between 10 and 15 kt; the best estimate is 11.8 ± 2.7 kt. This is a factor of four smaller than that announced by the Indian government casting serious doubts on the offical pronouncements. The seismograms (see figure) show a comparison of the May 11 test and the window of time reported for the May 13 test at the GSN station NIL (Nilore). NIL is located 740 km north of the test and is the closest open station to Pokharan. There is no seismic evidence that the May 13 test did occur. We searched the NIL record with several different techniques, but failed to detect any signal. The null result can be used to place some constraints on the size of the May 13 explosion: it must be less than 50 tons.

Open seismic stations provide an extremely important, independent monitoring resource for underground testing.

For further reading:

Gupta, V. and Pabian, F., Investigating the allegations of Indian nuclear test preparations in the Rajasthan Desert, 1996.

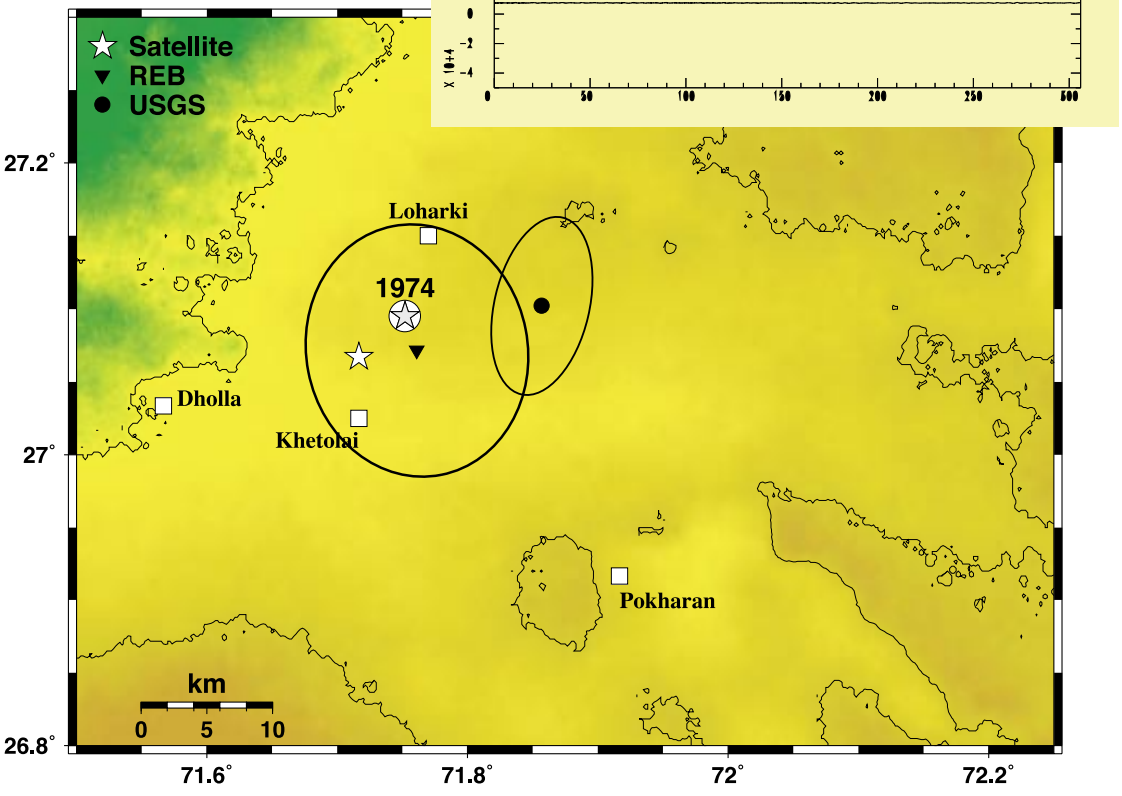

Location of the May 28, 1998 Pakistan Nuclear Test

Terry C. Wallace and Todd Bredbeck, University of Arizona

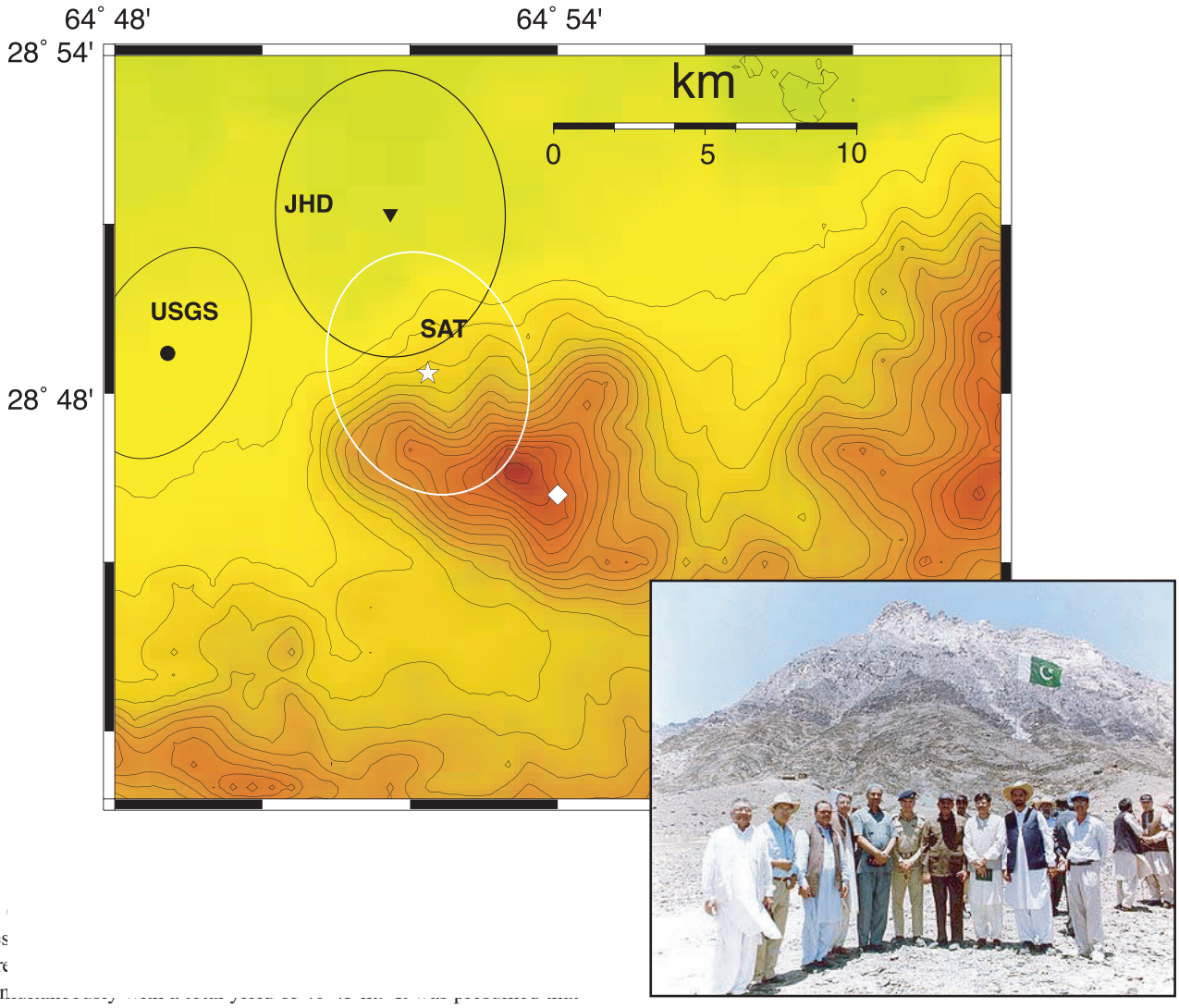

res
pr
si
the tests were conducted in a mountainous region in the western part of the country call the Ras Koh Range. This is the same place that Pakistan was reported to have conducted a "cold" test (no nuclear materials) in 1986.

The May 28 event was well recorded by the GSN. Unlike the Indian test site, the Ras Koh region is moderately seismically active. We used the arrival times of two nearby earthquakes (December 4, 1997 and January 5, 1998) along with the May 28 arrivals to perform a joint hypocenter determination (JHD). In the figure, the USGS location and error ellipse are shown along with the JHD location.

During the Pakistan press conference there were a series of photos shown including the picture of the testing team shown above. We infer that the tall mountain peak in the background is identical to the region of high topography shown on the map. Using the peak as a loose ground truth constraint we redid the JHD analysis and derived the location shown with the star. This location is within 6 km of the exact location later released by Pakistan (shown with the diamond on the map).

Open seismic data can be used with other information such as geologic and images to provide very accurate monitoring assessments.

Applying KNET Real-Time Regional Network Data for Verification Purposes

Jennifer A. Eakins, Scripps Institution of Oceanography
Frank L. Vernon, Scripps Institution of Oceanography
Terry C. Wallace, University of Arizona

In September of 1991, the 10 station Kyrgyz broadband seismic network (KNET) became operational. KNET is a cooperative project sponsored by IRIS and the government of Kyrgyzstan. It is operated by Kyrgyz Institute of Seismology (KIS) and the Institute of High Temperature Physics of the Russian Academy of Sciences (IVTAN).

The applicability of KNET for verification purposes became readily apparent in May 1998 after India and Pakistan performed their first underground nuclear tests. For the tests conducted by Pakistan, KNET returned the data in real-time giving a location within a few 10s of seconds after triggering. KNET was the closest operational broadband sensor to record in real-time as the GSN station NIL was disabled during the test. The second test performed by Pakistan was not detected by KNET due to a large earthquake that occurred in Afghanistan approximately 30 minutes prior to the nuclear detonation. On June 4, 2000 an event was located within 35 km of the test site in Pakistan. Real-time access to the waveforms from KNET allowed an analyst to confirm that an earthquake, not an explosion, had occurred.

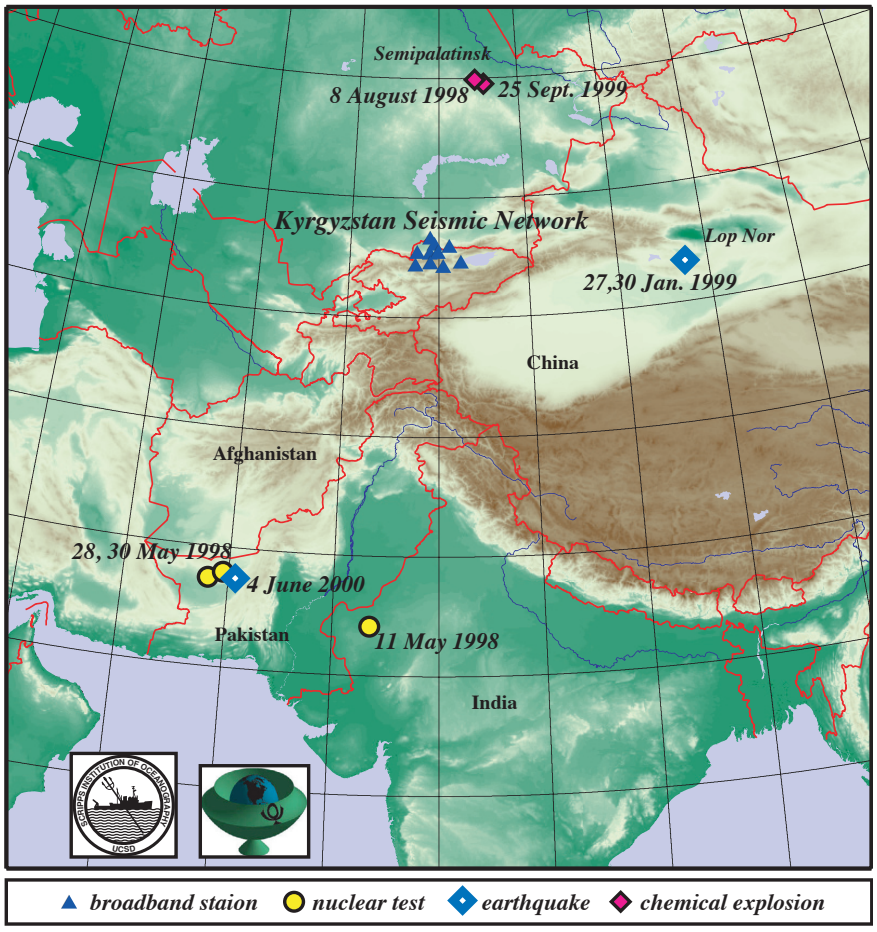

KNET is also ideally situated to record seismic events at the former nuclear test site at Semipalatinsk, Kazakstan and Lop Nor, China. The tunnels at Semipalatinsk are being destroyed by chemical explosions as part of the decomissioning effort. Two of those explosions have been recorded by KNET. At Lop Nor, in January 1999, two earthquakes occurred within the test site. Waveforms from KNET were essential in discriminating between an explosion and earthquake for these events. For each event discussed, all waveforms and source parameters were received from Central Asia within minutes and were made available to interested parties to allow real-time interpretation and analysis for event discrimination.

KNET and the Semipalatinsk and Lop Nor Test Sites

Terry Wallace, University of Arizona
Frank Vernon, Scripps Institution of Oceanography, University of California, San Diego
Jennifer Eakins, Scripps Institution of Oceanography, University of California, San Diego

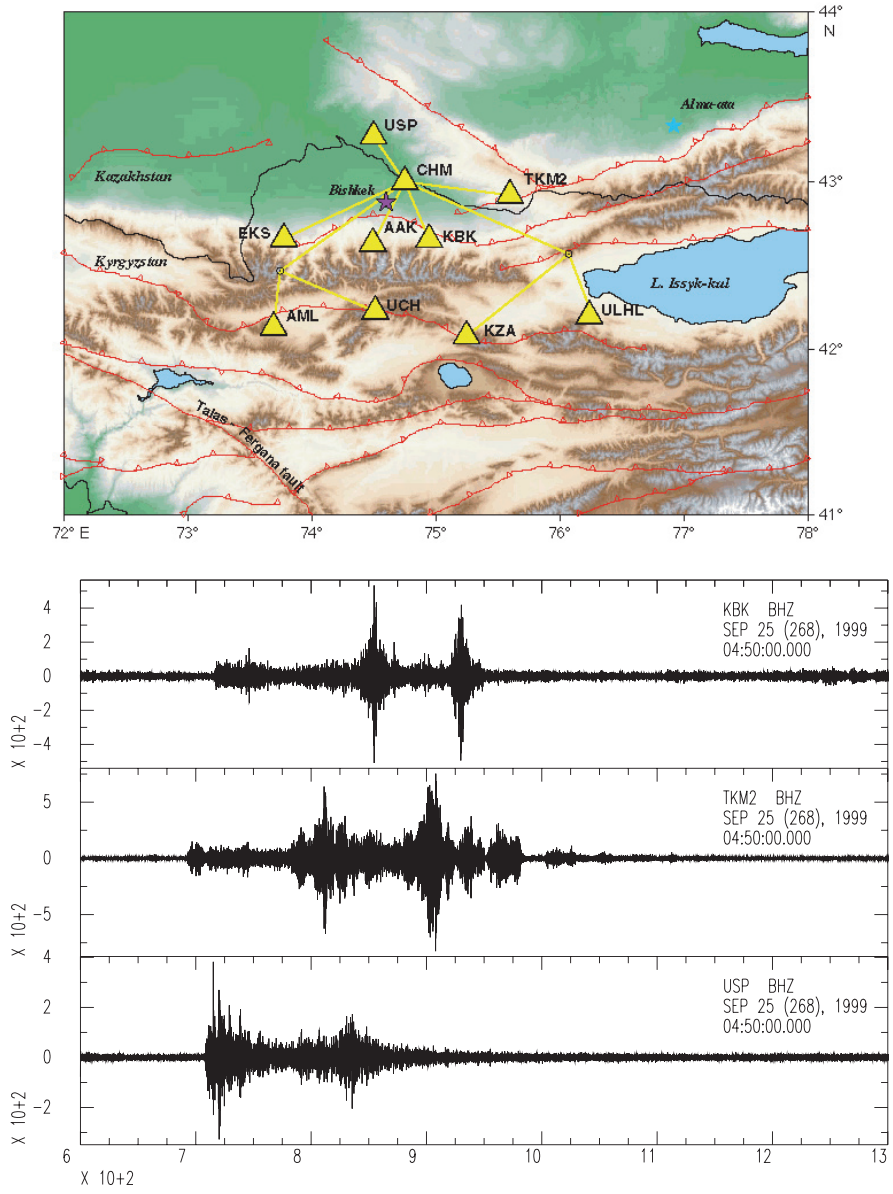

KNET, a broadband regional network installed by the IRIS JSP program, is situated at regional distances from Lop Nor (the PRC nuclear test site) and Semipalatinsk (former Soviet nuclear test site). The figure shows a series of seismograms from KNET stations for a 25 ton chemical explosion detonated at Semipalatinsk in September, 1999. The explosion was part of series of tests designed to test the effect of variations in the depth of burial on the character of seismic waves.

The waveforms can be used to measure the detection capability of KNET for monitoring Semipalatinsk. Individual stations in KNET can detect Semipalatinsk events with magnitudes of 2.9 or larger, however, it is possible to use KNET as a very wide aperture to spotlight events from this site. When this is done, the detection capability is reduced to 2.6. Similar analysis for Lop Nor gives an detection capability of 2.9.

Open seismic stations can provide a very important monitoring resource. At present, KNET is the closest group of seismic stations available in near-realtime to several regions of monitoring interest.

Complete Regional Waveform Modeling for Source and Structure: A Source Example Using the January 30, 2000 Mine Collapse in Wyoming

William R. Walter, Jennifer Swenson, William Foxall, Paul Vincent, Arthur J. Rodgers and Joydeep Bhattacharyya
Lawrence Livermore National Laboratory

Complete regional waveform modeling seeks to match synthetic seismograms to data in order to elucidate information about both the source of the seismic waves and the structure they propagate through. At intermediate periods (10-100 s) regional waveforms can usually be well matched using 1-D reflectivity synthetic seismograms. The normal procedure is to use larger, well-constrained sources to determine the structure (e.g., Rodgers et al., 1999, Bhattacharyya et al., 1999), then fix the structure to estimate the mechanisms of other sources. The advent of global and regional networks of easily accessible broadband seismometers greatly expands the regions where waveform modeling is effective, and lowers the magnitude threshold for determining source parameters using a few well-calibrated stations.

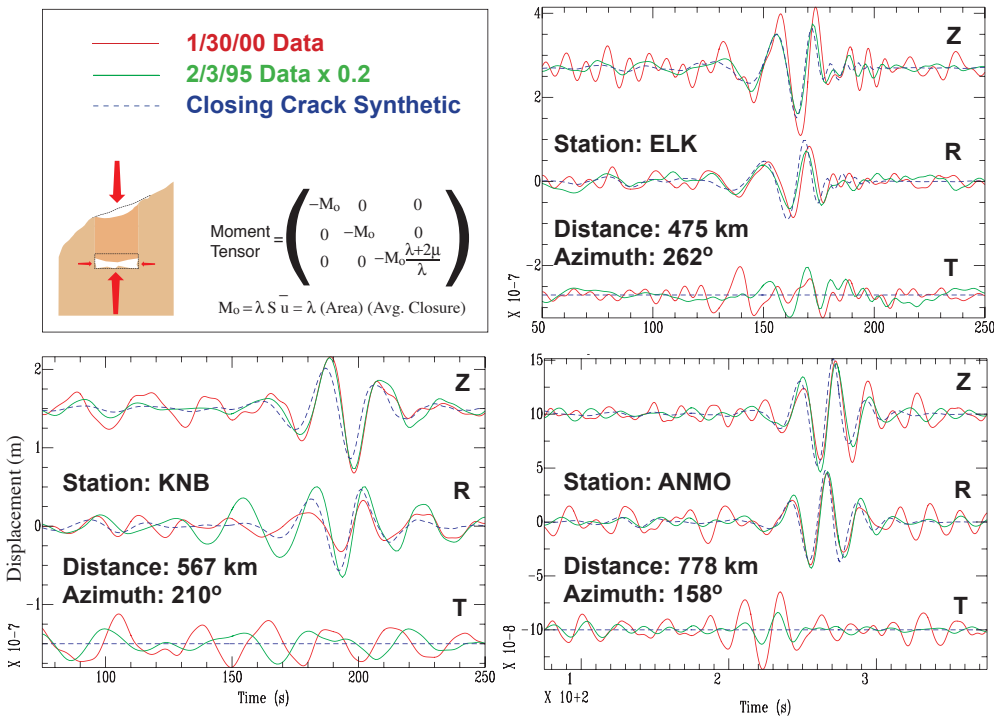

Here we show an example of waveform modeling the recent, January 30, 2000, mb 4.4 Wyoming mine collapse at the GSN station ANMO and the LLNL/USGS-NSN stations ELK and KNB. We have previously waveform modeled a larger mb 5.2 February 3, 1995 collapse from the same mine (Pechmann et al., 1995), so the paths are well calibrated. In the figure we compare the recent smaller event, the larger 1995 event which has been reducing in amplitude by a factor of 5, and synthetic seismograms for a closing crack model with a moment of 3.0 x 10^{15} N-m (Pechmann et al., 1995). Although the recent small event data is somewhat noisy, it is clear that there is good correlation between the new event, the previous collapse and our model synthetic waveform. If we assume the collapse height is similar to that in 1995, than we can estimate that the area of the new collapse is one-fifth the area of the 1995 event using just the seismic data. Preliminary indications from the mine appear to confirm this.

As was the case in 1995, the area involved in the recent event is also reflected in surface subsidence above the collapse zone. We are currently investigating the potential for using synthetic aperture radar interferometry (InSAR) to image this subsidence remotely to provide additional constraints on the underground failure source parameters. The combination of seismic modeling and InSAR has the potential to greatly improve our ability to remotely characterize unusual shallow seismic sources such as mine collapses.

For further reading:

Bhattacharyya, J., Sheehan, A.F., Tiampo K., and Rundle, J., Using a genetic algorithm to model broadband regional waveforms for crustal structure in the Western United States, *Bull. Seism. Soc. Am.*, **89**, 202-214, 1999.

Pechmann, J.C., Walter, W.R., Nava, S.J., and Arabasz, W.J., The February 3, 1995 ML 5.1 seismic event in the trona mining district of southwestern Wyoming, *Seism. Res. Lett.*, **66**, 25-34, 1995.

Rodgers, A., Walter, W.R., Zhang, Y., Mellors R., and Al-Amri, A.M.S., Lithospheric structure within the Arabian Peninsula from complete regional waveform modeling and surface wave group velocities, *J. Geo-*

Seismology as a Forensic Tool

Keith D. Koper and Terry C. Wallace, University of Arizona

As the number of permanently installed broadband seismometers continues to increase, it is becoming more common for ground motion from relatively small, non-earthquake sources to be recorded. Archives of continuous waveform data, such as those maintained by the IRIS DMC, allow such "exotic" source seismograms to be available even though the relevant time period is not associated with a specific earthquake. Examples of exotic sources include bolides, mine collapses, rockfalls, industrial explosions, and terrorist attacks. In the case of man-made exotic sources, the record of the source dynamics captured by seismic data can be useful to investigative organizations, to governmental agencies, and to insurance companies. Thus, the study of exotic sources is often motivated by the potential utility of seismology as a forensic tool.

There are numerous recent examples of forensic seismology. McCormack et al. (1999) analyzed seismic records of a plane crash to determine the precise time of impact and to conclude that the plane did not explode until it impacted the water. These facts aided the subsequent investigation by the Canadian Transportation Safety Board. Ichinose et al (1999) studied seismic records of a Nevada chemical plant explosion and determined the relative location of the two main pulses of seismic energy. Their results provided important corroboration of on-site analysis conducted by the U.S. Chemical Safety and Hazard Investigation Board. Recently we have studied seismic data (Figure) of the terrorist bombing of the U.S. Embassy in Nairobi, Kenya (Koper et al., 1999). These data helped constrain the precise time of the attack and the amount of explosive used, information that was of interest to F.B.I. investigators.

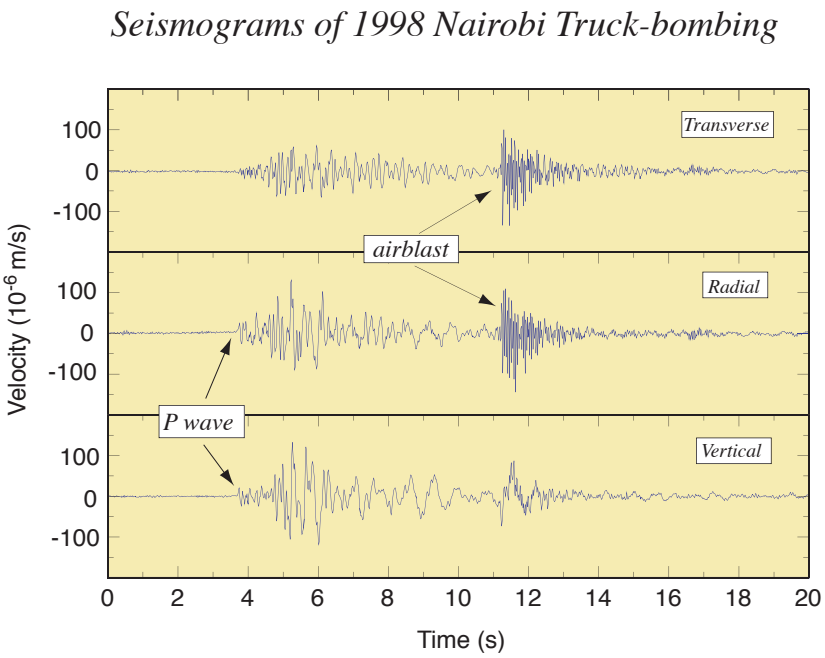

Velocity seismograms of the 7 August 1998 truck-bomb blast at the U.S.Embassy in Nairobi, Kenya. The station was located 3 km to the northwest of the blast.

The strongest yield constraint from the Nairobi data is provided by the airblast travel time. The shock wave nature of the airblast makes its arrival time a function of yield as well elastic atmospheric structure. Owing to the high frequency nature of the airblast pulse the arrival time can be measured with high precision. We determined the exact origin time of the blast using a waveform inversion technique, and converted the arrival time into a travel time. The explosive yield was then constrained using tables relating airblast characteristics to source properties for a reference chemical explosion. We are currently developing functional relations between seismic observables and source characteristics for chemical explosions.

For further reading:

Ichinose, G. A., Smith, K..D., and Anderson, J.G., Seismic analysis of the 7 January 1998 chemical plant explosion at Kean Canyon, Nevada, *Bull. Seismol. Soc. Am.*, **89**, 938-945, 1999.

Koper, K. D., Wallace, T.C., and Hollnack, D., Seismic analysis of the 7 August 1998 truck-bomb blast at the American Embassy in Nairobi, Kenya, *Seismol. Res. Lett.*, **70**, 512-521, 1999.

McCormack, D. A., Drysdale, J., and Bent, A.L., A seismological perspective on the crash of SwissAir Flight 111 near Halifax, Nova Scotia on 3 September 1998, (abstract), 11th annual IRIS Workshop, Fish Camp, CA, 1999.

Observing the Effects of Topography on Wave Propagation

Gary L. Pavlis and Christian Poppeliers, Indiana University

It has been known for decades that topography can significantly affect measurements of ground motion during a seismic event. Indeed, Barlow (1933) documented detectable variations in the intensity of shaking associated with topography almost seventy years ago. There is, however, a surprising lack of quality data on real wave interaction with topography. We know of no previous study which utilized a sufficient density of seismic stations to measure a spatially unbiased sample of the wavefield in the vicinity of a significant topographic feature. The reason that this is challenging is that the highest wavenumber feature created by topographic scattering (notably high frequency surface waves) can easily have wavelengths of only a few meters. With limited instrumentation available for measurements fixed arrays with station spacings of a few meters would be dismissed as a low priority. In fact, until the advent of PASSCAL, sufficient numbers of instruments to consider such an experiment simply did not exist.

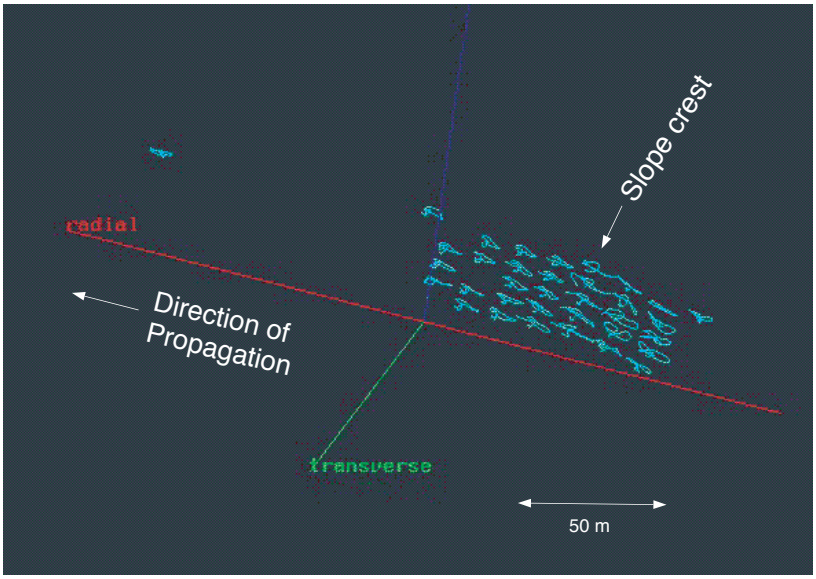

Particle motions of direct P wave showing topographic site effects. Blue figures are enlarged, three-dimensional paths of particle motion centered at the location of the corresponding station in space. The viewpoint is located above and parallel to the slope break line (approximately the transverse direction shown by the green line) across which the array was deployed. The slope break can be seen by the variations in elevation seen in the figure at the point marked. Note the approximate factor of two increase in amplitude at the slope break relative surrounding stations. We interpret this as a result of a site resonance associated with the slope.

In 1998 the Naval Surface Warfare Center, Crane Division, detonated a series of 20 explosions in a lake near Sullivan, Indiana, formed by an abandoned strip mine pit. We recorded these shots with 102 PASSCAL instruments equipped with 4.5 Hz, triaxial sensors. Sixty-three of the instruments were deployed in three linear profiles radiating from the shot point and the remaining instruments were deployed in a series of small aperture arrays. One of the arrays was deployed to study the effects of the major topographic discontinuity formed at the edge of the lake. That is, the edge of the lake on which this array was deployed had a near vertical underwater face from the water surface to a depth of approximately 25 m that was the highwall of the old strip mine. The top of the highwall had been tapered above the water surface to a slope of approximately 45 degrees to form an upward step in topography of approximately 10 m above the water. We deployed a grid array over this slope with a nominal spacing of 10 m between sensors. Using a three-dimensional particle motion visualization technique described by Repin and Pavlis (1997) we can observe remarkable details in the motion of the topographic slope induced by the explosions in the lake. A pulse we interpret as the direct P wave propagating through the low-velocity mining soil strikes the topographic slope polarized nearly horizontally and oriented approximately radially away from the slope face. The original animation cannot be captured completely here with the single static frame shown. The full visualization shows the incident wavefield induces motion on the stations at the lake shore (right side of figure) which can be observed propagating up the slope face. The stations above the lake shore lag behind this initial kick and then respond with a noticeable amplification of approximately a factor of two relative to stations an the lake shore. We quantified this further with spectral ratios computed from the array stations using the same approach as that described in a recent paper by Wilson and Pavlis (2000). The spectral ratio results suggest a strong site resonance at a frequency of approximately 8 Hz. The pattern of amplitude variations at this frequency indicate variations of a factor of two that occur over a scale length of less then 30 m. This is visually evident as well in the particle motion figure we show here. The only wave propagation mode with a velocity consist with this scale length is a high-frequency surface wave mode associated with the topographic slope break. This is loosely consistent with a number of numerical simulations of topography found in the literature that commonly show surface waves shed from topographic irregularities. These experimental data provide a useful reality test for anyone engaged in numerical modeling of wave propagation as this is the first experiment we know of that provides an unaliased record of ground motion effects induced by topography of this scale.

For further reading:

Barlow, N. Charles Darwin's Diary of the Voyage of H. M. S. Beagle, Cambridge Univ. Press, New York, 1933.

Repin, D.G. and Pavlis, G.L., Interactive three-dimensional visualization of seismic array data, *Computers and Geoscience*, **23**,1079-1092, 1997.

Wilson, D.C. and Pavlis, G.L., Near-surface site effects in crystalline bedrock: a comprehensive analysis of spectral amplitudes determined from a dense, three-component seismic array, *Earth Interactions*, **4**,4-002, (http://EarthInteractions.org/eij-bin/EntranceA), 2000.

Bringing Seismology into the Classroom

Christel B. Hennet, IRIS
Larry Braile, Purdue University

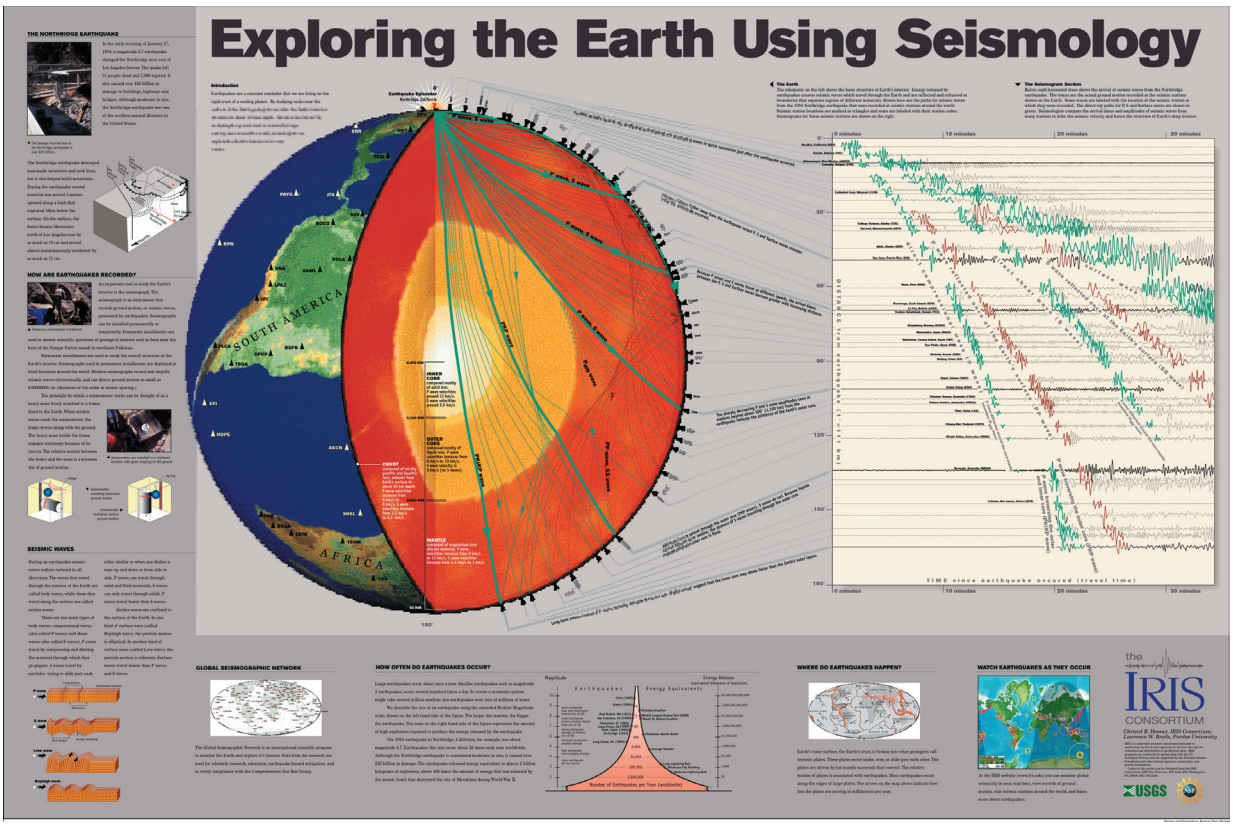

As part of our Education and Outreach Program, the IRIS Consortium has developed a poster to illustrate how seismology is used to explore the deep interior of our planet.

The poster consists of a high resolution schematic Earth cut open to reveal its basic structure, a seismogram section, and explanations of how we use seismology to infer the structure of the Earth's interior. The seismogram section shows traces of actual ground motion recorded during the 1994 Northridge earthquake. All major phases, such as P, S, PP, SS, PKP, PKIKP, and surface waves, are identified and highlighted. The schematic Earth shows the paths for all the rays identified on the seismogram section. Seismographic stations are marked at their angular distances from the epicenter, labelled, and visually linked to enhance the relationship between the individual ray paths, the locations at which the seismograms are recorded, and the composite seismogram section. The border of the poster includes descriptions of the Northridge earthquake, seismicity patterns, types of seismic waves, functions of a seismometer, and the Global Seismographic Network. Much of the information in the border of the poster is available as individual one-page handouts from IRIS. A one-pager of the main section of the poster is also available.

The IRIS E&O program is currently developing a teachers' guide for grades K-12 to accompany the poster. The poster is used in teacher workshops run by the E&O program at meetings such as the National Science Teachers Association convention and at teacher workshops run at individual IRIS member institutions. Copies have also been distributed to schools participating in the Princeton Earth Physics Project (PEPP).

Accessing Under Resourced Schools

Abigail Paske, Teach For America

Summer has come to a close and I am heading back to San Jose, California. During the school year, I teach high school as part of Teach for America, an Ameri Corps sponsored program that addresses the current teacher shortage by placing recent college graduates in under-resourced public schools across the country. Teach for America is a two-year commitment to the students and community. As part of our commitment to lifelong learning, Teach for America encourages math and science majors to participate in science-oriented internships during the summer between the first and second year. At the end of August I will begin my second year of teaching chemistry, physics, and perhaps most importantly, Introduction to Science, which is a mandatory yearlong course to give high school freshman an overview of scientific processes. One of the major components of this course is a unit on Earth Science.

Last summer, as an IRIS intern, I worked on a hands-on thematic unit for my freshmen. With the help of Greg van der Vink and Christel Hennet, I put together about 14 lesson plans in a unit designed to motivate and teach seismology to high school students. From my brief experience teaching, I have noticed that students are morbidly fascinated by anything that explodes or is dangerous to their personal well-being. To this end, the unit we designed was loosely based on Greg, Christel, and Danny Harvey's analysis for the US Senate, of the Japanese terrorist cult, Aum Shinrikyo. After the cult released Sarin nerve gas into the Tokyo subway system, there was some question of whether they performed an underground nuclear test on a sheep ranch in Western Australia a couple of years earlier. In the lesson, students use various scientific techniques to figure out if the terror-cult really did have nuclear capability or if the incident was simply an aberrant earthquake. It is my belief that students will be motivated to learn seismology when presented with such a relevant and engaging scenario — even if the initial interest is simply in hearing about big explosions.

Also that summer, Catherine Johnson advised me on research for an educational poster to highlight our changing view of the interior of the Earth. Investigating the history of seismology gave me valuable insight into the science and how best to teach it. The research lead me on a wild goose chase through the far nether-regions of the Internet and then lead me to the Still Picture Gallery of the National Archives where I donned white gloves and sorted through boxes of images to use on the poster. If you ever have a chance (or a good excuse) to visit the National Archives, I highly recommend it. The poster is still in the construction stages but will be finished over the next few months.

Exciting upcoming events include implementing the Aum Shinrikyo lessons in my classroom and the classrooms of other Teach for America Corps members. Additionally, I will be writing numerous grant proposals to have a high quality seismometer installed at the school where I teach in San Jose. If you happen to have a spare seismometer kicking around your basement, let me know!

It was a productive and fruitful summer of collaboration. I hope that future Teach for America Corps members will have a chance to participate in expanding the excellent Education and Outreach program at IRIS and to have a brush with seismology on the front lines.

Reaching K-12 Students Through Teacher Workshops

Larry Braile, Purdue Univsrsity

The IRIS Education and Outreach Program has sponsored several one-day intensive workshops for teachers in the past 3 years. The workshops focus on earthquakes and related seismology, plate tectonics and Earth science. The teachers are provided with extensive materials (maps, posters, books, curriculum guides, demo/lesson/activity descriptions) and participate in conducting the hands-on activities during the day. The topics covered include: Seismic waves (see "human wave" demonstration in top photo above), Plotting earthquake epicenters, Plate puzzle, Teaching about plate tectonics with foam models, Plate tectonics flip book, Reflection and refraction, SeisVole and GIS epicenter plotting programs, Walk-run S-P earthquake location simulation, Earth's interior structure, 3-D Earth structure model, Stick-slip earthquake generation simulation, Earthquake engineering – shear wall model (see lower photo), and Building contest with shake table testing. We have received excellent feedback from the teachers on the effectiveness of the workshops and on the use of the materials in their classrooms. We have expanded the program to include a workshop for college faculty at the GSA meeting and to provide a "training workshop" for seismologists (Seismologists Learning to Teach the Teachers) that prepares members of the IRIS community to conduct workshops for K-12 teachers in their local area. Several of these local workshops have now been conducted. Through these programs, we are now reaching over 100 people a year with a significant seismology education impact. Instructors in the one-day teacher workshops and the seismologists learning to teach the teachers workshops have included: Michelle Hall-Wallace, Larry Braile, Catherine Johnson, Jeff Barker, Sheryl Braile (K-12 teacher), Rob Mellors, John Lahr, Graciela Rendon-Coke (K-12 teacher).

Seismic Waves and the Slinky: A Guide for Teachers

Lawrence W. Braile, Purdue University

"Seismic Waves and the Slinky" is a teaching guide designed to introduce the concepts of waves and seismic waves that propagate within the Earth, and to provide ideas and suggestions for how to teach about seismic waves. The guide provides information on the types and properties of seismic waves and instructions for using some simple materials – especially the slinky – to effectively demonstrate seismic wave characteristics and propagation. Most of the activities described in the guide are useful both as demonstrations for the teacher and as exploratory activities for students. Sections of the guide are: Objectives, Waves, Waves in Water Experiment, Elasticity, Elasticity of a Spring Experiment, Seismic Waves, Slinky Demonstrations of P and S Waves, Illustration of Energy Carried by the Waves, Waves Propagation in All Directions, Human Wave Demonstration – P and S Waves in Solids and Liquids, Velocity of Wave Propagation Experiment, Attenuation of Waves, Reflection of Waves, Surface Waves, Oscillations of the Whole Earth, Seismic Waves in the Earth, The Slinky, Summary, Notes to the Teacher (including suggestions for assessment activities and discussion of the relationship to the National Science Education Standards), and References. The guide contains 18 color figures and 4 tables. It is intended primarily for K-12 teachers although most of the material is also appropriate for use in beginning college level Earth science courses. The complete document is available at http://www.eas.purdue.edu/~braile. Over a thousand copies of earlier versions of the document have been distributed by the IRIS E&O program to teachers at National Science Teachers Association conventions in the past two years.

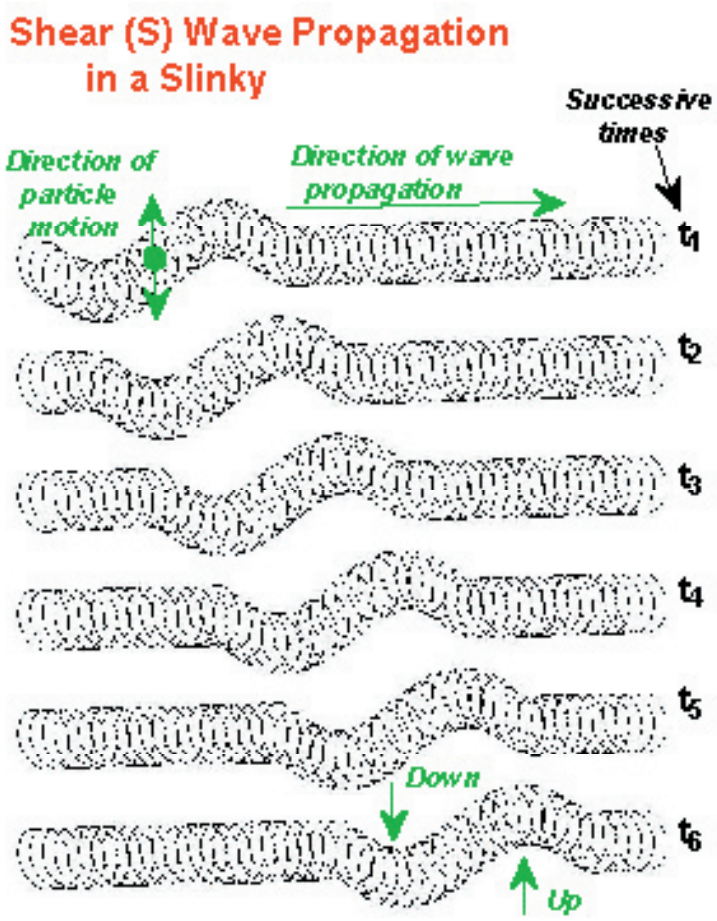

IRIS Seismographs in Schools Program

L. Braile, M. Hall-Wallace, L. Gee, J. Barker, G. Kroeger, J. Lahr, R. Mellors and C. Johnson, A. Jones, IRIS Education and Outreach Committee

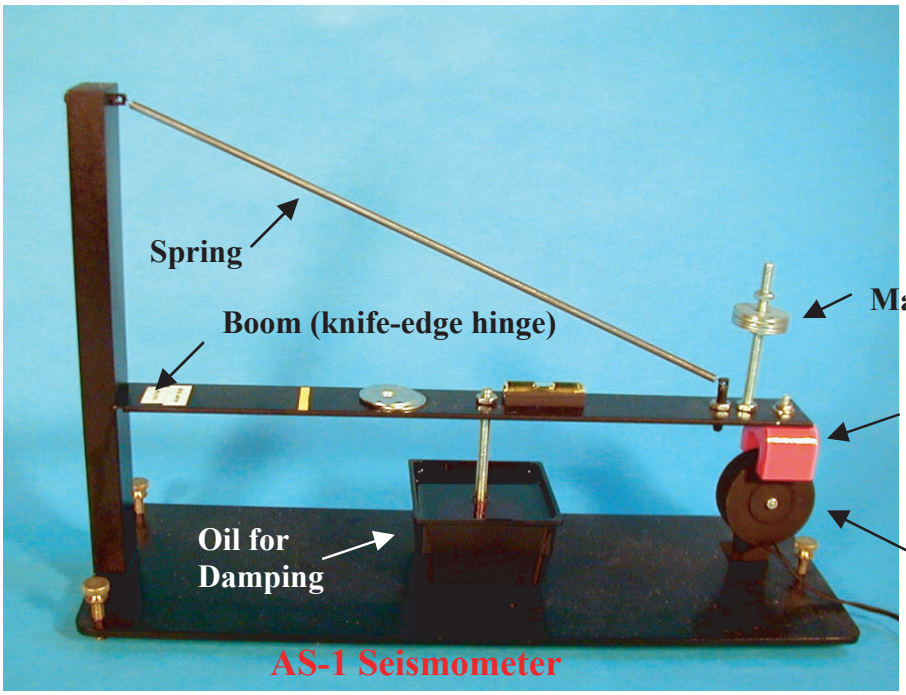

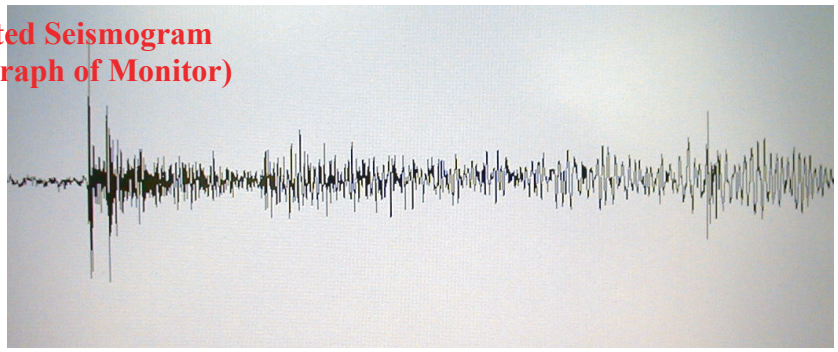

The IRIS Education and Outreach Committee has initiated a Seismographs in Schools program for K-12 schools using the AS-1 seismograph (www.primenet.com/~seismo, pictured above). The seismograph is inexpensive, easy to use for laboratory demonstrations and earthquake monitoring, and is effective for educational purposes because of its simple design (basic principles of seismometry are visible) and ease of data management. The seismograph attaches to a computer (WIN 95 and 98) for data display and archiving of recorded data. The seismograph has recently been enhanced by the addition of more versatile and powerful software (AmaSeis, written by Alan Jones, SUNY, Binghamton, www.geology.binghamton.edu/faculty/jones/) that provides a helicorder-like screen display of 24 hours of data (see screen display lower left, note 05/12/2000 M7 earthquake from Argentina recorded in Indiana) and various data management and screen display options (extracted earthquake trace at lower right, first two arrivals are P and pP phases which can be compared on the screen with standard travel time curves). An extensive set of teaching materials to accompany the AS-1 seismograph is currently being developed with the help of three "master teachers." We will have the first 35 seismographs in classrooms in Fall, 2000 and an additional 40 seismographs in classrooms by April, 2001.

AmaSeis: A Program to Capture Seismic Data From the AS-1 Seismometer

Alan Jones, SUNY Binghamton

The AS-1 Seismometer is being made available to schools through the IRIS Education and Outreach program. The Windows program AmaSeis retrieves data from the AS-1 and presents it on the screen in a helicorder-like display. Many days worth of data can be reviewed by scrolling back in time.

If an event is seen, it can be marked with the mouse and the event extracted into an event-analysis screen. The gain of the trace can be altered interactively as well as the time base. When the time base is expanded, the entire trace is not visible at one time but the trace can be scrolled through. A low-pass filter can be applied.

Arrivals can be picked with the mouse. These arrivals can then be overlaid on travel time curves and interactively moved around on the curves to find the most likely great circle arc distance to the epicenter.

The event can be saved in SAC or PEPP format. Also, an external SAC or PEPP file an be imported into the program for analysis. A SAC file can be saved as a PEPP file and a PEPP file can be saved as a SAC file.

It is hoped that the existence of the program will add excitement to earth science studies in schools since students can check for events first thing in the morning. If there is a new event they can extract it, analyze it, and share it with other participating schools.

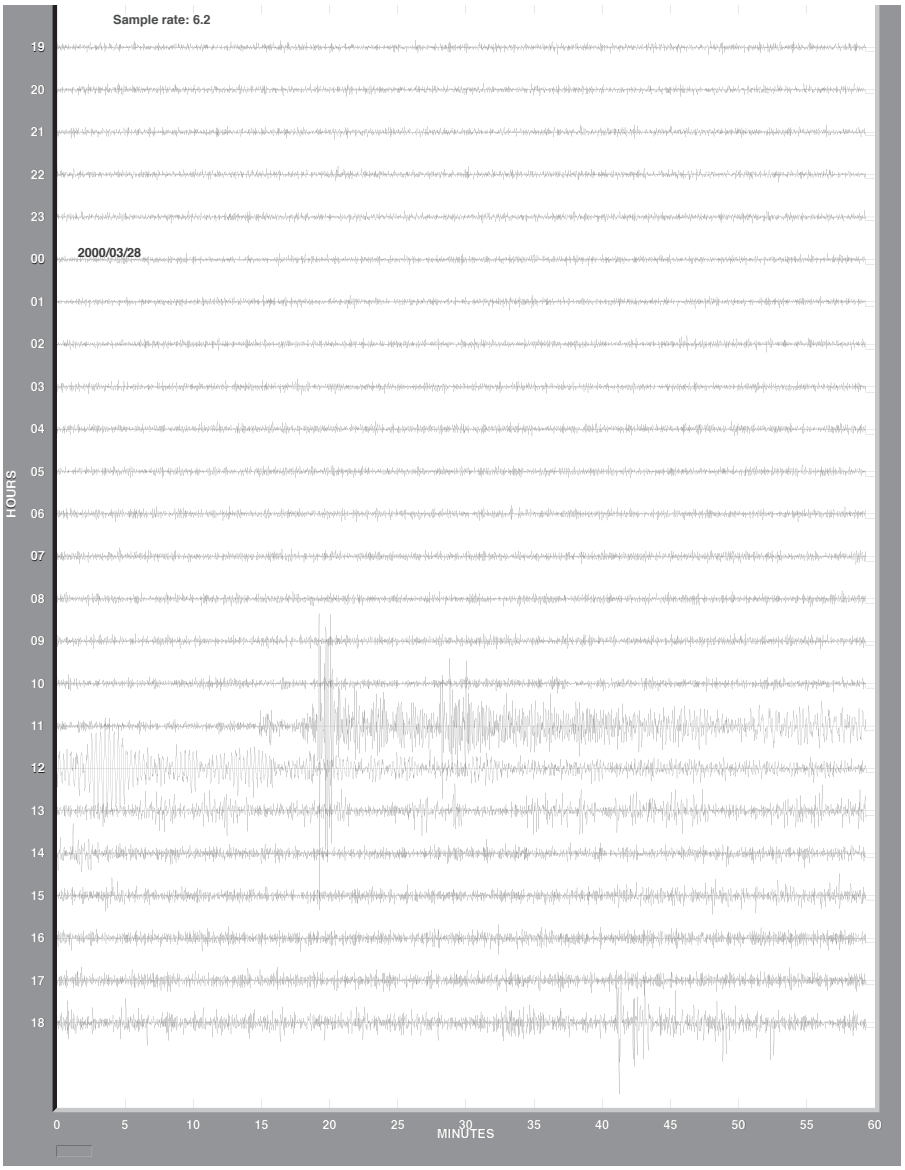

PEPP: Network of Seismic Stations in High Schools

Robert A. Phinney and Daniel Steinberg, Princeton University
Darell Speer, Rocky Mountain High School

Twelve IRIS institutions now serve as sponsors of operating seismic stations in high schools around the country, including the ten PEPP universities, the pioneering effort in Michigan, and a newly funded state-wide program in South Carolina. While the idea of seismometers in schools is not a new one, only now is it possible, via the Internet, for such stations to constitute a network. The Internet permits data to be shared among schools, access to global datasets, and classroom activities to take advantage of the real-time nature of earthquake occurrence. These are pioneering classroom efforts in several respects: (1) it involves students in a real scientific data acquisition program, (2) it requires the evolution of a support network of researchers in universities and colleges to collaborate with high school teachers and (3) it challenges the research community to understand the nature of K-12 science teaching. A series of regional teachers' workshops has evolved as a primary modality for scientists to learn to communicate effectively with teachers and for teachers to become familiarized with the novelty and challenge of this kind of program.

Students at Rocky Mountain High School in Fort Collins are reviewing a seismogram from their own Princeton Earth Physics Project (PEPP) station.

The nascent market for affordable seismometers is encouraging the development of instruments which can be acquired by students, teachers, museums and amateurs; the goal is to foster the growth of an international network of amateur seismologists. Educationally, these programs serve as an exemplar of many of the principles in the National Science Education Standards.

It is envisioned that the networked seismic data from the educational world will be joined with the international archive of data being acquired for research and societal purposes. School access to global data greatly enhances the activities in class, and the educational data has the potential to greatly densify the research networks. In seismically active regions, schools are prime candidates for the siting of strong motion sensors.

For further reading:

Princeton Earth Physics Project: http://lasker.princeton.edu/index.shtml.

Educational Earthquake Visualization

Saadia A. Baqer and Michael E.Wysession, Washington University

A series of animations are presented by which the propagation of seismic shear waves from deep and shallow earthquakes are visualized. The wavefront movies are created by taking multiple time slices of synthetic seismograms across a grid of points throughout the mantle, from the surface to the core and from the focus to the antipode. The large number of synthetic seismograms are computed across a two-dimensional grid using a summation of Earth's torsional modes of oscillations. This yields a complete record of the SH wavefield. The top of the figure shows the three seismogram traces that would be recorded at the surface at distances of 30, 60, and 90 degrees. The bottom part represents the seismic shear waves propagation through Earth's mantle. For comparison, ray-tracing of the waves shown are also presented for a slice across a spherically symmetric mantle model. The associated time-distance curves for specific SH motion are visualized to demonstrate the unique relation between a given ray path and its arrival time. The effect of the earthquake focal depth and station azimuth on the wave shape and amplitude is demonstrated. The movies show how the initially spherical SH wavefront becomes many different seismic phases after its interaction with Earth's major interfaces such as the surface, upper-mantle and core-mantle discontinuities. The movies are in Shockwave format, available for public use through Netscape at { http://epsc.wustl.edu/admin/people/baqer.html} . A VHS video version of this may be distributed through IRIS's Education and Outreach Program.

For further reading:

Wysession M. E. and Shore, P. J., Visualization of whole mantle propagation of seismic shear energy using normal mode summation, *Pure and Appl. Geophys.*, **142**, 295-310, 1994.

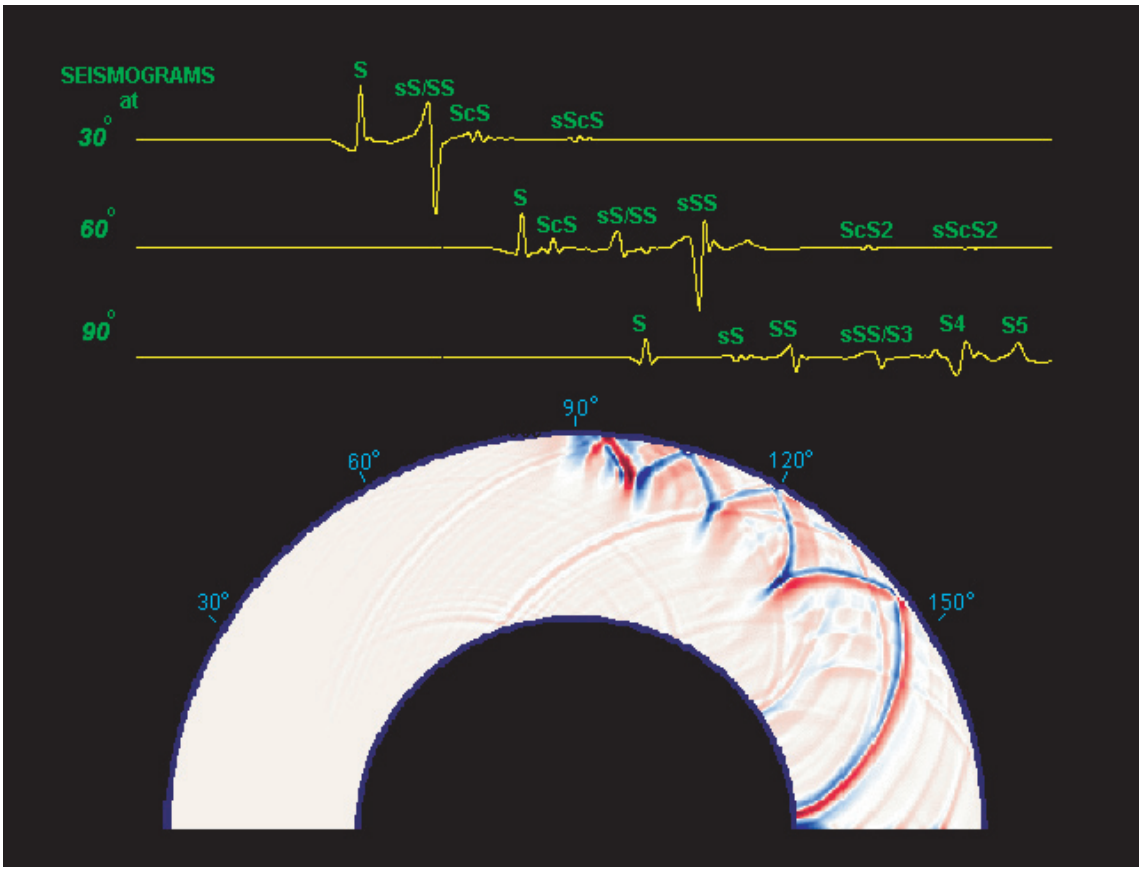

Sample Publication List

Below is a partial list of publications that have appeared in the following 15 journals during the 1999 calendar year and that specifically acknowledge IRIS data or instruments.

Bulletin, Geological Society of America
Bulletin, Seismological Society of America
Earth and Planetary Science Letters
Geology
Geophysical Journal International
Geophysical Research Letters
Journal of Geophysical Research
Nature
Physics of the Earth and Planetary Interiors
Pure and Applied Geophysics
Reviews of Geophysics
Science
Seismological Research Letters
Tectonics
Tectonophysics

Al-Amri, M. S. and A. M. Al-Amri "Configuration of the seismographic networks in Saudi Arabia." *Seismological Research Letters* (1999) 70: 322-331.

Allen, R. M., et.al. "The thin hot plume beneath Iceland." *Geophysical Journal International* (1999) 137: 51-63.

Antolik, M., D. et al. "Rupture processes of large deep-focus earthquakes from inversion of moment rate functions." *Journal of Geophysical Research* (1999) 104: 863-894.

Banka, D. D. and D. Crossley "Noise levels of superconducting gravimeters at seismic frequencies." *Geophysical Journal International* (1999) 139: 87-97.

Barruol, G. and R. Hoffmann "Upper mantle anisotropy beneath the Geoscope stations." *Journal of Geophysical Research* (1999) 104: 10757-10773.

Baumont, D., et.al. "Strong crustal heterogeneity in the Bolivian Altiplano as suggested by attenuation of Lg waves." *Journal of Geophysical Research* (1999) 104: 20287-20305.

Bear, L. K. and G. L. Pavlis "Multi-channel estimation of time residuals from broadband seismic data using multi-wavelets." *Bulletin of the Seismological Society of America* (1999) 89: 681-692.

Bear, L. K., G. L. Pavlis, et al. "Multi-wavelet analysis of three-component seismic arrays: Application to measure effective anisotropy at Pinon Flats, California." *Bulletin of the Seismological Society of America* (1999) 89: 693-705.

Berberiam, M., et.al. "The 1997 May 10 Zirkuh (Qa'enat) earthquake (Mw 7.2): Faulting along the Sistan suture zone of eastern Iran." *Geophysical Journal International* (1999) 137: 671-694.

Beucler, E., S. Chevrot, et al. "The Snake River Plain experiment revisited: Relationships between a Farallon plate fragment and the transition zone." *Geophysical Research Letters* (1999) 26: 2673-2676.

Bezzeghoud, M. and E. Buforn "Source parameters of the 1992 Melilla (Spain, Mw=4.8), 1994 Alhoceima (Morocco, Mw=5.8), and 1994 Mascara (Algeria, Mw=5.7) earthquakes and seismotectonic implications." *Bulletin of the Seismological Society of America* (1999) 89: 359-372.

Bhattacharyya, J., et.al. "Using a genetic algorithm to model broadband regional wave forms for crustal structure in the western U.S." *Bulletin of the Seismological Society of America* (1999) 89: 202-214.

Bilek, S. L. and T. Lay "Rigidity variations with depth along interplate megathrust faults in subduction zones." *Nature* (1999) 400: 443-446.

Bondar, I. and R. G. North "Development of calibration techniques for the CTBT International Monitoring System." *Physics of the Earth and Planetary Interiors* (1999) 113: 11-24.

Bondar, I., R. G. North, et al. "Teleseismic slowness-azimuth station corrections for the International Monitoring System Seismic Network." *Bulletin of the Seismological Society of America* (1999) 89: 989-1003.

Breger, L. et al. "PKP(BC-DF) travel time residuals and short scale heterogeneity in the deep earth." *Geophysical Research Letters* (1999) 26: 3169-3172.

Brisbourne, A., G. Stuart, et al. "Anisotropic structure of the Hikurangi subduction zone, New Zealand - integrated interpretation of surface-wave and body-wave observations." *Geophysical Journal International* (1999) 137: 214-230.

Castle, J. C. and K. C. Creager "A steeply dipping discontinuity in the lower mantle beneath Izu-Bonin." *Journal of Geophysical Research* (1999) 104: 7279-7292.

Chernobay, I. P. and I. P. Gabsatarova "Source classification in the northern Caucasus." *Physics of the Earth and Planetary Interiors* (1999) 113: 183-201.

Chevrot, S., et al. "Global-scale analysis of the mantle Pds phases." *Journal of Geophysical Research* 104: 20203-20219.

Comte, D., et.al. "A double-layered seismic zone in Arica, northern Chile." *Geophysical Research Letters* (1999) 26: 1965-1968.

Cotte, N., et.al. "Determination of the crustal structure in southern Tibet by dispersion and amplitude analysis of Rayleigh waves." *Geophysical Journal International* (1999) 138: 809-819.

Creager, K. C. "Large-scale variations in inner core anisotropy." *Journal of Geophysical Research* (1999) 104: 23127-23139.

Dahm, T. and F. Krueger "Higher-degree moment tensor inversion using far-field broad-band recordings: Theory and evaluation of the method with application to the 1994 Bolivian deep earthquake." *Geophysical Journal International* (1999) 137: 35-50.

Dalton, R. "Quake-spotting 'telescope' may map North American continent." *Nature* (1999) 399: 91.

Davidson, M. E. and L. W. Braile "Vibroseis recording techniques and data reduction from the Jemez Tomography Experiment." *Bulletin of the Seismological Society of America* (1999) 89: 1352-1365.

Debayle, E. "SV-wave azimuthal anisotropy in the Australian upper mantle: Preliminary results from automated Rayleigh waveform inversion." *Geophysical Journal International* (1999) 137: 747-754.

Douglas, A., et.al. "Putting nuclear-test monitoring to the test." *Nature* (1999) 398: 474-475.

Du, Z. J. and G. R. Foulger "The crustal structure beneath the northwest fjords, Iceland, from receiver functions and surface waves." *Geophysical Journal International* (1999) 139: 419-432.

Dziewonski, A. M. et al. "Centroid-moment tensor solutions for April-June 1997." *Physics of the Earth and Planetary Interiors* (1999) 112: 1-9.

Dziewonski, A. M. et al. "Centroid-moment tensor solutions for July-September 1998." *Physics of the Earth and Planetary Interiors* (1999) 114: 99-107.

Dziewonski, A. M. et al. "Centroid-moment tensor solutions for October-December 1998." *Physics of the Earth and Planetary Interiors* (1999) 115: 1-16.

Earle, P. S. "Polarization of the earth's teleseismic wavefield." *Geophysical Journal International* (1999) 139: 1-8.

Estabrook, C. H. "Bodywave inversion of the 1970 and 1963 South American large deep-focus earthquakes." *Journal of Geophysical Research* (1999) 104: 28751-28767.

Flanagan, M. P. and P. M. Shearer "A map of topography on the 410-km discontinuity from PP precursors." *Geophysical Research Letters* (1999) 26: 549-552.

Fliedner, M. M. and S. L. Klemperer "Structure of an island arc: Wide-angle seismic studies in the eastern Aleutian Islands, Alaska." *Journal of Geophysical Research* (1999) 104: 10667-10694.

Frankel, A., et.al. "Site response for Seattle and source parameters of earthquakes in the Puget Sound region." *Bulletin of the Seismological Society of America* (1999) 89: 468-483.

Freybourger, M., F. Kruger, et al. "A 22 degree long seismic profile for the study of the top of D"." *Geophysical Research Letter*s (1999) 26: 3409-3412.

Gaherty, J. B. et al. “Seismological structure of the upper mantle: a regional comparison of seismic layering.” *Physics of the Earth and Planetary Interiors* (1999) 110: 21-41.

Gomberg, J., et al. “The strain in the array is mainly in the plane.” *Bulletin of the Seismological Society of America* (1999) 89: 1428-1438.

Gorman, A. R. and R. M. Clowes “Wave-field tau-p analysis for 2-D velocity models: Application to western North American lithosphere.” *Geophysical Research Letters* (1999) 26: 2323-2326.

Gusev, A. A. and I. R. Abubakirov “Vertical profile of effective turbidity reconstructed from broadening of incoherent body-wave pulses - II. application of Kamchatka data.” *Geophysical Journal International* (1999) 136: 309-323.

Henderson, J. R., D. J. Barton, et al. “Fractal clustering of induced seismicity in the Geysers geothermal area, California.” *Geophysical Journal International* (1999) 139: 317-324.

Huang, H.-C. and T.-L. Teng “An evaluation of H/V ratio versus spectral ratio for site-response estimation using the 1994 Northridge earthquake sequences.” *Pure & Applied Geophysics* (1999) 156: 631-649.

Husebye, E. S. and F. U. Dowla “Editorial.” *Physics of the Earth and Planetary Interiors* (1999) 113: 1-3.

Inc., S. H. “Data Collection Center software.” *Seismological Research Letters* (1999) 70: 335.

Jih, R.-S. “Epicenter estimation using erroneous crustal model(s) and skew regional networks.” *Physics of the Earth and Planetary Interiors* (1999) 113: 303-319.

Kaneshima, S. and G. Helffrich “Dipping low-velocity layer in the mid-lower mantle: Evidence for geochemical heterogeneity.” *Science* (1999) 283: 1888-1891.

Kato, M. and T. H. Jordan “Seismic structure of the upper mantle beneath the western Philippine Sea.” *Physics of the Earth and Planetary Interiors* (1999) 110: 263-283.

Kay, I., et.al. “Shear wave splitting observations in the Archean craton of western Superior.” *Geophysical Research Letters* (1999) 26: 2669-2672.

Kay, I., et.al. “Imaging the Moho and Vp/Vs ratio in the western Superior Archean Craton with wide angle reflections.” *Geophysical Research Letters* (1999) 26: 2585-2588.

Kerr, R. A. “The great African plume emerges as a tectonic player.” *Science* (1999) 285: 187-188.

Kim, S. G. and N. Kraeva “Source parameter determination of local earthquakes in Korea using moment tensor inversion of single station data.” *Bulletin of the Seismological Society of America* (1999) 89: 1077-1082.

Klosko, E. R., et.al. “Upper mantle anisotropy in the New Zealand region.” Geophysical Research Letters (1999) 26: 1497-1500.

Kohler, M. D. “Lithospheric deformation beneath the San Gabriel Mountains in the southern California Transverse Ranges.” *Journal of Geophysical Research* (1999) 104: 15025-15041.

Koper, K. D., et al. “Multimodal function organization with a niching genetic algorithm: A seismological example.” *Bulletin of the Seismological Society of America*, (1999) 89: 978-988.

Koper, K. D., et.al. “Constraints on the origin of slab and mantle wedge anomalies in Tonga from the ratio of S to P velocities.” *Journal of Geophysical Research* (1999) 104: 15089-15104.

Kosarev, G., et.al. “Seismic evidence for a detached Indian lithospheric mantle beneath Tibet.” *Science* (1999) 283: 1306-1309.

Kuo, B.-Y. “Amplitude of Sdiff across Asia: Effects of velocity gradient and Qs in the D” region and the aspericity of the mantle.” *Earth & Planetary Science Letters* (1999) 173: 101-112.

Kushnir, A. F., et.al. “Statistical classification approach to discriminataion between weak earthquakes and quarry blasts recorded by the Israel Seismic Network.” *Physics of the Earth and Planetary Interiors* (1999) 113: 161-182.

Kvaerna, T. and F. Ringdal “Seismic threshold monitoring for continuous assessment of global detection capability.” *Bulletin of the Seismological Society of America* (1999) 89: 946-959.

Laske, G. and G. Masters “Limits on differential rotation of the inner core from an analysis of the earth’s free oscillations.” *Nature* (1999) 402: 66-69.

Laske, G., et al. “First results from the Hawaiian SWELL pilot experiment.” *Geophysical Research Letters* (1999) 26: 3397-3400.

Leach, R. R. J., et al. “Optimal filter parameters for low SNR seismograms as a function of station and event location.” *Physics of the Earth and Planetary Interiors* (1999) 113: 213-226.

Leborgne, S. and R. Madariaga “Body waveform modeling of east Mediterranean earthquakes at intermediate distances (17-30 degrees) with a Gaussian beam summation method.” *Journal of Geophysical Research* (1999) 104: 28813-28828.

Lemonnier, C., et.al. “Electrical structure of the Himalaya of central Nepal: High conductivity around the mid-crustal ramp along the MHT.” *Geophysical Research Letters* (1999) 26: 3261-3264.

Levin, V., et al. “Shear wave splitting in the Appalachians and the Urals: A case for multilayered anisotropy.” *Journal of Geophysical Research* (1999) 104: 17975-17993.

Levshin, A. L., et al. “Source effects on surface wave group travel times and group velocity maps.” *Physics of the Earth and Planetary Interiors* (1999) 115: 293-312.

Li, Y.-G., et.al. “Shallow structure of the Landers fault zone from explosion-generated trapped waves.” *Journal of Geophysical Research* (1999) 104: 20257-20275.

Ligorria, J. P. and C. J. Ammon “Iterative deconvolution and receiver-function estimation.” *Bulletin of the Seismological Society of America* (1999) 89: 1395-1400.

Lodge, R. L. E., et al. “Fundamental leaking mode (PL) propagation along the Tonga-Kermadec-Hikurangi-Macquarie margin.” *Geophysical Journal International* (1999) 137: 675-690.

Lutter, W. J., et.al. “Tomographic images of the Upper crust from the Los Angeles basin to the Mojave Desert, California: Results from the Los Angeles Region Seismic Experiment.” *Journal of Geophysical Research* (1999) 104: 25543-25565.

Makovsky, Y. and S. L. Klemperer “Measuring the seismic properties of Tibetan bright spots: Evidence for free aqueous fluids in the Tibetan middle crust.” *Journal of Geophysical Research* (1999) 104: 10795-10825.

Malone, S. “Seismic network recording and processing systems.” *Seismological Research Letters* (1999) 70: 175-178.

Mangino, S., et al. “The receiver structure beneath the China Digital Sesimograph Network stations.” *Bulletin of the Seismological Society of America* (1999) 89: 1053-1076.

Martynov, V. G., et.al. “High-frequency attenuation in the crust and upper mantle of the northern Tien Shan.” *Bulletin of the Seismological Society of America* (1999) 89: 215-238.

Megnin, C. and B. Romanowicz “The effects of the theoretical formalism and data selection on mantle models derived from waveform tomography.” *Geophysical Journal International* (1999) 138: 366-380.

Meissner, R. and W. Rabbel “Nature of crustal reflectivity along the DEKORP profiles in Germany in comparison with reflection patterns from different tectonic units worldwide: A review.” *Pure & Applied Geophysics* (1999) 156: 7-28.

Mellors, R. J., et.al. “Regional waveform propagation in the Arabian peninsula.” *Journal of Geophysical Research* (1999) 104: 20221-20235.

Mendoza, C. and S. Hartzell “Fault-slip distribution of the 1995 Cojima-Jalisco, Mexico, earthquake.” *Bulletin of the Seismological Society of America* (1999) 89: 1338-1344.

Midzi, V., et.al. “Transitional continental-oceanic structure beneath the Norwegian Sea from inversion of surface wave group velocity data.” *Geophysical Journal International* (1999) 139: 433-446.

Mitchell, B. J. and R. Buland “BILLIKEN.” *Seismological Research Letters* (1999) 70: 341-347.

Muyzert, E., et al. “A Seismic cross-section through the east European continent.” *Geophysical Journal International* (1999) 137: 695-704.

Myers. S., et al. “Observations in support of Rg scattering as a source for explosion S waves: Regional and local recordings of the 1997 Kazakhstan depth of burial experiment.” *Bulletin of the Seismological Society of America* (1999) 89: 544-549.

Neal, S. L. and G. L. Pavlis “Imaging P-to-S conversions with multichannel receiver functions.” *Geophysical Research Letters* (1999) 26: 2581-2584.

Nettles, M., et al. “The March 25, 1998, Antarctic plate earthquake.” *Geophysical Research Letters* (1999) 26: 2097-2100.

Nishida, K. and N. Kobayashi “Statistical features of earth’s continuous free oscillations.” *Journal of Geophysical Research* (1999) 104: 28741-28750.

Nowack, R. L. and W.-P. Chen “Source-receiver reciproc-

ity and empirical Green's functions from chemical blasts." *Bulletin of the Seismological Society of America* (1999) 89: 538-543.

Oliver, M. and G. Ekström "Rupture depths and source processes of the 1997-1998 earthquake sequence in central Italy." *Bulletin of the Seismological Society of America* (1999) 89: 305-310.

Ottemoller, L. and J. Havskov "Seisnet: A general purpose virtual seismic network." *Seismological Research Letters* (1999) 70: 522-528.

Ozalaybey, S. and W.-P. Chen "Frequency-dependent analysis of SKS/SKKS waveforms observed in Australia: Evidence for null birefringence." *Physics of the Earth and Planetary Interiors* (1999) 114: 197-210.

Parsons, T., et.al. "Three-dimensional velocity structure of Siletzia and other accreted terranes in the Cascadia forearc of Washington." *Journal of Geophysical Research* (1999) 104: 18015-18039.

Petukhin, A. G., et.al. "Preliminary model for scaling of Fourier spectra of strong ground motion recorded on Kamchatka." *Pure & Applied Geophysics* (1999) 156: 445-468.

Phillips, W. S. "Empirical path corrections for regional-phase amplitudes." *Bulletin of the Seismological Society of America* (1999) 89: 384-393.

Pillet, R., et.al. "Crust and upper mantle heterogeneities in the southwest Pacific from surface wave phase velocity analysis." *Physics of the Earth and Planetary Interiors* (1999) 110: 211-234.

Priestley, K. and F. Tilmann "Shear-wave structure of the lithosphere above the Hawaiian hot spot from two-station Rayleigh wave phase velocity measurements." *Geophysical Research Letters* (1999) 26: 1493-1496.

Quintanar, L., et al. "Source mechanism of two 1994 intermediate-depth-focus earthquakes in Guerrera, Mexico." *Bulletin of the Seismological Society of America* (1999) 89: 1004-1018.

Rangin, C., et.al. "Plate convergence measured across the Sundaland/Philippine Sea plate deformed boundary: The Philippines and eastern Indonesia." *Geophysical Journal International* (1999) 139: 296-316.

Raoof, M., et al. "Attenuation and excitation of three-component ground motion in Southern California." *Bulletin of the Seismological Society of America* (1999) 89: 888-902.

Rebollar, C. J., et.al. "Source process of the Chiapas, Mexico, intermediate-depth earthquake (Mw=7.2) of 21 October 1995." *Bulletin of the Seismological Society of America* (1999) 89: 348-358.

Reese, C. C., et al. "Lateral variation of Pn and Lg attenuation at the CDSN station LSA." *Bulletin of the Seismological Society of America* (1999) 89: 325-330.

Restivo, A. and G. Helffrich "Teleseismic shear wave splitting measurements in noisy environments." *Geophysical Journal International* (1999) 137: 821-830.

Ritsema, J., H. et al. "Complex shear wave velocity structure imaged beneath Africa and Iceland." *Science* (1999) 286: 1925-1928.

Rodgers, A. J., et.al. "Lithospheric structure of the Arabian Shield and Platform from complete regional waveform modeling and surface wave group velocities." *Geophysical Journal International* (1999) 138: 871-878.

Rodgers, A. J., et.al. "A comparison of methodologies for representing path effects on regional P/S discriminants." *Bulletin of the Seismological Society of America* (1999) 89: 394-408.

Roth, E. G., et.al. "Seismic attenuation tomography of the Tonga-Fiji region using phase pair methods." *Journal of Geophysical Research* (1999) 104: 4795-4809.

Roth, E. G. and D. A. Wiens "Depression of the 660-km discontinuity beneath the Tonga slab determined from near-vertical ScS reverberations." *Geophysical Research Letters* (1999) 26: 1223-1226.

Roult, G., et.al. "The GEOSCOPE program: Its data center." *Physics of the Earth and Planetary Interiors* (1999) 113: 25-43.

Ruff, L. J. "OhioSeis and PS." *Seismological Research Letters* (1999) 70: 332-333.

Ruff, L. J. and M. Hall-Wallace "Instructional software for seismology." *Seismological Research Letters* (1999) 70: 85-86.

Russell, S. A., et al. "Small-scale lateral shear velocity and anisotropy heterogeneity near the core-mantle boundary beneath the central Pacific imaged using broadband ScS waves." *Journal of Geophysical Research* (1999) 104: 13183-13199.

Ryberg, T. and F. Wenzel "High-frequency wave propagation in the uppermost mantle." *Journal of Geophysical Research* (1999) 104: 10655-10666.

Sain, S. R., et.al. "Outlier detection from a mixture distribution when training data are unlabeled." *Bulletin of the Seismological Society of America* (1999) 89: 294-304.

Sarker, G. and G. A. Abers "Lithospheric temperature estimates from seismic attenuation across range fronts in southern and central Europe." *Geology* (1999) 27: 427-430.

Schoffel, H.-J. and S. Das "Fine details of the Wadati-Benioff zone under Indonesia and its geodynamic implications." *Journal of Geophysical Research* (1999) 104: 13101-13114.

Schultz, C. A., et.al. "Nonstationary Bayesian kriging: A predictive technique to generate spatial corrections for seismic detection, location and identification." *Physics of the Earth and Planetary Interiors* (1999) 113: 321-338.

Schwartz, S. Y. "Noncharacteristic behavior and complex recurrence of large subduction zone earthquakes." *Journal of Geophysical Research* (1999) 104: 23111-23125.

Schweitzer, J. and T. Kvaerna "Influence of source radiation patterns on globally observed short-period magnitude estimates (mb)." *Bulletin of the Seismological Society of America* (1999) 89: 342-347.

Scrivner, C. W. and D. V. Helmberger "Variability of ground motions in Southern California — Data from the 1995 to 1996 Ridgecrest sequence." *Bulletin of the Seismological Society of America* (1999) 89: 626-639.

Shearer, P. M. and M. P. Flanagan "Seismic velocity and density jumps across the 410- and 660-kilometer discontinuities." *Science* (1999) 285: 1545-1548.

Sipkin, S. A., et al. "Moment tensor solution estimated using optimal filter theory: Global seismicity, 1997." *Physics of the Earth and Planetary Interiors* (1999) 114: 109-117.

Suárez, G., et.al. "The December 11, 1995, earthquake (Mw = 6.4): Implications for the present-day relative motion on the Rivera-Cocos plate boundary." *Geophysical Research Letters* (1999) 26: 1957-1960.

Suetsugu, D. "Defocusing of teleseismic P-waves by the Tonga-Kermadec slab." *Geophysical Research Letters* (1999) 26: 2785-2788.

Swenson, J. L., et al. "Regional distance shear-coupled PL propagation within the northern Altiplano, central Andes." *Geophysical Journal International* (1999) 139: 743-753.

Tanimoto, T. "Excitation of normal modes by atmospheric turbulence: Source of long-period seismic noise." *Geophysical Journal International* (1999) 136: 395-402.

Tanimoto, T. and J. Um "Cause of continuous oscillations of the Earth." *Journal of Geophysical Research* (1999) 104: 28723-28739.

Tarvainen, M., et al. "Locating regional seismic waves with global optimization based on interval arithmetic." *Geophysical Journal International* (1999) 138: 879-885.

Thio, H. K., et.al. "Seismic source and structure estimation in the western Mediterranean using a sparse broadband network." *Journal of Geophysical Research* (1999) 104: 845-861.

Tibi, R., et al. "The 1996 June 17 Flores Sea and 1994 March 9 Fiji-Tonga earthquakes: Source processes and deep earthquake mechanisms." *Geophysical Journal International* (1999) 138: 625-642.

van Eck, T. and B. Dost "ORFEUS a European initiative in broadband seismology: Status and future plans." *Physics of the Earth and Planetary Interiors* (1999) 113: 45-55.

Van Heijst, H. J. and J. Woodhouse "Global high-resolution phase velocity distributions of overtone and fundamental-mode surface waves determined by mode branch stripping." *Geophysical Journal International* (1999) 137: 601-620.

Vdovin, O., et.al. "Group-velocity tomography of South America and the surrounding oceans." *Geophysical Journal International* (1999) 136: 324-340.

Viejo, G. F., et al. "Imaging the lithospheric mantle in northwestern Canada with seismic wide-angle reflections." *Geophysical Research Letters* (1999) 26: 2809-2812.

Vinnik, L., et.al. "Teleseismic travel time residuals in North America and anelasticity of the asthenosphere." Physics of the Earth and Planetary Interiors (1999) 116: 93-103.

Wilcock, W. S. D., et al. "The effect of local wind on seismic noise near 1 Hz at the MELT site and in Iceland." *Bulletin of the Seismological Society of America* (1999) 89: 1543-1557.

Winslow, N. W. and L. J. Ruff "A hybrid method for calculating the radiated wave energy of deep earthquakes." *Phys-*

ics of the Earth and Planetary Interiors (1999) 115: 181-190.

Wolfe, C. J., F. et al. “Shear-wave splitting across western Saudi Arabia: The pattern of upper mantle anisotropy at a Proterozoic Shield.” *Geophysical Research Letters* (1999). 26: 779-782.

Wright, T. J., et.al. “Source parameters of the 1 October 1995 Dinar (Turkey) earthquake from SAR interferometry and seismic bodywave modeling.” *Earth & Planetary Science Letters* (1999) 172: 23-37.

Wu, L.-R. and W.-P. Chen “Anomalous aftershocks of deep earthquakes in Mariana.” *Geophysical Research Letters* (1999) 26: 1977-1980.

Wysession, M. E., et. al. “Lateral variations in compressional/shear velocities at the base of the mantle.” *Science* (1999) 284: 120-125.

Xie, J. and H. J. Patton “Regional phase excitation and propagation in the Lop Nor region of central Asia and implications for P/Lg discriminants.*” Journal of Geophysical Research* (1999) 104: 941-954.

Yoshizawa, K., et al. “Resolving power of surface polarization data for higher-order heterogeneities.” *Geophysical Journal International* (1999) 138: 205-220.

Zadeh, M. A. and P. Nassery “Application of quadratic neural networks to seismic signal classification.” *Physics of the Earth and Planetary Interiors* (1999) 113: 103-110.

Zhao, M., et.al. “Upper mantle velocity structure beneath southern Africa from modeling regional seismic data.” *Journal of Geophysical Research* (1999) 104: 4783-4794.

Zhao, Y. and K. Takano “An artificial neural network approach for broadband seismic phase picking.” *Bulletin of the Seismological Society of America* (1999) 89: 670-680.